WARWICK
THE UNIVERSITY OF WARWICK

A Thesis Submitted for the Degree of PhD at the University of Warwick

Permanent WRAP URL:

http://wrap.warwick.ac.uk/101773

Copyright and reuse:
This thesis is made available online and is protected by original copyright.
Please scroll down to view the document itself.
Please refer to the repository record for this item for information to help you to cite it.
Our policy information is available from the repository home page.

For more information, please contact the WRAP Team at: wrap@warwick.ac.uk

warwick.ac.uk/lib-publications

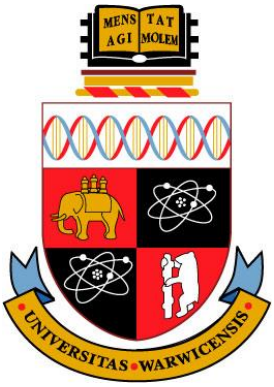

Detergent-free approach to the studies of bacterial cell division membrane proteins using styrene maleic acid copolymer

Alvin Chen Kuang Teo

Submitted in partial fulfilment of the requirements
for the degree of Doctor of Philosophy

School of Life Sciences & Department of Chemistry
July 2017

WARWICK
THE UNIVERSITY OF WARWICK

Contents

Table of Contents

List of Tables

List of Figures

Acknowledgements

First and foremost, I am grateful to my supervisor, Prof. David Roper for selecting me for this research project and his guidance and support throughout my PhD studies. I would also like to express my sincere thanks to all the members (both past and present) in the C10 Structural Laboratory at the School of Life Sciences, University of Warwick, for their help and input during my time in the lab. Special thanks go to:

- Anita and Julie for all the kind assistance in the lab;
- Amy and Dean for help with enzyme assays;
- Michael and Mary for help in transmission electron microscopy;
- Dan for help with microbiology;
- Debs for advice in membrane protein overexpression;
- Mussa for help with chemistry and computer-related matters.

I would like to thank Kasra and Meropi for help with FTIR analysis; Dr. Philip Young and Dr. Tauqeer Alam for statistical advice; Dr. Cleidiane Zampronio for mass spectrometry advice; and Dr. E. Peter Magennis and Dr. David Scurr for help with principal component analysis.

A heartfelt appreciation to Naomi Grew for her phenomenal administrative support to CAS-IDP, and to all the CAS-IDP fellows, your comradeship would never be forgotten! Huge thanks to Prof. Alison Rodger for running CAS-IDP and advice in circular dichroism spectroscopy. The funding from the European Union for my PhD studies is also greatly acknowledged.

An earnest thanks to Prof. Timothy Dafforn for hosting me in his group for the work in SMALP. Special thanks to Craig who initiated me into the exciting SMALP technology; Rosemary for looking after me when I am in the 7th floor lab; Sarah and Naomi Pollock for the fruitful collaboration in the SMALP lipidomic work; Stephen Hall for providing the protein sample; Julia, Richard, and Mohammed for all the advice and assistance during my time in Birmingham.

I am indebted to Prof. Corinne Spickett for hosting me in her group as a year-long visiting researcher. Special thanks to Alpesh for introducing me to LC-MS and all the help with the initial method development; Prof. Andrew Pitt who ignited my passion for MS; Ivana for all the help and advice in MS, especially the late night and weekend troubleshooting sessions; Iru for advice in lipidomics; Dr. Alice Rothnie for advice in the de-SMALP method development; and other members in the Spickett and Pitt groups for their assistance during my time in Aston.

Last but not least, I thank my family for their unconditional love and support, and my beloved wife, Yvonne for her unwavering love and faith in me completing my PhD over all these years, especially during the thesis writing period. Most importantly, I acknowledged my Lord and saviour, Jesus Christ, to God be all the glory!

‘I can do all things through Christ who strengthens me’
Philippians 4:13 (NKJV)

Declaration

This thesis is submitted to the University of Warwick in support of my application for the degree of Doctor of Philosophy. I hereby declare that I have personally carried out the work submitted in this thesis under the primary supervision of Prof. David I. Roper at the School of Life Sciences, University of Warwick. Parts of the work were also conducted in the University of Birmingham and Aston University in collaboration with the groups of Prof. Timothy R. Dafforn and Prof. Corinne M. Spickett respectively. Where work had been contributed to by other individuals it is specifically stated in the text. No part of this work has previously been submitted to be considered for a degree or qualification. All sources of information have been specifically acknowledged in the form of references.

Some of the initial literature review work of this thesis has been published and the SMALP lipidomic work is to be submitted for publication.

- Teo, A.C.K., Roper, D.I., 2015. Core steps of membrane-bound peptidoglycan biosynthesis: Recent advances, insight and opportunities. Antibiot (Basel). 4, 495–520.

- Teo, A.C.K., Lee, S.C., Pollock, N.L., Thakker, A., Pitt, A.R., Dafforn, T.R., Spickett, C.M., Roper, D.I., Analysis of SMALP co-extracted lipids of three classes of bacterial membrane proteins (*Manuscript in preparation*).

Abstract

Membrane proteins represent a subset of proteins embedded in or associated with the biological membrane. Despite accounting for 30% of the prokaryotic and eukaryotic proteomes and over 50% of current therapeutic targets, the structural and functional studies of membrane proteins still largely lag behind their soluble counterparts. This is predominantly due to the challenges in the isolation and purification of these proteins from their native membrane environment. Traditionally, detergents are employed for the extraction of membrane proteins from the native membrane, with subsequent solubilisation in mixed micelles. However, the surrounding lipids could be sequestered and lost during this process, which is potentially denaturing to the proteins.

A novel method exploiting the styrene maleic acid (SMA) copolymer for membrane solubilisation (in the total absence of detergents) results in the generation of SMA/lipid particles (SMALPs) or 'native nanodiscs' of polymer-encapsulated membrane proteins together with their surrounding lipid moieties. Besides allowing the direct solubilisation of target membrane proteins from their native environment, analyses of native protein-lipid interactions and the characterisation of membrane lipidomes could be implemented, which may provide pivotal information to underpin the development of the next-generation antimicrobial agents.

This detergent-free approach was successfully applied to the two cell division proteins, *i.e.* ZipA and FtsA and another integral membrane lipid phosphatase - PgpB from *Escherichia coli*. An analytically robust 'SMALP lipidomics' method based on liquid chromatography-tandem mass spectrometry (LC-MS/MS) was developed to elucidate the co-extracted membrane lipidomes of these proteins, resulting in the first comprehensive report of their respective native phospholipid compositions. Biophysical and biochemical characterisations were also conducted on PgpB in the context of SMALP and a detergent benchmark to facilitate the direct comparison between these two approaches for membrane protein studies.

Keywords: Cell division, divisome, membrane proteins, styrene maleic acid copolymer, SMALP, ZipA, FtsA, PgpB, lipidomics, LC-MS/MS

Abbreviations

ACN	Acetonitrile
AMR	Antimicrobial resistance
ANOVA	Analysis of variance
APS	Ammonium persulfate
ATR-FTIR	Attenuated total reflectance-Fourier transform infrared
BHT	Butylated hydroxytoluene
BLM	Black lipid membrane
βME	β-Mercaptoethanol
C_{55}-P	Undecaprenyl phosphate
C_{55}-PP	Undecaprenyl pyrophosphate
C-terminal	Carboxyl-terminal
CD	Circular dichroism
CHAPS	3-[(3-Cholamidopropyl) dimethylammonio]-1-propanesulfonate
CID/CAD	Collision-induced/activated dissociation
CL	Cardiolipin
CMC	Critical micelle concentration
Cryo-EM	Cryo-electron microscopy
CPM	7-Diethylamino-3-(4'-maleimidylphenyl)-4-methylcoumarin
DDA/IDA	Data/information-dependent acquisition
DDM	*n*-Dodecyl-β-D-maltopyranoside
DFT	Dynamic fill time
DGPP	Diacylglycerol pyrophosphate
DHPC	1,2-Dihexanoyl-*sn*-glycero-3-phosphocholine
DMPC	1,2-Dimyristoyl-*sn*-glycero-3-phosphocholine
DMSO	Dimethyl sulfoxide
DNA	Deoxyribonucleic acid
E. coli	*Escherichia coli*
EDTA	Ethylenediaminetetraacetic acid
EIC/XIC	Extracted ion chromatogram
EM	Electron microscopy

EMS	Enhanced mass spectrometry scan mode
EPI	Enhance product ion scan mode
ESI	Electrospray ionisation
GC	Gas chromatography
GS1	Nebuliser gas
GS2	Auxiliary/turbo gas
HPLC	High performance liquid chromatography
IMAC	Immobilised metal affinity chromatography
IPTG	Isopropyl β-D-1-thiogalactopyranoside
IPA	Isopropyl alcohol
IS	Internal standard
LB	Luria-Bertani or lysogeny broth
LC-MS	Liquid chromatography-mass spectrometry
LC-MS/MS	Liquid chromatography-tandem mass spectrometry
LCP	Lipidic cubic phase
LDAO	Lauryldimethylamine oxide or *N*,*N*-Dimethyldodecylamine *N*-oxide
LPA	Lysophosphatidic acid
LoD	Limit of detection
LoQ	Limit of quantification
LUV	Large unilamellar vesicle
MALDI	Matrix-assisted laser desorption/ionisation
MCA	Multichannel analysis
MeOH	Methanol
MESG	7-Methyl-6-thioguanosine
MLV	Multilamellar vesicle
MRM	Multiple reaction monitoring
MS	Mass spectrometry
MS/MS (MS^2)	Tandem mass spectrometry
MSP	Membrane scaffold protein
MTBE	Methyl *tert*-butyl ether
MTS	Membrane targeting sequence
NAO	10-*N*-nonyl acridine orange

NL	Neutral loss
NMR	Nuclear magnetic resonance
N-terminal	Amino-terminal
OD600	Optical density measured at 600 nm
PA	Phosphatidic acid
PBP	Penicillin-binding protein
PCA	Principal component analysis
PDB	Protein Data Bank
PE	Phosphatidylethanolamine
PG	Phosphatidylglycerol
PGP	Phosphatidylglycerol phosphate
PIS	Precursor ion scan mode
PNP	Purine nucleoside phosphorylase
POPG	1-Palmitoyl-2-oleoyl-*sn*-glycero-3-phospho-(1'-*rac*-glycerol) (16:0/18:1 PG)
POPE	1-Palmitoyl-2-oleoyl-*sn*-glycero-3-phosphoethanolamine (16:0/18:1 PE)
PS	Phosphatidylserine
RAFT	Reversible addition-fragmentation chain transfer
RSD	Relative standard deviation
R. sphaeroides	*Rhodobacter sphaeroides*
S1P	Sphingosine-1-phosphate
S. aureus	*Staphylococcus aureus*
SANS	Small angle neutron scattering
SAXS	Small angle X-ray scattering
SDS	Sodium dodecyl sulfate
sCO_2	Supercritical carbon dioxide
SDS-PAGE	Sodium dodecyl sulfate-polyacrylamide gel electrophoresis
SEC	Size exclusion chromatography
SFC	Supercritical fluid chromatography
SIMS	Secondary ion mass spectrometry
SMA	Styrene maleic acid
SMAn	Styrene maleic anhydride

S:MA	Styrene-to-maleic acid ratio
SMALP	Styrene maleic acid/lipid particle
SRM	Selected reaction monitoring
SLB	Supported lipid bilayer
TEM	Transmission electron microscopy
TEMED	Tetramethylethylenediamine
THF	Tetrahydrofuran
TLC	Thin layer chromatography
TM	Transmembrane
TOCL	1,1',2,2'-Tetraoctadecenoyl cardiolipin or 1',3'-Bis[1,2-dioleoyl-*sn*-glycero-3-phospho]-*sn*-glycerol (18:1/18:1/18:1/18:1 CL)
ToF	Time-of-flight mass analyser
Tris	Tris(hydroxymethyl)aminomethane

Units of Measurement

Å	Angstrom
x *g*	Centrifugal force
cps	Counts per second
CV	Column volume or resin bed volume
Da	Dalton
°C	Degree Celsius
θ	Ellipticity (measured in millidegrees)
g	Gram
h	Hour
kDa	KiloDalton
kpsi	Kilopound per square inch
µL	Microliter
µM	Micromolar
µg	Microgram
mg/mL	Milligram per millilitre
mg	Milligram

mM	Millimolar
min	Minute
M	Molar
$\Delta\varepsilon$	Molar differential extinction coefficient
MW	Molecular weight
ng	Nanogram
nL	Nanolitre
nm	Nanometre
pH	$-\log_{10}[H^+]$ (potential of hydrogen)
rpm	Rotations per minute
s	Second
V	Volt
v/v	Volume-to-volume ratio
w/v	Weight-to-volume ratio
λ	Wavelength of light

Other abbreviations are explained in the text where appropriate.

Chapter 1: General Introduction

1.1 Antimicrobial resistance

In this era of antimicrobial resistance (AMR), the emerging reports of multidrug resistance bacteria afflicting the human race are ever increasing to warrant considerable attention from the government and general public (O'Neill, 2014; WHO, 2014). In fact, the need to address the resistance of bacteria to existing antibiotics is never ever in such desperate demand. Without effective intervention, it is forecasted by the year 2050, untreated bacterial infections could result in ten million deaths per year (more than the current 8.2 million deaths caused by cancer), equating to a staggering amount of one person dying from AMR every three seconds. AMR is also estimated to cost the global economy up to $100 trillion by 2050, posing an enormous global healthcare and economical challenge (O'Neill, 2014). In the UK, at least 5,000 people die per year from resistant infections caused by antibiotic-resistant bacteria, such as methicillin-resistant *Staphylococcus aureus* (MRSA) (National Audit Office, 2004). Over-prescription of antibiotics, the use of antibiotics in agricultural sectors, increasing population growth, and global travel are among the key factors identified to contribute to the issue of AMR. In addition, there has been a drug discovery void for the past 30 years, whereby no novel classes of antibiotics was developed since the discovery of daptomycin in 1987 (Broughton *et al.*, 2016).

1.2 Bacterial cell division and antibiotic discovery

Since the serendipitous discovery of the β-lactam antibiotic - penicillin by Sir Alexander Fleming in 1928, he had forewarned about the emergence of drug resistant bacteria in his Nobel Prize speech in 1945. In fact, bacteria have since exploited multiple ways to modify their cell wall (which is the target for β-lactam antibiotics), in order to resist the action of such antibacterial agents (WHO, 2014). β-lactam antibiotics target a group of enzymes, collectively known as the penicillin-binding proteins (PBPs) involved in the biosynthesis of the peptidoglycan cell wall in bacteria (Silver, 2013). Peptidoglycan, the fundamental structural component of bacterial cell wall is a mesh-like, discontinuous, heteropolymeric sacculus serves to preserve cellular integrity by providing structural support, maintaining the cell shape and morphology, and preventing the cells from osmotic rupture due to the large internal turgor pressure

(Typas *et al.*, 2012). It is therefore unsurprisingly that many enzymes involved in the peptidoglycan biosynthetic pathway, especially the soluble Mur ligases A-F (Figure 1.1A) have been shortlisted for antibiotic discovery (Hrast *et al.*, 2014; Silver, 2013). The synthesis of cell wall in bacteria is inherently linked to its division process, as the cell wall material has to be made and remodelled in a highly controlled fashion to enable the binary fission process to occur. The generalised bacterial divisome model is illustrated in Figure 1.1 (A). It is a complex ensemble of protein components, spanning both sides of the cell membrane into a dynamic hyperstructure that is linked to the cell cycle, to coordinate the various cell division events, leading to complete cell envelope invagination during cytokinesis (den Blaauwen *et al.*, 2017; Trip and Scheffers, 2015; Vischer *et al.*, 2015).

Figure 1.1 (B) illustrates the hierarchical recruitment of the protein components within the divisome, underlining the numerous protein-protein interactions (Egan and Vollmer, 2013). The discovery of the Z-ring (made up of FtsZ protein filaments) in 1991 was considered a defining moment for the field of bacterial cell division and had since motivated over 25 years of in-depth research regarding this bacterial tubulin homolog that serves as scaffold for the division machinery and other divisome protein components (den Blaauwen *et al.*, 2017). During the formation of the divisome complex, the protein components arrive at the septum sequentially, starting with the formation of a proto-ring consisting of FtsZ proteins stabilised by ZipA, FtsA, and Zap proteins. Subsequently, FtsE/X, FtsK, FtsQ/L/B, FtsW, FtsI(PBP3) and lastly FtsN arrive at the divisome prior to cytokinesis (de Boer, 2010; Egan and Vollmer, 2013).

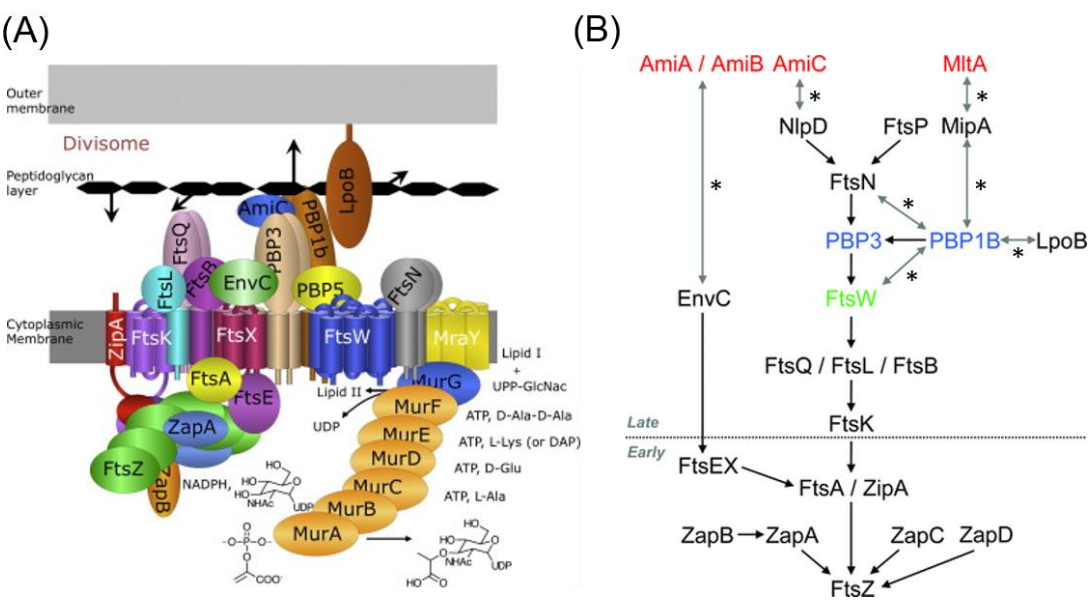

Figure 1.1 The generalised bacterial divisome model and protein-protein interactions within the divisome. (A) The bacterial divisome is a dynamic complex involving many proteins that spans both sides of the cell membrane. (B) The hierarchical recruitment of the protein components within the divisome, black arrows indicate dependency on septal localisation mediated by the proposed protein-protein interactions; gray arrows (with asterisks) indicate further direct interactions involving the peptidoglycan enzymes. Figures are adopted from den Blaauwen *et al.* (2014) and Egan and Vollmer (2013) with permission.

1.2.1 Divisome membrane proteins as antibiotic target

The mature divisome of the Gram negative model bacterium - *Escherichia coli* is known to comprise of more than 30 different protein components, among which ten of them, namely FtsZ, ZipA, FtsA, FtsK, FtsQ, FtsL, FtsB, FtsW, FtsI(PBP3), and FtsN are essential to the cell division process (de Boer, 2010; Egan and Vollmer, 2013). These proteins are thus considered the core of the division apparatus and many of them are membrane proteins in nature. They can either attach to the cell membrane (peripheral membrane protein), or embed within the cell membrane either through a single spanning transmembrane (TM) helix (bitopic membrane protein) or multiple spanning TM helices (polytopic integral membrane protein).

There is currently no drug in the clinic that targets the membrane proteins in the divisome besides the PBPs. In order to explore these other divisome members as

potential antibiotic target, it is impetus to develop robust analytical tools to perform in-depth structural and functional studies on these proteins. However, given that their nature as membrane proteins, they are not readily amenable to conventional *in vitro* biochemical and/or biophysical studies in aqueous environments without utilising an appropriate membrane solubilisation agent. While studying these membrane proteins, careful examination of the interaction of these proteins with the surrounding membrane lipids, and/or the numerous protein-protein interactions within the divisome complex may aid in the design of new and novel antibacterial means. It is with hope that the progress made in deciphering the bacterial cell division through detailed investigation of these membrane proteins could one day underpin the development of next-generation antibiotics (den Blaauwen *et al.*, 2014).

1.3 Membrane solubilisation agents and mimetics

The development of membrane solubilisation agents and mimetics have greatly facilitated the studies of membrane proteins *in vitro.* Detergents are the most common agents to solubilise membrane proteins which enable subsequent purification of target proteins for downstream analyses (Seddon *et al.*, 2004). The alternative membrane mimetics to detergents developed over the years are also discussed in the following sections.

1.3.1 Detergents

Detergents are amphipathic molecules comprising of a polar head group and a hydrophobic tail that preferentially absorbed at interfaces and spontaneously form spherical micellar structures in solution (Garavito and Ferguson-Miller, 2001; Otzen, 2011; Seddon *et al.*, 2004). Detergents are surface active agents (also known as surfactants) and they can generally be classified as ionic, zwitterionic, nonionic or bile acid salts (Seddon *et al.*, 2004). The critical micelle concentration (CMC) of a detergent is defined as the minimum concentration for individual detergent monomers to cluster and form micelles, which results in a sudden change in surface tension and other physical properties (Garavito and Ferguson-Miller, 2001). The CMC of a detergent is governed by the combined effect of the repulsive forces from the headgroup and the hydrophobic interactions of the tails, which varies with different pH, ionic strength, temperature, as well as the presence of other proteins, lipids, and/or detergent molecules

(Seddon *et al.*, 2004). Figure 1.2 is a cartoon illustration of the solubilisation of a membrane protein(s)-containing lipid membrane.

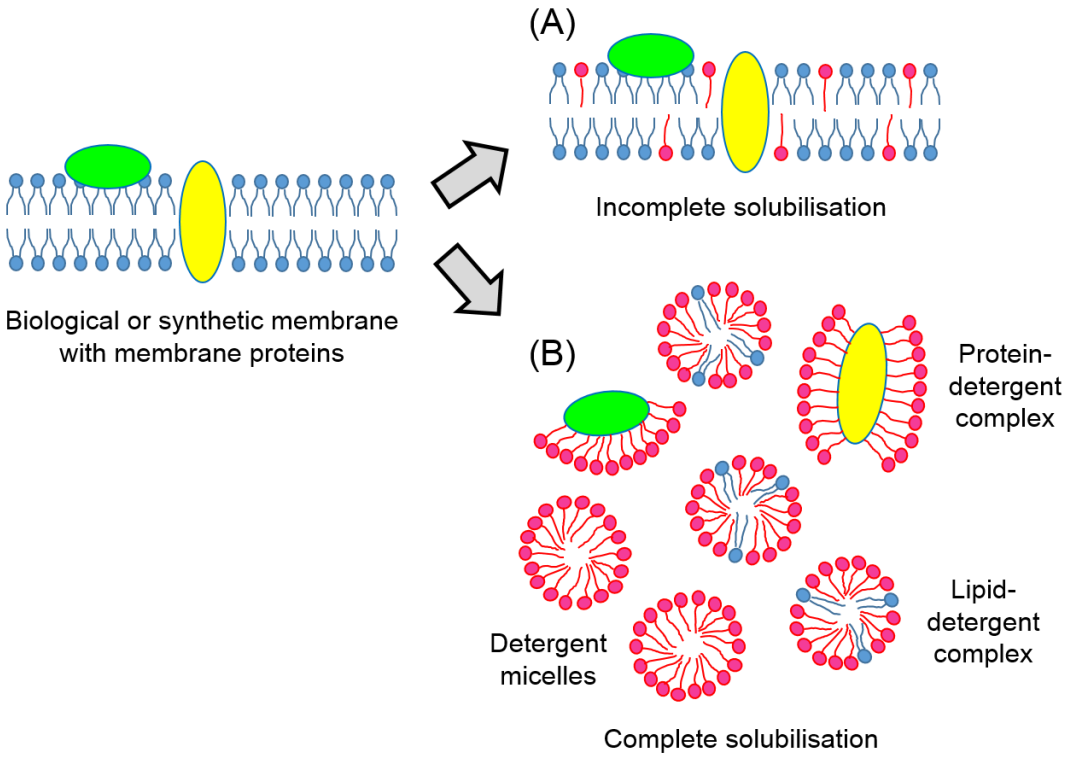

Figure 1.2 Solubilisation of biological or synthetic lipid membrane containing proteins by detergents. (A) Incomplete/partial solubilisation results only in the intercalation of detergent monomers into the lipid bilayer, normally at a low detergent concentration. (B) Complete solubilisation happens above the CMC of the detergent used, which leads to a rapid fragmentation of the lipid membrane, resulting in a heterogeneous mixture of detergent micelles, detergent-lipid, detergent-protein complex. Figure is modified from https://www.jenabioscience.com/crystallography/screening-membrane-proteins/jbscreen/detergents.

Nonionic detergents, for example *n*-Dodecyl-β-D-maltopyranoside (DDM) is commonly used for the extraction of membrane proteins (Mancia and Love, 2010). They tend to have a higher aggregation number (*i.e.* the number of detergent monomers in a micelle) and are generally considered mild and relatively non-denaturing as only lipid-lipid and/or protein-lipid interactions are disrupted instead of protein-protein interactions during the detergent solubilisation process. Nevertheless, nonionic

detergents with shorter hydrophobic chains (*e.g.* C7-C10) can lead to the deactivation of membrane proteins (Seddon *et al.*, 2004).

Although the use of detergents present a relatively convenient means to extract the membrane proteins of interest from the native membrane milieu into aqueous solution for downstream analyses, this technique of membrane solubilisation still poses a range of drawbacks that have to be seriously considered by the protein scientists. First and foremost, the detergent micelle is a poor membrane mimetic in comparison to the native biological membrane. As a matter of fact, the primary task of a membrane mimetic is to replicate the complex native membrane milieu that the protein resides in (Lee *et al.*, 2016a). However, the detergent micelles represent a highly disordered environment with very different physicochemical properties to the native membrane, such as lateral pressure and water permeability (Dörr *et al.*, 2016; Hardy *et al.*, 2016; Serebryany *et al.*, 2012). In addition, the monomer-micelle equilibrium can cause detergent monomers to rapidly exchange between the micellar and soluble pool. This phenomenon increases the dynamics of the protein environment in a negative manner that could lead to reduced stability (*i.e.* inactivation and/or aggregation) of the solubilised membrane proteins due to transient aqueous solvent exposure of the TM surfaces of the proteins (Dörr *et al.*, 2016). Detergents can also disrupt intermolecular interactions that might be essential for the structure integrity and function of the membrane proteins (Lee *et al.*, 2016a). Although some membrane proteins remain functionally active (to a certain degree) in detergent micelles, the destabilisation of extracted proteins can still happen over time (Parmar *et al.*, 2016; Seddon *et al.*, 2004).

Furthermore, there is no universal detergent for the studies of membrane proteins. Therefore, very often a time-consuming and costly empirical screening of detergents has to be implemented to identify the best detergent to extract and purify the membrane proteins of interest (Dörr *et al.*, 2016; Parmar *et al.*, 2016). The right balance has to be struck to maximise the extraction of membrane proteins from their native environment without denaturing them upon solubilisation. Subsequent to the detergent screen, laborious detergent exchange might incur as the detergent used to extract and purify a membrane protein might not be suitable for the intended functional and structural assays, adding a further level of complexity (Parmar *et al.*, 2016). Once the target membrane proteins have been solubilised in detergent micelles, the concentration of

detergents must be maintained above its CMC at all times (including downstream protein purification and characterisation) to preserve the stability of the proteins. However, the presence of free detergent micelles can interfere with some analytical studies (Serebryany *et al.*, 2012).

Last but not least, the process of extracting the membrane proteins using detergents can lead to delipidation, *i.e.* the stripping of surrounding membrane lipids from the protein during the solubilisation process. Small or loosely bound protein subunits may also disassociate along with the native membrane lipids during detergent solubilisation (Dörr *et al.*, 2016). Consequently, the loss in crucial protein-lipid and/or protein-protein interactions could compromise the stability of the proteins in detergent micelles and might even rendered some functional states inaccessible (Phillips *et al.*, 2009). The extent of delipidation would depend on the types and concentration of the detergent employed. In order to address the limitations posed by the use of detergents in the studies of membrane proteins, other membrane mimetics as an alternative to detergents (shown in Figure 1.3) have been developed in the field over the years and will be discussed in the following sections.

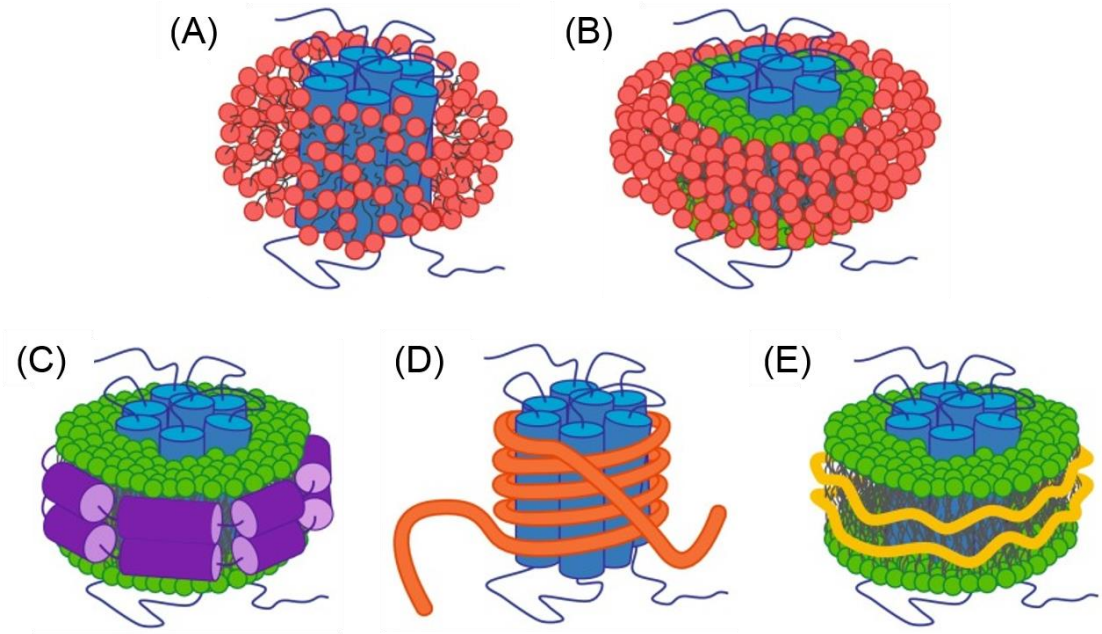

Figure 1.3 Detergents and several membrane mimetics employed in the studies of membrane proteins. (A) Detergent micelle; (B) bicelle; (C) membrane scaffold protein (MSP)-nanodisc; (D) amphipol; (E) and styrene maleic acid/lipid particle (SMALP). Figure is adapted from Dörr *et al.* (2016) with permission.

1.3.2 Liposomes

Liposome, which is a spherical vesicle that contains at least one lipid bilayer are frequently used as membrane mimetic during protein reconstitution after the target membrane proteins have been solubilised in detergents (Knol *et al.*, 1998; Rigaud and Levy, 2003). The reconstitution of membrane proteins into liposomes (resulting in proteoliposomes) represents an excellent analytical tool and the current gold standard to the elucidation of membrane protein structure and function *in vitro* (Seddon *et al.*, 2004). Compartmentalisation is allowed when membrane proteins are reconstituted in liposomes, which can facilitate the examination of vectorial transport of membrane channel and transport proteins (Dörr *et al.*, 2016; Parmar *et al.*, 2016). In addition, the lipid composition of the liposomes can be systematically varied during protein reconstitution to study the impact of lipid composition on the structure and function of the membrane proteins of interest.

Multilamellar vesicles (MLVs) with multiple concentric lipid bilayers (up to tens of μm) will form spontaneously upon the hydration of dried lipid film above the phase transition temperature of the lipid(s) (Goddard *et al.*, 2015). By adjusting the ratio and composition of lipids, the nature and size of the liposomes can be manipulated (Parmar *et al.*, 2016). Due to the heterogeneity in size, MLVs are less desirable for membrane proteins studies. MLVs can be downsized into large unilamellar vesicles (LUVs) or small unilamellar vesicles (SUVs) using various processing methods, including multiple freeze-thaw cycles, French press, sonication and extrusion (Akbarzadeh *et al.*, 2013). LUVs are normally produced in homogenous form via extrusion through pre-defined pore size polycarbonate filters of 100-400 nm, which can be stable for weeks when stored at -80°C (Goddard *et al.*, 2015; Knol *et al.*, 1998). Sonication can be utilised to yield SUVs (15-50 nm), however the high level of curvature and surface tension renders them relatively unstable and thus tend to fuse spontaneously when drop below the phase transition temperature (Goddard *et al.*, 2015). To reconstitute detergent-solubilised membrane proteins into these lipid vesicles, polystyrene absorbent beads or dialysis are typically employed for detergent removal (Goddard *et al.*, 2015; Knol *et al.*, 1998; Seddon *et al.*, 2004). The abovementioned different types of lipid vesicles, including MLV, LUV, and SUV are depicted in Figure 1.4.

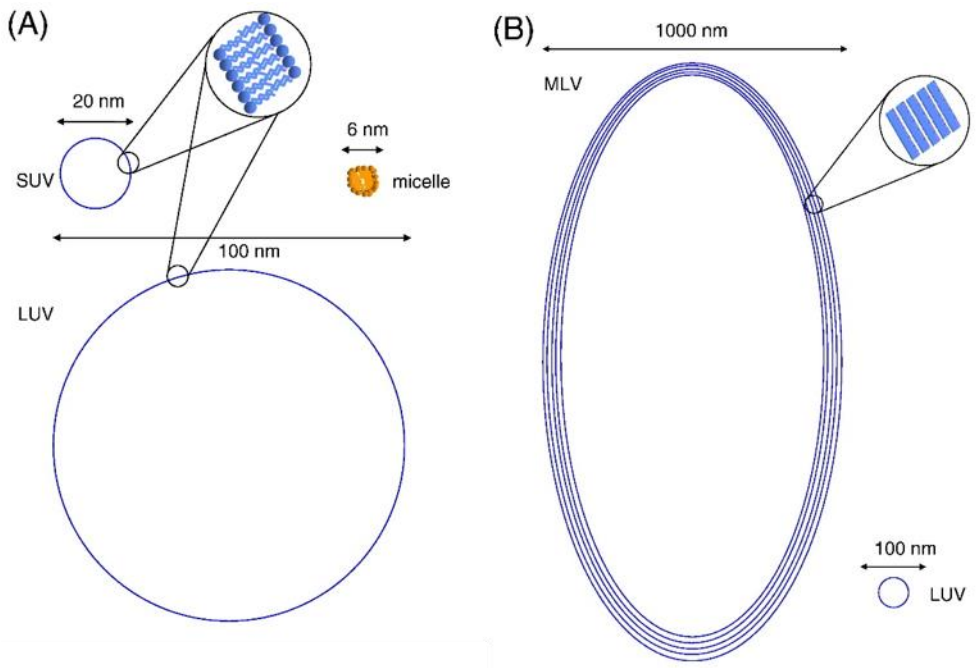

Figure 1.4 Types of lipid vesicles used for membrane protein reconstitution studies. (A) Size comparison of SUV and LUV vs a detergent micelle; (B) MLV is composed of multiple concentric bilayers. Figure is adopted from Warschawski *et al.* (2011) with permission.

It is important to note that the use of liposomes present considerable challenges and shortcomings to membrane protein studies. Firstly, the production of stable and functional proteoliposomes is technically challenging and time consuming, which can hinder high-throughput analysis of target membrane proteins. The large size and light scattering property of LUVs, which are commonly used in membrane protein reconstitution could impede spectroscopic studies (Dörr *et al.*, 2016). On the other hand, the usefulness of liposomes for the examination of vectorial transport is offset when the both sides of the target membrane proteins are to be assessed, for instance in ligand binding studies. It is also difficult to evenly distribute the membrane proteins with defined orientation within the liposomes (Seddon *et al.*, 2004).

1.3.3 Planar lipid bilayers

Planar lipid bilayers exemplify another membrane mimetic, often exploited to examine the electrophysiological properties of reconstituted membrane channel proteins, as the setup allows transport measurements to be made across the membrane in the two different solutions to give physiological membrane potentials. In general, there are two

types of planar lipid bilayers, namely black lipid membranes (BLMs) and supported lipid bilayers (SLBs) (Parmar *et al.*, 2016; Serebryany *et al.*, 2012). The term 'black lipid' refers to the fact that the lipid bilayer actually appears black in colour under reflected light, and BLMs are normally formed in an aperture created in thin layer of lipids, part of the wall that separates two different solution chambers. Detergent-solubilised membrane proteins can be spontaneously incorporated into preformed BLMs (Serebryany *et al.*, 2012). On the other hand, SLBs are typically constructed by lipid vesicle fusion or Langmuir transfer onto a suitable solid surface, such as gold (Chan and Boxer, 2007). Tethered bilayer lipid membranes is a variant to SLBs, in which the lipids are chemically anchored to the solid support via a spacer. The aim is to introduce some space between the solid support and the lipid bilayer, which is useful for the incorporation of membrane proteins with large cytoplasmic or extracellular domains (Parmar *et al.*, 2016).

BLMs have a short lifetime (less than 1 h) and thus do not support long experiments. In contrast, SLBs can offer prolonged stability, allowing longer experiments to be conducted, which improves the reproducibility of this method for membrane protein studies through multiple runs on the same SLB (Parmar *et al.*, 2016). In addition, SLBs are also relatively easy to prepare and patterned, besides being amenable to a range of surface characterisation techniques, such as secondary ion mass spectrometry (SIMS) (Chan and Boxer, 2007). Due to the immobilisation nature of planar lipid bilayers, this format of experimental setup for membrane proteins is not suitable for many solution-based analytical methods (Dörr *et al.*, 2016). For SLBs, there is a loss in lateral mobility towards the protein function once reconstituted, and the bottom side of the lipid bilayer is not accessible upon immobilisation on the solid support (Chan and Boxer, 2007; Serebryany *et al.*, 2012).

1.3.4 Bicelles

Bicelles are self-assembled, solubilised lipid bilayer discs (around the size of 8-50 nm), formed by mixing a short chain lipid (or detergent) with a long chain lipid, as depicted in Figure 1.3 (B) (Dörr *et al.*, 2016; Seddon *et al.*, 2004). The reconstituted membrane proteins are surrounded by the long chain lipid, which is stabilised at the edge of bilayer by the short chain lipid bilayer (Serebryany *et al.*, 2012). In terms of lipid choice, 1,2-Dihexanoyl-*sn*-glycero-3-phosphocholine (DHPC) is commonly employed as the short

chain lipid, while 1,2-Dimyristoyl-s*n*-glycero-3-phosphocholine (DMPC) is utilised as the long chain lipid. The zwitterionic detergent, 3-[(3-Cholamidopropyl) dimethylammonio]-1-propanesulfonate (CHAPS) can also replace DHPC to form bicelles with DMPC (Dürr *et al.*, 2012; Jamshad *et al.*, 2011). Bicelles can adopt different conformation depending on several experimental parameters, including the molar ratio of long chain to short chain lipids (known as the *q*-ratio), temperature, pH, and salt concentrations (Parmar *et al.*, 2016). Homogenous sample of bicelles are readily obtainable and due to the fact that bicelles can be aligned in magnetic field, they are the preferred tool in NMR studies (Dürr *et al.*, 2012). A number of protein structures had been solved using bicelles as the membrane mimetic (Dörr *et al.*, 2016; Seddon *et al.*, 2004). The major drawback of application of bicelles for membrane protein studies is the tight *q*-ratio, thus limiting the choice of lipid compositions for bicelle formation (Dörr *et al.*, 2016; Jamshad *et al.*, 2011).

1.3.5 Membrane scaffold protein-nanodiscs

Figure 1.3 (C) depicts the MSP-nanodiscs technology, as developed and introduced by Sligar and co-workers in 2002 (Bayburt *et al.*, 2002). This membrane mimetic consists of a bilayer of 130-160 lipid molecules, surrounded by an amphipathic helical lipoprotein belt - termed the MSP. This genetically engineered MSP was based upon the concept of the human serum apolipoprotein A-1 (Dörr *et al.*, 2016; Jamshad *et al.*, 2011; Lee *et al.*, 2016a; Parmar *et al.*, 2016). The MSP-nanodisc complex is stable and monodisperse, with a size around 10-20 nm depending on the MSP used for protein reconstitution. The empty of a MSP-nanodisc (in the absence of reconstituted membrane protein) is approximately 150 kDa and its size can be adjusted to encapsulate just a single membrane protein per MSP-nanodisc (Jamshad *et al.*, 2011). Alternatively, the length of the MSP can be tuned to encapsulate membrane proteins in defined oligomeric state to facilitated downstream structural and functional studies (Chan and Boxer, 2007). The lipid composition of the MSP-nanodiscs can be adjusted to allow the systematic analysis of lipid effect towards the reconstituted membrane proteins. Both surfaces of the reconstituted membrane proteins are also accessible for substrate interaction within the MSP-nanodiscs, which in turns facilitates ligand binding studies. (Dörr *et al.*, 2016).

Despite the many advantages presented by this technology, it is limited by the very core nature of its MSP-based encapsulation approach. Firstly, the MSPs need to be produced and purified, prior to mixing with the correct composition of detergent-solubilised target membrane proteins and lipids with subsequent detergent removal to generate the intended MSP-nanodiscs. This is inherently a multistep, lengthy and laborious process (Parmar *et al.*, 2016). Although there is no strict lipid restriction (as per bicelles), the presence of the MSP, being proteinaceous itself can interfere and complicate downstream spectroscopic studies of the target membrane proteins due to its own absorbance properties (Jamshad *et al.*, 2011).

1.3.6 Amphipols

Amphipols, as depicted in Figure 1.3 (D) are a group of short, linear, water-soluble amphipathic copolymers comprise of hydrophilic backbones with closely spaced hydrophobic side chains, first introduced by Popot and co-workers (Tribet *et al.*, 1996). Under defined conditions, the periodicity of the amphipols can promote hypercoiling (Rajesh *et al.*, 2011). When encountering detergent-solubilised membrane proteins in solution, the amphipols can coil around their hydrophobic TM regions, which shield the membrane proteins from the aqueous milieu and thus stabilising them in solution (Jamshad *et al.*, 2011; Parmar *et al.*, 2016; Rajesh *et al.*, 2011; Seddon *et al.*, 2004). The different chemical types of amphipols include the polyacrylate-based (*e.g.* A8–35), phosphorylcholine-based (*e.g.* C22–43), nonionic glucose-based, sulfonated, and the zwitterionic alkyl-poly(maleic anhydride) series (*e.g.* PMAL-C8) (Zoonens and Popot, 2014). Due to the relatively low exchange rate of membrane protein-bound amphipols and free amphipols in solution (if compared to detergents), it confers a high stability to this membrane mimetic system for membrane protein studies. In addition, the working concentration of amphipols is also lower than the requirement for detergents (Dörr *et al.*, 2016).

1.3.7 Styrene maleic acid copolymer

It is important to note that all of the aforementioned membrane mimetics are mainly for membrane protein reconstitution upon detergent extraction rather than acting as the actual extraction agent. Therefore, they are all susceptible to the drawbacks of detergent employment. A recently developed membrane mimetic technology employs the amphipathic styrene maleic acid (SMA) copolymer as the membrane solubilisation and

subsequent protein encapsulation agent, as depicted in Figure 1.3 (E). The SMA copolymer was discovered to spontaneously encapsulate portions of the lipid membrane (both biological and synthetic) into stable, disc shaped, water-soluble, nanosized particles (10-24 nm) containing both membrane lipids and protein(s) surrounded by the polymer annulus in a pH-dependent manner (Dörr *et al.*, 2016; Lee *et al.*, 2016a). The membrane solubilisation and encapsulation property of the SMA copolymer was first described by Dafforn and co-workers using a low molecular weight SMA copolymer of 2:1 styrene-to-maleic acid (S:MA) ratio. They aptly named these polymer-stabilised lipid particles as styrene maleic acid/lipid particles (SMALPs) (Knowles *et al.*, 2009). Subsequently, Orwick *et al.* (2012) reported similar observation to generate 'lipodisq' particles using a 3:1 SMA copolymer. This technique was also coined 'native nanodisc' by the Killian group to differentiate the SMA-bounded nanodiscs from the MSP-nanodiscs technology, especially when the target membrane protein(s) are encapsulated within the polymer disc with the surrounding lipid moieties (Dörr *et al.*, 2014). For the rest of the thesis, the term 'SMALP' would be used exclusively to describe such nanoparticles of membrane proteins and lipids encapsulated by the SMA copolymer.

The raw material for this technology, *i.e.* the styrene maleic anhydride (SMAnh) copolymer (of various molecular weight and S:MA ratio) is commercially available in large quantities from major chemical suppliers such as TOTAL Cray Valley (USA) and Polyscope (The Netherlands). The starting SMAnh copolymer would have to be hydrolysed to the acid form prior to any intended biological applications (Lee *et al.*, 2016b). The hydrolysed form of the SMA copolymer is also available in small quantities from Sigma-Aldrich (USA). Before its discovery as a novel tool for membrane proteins studies, the SMA copolymer was originally described as conjugate for drugs in cancer therapy and later for drug delivery (Dörr *et al.*, 2016). The SMA copolymer has been demonstrated to extract and solubilise membrane proteins from both synthetic proteoliposomes and native membranes of bacterial, yeast, insect, and mammalian origin (Dörr *et al.*, 2016; Lee *et al.*, 2016a). To this point, the 2:1 SMA was reported to be the most efficient membrane solubiliser across a wide pH range (Morrison *et al.*, 2016; Scheidelaar *et al.*, 2016). The SMALP technology has been gaining popularity and acceptance in the field of membrane proteins studies. In fact, an exponential increase in publications is seen since 2012 (as shown in Figure 1.5) of

successful applications of this emerging membrane mimetic for the studies of membrane protein studies (Lee and Pollock, 2016).

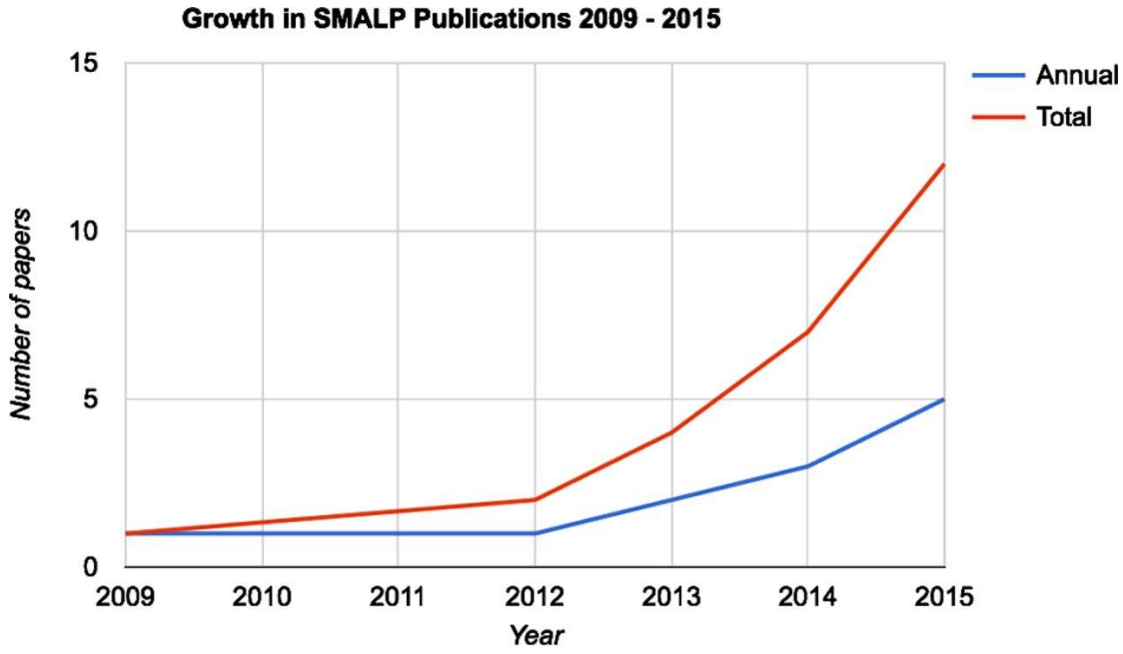

Figure 1.5 Growth in publications describing the use of the SMALP technology for membrane protein studies over a six-year period (2009-2015). Figure is adopted from Lee and Pollock (2016) with permission.

One of the distinct advantage of the SMALP technology when compared to the other membrane mimetics is the co-extraction of surrounding lipid moieties together with the proteins during the extraction and solubilisation process. In other words, the membrane proteins of interest once extracted can still be interrogated in a physiologically relevant native membrane bound state. This is in stark contrast to the other membrane mimetics such as bicelles or MSP-nanodiscs, whereby a selection of lipids are specifically added during the reconstitution process. Due to the fact that it is very difficult (if not impossible) to exactly reconstitute the extracted target membrane proteins back into its native membrane environment, it would be much more pragmatic to have a tool to literally excise the membrane proteins out of their native membrane milieu together with the surrounding lipids in order to facilitate optimal downstream analytical studies (Lee *et al.*, 2016a). Thus, the 'molecular cookie cutter' analogy was given to this SMALP technology to portray this membrane excising mechanism (Parmar *et al.*, 2016). Although some membrane lipids are still retained upon mild detergent extraction for certain membrane proteins, it often results in the selective co-purification of the

annular lipids that are tightly bound to the protein. On the other hand, part of the surrounding membrane environment of the target membrane protein is co-extracted during the SMALP encapsulation process, which reflects a more realistic snapshot of the native environment for the protein (Dörr *et al.*, 2016).

Protein samples had been purified to homogeneity even with a single affinity purification step using the SMALP technology. In contrast to detergents, no additional SMA copolymer is to be supplemented after the protein extraction process, which present a huge cost-saving advantage (Hardy *et al.*, 2016). In addition, the relatively small size of SMALPs (10-24 nm) makes them amenable to range of spectroscopic techniques, including dynamic light scattering, circular dichroism (CD), nuclear magnetic resonance (NMR), electron paramagnetic resonance (EPR), and analytical ultracentrifugation (Dörr *et al.*, 2016; Jamshad *et al.*, 2011; Lee *et al.*, 2016a). It has been reported that the size of SMALPs can be tuned by varying the SMA copolymer to lipid ratios (Vargas *et al.*, 2015; Zhang *et al.*, 2015). The size of SMALPs can also be adjusted via the controlled synthesis of the SMA copolymer by exploiting the reversible addition-fragmentation chain transfer (RAFT) polymerisation method for different S:MA ratio (Craig *et al.*, 2016).

The SMA copolymer has been reported to extract a variety of membrane proteins, ranging from peripheral to integral membrane proteins (both β-barrel and α-helical proteins). For α-helical proteins, SMALPs were demonstrated to accommodate zero up to 36 TM helices (Dörr *et al.*, 2016; Lee *et al.*, 2016a). Furthermore, native protein complexes have also been encapsulated with the SMALP technology (Paulin *et al.*, 2014; Prabudiansyah *et al.*, 2015). Similar to the MSP-nanodisc technology, both sides of the protein in SMALPs are amenable to ligand binding studies (Dörr *et al.*, 2016; Lee *et al.*, 2016a). While the MSP can be genetically modified to introduce label or affinity tags, the SMA copolymer can be covalently modified by grafting the polymer with cysteamine to create solvent-exposed sulfhydryl groups to allow further modification and functionalisation via thiol-reactive chemistry (Lindhoud *et al.*, 2016). Membrane proteins in SMALPs have been reported to display enhanced storage and thermostability, *i.e.* resilient to multiple freeze-thaw cycles and desiccation by lyophilisation, in comparison to the detergent solubilised membrane proteins (Jamshad *et al.*, 2015a, 2011).

1.3.7.1 Interaction of the SMA copolymer with lipid bilayer

The interactions of the SMA copolymer with pure lipid bilayer (in the absence of membrane protein) have been systematically analysed using a range of biophysical techniques (Jamshad *et al.*, 2015b; Orwick *et al.*, 2012). Utilising small angle X-ray and neutron scattering (SAXS and SANS), the disc-shaped SMALPs were showed to harbour a circular cross-section, with the height of each SMALP disc matching the dimension of an intact lipid bilayer. Some degree of penetration (or intercalation) of the phenyl group from the SMA copolymer into the fatty acyl region of the lipid bilayer was suggested by SANS, SAXS and attenuated total reflectance-Fourier transform infrared (ATR-FTIR) spectroscopic studies, with the phenyl groups being parallel to the long axis of the lipid acyl chains (Jamshad *et al.*, 2015b). EPR studies also showed that carbon atoms at certain positions in the lipid acyl chains were restricted in motion, which is consistent with the notion of phenyl group insertion (Orwick *et al.*, 2012).

Differential scanning calorimetry studies provided information on phase transition behaviour of the lipid bilayer encapsulated within the SMALP discs. There was a much broader change in phase transition, which indicated a lower level of cooperativity for SMALPs in contrast to a sharp change in phase transition for the unencapsulated lipid bilayers. The 2:1 SMA copolymer displayed a smaller perturbation (*i.e.* reduction in the phase transition temperature) than the 3:1 SMA copolymer. In contrast, an increase in phase transition temperature (which prevents the melting of lipid bilayer) was observed for the MSP-nanodisc system. This is likely the result of an increase in lateral pressure to the encapsulated lipids within the MSP-nanodiscs (Jamshad *et al.*, 2015b; Lee *et al.*, 2016a; Orwick *et al.*, 2012).

A three-step molecular model describing the membrane solubilisation action of the SMA copolymer was proposed by Scheidelaar *et al.* (2015). Firstly, the SMA copolymer binds to the surface of a lipid bilayer as a function of polymer concentration. This initial polymer binding is modulated by electrostatic interactions. For instance, the presence of anionic lipids would lead to charge repulsion, thus preventing the binding of the negatively charged SMA copolymer to the lipid bilayer. Subsequently, the SMA copolymer would insert into the hydrophobic core of the lipid bilayer and this insertion depends strongly on lipid packing factors such as membrane fluidity and lateral pressure. In essence, a tight lipid packing and thick membrane would prevent the

penetration of the SMA copolymer into the lipid bilayer. Lastly, due to the large enthalpic penalty incurred for the insertion of the SMA copolymer into the hydrophobic core of the lipid bilayer, solubilisation takes place in terms of the thermodynamically favourable formation of SMALPs (Scheidelaar *et al.*, 2015).

1.3.7.2 Application of SMALP for structural biology

Unlike the MSP, the SMA copolymer does not display much electron density. As a result, the polymer annulus does not dominate the electron microscopy (EM) images and EM has been widely utilised to characterise the size of SMALPs (Dörr *et al.*, 2016; Hardy *et al.*, 2016). To date, structural studies of membrane proteins in SMALP using EM have been successful with negative stain and cryo-EM approaches (Gulati *et al.*, 2014; Postis *et al.*, 2015). The SMALP technology has also facilitated structural determination of other membrane proteins through X-ray crystallography and solid state NMR. Broecker *et al.* (2017) reported the successful transfer of a bacteriorhodopsin (encapsulated in 3:1 SMA copolymer) to a monoolein lipidic cubic phase (LCP) that crystallised *in meso* and produced crystals that diffracted to a 2 Å resolution structure, which was comparable to the conventional detergent approach. In addition, the structure of another bacterial protein (encapsulated in both 2:1 and 3:1 SMA copolymers) was solved using solid state NMR (Bersch *et al.*, 2017). These recent discoveries highlighted the enormous potential for the SMALP technology in structural biology studies. The fact that most X-ray crystal structure of membrane proteins in the Protein Data Bank (PDB) originated from detergent-solubilised membrane protein preparations (which could have suffered from delipidation), it is impetus to derive structural information from native membrane-like environment by capitalising on the SMALP technology (Yeagle, 2014).

1.3.7.3 Limitations of the SMALP technology

Despite the many advantages offered by the SMALP technology, it is critical to note that this is not a magic technique or panacea to resolve all the issues posed by the conventional approaches utilising detergents. The presence of the polymer annulus for membrane protein stabilisation means that SMALPs can pose a constraint to the diffusion of certain encapsulated protein within the nanodisc in ways similar to the MSP-nanodisc system, thus hindering the examination of transmembrane movements in certain functional studies (Serebryany *et al.*, 2012). Due to the polymeric nature of

the SMA copolymer (analogous to amphipols), it is difficult to obtain monodisperse polymer samples and the impact of polydispersity towards membrane solubilisation has not been systematically reported. The advent of controlled polymer synthesis methods, such as RAFT should be explored to generate monodisperse SMA copolymer to aid in future mechanism studies of SMALP, while bearing in mind the feasibility of scaling up the polymer production. Last but not least, the chemical nature of the SMA copolymers makes them sensitive to acidic pH and divalent metal cations, which can lead to polymer and protein aggregation (Jamshad *et al.*, 2011; Lee and Pollock, 2016).

1.4 The local lipid environment of membrane proteins

The lipid moieties within the cell membrane that the membrane proteins resides in are not just passive and inert bystander, but decades of research have demonstrated that some of them actually influence the function and/or localisation of the proteins within this membrane landscape (Barák and Muchová, 2013; Phillips *et al.*, 2009). Therefore, it is imperative for the studies of membrane proteins to take these membrane lipid components into serious consideration.

1.4.1 Chemical diversity and biosynthesis of membrane phospholipids

The prokaryotic and eukaryotic cell membranes are composed of chemically diverse groups of lipid molecules, varying in size and structure, with different polar headgroups and fatty acyl chain combinations. The cell membranes of *E. coli* are generally composed of 70% phosphatidylethanolamine (PE), and 20-25% phosphatidylglycerol (PG) and 5-10% cardiolipin (CL) (Mileykovskaya and Dowhan, 2005). PE is zwitterionic in nature, while PG and CL are both anionic lipids (Barák and Muchová, 2013). The biosynthetic pathways for the membrane phospholipids in *E. coli* is shown in Figure 1.6. Phosphatidic acid (PA) is the precursor for the different membrane phospholipids found in *E. coli*. PE is synthesised from the decarboxylation from a phosphatidylserine (PS) precusor, while PG is synthesised upon the dephosphorylation of a phosphatidylglycerol phosphate (PGP) pecursor. CL is made from the condensation of two PG molecules or through a PE precursor (Parsons and Rock, 2013).

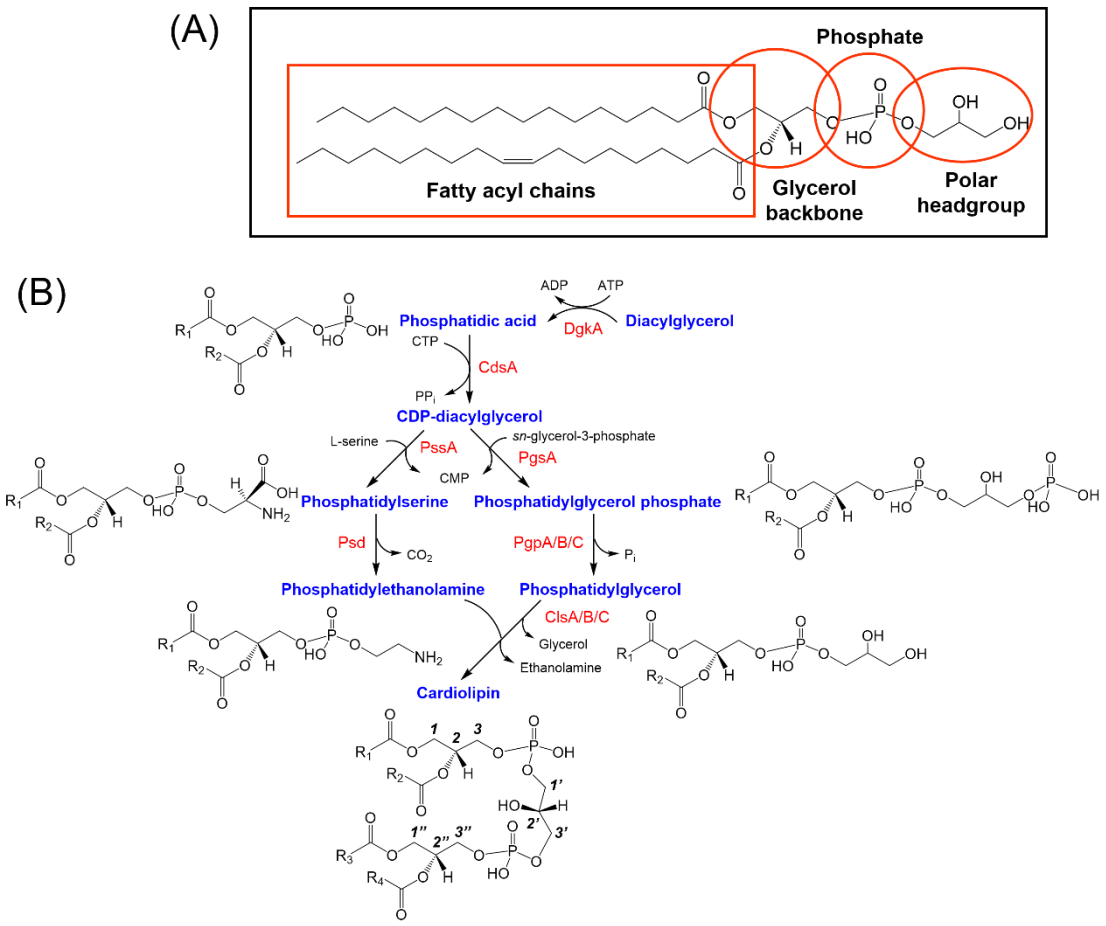

Figure 1.6 Biosynthesis of membrane phospholipids in *E. coli*. (A) General chemical structure of a phospholipid. (B) Representative structrures of PA, PS, PE, CL, PG and PGP are presented in the biosynthetic pathways of membrane phospholipids in *E. coli* (Parsons and Rock, 2013). The number of glycerol carbons for CL is specified in stereospecific numbering convention with $R_{1\text{-}4}$ representing the fatty acyl chains (Garrett *et al.*, 2007).

The complex mixture of lipids within the cell membrane has endowed it with a set of unique physicochemcial properties. The polar headgroups can harbour different polarities and charges under physiological pH, while the geometry of unsaturated double bonds can vary within the fatty acyl chains. Consequently, different lipid headgroups can affect the interface properties of the lipid bilayer, while different fatty acyl chain compositions can influence the thickness of the lipid bilayer (Dowhan *et al.*, 2004). The different chemical structures of fatty acyl moities present in membrane phospholipids is depicted in Figure 1.7. The odd numbered fatty acyl chains found in some bacteria can be either be in the form of cyclopropane rings or branched chains

(Zhang and Rock, 2008). The cyclopropane fatty acids are synthesised by the addition of a methylene group from *S*-Adenosyl-L-methionine to the *cis* double bond of an unsaturated fatty acyl chain (Grogan and Cronan, 1997), while the iso- and anteiso-branched chain fatty acids are synthesised using leucine and isoleucine as substrates (Kaneda, 1991). The presence of saturated fatty acids can reduce the membrane fluidity, while the presence of *cis*-unsturated fatty acids increases the membrane fluidity through the formation of a kink in the fatty acyl chain due to the *cis*-double bond. Membrane fluidity is also reduced in the presence of iso-branched fatty acids in comparison to anteiso- counterparts (Zhang and Rock, 2008). *Trans*-unsaturated fatty acids display similar properties to the saturated fatty acids, resulting in cell membranes with a higher phase transition temperature, and provide resistance to solvents and growth temperature surge (Zhang and Rock, 2008). The cyclopropane fatty acids which normally observe to increase during stationary growth phase also display similar properties as the saturated fatty acids, which render the cell membrane less susceptible to environment insults (Grogan and Cronan, 1997).

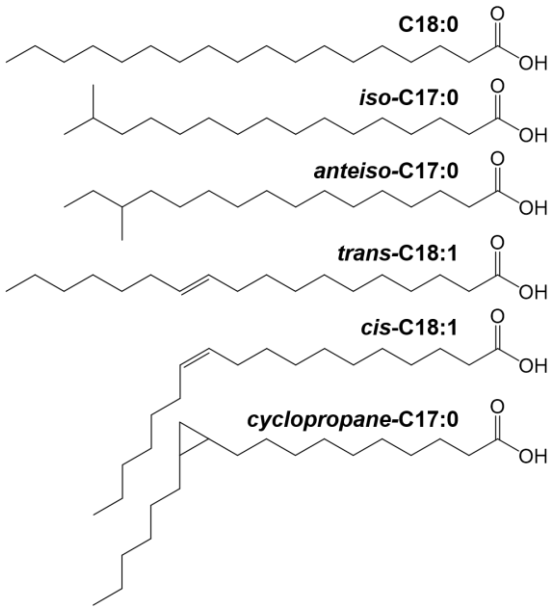

Figure 1.7 Chemical structures of different fatty acyl moities present in membrane phospholipids (Zhang and Rock, 2008).

Due to the central and bioenergetics role governed by membrane lipids, robust mechanism takes place to maintain lipid homeostasis to ensure appropriate membrane fluidity for the optimal function of membrane proteins (Zhang and Rock, 2008). It was

reported that an *E. coli* K-12 strain modified its membrane phospholipid composition, including the elongation, cyclopropanation of fatty acids and an increase in CL formation as an reaction to starvation (Wehrli *et al.*, 2016). In addition, lipid remodelling was also found to be a critical conserved response towards environmental adaptation for phylogenetically diverse marine bacteria under phosphorus-deficient condition (Sebastián *et al.*, 2016).

1.4.2 Membrane heterogeneity and lipid microdomains

Since the proposal of the fluid mosaic model by Singer and Nicolson (1972) as illustrated in Figure 1.8 (A) for the generalised conceptualisation of the cell membrane architecture, the cell membrane is now regarded to be more mosaic than fluid, being made up by heterogeneous, segregated patches of lipids and proteins as supported by experimental observations. The cell membrane architecture in the revised model, as portrays in Figure 1.8 (B) consists of lipid regions vary in thickness and composition in a crowded milieu (Engelman, 2005). It can thus be envisaged that the lateral heterogeneity of the cell membrane could produce specific domains for membrane proteins to locate and function. Indeed, there have been numerous reports of preferential interaction of integral membrane proteins with certain lipid polar headgroups (Contreras *et al.*, 2011; Dowhan *et al.*, 2004; Lee, 2004). In addition, some peripheral membrane proteins that associate weakly with the membrane lipids were reported to aid the formation of specific membrane domains and if the proteins themselves interact with other protein partners, they could assist in the co-localisation of these protein partners to the domain (Matsumoto *et al.*, 2015).

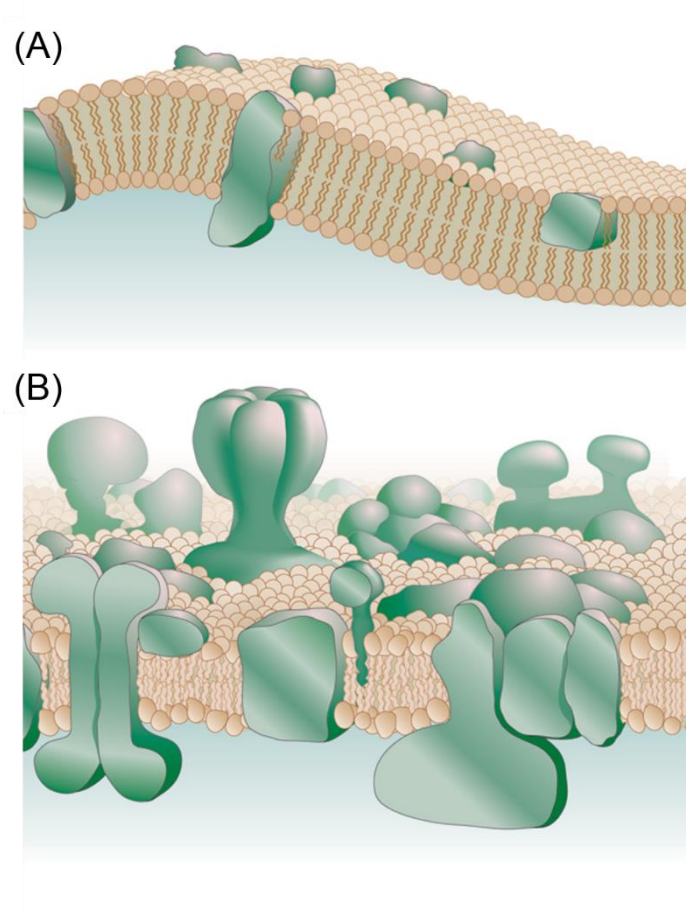

Figure 1.8 The cell membrane architecture models. (A) Singer and Nicholson fluid mosaic model; (B) revised model showing a patchy membrane with a higher protein content and variable lipid thickness and compositions. Figure is adopted from Engelman (2005) with permission.

In the context of bacterial cell division, microdomains enriched in anionic phospholipids (including PG and CL) have been reported at the cell poles and division septum (Barák and Muchová, 2013; Mileykovskaya and Dowhan, 2005). These anionic lipids appear to bind the MinD and MinE proteins, which is part of the Min system that spatially regulates the Z-ring positioning to prevent aberrant localisation of the cell division machinery at the cell poles (Renner and Weibel, 2012). PG and CL were also found to interact with the bacterial actin homolog - MreB that regulates the formation and maintenance of rod-shape cell morphology and these lipids prevented the localisation of MreB to the cell poles (Kawazura *et al.*, 2017). *E. coli* MraY, an integral membrane protein that catalyses the formation of the lipid-linked peptidoglycan precursor - Lipid I was reported to be active *in vitro* only when PG lipids were supplemented in preformed MSP-nanodiscs prepared through the cell-free expression

platform. PG was thus postulated to stabilise the proper folding and activity of MraY *in vitro* (Henrich *et al.*, 2015). The membrane-associated MurG, which transfers a sugar moiety onto Lipid I to generate Lipid II was observed to localise to CL-rich microdomains in the Gram-positive *Bacillus subtilis*. Furthermore, MurG requires CL to localise to the forespore during the sporulation process (Gifford and Meyer, 2015). These observations thus strongly imply that for important physiological processes to occur, there exist a distinct and unique composition of lipids and possibly transient and dynamic protein-lipid interactions within the membrane microdomains.

It is technically challenging for the *in vivo* examination of these small membrane microdomains. Although the trans-bilayer movement of lipids are relatively slow without perturbations, the lateral movements of lipid molecules within a leaflet are rapid, and thus can result in the formation and disappearance of microdomains over millisecond timescale to warrant measurements by spectroscopic techniques (Janmey and Kinnunen, 2006). CL-rich microdomains have been detected at the cell poles and septum of *E. coli* and *B. subtilis* using a fluorescent dye, 10-*N*-nonyl acridine orange (NAO) that was reported to specifically bind to CL *in vivo*, producing a unique intense Stokes shift fluorescence signal (Mileykovskaya and Dowhan, 2009). However, recent investigation into the photophysical properties of this fluorescent dye has questioned the specificity of NAO for CL, showing evidence that NAO was actually rather less specific in lipid binding, showing no preference in the binding of PG and CL, but there was a higher affinity for these lipids than the other anionic lipids such as PA and PS (Oliver *et al.*, 2014). Another studies using fluorescently-labelled phospholipids containing eicosapentaenoic acid (*cis*-C20:5) revealed that phospholipids containing the eicosapentaenyl group are enriched in a specific microdomains at the division site of the Gram-negative psychrotrophic bacterium - *Shewanella livingstonensis.* The specific accumulation of phospholipids containing the *cis*-20:5 fatty acid was postulated to allow for a larger diversity of energetically accessible conformational states than the saturated fatty acids counterpart for the solvation of membrane proteins with rough surfaces with little energetic penalty (Sato *et al.*, 2012).

1.4.3 Membrane biophysics

While investigating the specific mechanism of the localisation of membrane proteins to certain lipid microdomains, it is worth considering the biophysical properties of the

lipids within the cell membrane to regulate and modulate such protein-lipid interactions. Although the majority of the membrane lipids may reside in the bulk lipid phase and do not directly interact with the membane proteins, they still influence the biophysical properties of the cell membrane. The emergent properties imparted from these membrane lipids including lateral pressure profile, hydrophobic thickness, and curvature stress could be used to control membrane protein function and localisation (Jensen and Mouritsen, 2004).

1.4.3.1 Lateral pressure

Lateral pressure describes the compresive force or pressure exerted by the lipids on the proteins residing within the cell membrane (Janmey and Kinnunen, 2006). It has a directionality perpendicular to the membrane normal, and can be modulated by the degree of order of the surrounding lipids, as well as the degree of hydrophobic mismatch within the cell membrane (Contreras *et al.*, 2011). The lipid bilayer might be stable as an entirety, but there are parts within the bilayer that can be highly stressed. Interfacial tension is created through the hydrophobic-hydrophilic interface that exerts a force to pull the solvated macromolecules within the lipid bilayer together. Within the lipid bilayer, the contacts of the lipid acyl chains with the aqueous environment is minimised by the hydrophobic effect. This is further balanced by the steric repulsion between the polar headgroups and entropic repulsion between the lipid acyl chains in the monolayer leaftlet (Janmey and Kinnunen, 2006). Consequentially, proteins embedded within the lipid membrane tends to be compressed by the lateral pressure and this biophysical property has been shown to be crucial in maintaining the native fold and activity of membrane proteins (Janmey and Kinnunen, 2006; Wheatley *et al.*, 2016).

1.4.3.2 Hydrophobic thickness and mismatch

Hydrophobic mismatch (as depicted in Figure 1.9) occurs when there is difference between the thickness of the hydrophobic core of the lipid bilayer and the hydrophobic region of the TM proteins residing within it (Phillips *et al.*, 2009). During hydrophobic mismatch, the lipid bilayer might distort to cover the hydrophobic surface of the TM proteins. Such local distortion of membrane lipids can occur in microdomains of high protein-to-lipid ratios, resulting in membrane curvature if the distortion is asymmetrical across the lipid bilayer (Engelman, 2005). Alternatively, the membrane lipids might

force the embedded proteins to alter their conformations (by tilting or bending its TM segments) in order to bury their hydrophobic surfaces within the limited thickness of the hydrophobic core of the lipid bilayer. This can impact the function and stability of the membrane proteins considerably (Contreras *et al.*, 2011; Janmey and Kinnunen, 2006; Yeagle, 2014). Essentially, an integral TM protein would be solvated optimally in a lipid bilayer with matching hydrophobic thickness as dictated by the lipid composition.

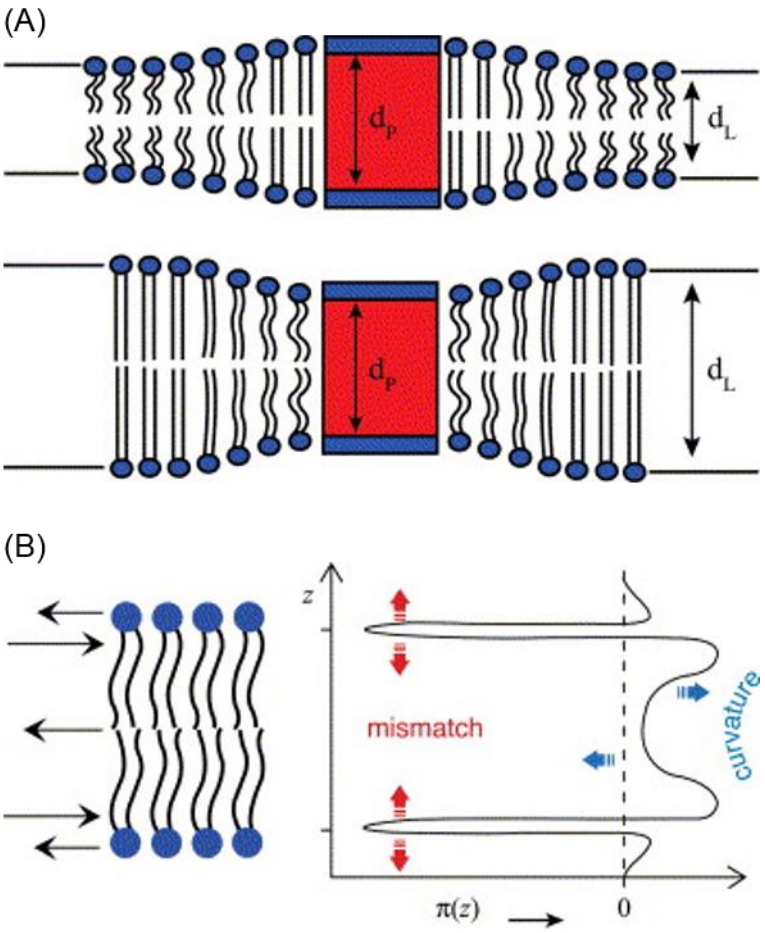

Figure 1.9 Hydrophobic mismatch of an integral membrane protein residing in lipid bilayers of different hydrophobic thickness. (A) Lipid distortion occurs when the hydrophobic thickness (d_P) of the TM protein is larger or smaller than the thickness (d_L) of the lipid bilayer. (B) The forces operating within a lipid bilayer with corresponding lateral pressure profile, $\pi(z)$ at different distance (z) across the bilayer thickness is shown, illustrating the effects of hydrophobic mismatch and curvature stress. Figure is adopted from Jensen and Mouritsen (2004), Perozo *et al.* (2002) and Dumas *et al.* (1999) with permission.

1.4.3.3 Membrane curvature

The default shape of a lipid membrane is not flat and depends on the shapes of the constituent lipid molecules. The shape-structure concept of lipid polymorphism is shown in Figure 1.10. Generally, molecules with an overall inverted conical shape, such as detergents and lysophopholipids will form tubular (H_I) phase or spherical micellar structures with a positive membrane curvature. Cylindrical molecules, for instance phosphatidylcholine (PC), PG, and PI will preferentially form a flat lamellar phase or bilayer structure with zero membrane curvature. In contrast, molecules with an overall conical shape, including PE, PS, PA, CL and diacylglycerol have the tendency to form inverted hexagonal (H_{II}) or cubic bicontinuous phase, with a negative membrane curvature (Janmey and Kinnunen, 2006; Jouhet, 2013). A positive membrane curvature produces a dome-like convex surface that curves inwards towards the cytoplasm, while a negative membrane curvature has a concave surface that curve outwards from the cytoplasm (McMahon and Gallop, 2005).

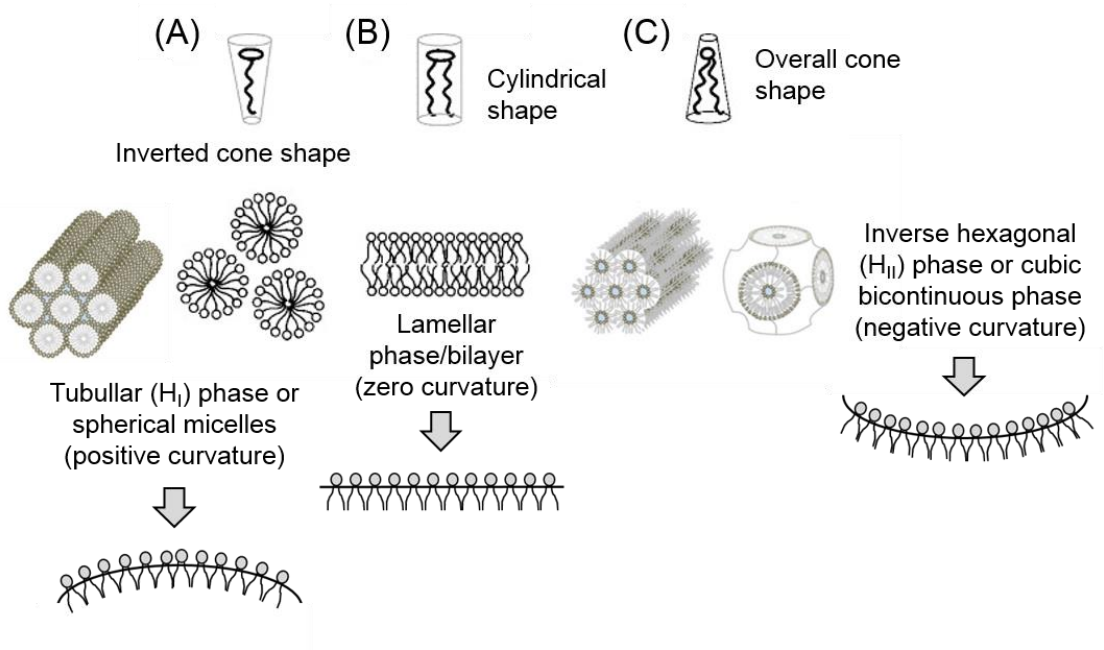

Figure 1.10 The shape-structure concept of lipid polymorphism. (A) Inverted cone shaped molecules will form tubular (H_I) phase or spherical micellar structures with a positive membrane curvature. (B) Cylindrical shaped molecules will form a lamellar phase or bilayer structure with zero membrane curvature. (C) Overall cone shaped molecules will form inverse hexagonal (H_{II}) or cubic bicontinuous phase with a

negative membrane curvature. Figure is adapted and modified from van den Brink-van der Laan *et al.* (2004) and Jouhet (2013) with permission.

It is crucial for the bacterial cells to maintain a balance between bilayer and non-bilayer forming lipids by adjusting the lipid compositions, *i.e.* headgroups and fatty acyl chain distribution during their life cycle. The phase transition temperature of a lipid membrane can be modified through the synthesis of different lipid combinations, in order to maintain the lamellar liquid crystalline phase and avoid the formation of lamellar gel phase or reverse non-lamellar phase unless deemed necessary (Jouhet, 2013; Rilfors and Lindblom, 2002). It has been postulated that the localisation of specific proteins to the cell poles and division septum in bacteria could arise from the negative membrane curvature in which the lipid microdomains are established (Barák and Muchová, 2013; Furse *et al.*, 2015b; Mileykovskaya and Dowhan, 2005). In particular, the concept of curvature-mediated microphase separation of CL in bacterial cell membranes was suggested. The unique chemical structure of CL, being a dimeric lipid with a small headgroup in relation to its four fatty acyl chains, induces in a large intrinsic negative curvature (Lin and Weibel, 2016). As a result, CL clusters with high intrinsic curvature would incur a lower energy penalty when they are positioned at curved membrane regions, such as the cell poles or septum. This provides a plausible explanation to the basis of CL microdomains in the cell membrane (Schlame, 2008). The different headgroups of membrane lipids can also act as the attachment sites for peripheral membrane proteins, which in turn facilitate in the recruitment of proteins necessary to generate the desired membrane curvature. Upon attaching to the lipid membrane via the headgroups, the peripheral proteins can interact with the membrane on a larger surface through hydrophobic interaction (McMahon and Gallop, 2005).

1.4.4 Using SMALP to examine protein-lipid interaction

The activities of many membrane proteins are regulated by direct protein-lipid interactions with specific lipids acting as allosteric regulators. Alternatively, the membrane lipids can exert an influence on the proteins through altering the physical state of the membrane (Janmey and Kinnunen, 2006). With the development of the various membrane mimetic systems, especially the SMALP technology, it is timely to study the membrane proteins not as isolated entities in mixed detergent micelles, but to examine the proteins in its native lipid environment. The survey of the local lipid

membrane landscape (in terms of lipid composition and resulting physicochemical properties) that the proteins reside via state-of-the-art lipidomic studies is a particularly exciting area of research for the analysis of protein-lipid interactions.

Due to the delipidation effect of conventional detergent extraction approaches, very often only the tightly bound annular lipids are left with the solubilised membrane proteins. Annular lipid or lipid shell is defined as the lipid species that preferentially bind to the surfaces of membrane proteins, with a longer residence time as compared to the bulk lipids, which diffuse rapidly within the bilayer plane (*i.e.* fast exchange with neighbouring lipids) and thus exhibit a low degree of interaction with the membrane proteins (Contreras *et al.*, 2011). On the other hand, nonannular lipids or co-factor lipids are found residing within membrane protein complexes to serve diffferent roles, such as structural building blocks or allosteric effectors (Contreras *et al.*, 2011). The SMALP technology allows the wider interogation of the surrounding bulk lipids that are co-extracted with the target membrane proteins besides the annular or co-factor lipid species that have resisted detergent sequestration.

1.5 Lipidomics

Lipidomics is the emerging 'omics' discipline studying the full lipid complement of cells, tissues and organisms (Shevchenko and Simons, 2010). It is a rapidly expanding research field whereby multiple analytical techniques are employed to characterise and quantify hundreds of chemically distinct lipid species, with the ultimate goal to decipher the molecular mechanisms, networks and pathways through which these hydrophobic biomolecules facilitate in cells (Han and Gross, 2003; Vaz *et al.*, 2014). A host of techniques used in lipidomic studies are discussed in the following sections.

1.5.1 Lipid extraction

Prior to any lipidomic analysis, the target lipid analytes have to be extracted from the biological samples. The combination of chloroform ($CHCl_3$) and methanol (MeOH) remains one of the most common solvents of choice for lipid extraction (Cajka and Fiehn, 2014; Furse *et al.*, 2015a; Milne *et al.*, 2006; Vaz *et al.*, 2014), derived from two methods published in the late 1950s (Bligh and Dyer, 1959; Folch *et al.*, 1957). There can be strong interactions between the lipids and various biopolymers (*e.g.* proteins and polysaccharides) in a sample that might hinder the complete extraction of lipids (Pati

et al., 2016). It is thus critical to ensure the complete removal of non-lipid contents to maximise lipid extraction. The extracted lipids should be resuspended in appropriate solvent choice that is compatible to downstream analysis such as liquid chromatography (LC) separation (Cajka and Fiehn, 2014).

For polar lipids with both hydrophilic and hydrophobic groups, solvents including MeOH and $CHCl_3$ are commonly employed for extraction. MeOH does not typically serves as a lipid extraction agent because of its miscibility with water. Nonetheless, given its high polarity and dielectric constant, it is capable of accessing regions of ion-dipole interactions and hydrogen bonds, so as to disrupt the association between the lipids and the non-lipid components to aid extraction (Pati *et al.*, 2016; Reis *et al.*, 2013). On the other hand, alkane solvents are more suitable to extract non-polar lipids lacking the hydrophilic groups, such as triacylglycerols and sterols (Pati *et al.*, 2016). Adding an acidification step can sometimes be effective to increase the extraction efficiency as negatively charged molecules (*e.g.* anionic lipids or other biopolymers) are converted into their non-ionised forms under acidic condition, which interrupts with their ionic interactions with other biomolecules to support lipid extraction (Myers *et al.*, 2011; Pati *et al.*, 2016). However, care must be taken during the acidification step to prevent the hydrolysis of lipid ester bonds that are acid-labile under prolonged exposure.

In some studies, dichloromethane (which is less toxic than $CHCl_3$ to human) was chosen to substitute $CHCl_3$, while MeOH was replaced with ethanol instead for similar occupational health and safety reason (Cajka and Fiehn, 2014; Fang and Barcelona, 1998; Gidden *et al.*, 2009). A recent alternative to the $CHCl_3$/MeOH-based liquid-liquid extraction combination was based on the methyl *tert*-butyl ether (MTBE)/MeOH combination. The benefit of this approach is the low density of MTBE which results in the lipid containing phase to be in the upper layer, facilitating the centrifugation of the samples to remove the unwanted denatured materials (Matyash *et al.*, 2008). Furthermore, MTBE is non-toxic and non-carcinogenic to human in comparison to $CHCl_3$.

1.5.2 Phosphate quantification

Phosphate quantification is one of the most traditionally used method to analyse phospholipids. Although this analytical method provides a rough estimation of the

number of phosphate molecules within a lipid sample, it requires treating the sample with strong acids, such as sulfuric or perchloric acids, at a high temperature (typically around 170-220°C) to liberate the free phosphates, which thereafter formed complex with colorimetric reagents, *e.g.* malachite green or ammnonium molybdate to allow subsequent colorimetric absorbance measurement (Mrsny *et al.*, 1986; Rouser *et al.*, 1970; Zhou and Arthur, 1992). Ammonium ferrothiocyanate is another reagent for phosphate quantification and this method eliminates the prior need of acid digestion (Stewart, 1980). A phosphate standard curve is normally plotted using phospholipid standards or inorganic phosphates to facilitate the estimation of phosphate concentration from absorbance measurements. However, the presence of two phosphate moieties on a CL molecule is normally not taken into account during phosphate quantification, thus likely to skew the result to over account for the amount of phospholipids.

1.5.3 Thin layer chromatography

Thin layer chromatography (TLC) is also routinely used for lipid analysis. In comparison to phosphate quantification, this technique provides an additional dimension of information with regards to the characterisation of different classes of lipids (and their relative abundances) in a lipid sample. It is relatively simple to perform and require inexpensive equipment setup and thus more readily established in the laboratories (Fuchs *et al.*, 2011). However, it is a relatively low resolution and insensitive technique, thus necessitating a high loading of lipid analytes. Consequently, it is more applicable for the analysis total membrane extracts, as it would be very challenging to analyse the co-extracted lipids from purified membrane proteins. The main shortcoming of TLC is that the differences in fatty acids composition for each lipid class cannot be readily distinguished, as it provides only class-based separation (Pati *et al.*, 2016).

1.5.4 Gas chromatography

Gas chromatography (GC) is a more advanced analytical technique for the analysis of lipids in comparison to phosphate quantification and TLC. However, due to the nature of GC, the fatty acyl chains must be released via alkaline hydrolysis, followed by chemical derivitisation, for example into the forms of methyl esters, picolinyl esters, or pentafluorobenzyl esters to facilitate subsequent detection (Oursel *et al.*, 2007a). This

treatment thus relinquish the information of the lipid headgroups and therefore GC analysis can be coupled to TLC analysis to obtain complementary lipid class-based information (Dörr *et al.*, 2014). Difficulty can however arises in the interpretation of results pertaining to the origin of the fatty acyl chains, which might be derived from lipopolysaccharides or lipoproteins besides phospholipids (Benamara *et al.*, 2014). Nevertheless, GC analysis of lipids provides the additional account of fatty acyl chain compositions that is not attainable through TLC analysis.

1.5.5 Nuclear magnetic resonance

Although ^{1}H and ^{13}C NMR can be used for lipid analysis, but they are only applicable for individual phospholipid species due to the complex lipid mixtures in a biological sample. On the other hand, ^{31}P NMR is more useful for the analysis of mixed lipids in biological samples, as the molar quantities of phosphorus can be measured and separate signals can be acquired for different phospholipid classes (Sotirhos *et al.*, 1986). However, due to the relatively large sample requirement for NMR (due to its low sensitivity) and the lack of detail characterisation in comparison to other analytical techniques such as mass spectrometry, it is not routinely used for lipid analysis (Adosraku *et al.*, 1994; Sotirhos *et al.*, 1986).

1.5.6 Mass spectrometry

Mass spectrometry (MS) is inevaitably the present-day analytical method of choice for lipidomic experiments as it provides superior qualitative and quantitaive information regarding the lipidome in a sample (Köfeler *et al.*, 2012; Li *et al.*, 2014; Murphy and Gaskell, 2011). To date, no other analytical method is capable of offering both the simultaneous and differential detection of individual lipid species, with detailed structural charcterisation (headgroups and fatty acyl chains distribution) except through the employment of MS (Ellis *et al.*, 2013). The remaining sections in this chapter would thus focus on discussion on the use of MS-based approaches for lipidomic analysis.

1.5.6.1 Ionisation methods

The advent of soft ionisation techniques, namely matrix-assisted laser desorption ionisation (MALDI) and electrospray ionisation (ESI) have immensely faciliated intact lipid analysis using MS (Murphy and Gaskell, 2011). For MALDI-MS approach, the lipid sample is mixed with a suitable matrix, *e.g.* 2,5-Dihydroxybenzoic acid, α-Cyano-

4-hydroxycinnamic acid, or 9-Aminoacridine and subsequently spotted onto a MALDI target plate to dry and form crystals (Ellis *et al.*, 2013; Köfeler *et al.*, 2012; Li *et al.*, 2014). Alternatively, sublimination (under conditions of reduced pressure and elevated temperature) can be used for matrix application (Hankin *et al.*, 2007). The firing of a laser beam onto the dried matrix crystals enables the lipids to absorb the laser enegry, resulting in desorption and ionisation of the lipid analytes for subsequent MS analysis, normally through a time-of-flight (ToF) mass analyser (Vaz *et al.*, 2014).

The matrix effect represents a considerable disadvantage to the use of the MALDI-MS approach. Due to the matrix interference which results in a myriad of matrix peaks at 100-500 Da, the analysis of analyte peaks below *m/z* 500 can be very challenging without careful sample preparation (Köfeler *et al.*, 2012; Li *et al.*, 2014). The use of 1,8-Bis(dimethylamino)napthalene as the matrix for MALDI-MS analysis provided a promising solution to this matrix interference problem as it was reported to display little to none matrix effect, and thus revealing the presence of free fatty acids that would normally be masked by the high intensities of matrix peaks when other matrices were employed (Doubsky, 2009). Besides the issue of matrix effect, the MALDI-MS approach has been critised of being rather poor in reproducilibity, due to the heterogeneity of matrix-analyte crystals, which compromises quantitative lipid analysis (Li *et al.*, 2014). For hyphenated approaches, MALDI would be more suitable to be coupled a TLC-based separation system for lipid analysis rather than LC-based separation common to ESI-MS (Calvano *et al.*, 2014).

ESI is extensively utilised to ionise thermally labile and mostly non-volatile molecules, allowing this ionisation method to be applied to almost all lipid categories (Vaz *et al.*, 2014). Figure 1.11 depicts the generalised ESI process to produce gas-phase ions for subsequent MS analysis. Essentially, the lipid analytes are passed through a highly charged capillary (3-5 kV) into a curtain of heated, inert nebulising gas (usually nitrogen) to aid the desolvation of the solvent. The electrical potential difference between the capillary and the inlet of the mass spectrometer results in the formation of a Taylor Cone at the tip of the capillary with a plume of small charged droplets containing the analytes. The evaporation of solvent in the lipid droplets causes increasing charge density, eventually leading to Coulombic-driven explosion upon reaching the Rayleigh limit, breaking up the droplets into smaller droplets and increases

the available surface area. Consequently, intact gas-phase lipid ions (containing pseudo molecular ions) are produced for subsequent MS analysis (Brouwers, 2011; Ellis *et al.*, 2013; Milne *et al.*, 2006; Spickett *et al.*, 2011; Vaz *et al.*, 2014; Wilm, 2011). For an effective ESI process, the solvent used has to be sufficiently conductive (Brouwers, 2011). One of the approaches for MS-based lipidomic analysis is via a shotgun approach, *i.e.* by directly infusing a lipid extract into the mass spectrometer for analysis through ESI without any prior separation step.

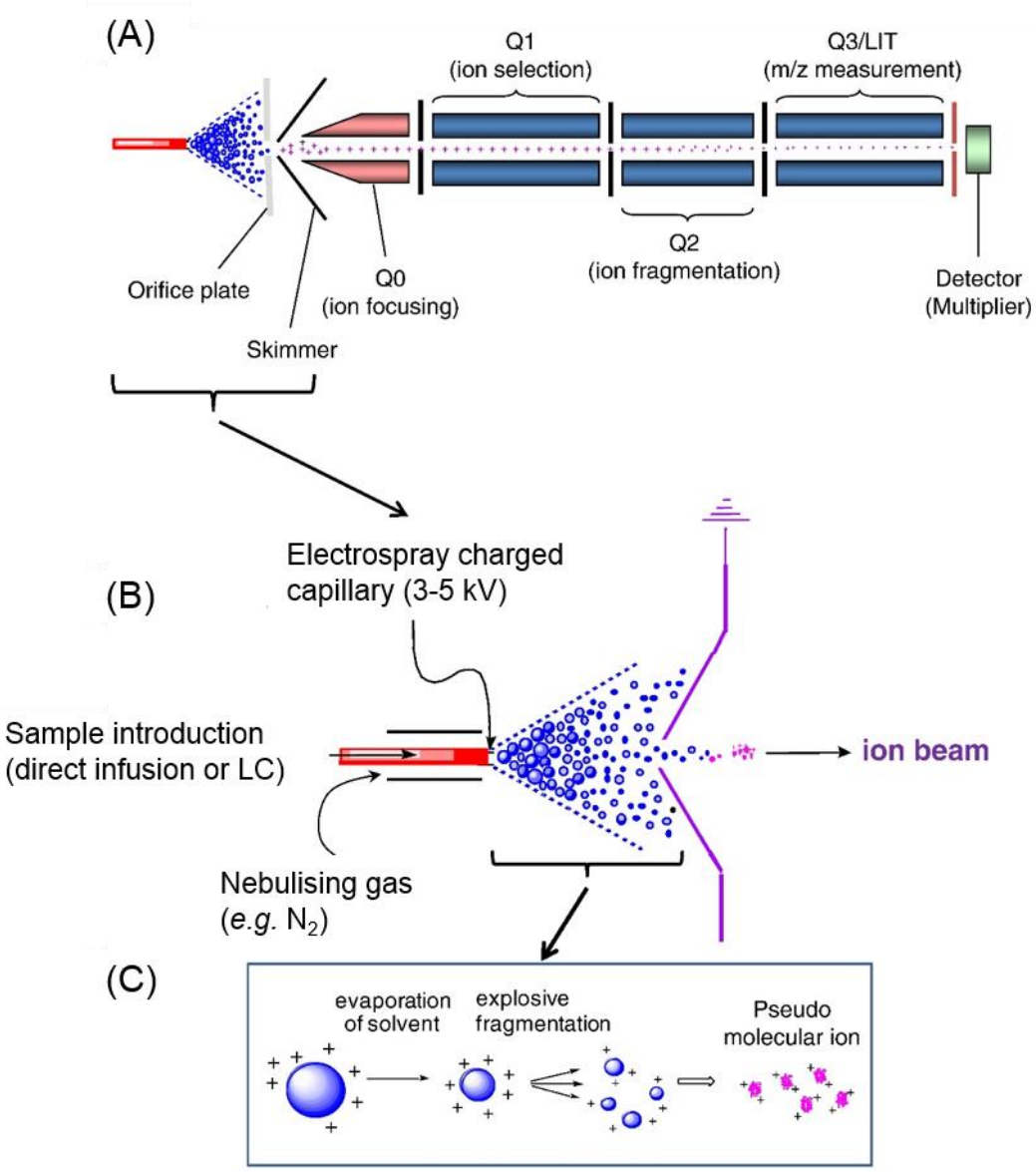

Figure 1.11 ESI process to produce gas-phase analyte ions for subsequent MS analysis. (A) The schematic diagram of an ESI source coupled to a hybrid triple quadrupole-linear ion trap (QqQ/LIT) mass spectrometer. (B) Sample containing the analytes of interest is sprayed through a charged capillary at high voltage and the evaporation of

solvent is aided by a sheath of heated, inert nebulising gas. (C) Pseudo molecular ions for subsequent MS analysis are formed through Coloumbic-driven explosion upon reaching the Rayleigh limit as the droplet dries. Figure is adapted from Spickett *et al.* (2011) with permission.

1.5.6.2 Liquid chromatography-mass spectrometry

Although MS-based lipidomic analysis can be readily implemented through the shotgun direct infusion approach, the inclusion of a prior separation step utilising LC can aid in the analysis of complex lipid mixtures in a biological sample. In particular, ion suppression and/or enhancement effects which can be a major problem in shotgun lipidomics can be effectively minimised with the employment of liquid chromatography-mass spectrometry (LC-MS) (Brouwers, 2011). With LC separation, the interferences from the more abundance or better ionised lipid species is counteracted, and the lower abundance species are simultaneously enriched along the separation gradient to facilitate detection and quantification (Yang and Han, 2011). In addition, LC can facilitate the separation of isobaric species of very similar mass-to-charge ratio (*m/z*) and/or isomeric species (Brouwers, 2011). The occasional occurrence of in-source fragmentation, whereby gas-phase analyte ions undergo fragmentation in the ESI source before reaching the mass analyser can complicate lipid analysis. For instance, a PS species can generate a PA species when the serine headgroup is lost and this phenomenon can complicate the identification of PA in direct infusion MS experiments. However, with LC-MS, the PS-derived PA would be separated from the endogenous PA and thus enable more accurate analysis (Brouwers, 2011).

1.5.6.3 Normal-phase and hydrophilic interaction LC

In principle, the lipids separate on the basis of polar interactions between the stationary phase (usually unmodified silica particles with free silanol group) in normal-phase liquid chromatography (NPLC) (Brouwers, 2011). Generally, highly non-polar solvents such as hexane with low ionisation capacity are used in NPLC and problem with ESI may arise at the beginning of the LC gradient when the content of non-polar solvent is the highest (Brouwers, 2011). The use of the normal-phase type solvents are also viewed as environmentally unfriendly in modern laboratories and expensive in terms of disposal of the toxic eluents.

Hydrophilic interaction liquid chromatography (HILIC) can be considered an alternative variant to NPLC (Buszewski and Noga, 2012). Instead of employing highly non-polar solvents for the separation of polar compounds, it utilises water and water-miscible organic solvents, such as acetonitrile (ACN) to achieve the liquid-liquid partitioning of the analytes on a water-rich layer created on the polar stationary phase (Cajka and Fiehn, 2014). In HILIC, the retention of analytes on the polar stationary phase is influenced by the differences in terms of hydrogen bonding and electrostatic forces between stationary and mobile phases. In comparison to NPLC, HILIC results in lower back pressures, higher sensitivity, better reproducibility, and is more compatible with downstream ESI-MS analysis (Cajka and Fiehn, 2014; Pati *et al.*, 2016; Schwalbe-Herrmann *et al.*, 2010).

1.5.6.4 Reverse-phase LC

The lipids are separated based on differences in their polar headgroups (by class) in NPLC and HILIC. In contrast, the separation of lipids is based on hydrophobicity or lipophilicity (as governed by the number of carbon atoms and double bonds) in reverse-phase liquid chromatography (RPLC), typically on alkyl chain bonded silica columns (*e.g.* C8 and C18) (Cajka and Fiehn, 2014). It is common to add mobile phase additives, such as ammonium formate, ammonium acetate, and/or formic acid in RPLC to faciliate the ionisation of analytes, while reducing the formation of mixed adducts with the counterions present in a biological sample. It is important to note that the use of relatively polar mobile phase at the beginning of the LC gradient could potentially result in sample solubility issue that leads to different apparent ionisation efficiency and resulting in ionisation instability during elution (Yang and Han, 2011). Generally, due to the diverse ionisable sites on different lipid classes, the chosen LC-MS method should ideally be efficient and robust to be implemented in both positive and negative ion modes, in order to achieve a comprehensive coverage (Bird *et al.*, 2011). In comparison to NPLC, the analysis time of RPLC is usually shorter (Cajka and Fiehn, 2014; Schwalbe-Herrmann *et al.*, 2010).

1.5.6.5 Targeted MS approach

The employment of tandem mass spectrometers (with more than one mass analysers) such as a triple quadrupole instrument facilitate tandem MS approaches, which are applicable to both shotgun and LC-MS-based lipidomic analysis (Vaz *et al.*, 2014; Wolf

and Quinn, 2008). During tandem MS, the lipid analytes are fragmented in a collision cell based on collision-induced/activated dissociation (CID/CAD), and the resulting fragment ions can be mapped to the structural features on the target lipid analytes. Based on well studied fragmentation process for phospholipids, structural information can be readily obtained for fatty acyl chains at the *sn*-1 and *sn*-2 positions (by comparing their relative ion intensities), as the the fragmentation processes that leads to ion formation are sterically more favourable at the *sn*-2 position than *sn*-1 (Hsu and Turk, 2001; Smith *et al.*, 1995).

Figure 1.12 shows the different targeted MS approaches utilising tandem mass spectrometers that increase the selectivity of the mass spectrometer to detect specific phospholipid classes. When the headgroup of a lipid class is lost as a charged fragment, precursor ion scan (PIS) mode can be implemented to selectively detect that class of lipids. It works by setting the second mass analyser to transmit only the ions harbouring the *m/z* value corresponding to the selected headgroup fragment (*e.g.* PIS 184 for PC headgroup), while allowing the first mass analyser to scan across a preselected *m/z* range (Brügger *et al.*, 1997; Myers *et al.*, 2011; Spickett *et al.*, 2011). On the other hand, neutral loss (NL) scans are utilised when the lipid headgroup is lost as a neutral (uncharged) fragment (*e.g.* NL 141 for PE headgroup), whereby both mass analysers are programmed to scan in unison, with a specific *m/z* offset (matching the corresponding neutral loss) between the mass analysers (Brügger *et al.*, 1997; Spickett *et al.*, 2011).

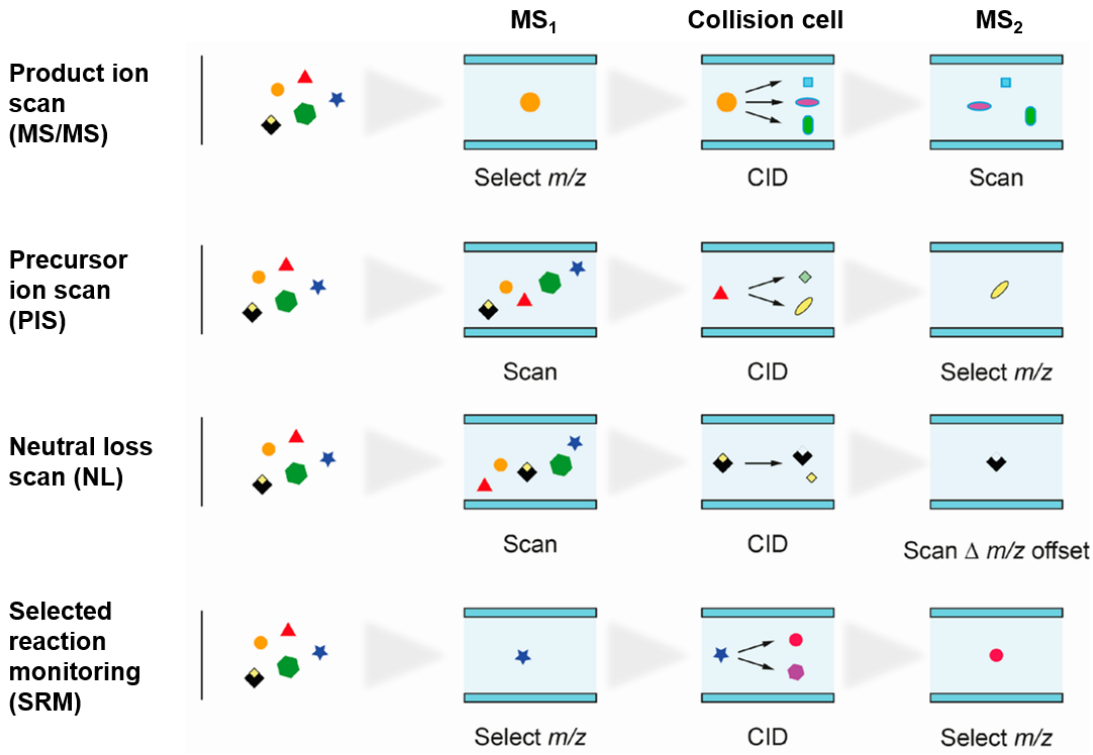

Figure 1.12 Targeted MS scan modes utilising tandem mass spectrometers for lipidomic analysis. MS_1 and MS_2 represent the two mass analysers. Figure is adopted from Markgraf *et al.* (2016) with permission.

Another type of tandem MS approach utilises selected reaction monitoring (SRM) to accurately quantify a small subset of lipids, based on the known transitions between the parent and product ions. In SRM, the first mass analyser is fixed on a specific precursor ion, while the second mass analyser is locked on a specific product ion (Harkewicz and Dennis, 2011). Multiple reaction monitoring (MRM) takes place when multiple of such transitions are monitored in an experiment, essentially getting the mass spectrometer to cycle through multiple SRM pairs in a repeated manner (Han *et al.*, 2012; Harkewicz and Dennis, 2011). The *a priori* knowledge about the target lipid species is indispensable for SRM/MRM types of investigation (Checa *et al.*, 2015; Myers *et al.*, 2011).

Data/information-dependent acquisition (DDA/IDA) approach can be employed for automated real-time selection of ions for tandem MS analysis to augment the information obtained from the general survey scan during a lipidomic experiment. It consists of a general survey scan (of a preselected *m/z* range), whereby precursor ions

exceeding a predefined intensity threshold are automatically isolated for fragmentation in the collision cell and the resulting product ions are detected for further structural characterisation of the analytes (Cajka and Fiehn, 2014; Vaz *et al.*, 2014). DDA/IDA type of MS approach is strongly dependent on the acquisition rate of the mass spectrometer for the amount of scans that can be perfomed in a given amount of time for the predefined *m/z* range (Vaz *et al.*, 2014).

1.5.6.6 Experimental design for MS-based lipidomics

Due to the inherent complexity of a MS-based lipidomic experiment, it is pivotal to design the experiment in such a way to maximise the information obtainable from the dataset. Experimental parameters, such as sample size (biological and technical replicates), internal standards (for data normalisation), and quality control (QC) samples (to account for prolonged LC-MS runs) must be given due consideration (Vaz *et al.*, 2014). MS is not inherently quantitative, *i.e.* the intensity for each ion peak does not correlate directly to its concentration due to the differences in ionisation efficiency. Consequently, different approaches have to be employed to facilitate absolute or relative quantification in a lipidomic experiment. Absolute quantification emphasises the accurate determination of the amount of individual lipid species in the lipidome, while relative quantification examines the global pattern change in the lipidome (Yang and Han, 2011). Absolute quantification is still rare for lipidomics, unless a specific small sets of lipids are to be monitored, and SRM/MRM approach would be the method of choice. On the other hand, relative quantification normally uses stable isotope labelling of biological samples or the inclusion of internal standards (IS) for the normalisation of ion intensities (Cajka and Fiehn, 2014). In lipidomic analysis, either the deuterated version of the lipids of interest, or non-natural lipids (*i.e.* lipid species that are not normally present in the organism or sample being studied) can be exploited as the IS (Brouwers, 2011; Brügger *et al.*, 1997; Cajka and Fiehn, 2014; Fang and Barcelona, 1998; Layre and Moody, 2013; Myers *et al.*, 2011; Vaz *et al.*, 2014; Yang and Han, 2011). However, for more accurate quantification, the deuterated IS is preferred due to similar ionisation efficiency, but the availability of the deuterated IS might be an issue. The IS should be added in at the earliest step during sample preparation (prior to lipid extraction), in order to be processed and analysed simultaneously with the analytes (Yang and Han, 2011).

1.5.6.7 Bacterial membrane lipidomics

Several research groups have utilised LC-MS to study the *E. coli* membrane composition. Oursel *et al.* (2007b) evaluated the membrane composition of a wild type *E. coli* K12 strain (LM 3118) utilising a RPLC-MS approach. Relative quantification was performed using PE 12:0/12:0 (24:0) as the IS. A total of 30 PE and PG lipids (including the isobaric species) was detected, but the method employed failed to detect CL due to inadequate elution from the C18 reverse-phase column (Oursel *et al.*, 2007b). Garrett *et al.* (2012) built upon the abovementioned work and specifically investigated the CL species in another *E. coli* K12 strain (W3110) with a NPLC-MS approach instead. The CL species were identified as doubly charged species $[M\text{-}2H]^{2-}$ in the negative ion mode. Upon thorough analytical investigation, CL 14:1/14:1/14:1/15:1 (57:4) was selected by as the IS. Although CLs were eluted from the silica column, this method did not always separate PG and CL, which inadvertently complicated the quantification process (Garrett *et al.*, 2012). In a separate experiment whereby a C8 reverse-phase column was used, CL was found to co-elute with PE (Garrett *et al.*, 2007). A total of 56 different molecular species of CL, ranging from 60-72 number of carbons with zero to four unsaturations were identified in the *E. coli* W3110 lipid extracts (Garrett *et al.*, 2012). The vast diversity of CL molecular species was unsurprising given the tetraacylated nature of CL, which can in principle result in n^4 potential molecular species for n types of fatty acids. Thus, considering the common fatty acids found in the *E. coli* membrane, including C12:0, C14:0, cyC15:0, C16:0, C16:1, C17:0, cyC17:0, C18:0, C18:1, cyC19:0 (Garrett *et al.*, 2012; Oursel *et al.*, 2007a), the potential combination of CL reaches 10,000, without even factoring the double bond stereoisomers for the unsaturated CL species (Schlame, 2008).

While characterising *E. coli* CL species using a multiple-stage ion trap approach (without LC separation), Hsu and Turk (2006) detected CL species as $[M\text{-}2H+Na]^-$ ions for 14 CL species, including CL 64:2, 65:2, 66:2, 67:2, 67:3, 68:3, 69:3, 70:4, 70:3, 71:4, 71:3, 72:4, 73:4, 74:3 from a commercial *E. coli* CL extract. Using a RPLC-MS approach, Fang and Barcelona (1998) observed many monounsaturated CL species, including CL 65:1, 66:1, 67:1, 68:1, 69:1, 70:1 , 71:1 and/or 72:4 as doubly charged ions from an *E. coli* CL extract. Among the three major membrane phospholipids in *E. coli*, CL is considered the most technically challenging for quantitative analysis due to its lower natural abundance, larger molecular structure and higher hydrophobicity than

PE and PG (Han *et al.*, 2006; Schlame, 2008). In addition, being the product of condensation between two molecules of PG can make CL difficult to analyse using tandem MS (in the absence of a prior separation step), due to the similarities in fragmentation patterns with PG.

1.6 Statistical analysis in lipidomics

Due to the vast and complex dataset obtained from lipidomic experiments, statistical analysis is routinely conducted to extract valuable information out of the dataset (Checa *et al.*, 2015). The common univariate and multivariate analyses applied to lipidomic dataset is disccused in the following sections.

1.6.1 Univariate analysis

Statistical hypothesis testing for the difference of means between two groups of samples is frequently used to analyse lipidomic data. Depending on the assumption regarding the probability distribution of the data, the statistics could be either parametric or non-parametric (Greenhalgh, 1997). For univariate analysis, the Student's *t*-test (equal variance) or Welch's *t*-test (non-equal variance) are utilised to compare the means of two groups of samples, for instance the lipid profiles between diseased and healthy tissues (Checa *et al.*, 2015). Analysis of variance (ANOVA) on the other hand can be seen as a generalisation of *t*-test to more than two groups of samples. In one-way ANOVA, there is a single measured variable and factor, such as the comparison of lipid concentration for samples subjected to different treatments. Two-way ANOVA deals with a single measured variable with more than one factor, such as the comparison of lipid concentration for samples subjected to various treatments and sampling times (Checa *et al.*, 2015).

1.6.2 Multivariate analysis

Principal component analysis (PCA) is one of the most common multivariate analysis method for lipidomic dataset. It is an unsupervised method for the projection of the original complex dataset (while preserving as much variance as possible) into a lower dimensionality plot to faciliatate data visualisation and sample classification (Checa *et al.*, 2015; Katajamaa and Orešič, 2007; Worley and Powers, 2013). The mathematical algorithm employed in PCA to reduce the dimensionality and complexity of the data, works by identifying directions called principal components, which are linear

combinations of the original variables, along which maximum variation in the data is captured. Generally, the first principal component portrays the direction along which the samples show the largest variation, while the second principal component shows the direction that is uncorrelated to the first component, along which the samples show the next largest variation. The output is visualised by plotting the scores plot to inspect similarities and differences between the samples and determine if the samples can be grouped (Ringnér, 2008). One caveat in PCA is that the within-group variation should be sufficiently less than the between-group variation for the analysis to be meaningful (Worley and Powers, 2013). PCA is frequently employed to distinguish bacteria species (up to subspecies level) in MS-based chemotaxonomic fingerprinting experiments. Membrane lipids were found to be the discriminating biochemical factors for taxonomic separation due to their vast chemical diversity (Ishida *et al.*, 2002; Meetani *et al.*, 2007; Santos *et al.*, 2015; Song *et al.*, 2007; Wehrli *et al.*, 2014; Zhang *et al.*, 2011).

1.7 Aim and objectives of thesis

The primary aim of the work in this thesis was to develop appropriate analytical approaches and tools to facilitate the *in vitro* analysis of bacterial membrane proteins with a particular focus on the divisome complex. To accomplish the aim of research, several key objectives have to be achieved as follows:

- Develop a robust SMALP lipidomic strategy to characterise the co-extracted membrane lipidomes of bacterial membrane proteins
- Perform relative quantification of the co-extracted membrane phospholipids to compare the phospholipid profiles obtained for different bacterial membrane proteins
- Explore the applicability of the SMALP technology to new bacterial membrane protein previously subjected to detergent studies, to facilitate the comparison of corresponding biophysical and biochemical properties besides the co-extracted membrane lipidomes in SMALP vs detergent

Chapter 2: Materials and Methods

2.1 General materials

Unless stated otherwise, all chemicals and reagents used in this project were purchased from Sigma-Aldrich (Dorset, UK), Fisher Scientific (Leicestershire, UK), or Melford Biolaboratories (Suffolk, UK). All organic solvents used in the mass spectrometry experiments were of high performance liquid chromatography (HPLC) grade, and LC-MS grade water was used.

Ultrapure (Milli-Q) water (18.2 MΩ.cm) was used to make the buffers. The buffers were filtered prior to use with a 0.2 µm polyethersulfone (PES) membrane filter. The pH of solutions was measured using either one for the following pH meters calibrated with appriopriate buffer standards, *i.e.* S20 SevenEasy^{TM} (Metler Toledo, Switzerland), Delta 320 (Metler Toledo, Switzerland) or Corning® 120 (Sigma-Aldrich, UK).

2.2 Styrene maleic acid copolymer preparation

The preparation of the SMA copolymer was based on Lee *et al.* (2016b). Firstly, 25 g of SMA® 2000 - 2:1 styrene-to-maleic anhydride ratio, average molecular weight: 7.5 kDa (Cray Valley, USA) was dissolved in 250 mL 1 M NaOH, using a 500 mL round bottom flask, and stirred overnight at room temperature. Subsequently, the polymer solution was heated under reflux for 2 h. A few anti-bumping granules were added to encourage smooth boiling. Upon cooling to room temperature (about 2 h), the SMA copolymer (now hydrolysed into the acid form) was precipitated by reducing the pH to below 6 using concentrated HCl (specific gravity: 1.18), with the pH being monitored using litmus test paper strips. The acid-precipitated polymer was then washed three times with ultrapure water to remove the water-soluble impurities. For each wash, the polymer suspension was centrifuged at 8000 rpm (11,300 x *g*) in a Beckman Coulter JA-10.500 rotor for 15 min at room temperature. The polymer precipitate upon the final wash was resuspended in 0.6 M NaOH and incubated overnight at 37°C, 180 rpm using an orbital shaker to fully dissolve the polymer. The final pH of the polymer solution was adjusted slowly to 8 using concentrated HCl. Note that when localised precipitations occurred, the precipitates were allowed to re-dissolve in solution prior to the addition of HCl and this step could take 2-3 h. The pH-adjusted polymer solution

was flash frozen using liquid nitrogen and subsequently lyophilised in a ScanVac CoolSafe^{TM} 55-9 PRO freeze dryer (LaboGene, Denmark) at around -50°C. The lyophilised polymer powder was subjected to Fourier transform infrared (FTIR) spectroscopic analysis utilising the Avatar 320 FT-IR spectrophotometer (Thermo Nicolet, USA) with attenuated total reflectance (ATR) as the sampling technique on a germanium lens. A total of 16 scans were averaged at a resolution of four. The ATR-FTIR analysis (Appendix) was conducted to confirm the full conversion of the anhydride to acid form of the SMA copolymer upon hydrolysis by noting the disappearance of the maleic anhydride carbonyl peak at 1778 cm^{-1}, with the concurrent appearance of the carboxylate carbonyl peak at 1568 cm^{-1} (Knowles *et al.*, 2009). The final hydrolysed SMA copolymer (about 30 g) was stored in separate parafilm-sealed Falcon® polypropylene tubes (Corning, USA) at room temperature in a dark cupboard prior to usage.

2.3 Preparation of chemically-induced competent *E. coli* cells

E. coli cells was inoculated in 2.5 mL Luria-Bertani (LB) medium (1% w/v tryptone, 0.5% w/v yeast extract, 1% w/v NaCl, pH 7.5) at 37°C, 180 rpm as overnight starter culture. The starter culture was used to inoculate 250 mL LB in 2 L baffled Erlenmeyer flask, supplemented with 20 mM $MgSO_4$. The *E. coli* cells were incubated at 37°C, 200 rpm until an optical density at 600 nm (OD_{600}) around 0.4-0.6, measured via the Ultrospec^{TM} 2100 pro UV/Vis spectrophotometer (Amersham Biosciences, USA). The *E. coli* cells were centrifuged at 4500 x *g* in a Beckman Coulter JA-14 rotor for 5 min at 4°C. The pelleted *E. coli* cells were resuspended in 100 mL ice-cold transformation buffer 1 (100 mM $RbCl_2$, 50 mM $MnCl_2$, 30 mM CH_3COOK, 10 mM $CaCl_2$, 15% w/v glycerol, pH 5.8) and incubated for 5 min at 4°C. The *E. coli* cells were centrifuged at 4500 x *g* in a Beckman Coulter JA-25.50 rotor for 5 min at 4°C. The pelleted *E. coli* cells were resuspended in 10 mL ice-cold transformation buffer 2 (10 mM $RbCl_2$, 10 mM 3-(*N*-morpholino)propanesulfonic acid, 75 mM $CaCl_2$, 15% w/v glycerol, pH 6.5) and incubated for 1 h at 4°C. Note that the pH of TFB1 was adjusted with 1 M acetic acid and TFB 2 with 1 M KOH; both buffers were filter-sterilised prior to use. The *E. coli* cells were aliquoted to 50 µL, flash frozen in liquid nitrogen, and stored at -80°C until further use. Competency test (using pUC19 control plasmid) and sterility test were conducted on the chemically-induced competent *E. coli* cells prior to use.

2.4 Bacterial transformation

Plasmid deoxyribonucleic acid (DNA) (1-2 µL) was added to 40-50 µL chemically-induced competent *E. coli* cells, and the cells were equilibrated on ice for 15-30 min prior to heat shock treatment for 45 s in a water bath set to 42°C. The *E. coli* cells were recovered on ice for 2-3 min, then supplemented with 150 µL Super optimal broth with catabolite repression medium (2% w/v tryptone, 0.5% w/v yeast extract, 10 mM NaCl, 2.5 mM KCl, 10 mM $MgCl_2$, 10 mM $MgSO_4$, 20 mM glucose) and allow to grow for 1 h at 37°C, 180 rpm. Transformed *E. coli* cells (100 µL) were plated onto LB agar (1% w/v tryptone, 0.5% w/v yeast extract, 1% w/v NaCl, 1.5% w/v agar) supplemented with appropriate antibiotic, and incubated overnight at 37°C.

2.5 Recombinant protein expression

2.5.1 ZipA and FtsA

A 10 mL overnight starter LB culture of transformed *E. coli* BL21(DE3) cells harbouring the plasmid encoding for ZipA or FtsA was used to inoculate each of the 6 x 500 mL LB in 2 L non-baffled Erlenmeyer flasks supplemented with 100 µg/mL ampicillin. The *E. coli* cells were incubated at 37°C, 180 rpm until OD_{600} around 0.6-0.8. Protein overexpression was induced by the addition of 1 mM Isopropyl β-D-1-thiogalactopyranoside (IPTG) with concurrent reduction of incubation temperature to 25°C for overnight incubation. The *E. coli* cells were harvested by centrifugation at 4000 rpm (3000 x *g*) in a Beckman Coulter JLA 10.500 rotor for 15 min at 4°C. The *E. coli* cell pellets were washed with 20 mL phosphate buffered saline (PBS) (137 mM NaCl, 2.7 mM KCl, 10 mM Na_2HPO_4, 1.8 mM KH_2PO_4) and centrifuged at 4000 rpm (3000 x *g*) in a Beckman Coulter JLA 10.500 rotor for 15 min at 4°C. The washed pellets were stored at -20°C until further use. Note that the ZipA plasmid harbours a C-terminal V5 epitode and hexahistine (His_6) tag after the *zipA* gene; recombinant protein weight 39.5 kDa (kind gift of Dr. Yu-pin Lin, University of Birmingham), while the FtsA plasmid harbours the hexahistidine tag at the end of the *ftsA* gene; recombinant protein weight 45 kDa (kind gift of Dr. Mohammed Jamshad, University of Birmingham). Both plasmids confer ampicillin resistance to the gene constructs.

2.5.2 PgpB

The overexpression of PgpB was based on Touzé *et al.* (2008). A 20 mL overnight starter LB culture of transformed *E. coli* C43(DE3) harbouring the plasmid encoding

for PgpB was used to inoculate each of the 6 x 1 L 2YT (1.6% w/v tryptone, 1% w/v yeast extract, 5.9 w/v NaCl, pH 7) in 2 L Ultra Yield Flask™ supplemented with 100 µg/mL ampicillin. The *E. coli* cells were incubated at 37°C, 180 rpm until OD_{600} around 0.8-1.0. Protein overexpression was induced by the addition of 1 mM IPTG with further incubation for 3.5-4.0 h. The *E. coli* cells were harvested by centrifugation at 4000 x *g* in a Beckman Coulter JLA 8.1000 rotor for 10 min at 4°C. The *E. coli* cell pellets were stored at -20°C until further use. Note that the PgpB plasmid harbours a C-terminal arginine-serine-hexahistidine tag (Arg-Ser-His_6) after the *pgpB* gene; recombinant protein weight 30 kDa (kind gift from Dr. Thierry Touzé, Université Paris-Sud).

2.6 *E. coli* cell disruption and membrane preparation

2.6.1 ZipA and FtsA

Thawed *E. coli* cell pellets were resuspended in 50-100 mL resuspension buffer A (50 mM Tris-HCl, 100 mM NaCl, 5% w/v glycerol, pH 8) supplemented with one to two Pierce™ Protease Inhibitor Tablet with ethylenediaminetetraacetic acid (EDTA) (Thermo Fisher Scientific, USA). The resuspended *E. coli* cells were subjected to cell disruption using the Emulsiflex-C3 Cell Disruptor (Avestin, Canada) for five to six passes at 25 kpsi. Upon cell disruption, the flow through was centrifuged at 11,500 rpm (10,000 x *g*) in a Beckman Coulter JA 20 rotor for 1 h at 4°C. For subsequent membrane preparation using ultracentrifugation, the resulting supernatant was centrifuged at 45,000 rpm (100,000 x *g*) in a Beckman Coulter 70.1 Ti rotor for 1 h at 4°C. Note that the ZipA and FtsA proteins used in the lipidomic experiments were prepared by Dr. Sarah Lee, Dr. Naomi Pollock, Rosemary Parslow and Stephen Hall (University of Birmingham).

2.6.2 PgpB

Thawed *E. coli* cell pellets were resuspended in five times volume of resuspension buffer B (50 mM Tris-HCl, 100 mM NaCl, 2 mM EDTA, 5% w/v glycerol, pH 8, for subsequent SMALP extraction and purification) or resuspension buffer C (20 mM Tris-HCl, 1 mM $MgCl_2$, 20 mM β-Mercaptoethanol (βME), 500 mM NaCl, 10% w/v glycerol, pH 7.5, for subsequent detergent extraction and purification), both supplemented with 1 µM Leupeptin, 1 µM Pepstatin A, and 0.2 mM phenylmethylsulfonyl fluoride. The resuspended *E. coli* cells were subjected to cell disruption using the Constant Cell Disruptor (Constant Systems, UK) for four passes at

30 kpsi with optional addition of Antifoam 204 and DNase I (from bovine pancreas) at the start of the second disruption cycle. Upon cell disruption, the flow through was centrifuged at 20,000 x *g* in a Beckman Coulter JA 25.50 or JA 14 rotor for 45 min at 4°C. For subsequent membrane preparation using ultracentrifugation, the resulting 20,000 x *g* supernatant was centrifuged at 100,000 x *g* in a Beckman Coulter 45 Ti rotor for 1 h at 4°C.

2.7 *E. coli* membrane solubilisation

2.7.1 ZipA, FtsA, and PgpB (SMALP)

The solubilisation of *E. coli* membrane using the SMALP technology was based on Lee *et al.* (2016b). The 100,000 x *g* membrane was resuspended in SMALP solubilisation buffer (50 mM Tris-HCl, 500 mM NaCl, 2.5% w/v SMA, 10% w/v glycerol, pH 8) at a wet membrane pellet weight of 40 mg/mL. The wet membrane pellet weight was used instead of specific membrane protein concentration as the SMA copolymer interacts with membrane lipids (Rothnie, 2016). The *E. coli* membrane was homogenised using a Potter-Elvehjem homogeniser and the homogenised membrane was incubated for 2.5 h at room temperature on a roller mixer. The solubilised *E. coli* membrane was centrifuged at 150,000 x *g* in a Beckman Coulter 45 Ti rotor for 1 h at 4°C.

2.7.2 PgpB (detergent)

The solubilisation of *E. coli* membrane using the non-ionic detergent, DDM was based on Touzé *et al.* (2008). The 100,000 x *g* membrane was resuspended in 50 mL DDM solubilisation buffer (20 mM Tris-HCl, 1 mM $MgCl_2$, 500 mM NaCl, 2% w/v DDM, 10% w/v glycerol, pH 7.5). The *E. coli* membrane was homogenised using a Potter-Elvehjem homogeniser and the homogenised membrane was incubated for 2.5 h at 4°C on a roller mixer. The solubilised *E. coli* membrane was centrifuged at 150,000 x *g* in a Beckman Coulter 45 Ti rotor for 1 h at 4°C.

2.8 Immobilised metal affinity purification

2.8.1 ZipA and FtsA (SMALP)

A total of 2 mL nickel^{2+}-nitriloacetic acid (Ni-NTA) resin (Generon, UK) in 50 mM Tris-HCl, 100 mM NaCl, 10% w/v glycerol, pH 8 was added to the 150,000 x *g* supernatant which corresponds to the SMALP-solubilised membrane. The solubilised protein sample was incubated overnight at 4°C on a roller mixer. Upon overnight

incubation, the solubilised protein sample was decanted into a gravity flow column. The Ni-NTA resin was allowed to settle for 15 min before the flow through was collected. The Ni-NTA resin was washed with 10 column volume (CV) of SMALP purification buffer 1 (50 mM Tris-HCl, 500 mM NaCl, 10 mM imidazole, 10% w/v glycerol, pH 8). ZipA and FtsA were eluted in 2 CV of SMALP elution buffer 1 (50 mM Tris-HCl, 500 mM NaCl, 300 mM imidazole, 10% w/v glycerol, pH 8).

2.8.2 PgpB (SMALP)

A total of 3.5 mL Ni-NTA resin (Qiagen, USA) in 50 mM Tris-HCl, 500 mM NaCl, 10 mM imidazole, 10% w/v glycerol, pH 8 was added to the 150,000 x *g* supernatant which corresponds to the SMALP-solubilised membrane. The solubilised protein sample was incubated overnight at 4°C on a roller mixer. Upon overnight incubation, the solubilised protein sample was decanted into a gravity flow column (with a reservoir attached). The resin was allowed to settle for 15 min before the flow through was collected. The Ni-NTA resin was washed with 20 CV of SMALP purification buffer 1 (50 mM Tris-HCl, 500 mM NaCl, 10 mM imidazole, 10% w/v glycerol, pH 8), followed by SMALP purification buffer 2 (50 mM Tris-HCl, 500 mM NaCl, 30 mM imidazole, 10% w/v glycerol, pH 8). PgpB was eluted with 2 CV of SMALP elution buffer 2 (50 mM Tris-HCl, 500 mM NaCl, 400 mM imidazole, 10% w/v glycerol, pH 8), followed by 2 CV of SMALP elution buffer 3 (50 mM Tris-HCl, 500 mM NaCl, 500 mM imidazole, 10% w/v glycerol, pH 8) and finally 2CV of SMALP elution buffer 3 (50 mM Tris-HCl, 500 mM NaCl, 1M imidazole, 10% w/v glycerol, pH 8).

2.8.3 PgpB (detergent)

A total of 2 mL Ni-NTA resin (Qiagen, USA) in 20 mM Tris-HCl, 1 mM $MgCl_2$, 500 mM NaCl, 2% w/v DDM, 10 mM imidazole, 10% w/v glycerol, pH 7.5 was added to the DDM-solubilised membrane. The solubilised protein sample was incubated overnight at 4°C on a roller mixer. Upon overnight incubation, the solubilised protein sample was decanted into a gravity flow column (with a reservoir attached). The Ni-NTA resin was allowed to settle for 15 min before the flow through was collected. The Ni-NTA resin was washed with 20 CV of DDM purification buffer 1 (20 mM Tris-HCl, 1 mM $MgCl_2$, 500 mM NaCl, 0.2% w/v DDM, 10 mM imidazole, 10% w/v glycerol, pH 7.5), followed by DDM purification buffer 2 (20 mM Tris-HCl, 1 mM $MgCl_2$, 500 mM NaCl, 0.2% w/v DDM, 30 mM imidazole, 10% w/v glycerol, pH 7.5). PgpB was

eluted with 2 CV of DDM elution buffer 1 (20 mM Tris-HCl, 1 mM $MgCl_2$, 500 mM NaCl, 0.2% w/v DDM, 400 mM imidazole, 10% w/v glycerol, pH 7.5), followed by 2 CV of DDM elution buffer 2 (20 mM Tris-HCl, 1 mM $MgCl_2$, 500 mM NaCl, 0.2% w/v DDM, 1M imidazole, 10% w/v glycerol, pH 7.5).

2.9 Sodium dodecyl sulfate-polyacrylamide gel electrophoresis

The purified protein samples were subjected to sodium dodecyl sulfate-polyacrylamide gel electrophoresis (SDS-PAGE) analysis, which is routinely used for the separation and visualisation of polypeptides under a denaturing condition (in the presence of SDS) and the employment a discontinuous polyacrylamide gel system (Laemmli, 1970). The 12% resolving and 4% stacking gels were prepared according to Tables 2.1 and 2.2. The purified protein samples were prepared for gel loading by mixing 15 µL of purified protein with 5 µL NuPAGE® lithium dodecyl sulfate sample buffer (4X) and 2 µL NuPAGE® reducing agent (10X). The protein samples were then incubated at 37°C for 30 min, prior to electrophoresis at 180V for 1 h under the SDS-PAGE running buffer (25 mM Tris-HCl, 0.19 M glycine, 0.1% w/v SDS, pH 8.3). The electrophoresed gel was stained with the InstantBlue™ solution (Expedeon, UK), which is a colloidal Coomassie Brilliant Blue G-250 dye-based gel staining reagent and the gel image was capture using a G:BOX gel documentation system (Syngene, UK) upon destaining the gel in ultrapure water.

Table 2.1 Recipe for 12% resolving gel (enough for two gels).

Reagent	Volume (mL)
1.5 M Tris-HCl, pH 8.8	2.82
Ultrapure water	3.78
AccuGel 29:1 (30% w/v 29:1 acrylamide:bis-acrylamide) (National Diagnostics, USA)	4.56
10% w/v SDS	0.12
10% w/v ammonium persulfate (APS)	0.12
Tetramethylethylenediamine (TEMED)	0.01
Total volume	**11.41**

Table 2.2 Recipe for 4% stacking gel (enough for two gels).

Reagent	Volume (mL)
1 M Tris-HCl, pH 6.8	0.63
Ultrapure water	3.40
AccuGel 29:1 (30% w/v 29:1 acrylamide:bis-acrylamide) (National Diagnostics, USA)	0.67
10% w/v SDS	0.05
0.1% w/v bromophenol blue	0.05
10% w/v APS	0.05
TEMED	0.005
Total volume	**4.855**

2.10 Protein dialysis and concentration

The eluted protein fractions upon SDS-PAGE analysis were pooled and dialysed in either 1 L SMALP dialysis buffer (50 mM Tris-HCl, 500 mM NaCl, 10% w/v glycerol, pH 8) or DDM dialysis buffer (20 mM Tris-HCl, 150 mM NaCl, pH 7.5) overnight at 4°C with constant stirring. The dialysed protein was concentrated using a Vivaspin® centrifugal concentrator (GE Healthcare, USA) with 10 kDa molecular weight cut-off (MWCO) PES membrane.

2.11 Protein concentration determination

The final concentration of the purified and concentrated protein was estimated utilising the Pierce^{TM} bicinchoninic acid protein assay (Thermo Scientific, USA) due to its compatibility to detergents and a selection of chemicals commonly used in the buffers for protein purification (Smith *et al.*, 1985) according to the manufacturer's instruction. A working reagent was prepared by the mixing Reagent A and B in a 50:1 ratio. A standard curve was prepared by employing bovine serum albumin as the protein standard, across a concentration range of 0.125-2 mg/mL. A total of 5 µL of the purified and concentrated protein sample was added to 1 mL of working reagent, and incubated for 30 min at 37°C. The protein sample was cooled to room temperature for 5 min, prior to absorbance measurement at 562 nm using a 6305 UV/Vis spectrophotometer (Jenway, UK). Note that appropriate dilution of the protein sample was carried out when the measured absorbance exceeded the standard curve range.

The final concentration of the purified and concentrated ZipA and FtsA was also estimated based on the A280 (absorbance at 280 nm) method using a NanoDrop® ND-

1000 spectrophotometer (Thermo Scientific, UK) and found to correspond the values obtained via the BCA method.

2.12 Size exclusion chromatography for ZipA and FtsA

Upon immobilised metal affinity purification (IMAC) purification, the concentrated ZipA or FtsA proteins in SMALP were subjected for further purification using size exclusion chromatography (SEC) prior to lipidomic analysis. The SMALP-proteins were loaded onto a Superdex® 200 Increase 10/300 column (GE Healthcare, USA) equilibrated with the SEC buffer (50 mM Tris-HCl, 150 mM NaCl, 10% w/v glycerol, pH 8), operated on a ÄKTA^{TM}purifier protein purification system (GE Healthcare, USA) at a flow rate of 0.5 mL/min. Fractions of 500 µL were collected. Note that the SEC purification of SMALP-ZipA and FtsA was conducted by Dr. Sarah Lee, Dr. Naomi Pollock and Stephen Hall (University of Birmingham). The purity of the SMALP-ZipA and SMALP-FtsA proteins used in the lipidomic experiments can be observed from the representative SDS-PAGE gel images of the purified SMALP proteins (Appendix B and C).

2.13 Preparation of *E. coli* membrane controls

A 10 mL overnight starter LB culture of transformed *E. coli* BL21(DE3) cells harbouring the plasmid encoding for ZipA or FtsA was used to inoculate 500 mL LB in 2 L non-baffled Erlenmeyer flasks supplemented with 100 µg/mL ampicillin. The *E. coli* cells were incubated at 37°C, 180 rpm until OD_{600} around 0.6-0.8. Protein overexpression was either induced by the addition of IPTG (induced control) or uninduced (nil IPTG - uninduced control) with concurrent reduction of incubation temperature to 25°C for overnight incubation. The *E. coli* cells were harvested by centrifugation at 4000 rpm (3000 x *g*) in a Beckman Coulter JLA 10.500 rotor for 15 min at 4°C. The *E. coli* cell pellets were washed with 20 mL PBS and centrifuged at 4000 rpm (3000 x *g*) in a Beckman Coulter JLA 10.500 rotor for 15 min at 4°C. The washed pellets were stored at -20°C until further use.

Thawed *E. coli* cell pellets were resuspended in 50 mL resuspension buffer A (50 mM Tris-HCl, 2 mM EDTA, 5% w/v glycerol, pH 8) supplemented with one Pierce^{TM} Protease Inhibitor Tablet, EDTA-free (Thermo Fisher Scientific, USA) using a Potter-Elvehjem homogeniser. The resuspended *E. coli* cells were subjected to cell disruption

using the Emulsiflex-C3 Cell Disruptor (Avestin, Canada) for four passes at 40 kpsi. Upon cell disruption, the flow through was centrifuged at 10,000 rpm (12,000 x g) in a Beckman Coulter JA 20 rotor for 30 min at 4°C. For subsequent membrane preparation using ultracentrifugation, the resulting supernatant was centrifuged at 40,000 rpm (100,000 x *g*) in a Beckman Coulter 70.1 Ti rotor for 45 min at 4°C. The resulting *E. coli* membranes were resuspended in membrane resuspension solubilisation buffer (50 mM Tris-HCl, 500 mM NaCl, 10% w/v glycerol, pH 8) at a wet membrane pellet weight of 80 mg/mL for subsequent membrane solubilisation using the 2:1 SMA copolymer (5% w/v) at equal volume. The *E. coli* membranes with the SMA copolymer were incubated for 2 h at room temperature on a roller mixer. The solubilised *E. coli* membrane was centrifuged at 50,000 rpm (100,000 x *g*) in a Beckman Coulter TLA 120.2 rotor for 1 h at 4°C and the membrane pellets were used for subsequent lipidomic analysis.

2.14 Circular dichroism spectroscopy

CD spectra were collected in the region of 180-300 nm using a J-815 Spectrophotometer (JASCO, Japan) and a 1 mm path length quartz cuvette containing 200 µL protein sample at room temperature. Each spectrum was collected with a data pitch of 0.1 nm, at a bandwidth of 2 nm, and an average of 32 scans per measurement. The spectrum for the buffer was used for background subtraction.

For concentration-independent comparison of CD spectra, the measured ellipticities (θ) were converted to the molar differential extinction coefficient ($\Delta\varepsilon$) using the formula below.

$$\Delta\varepsilon = \theta \text{ x } \frac{0.1 \text{ x MRW}}{\text{P x conc x } 3298}$$

Note that mean residue weight (MRW) = M/*N*-1, whereby M = molecular mass of protein in Da; *N*-1 = number of amino acids – 1 or number of peptide bonds. For the recombinant PgpB, the MRW is 30087.37/262-1 ≈ 115.28, which lies is in the normal MRW range of 110±5 Da (Kelly *et al.*, 2005).

2.15 Transmission electron microscopy

A total of 5 µL of SMALP-PgpB (0.1 mg/mL) was applied to glow-discharged carbon-coated copper grids and left to adsorb for 1 min. The excess protein sample was blotted off with filter paper. The grids were then stained with 5 µL 2% uranyl acetate solution for 2 min. The excess stain was blotted off with filter paper, followed by air-drying for 2 min. Electron micrographs were recorded on a JEOL 2010F field emission transmission electron microscope (JEOL, Japan) operating at 200 kV. For size determination, individual particles were measured using the image processing package Fiji (Schindelin *et al.*, 2012). Note that the transmission electron microscopy (TEM) images of SMALP-PgpB were acquired with the help of Dr. Michael Baker and Mary Halebian (University of Warwick).

2.16 Microscale fluorescent thermal stability assay

The microscale fluorescent thermal stability assay was conducted based on Sonoda *et al.* (2011) using the 7-Diethylamino-3-(4-maleimidophenyl)-4-methylcoumarin (CPM) dye, also known as the CPM assay. A total of 1 µL of the purified SMALP-PgpB (5.1 mg/mL) or DDM-PgpB (15.1 mg/mL) was added to 150 µL SMALP buffer (50 mM Tris-HCl, 500 mM NaCl, 10% w/v glycerol, pH 8) or DDM buffer (20 mM Tris-HCl, 1 mM MgCl2, 20 mM βME, 500 mM NaCl, 10% w/v glycerol, 0.2 % v/v DDM, pH 7.5) respectively in a 96-well black walled Nunc™ plate (Thermo Fisher Scientific, USA). The CPM dye (Thermo Fisher Scientific, USA) at 4 mg/mL in dimethyl sulfoxide (DMSO) was diluted 100-fold in the respective buffers and 3 µL of the diluted CPM dye was added to the protein sample. Fluorescence measurement was obtained using a CLARIOstar® multimode microplate reader (BMG LabTech, Germany) over 5 h with a 5-min time interval (total 60 cycles) at 40°C. The fluorescence setting was set at 40 flashes per well, excitation wavelength: 387 nm; emission wavelength: 463 nm, both at a bandwidth of 15 nm. Note that the CPM assay was conducted by Dr. Deborah Brotherton (University of Warwick).

2.17 Enzyme-coupled phosphate release assay

The assay was based on the enzyme-coupling mechanism of 7-Methyl-6-thioguanosine (MESG) and purine nucleoside phosphorylase (PNP) from Webb (1992) and the scheme is depicted in Figure 2.1. In principle, PNP converts MESG (strong absorbance at 330 nm, pH 7.6) to 7-Methyl-6-thioguanine (with absorbance shift to 355nm) in the

presence of phosphate ions, which can be monitored spectrophotometrically to track the phosphate release reaction in real time. Absorbance at 360 nm was selected to monitor the phosphate release reaction as a compromise between maximising the change in absorbance during the reaction and minimising the initial absorbance of the reaction mixture in the cuvette. The change in extinction coefficient at 360 nm, pH 7.6 is 11000 $M^{-1}cm^{-1}$ (Webb, 1992).

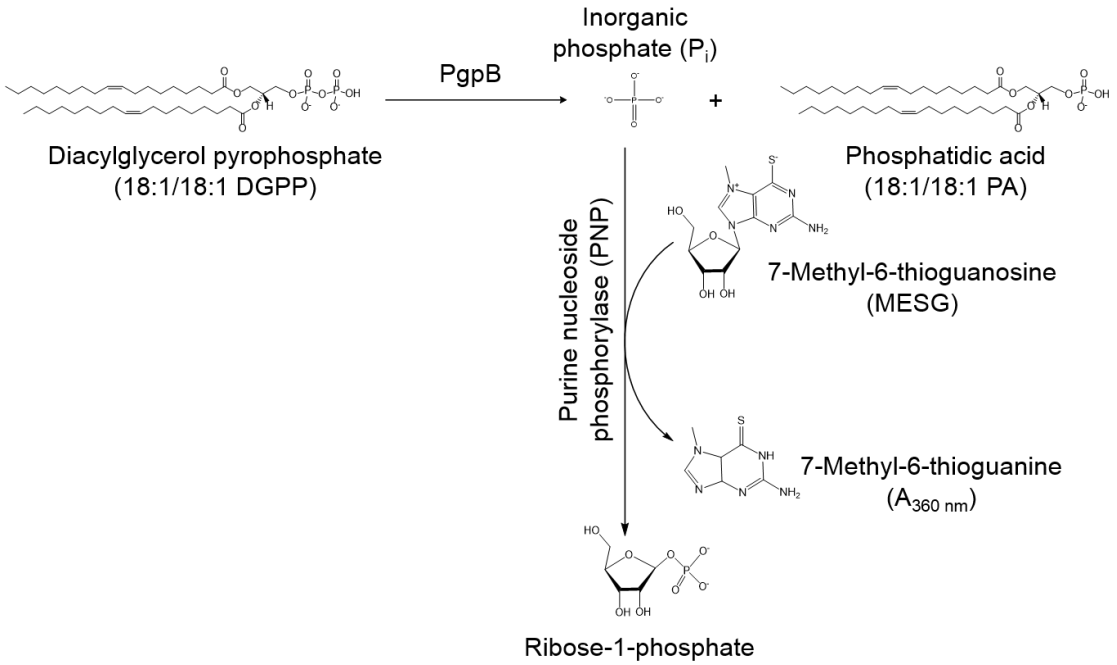

Figure 2.1 Continuous enzyme-coupled phosphate release assay for *in vitro* characterisation of PgpB activity. The reaction is initiated with the addition of PgpB into the quartz cuvette and the reaction is followed in real-time through the changes in absorbance at 360 nm.

All the reagents listed in Table 2.3 (except PgpB in SMALP or DDM) were pipetted into a 10 mm path length quartz cuvette and mixed well by repeated gentle pipetting. The background absorbance at 360 nm was monitored until a flat baseline was obtained. PgpB was then added to initiate the dephosphorylation reaction, while monitoring the absorbance change at 360 nm using a Cary® 100 Bio UV/Vis spectrophotometer (Varian Instruments, USA), operating at 37°C.

Table 2.3 Typical assay components for the enzyme-coupled phosphate release assay.

Stock concentration	Reagent	Final concentration	Volume (µL)
5X	Assay buffer	1X	40
1 mM	MESG	200 µM	40
140 or 163 U/mL	PNP	1U	7 or 6
-	Sterile water	-	to 200
5 mM	18:1 DGPP (Avanti Polar Lipids, USA)	100-400 µM	8
40 µM	PgpB	1 µM	5

Note that the 1X Assay buffer for SMALP-PgpB is 20 mM Tris-HCl, 150 mM NaCl, 0.1% w/v DDM, pH 7.5; for DDM-PgpB is 20 mM Tris-HCl, 150 mM NaCl, 2 mM βME, 0.12% w/v DDM, pH 8. The substrate - 18:1 DGPP was dried down under a gentle stream of nitrogen gas, then resuspended in 5 µL 0.1% w/v DDM for addition into the quartz cuvette.

2.18 de-SMALP PgpB with divalent metal cation

In order to release PgpB from SMALP, 0.5% w/v DDM was added to 1 mL of 2 µM SMALP-PgpB to create a micellar environment for subsequent reconstitution of the proteins upon de-SMALP. $MgCl_2$ was at added approximately 10 mM to disrupt the polymer-protein interaction, *i.e.* to de-SMALP. Three other concentrations of DDM at 1%, 1.5%, 2% were also tested for this divalent metal cation-based de-SMALP treatment. Upon incubation for 30 min at 4°C on a roller mixer, the protein samples were centrifuged at 50,000 rpm (100,000 x *g*) in a Beckman Coulter TLA 100.3 rotor for 1 h at 4°C. The supernatant and pellet fraction were subjected to SDS-PAGE analysis.

Based on the abovementioned divalent metal cation-based de-SMALP trials, 2% w/v DDM was selected to reconstitute the de-SMALP PgpB upon treatment with 10 mM $MgCl_2$. In practice, 2% w/v DDM was added to 100 µL of 40 µM SMALP-PgpB, prior to the addition of 10 mM $MgCl_2$ to de-SMALP. Upon incubation for 30 min at 4°C on a roller mixer, the sample was centrifuged at 56,000 rpm (130,000 x *g*) in a Beckman Coulter TLA 100.3 rotor for 1 h at 4°C. The supernatant containing the de-SMALP PgpB (now in DDM micelles) was subsequently subjected to biophysical and biochemical analyses. Note that in the abovementioned enzyme-coupled phosphate release assay, the 1X assay buffer for de-SMALP PgpB is 20 mM Tris-HCl, 150 mM

NaCl, 10 mM βME, 0.6% w/v DDM, pH 8. The lipid substrate - 18:1 DGPP was dried down under a gentle stream of nitrogen gas, then resuspended in 0.1% w/v DDM (5 µL for 100 and 200 µM substrate; 10 µL for 400 µM substrate) for addition into the quartz cuvette of 10 mm path length.

2.19 Lipidomic analysis

2.19.1 Preparation of internal standard mixture

The three synthetic phospholipids (Avanti Polar Lipids, USA) selected for the lipidomic analysis as internal standards (IS) are listed in Table 2.4.

Table 2.4 Synthetic phospholipids used in the lipidomic analysis as internal standards.

Phospholipid	Stock concentration	Molecular weight (Da)
PE 12:0/13:0 (24:0)	17.02 µM (10.11 µg/mL)	593.77
PG 12:0/13:0 (24:0)	16.68 µM (10.42 µg/mL)	624.78 (as ammonium salt)
CL 14:1/14:1/14:1/15:1 (57:4)	86.14 µM (114.24 µg/mL	1281.66 (as ammonium salt)

For both the PE 12:0/13:0 and PG 12:0/13:0 IS, 2 x 500 µL aliquots (5 µg each) were obtained and dried under a gentle stream of nitrogen gas. The CL14:1/14:1/14:1/15:1 IS was diluted down to 100 µg/mL with the addition of 140 µL of MeOH supplemented with 0.005% w/v butylated hydroxytoluene (BHT) to the stock solution (114.24 µg/mL). Upon dilution, 50 or 150 µL (5 or 15 µg) of the diluted CL IS was added to the PE and PG IS (5 µg each) to make up of the IS mixture. The IS mixture was dried under a gentle stream of nitrogen gas, then reconstituted in 500 µL MeOH (with 0.005% w/v BHT) to make up 30 or 50 µg/mL stock IS mixture. A loading guide for LC-MS based on the different concentration of stock IS mixture is listed in Table 2.5.

Table 2.5 Lipid loading guide for LC-MS.

Stock IS concentration (µg/mL)	LC load in 10 µL (ng)
1000	10000
100	1000
10	100
1	10
0.1	1

2.19.2 Preparation of quality control sample

The three synthetic phospholipids (Avanti Polar Lipids, USA) selected for the lipidomic analysis as quality control sample are listed in Table 2.6.

Table 2.6 Synthetic phospholipids used in the lipidomic analysis as quality control sample.

Phospholipid	Abbreviation	Molecular weight (Da)
PE 16:0/18:1 (34:1)	POPE	717.996
PG 16:0/18:1 (34:1)	POPG	770.989 (as sodium salt)
CL 18:1/18:1/18:1/18:1 (72:4)	TOCL	1501.959 (as disodium salt)

Note that all the double bond on the oleic acid is on the *cis*-9 (9Z) position.

Firstly, 25 mg of 1-Palmitoyl-2-oleoyl-*sn*-glycero-3-phosphoethanolamine (POPE) and 1-Palmitoyl-2-oleoyl-*sn*-glycero-3-phospho-(1'-*rac*-glycerol) (POPG) were dissolved individually in 5 mL 9:1 v/v MeOH:$CHCl_3$ and aliquoted into 500 µL (2.5 mg) fractions in Teflon-capped amber glass vials for storage at -20°C. Similarly, 25 mg of 1',3'-Bis[1,2-dioleoyl-*sn*-glycero-3-phospho]-*sn*-glycerol, also known as 1,1',2,2'-Tetraoctadecenoyl cardiolipin (TOCL) was dissolved in 5 mL 1:1 v/v MeOH:$CHCl_3$ and aliquoted into 500 µL (2.5 mg) fractions in Teflon-capped amber vials for storage at -20°C. Note that unsaturated lipids are difficult to weigh accurately due to their hygroscopic nature (Goddard *et al.*, 2015), thus all 25 mg of each of the synthetic phospholipid standard was made up into stock solution prior to aliquoting for storage. A phospholipid mixture at 3 mg/mL was prepared by mixing 200 µL POPE, POPG, and TOCL (1 mg each) and then made up to 1 mL with 400 µL 9:1 v/v MeOH:$CHCl_3$. The phospholipid mixture was vortexed and sonicated in ice bath to mix well. The phospholipid mixture was diluted 100-fold in the starting LC-MS solvent to serve as QC sample to detect any retention time drift or drop in MS signal intensity over the prolonged LC-MS runs (Cajka and Fiehn, 2014; Tiwari and Tiwari, 2010; Vaz *et al.*, 2014). Alternatively, the phospholipid mixture was diluted exponentially (from 100 ng to 0.039 ng) for limit of quantification (LoQ) determination.

2.19.3 Lipid extraction

The phospholipid IS mixture (40-100 µL) was added to the purified protein samples (in SMALP or DDM) or *E. coli* membranes prior to lipid extraction based on a modified

Folch method (Reis *et al.*, 2013). The general lipid extraction scheme is depicted in Figure 2.2. Firstly, 200 µL ice-cold MeOH (supplemented with 0.005% w/v BHT) was added to 400 µL sample containing IS, followed by 400 µL ice-cold $CHCl_3$ (using a 1 mL Hamilton syringe), and lastly 150 µL ice-cold ultrapure water. The sample was vortexed for 20 s and sonicated in ice bath for 15 min, after each solvent addition to facilitate rigorous mixing and extraction. The sample was then centrifuged at 13,000 rpm (16,000 x g) for 5 min at 4 °C using the Eppendorf® 5418R microcentrifuge to achieve phase separation. The lipid-containing (lower) organic layer was collected and the remaining aqueous phase was subjected to a second extraction by adding 400 µL ice-cold $CHCl_3$. The sample was centrifuged again at 13,000 rpm (16,000 x g) for 5 min at 4 °C to achieve phase separation and the organic layer was collected. The resulting lipid extract was dried under a gentle stream of nitrogen gas and reconstituted in 9:1 v/v MeOH:$CHCl_3$, followed by appropriate dilution for subsequent lipidomic analysis. Note that the denatured proteins and SMA copolymer can form an insoluble pellet between upper and lower layers upon centrifugation, in which mild acidification of the sample using 1-2 mM HCl can be employed to aid in the dissolution of this insoluble material.

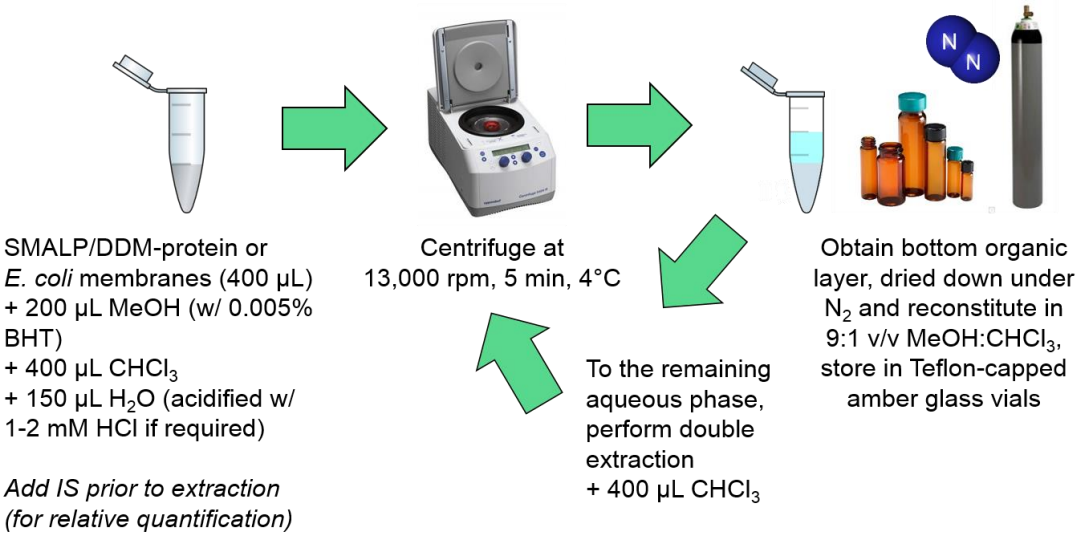

Figure 2.2 The lipid extraction protocol for the membrane proteins purified in SMALP or DDM, or *E. coli* membranes based on a modified Folch method.

For extraction efficiency verification, natural phospholipid samples (Sigma-Aldrich, UK) were used. For egg yolk PG and bovine heart CL, 100 µL of each of the 1 mg/mL

stock was dried under a gentle stream of nitrogen gas and resuspended in 200 µL ice-cold ultrapure water for lipid extraction separately as described above. For egg yolk PC and soybean PE, 300 µL PC was mixed with 300 µL PE (both of 1 mg/mL stock) with rigorous vortexing for 20 s and sonication in ice bath for 15 min. 200 µL PC/PE mixture (1 mg/mL) was diluted 2-fold by the addition of 200 µL buffer (50 mM Tris-HCl, 500 mM NaCl, 10% w/v glycerol, pH 8) prior to lipid extraction as described above. The LC-MS intensities for each class of phospholipid were compared against the non-extracted controls (at the same concentration) to examine the extraction efficiency for each phospholipid class.

2.19.4 Direct infusion MS

A 250 µL Hamilton syringe (2.3 mm inner barrel diameter) was flushed with MeOH for five times to minimise carry over from the previous sample. Similarly, the connecting polyetheretherketone (PEEK) tubing was flushed five times with MeOH and then with the positive (9:1 v/v MeOH:10% formic acid) or negative (9:1 v/v MeOH:10 mM ammonium acetate) ESI solvent for another two to three times. A QTRAP® 5500 hybrid triple quadrupole/linear ion trap mass spectrometer with a with a Turbo V™ ion source (AB Sciex, UK) was utilised. A flow rate of 20 µL/min was used to examine any carry over on the mass spectrometer by running an enhanced mass spectrometry (EMS) survey scan with dynamic fill time (DFT) over 10-15 min. In the EMS mode, there was no selection of precursor ions in the first quadrupole mass filter, and all the ions at different *m/z* were scanned and detected at the linear ion trap (LIT) which acts as the mass analyser. The instrument parameters were as follows: curtain gas: 35 psi, ion spray voltage: +5.5 kV (positive ion mode) or -4.5 kV (negative ion mode); temperature: 150°C; nebuliser gas (GS1): 13 psi; auxiliary/turbo gas (GS2): 0 psi; declustering potential: 50 V; entrance potential: 10 V; collision energy: 10 eV. The intensities of the solvent ions and the stability of the electrospray were examined prior to applying the lipid samples. The flow rate was reduced to 10 µL/min when characterising the lipid samples.

2.19.5 Tandem MS

For the precursor ion scan (PIS) mode, the Q3 quadrupole of the QTRAP® 5500 mass spectrometer was set to transmit only ions of *m/z* value of a selected fragment, *e.g.* 184 Da for PC headgroup in positive ion mode, while the Q1 quadrupole performs the

survey scans over the pre-selected *m/z* range (400-1000 Da). In contrast, both Q1 and Q3 quadrupoles were programmed to scan in a synchronised fashion with an offset of the desired neutral loss (NL), *e.g.* 141 Da for PE headgroup in positive ion mode, with the lower *m/z* value applied to the Q3 quadrupole. For enhanced product ion (EPI) mode, the precursor ions to be fragmented by collision induced dissociation (CID) was selected in the Q1 quadrupole (with a *m/z* window of 1 Da wide) and the resulting MS/MS fragments (*m/z* 100-1000) were scanned in Q3/LIT. Appropriate collision energy (typically in the range of 30-50 eV) was set for CID in each of the tandem MS-based scans.

2.19.6 LC-MS/MS

Firstly, 10 µL of reconstituted lipid extract was injected onto a Luna® C8(2) 100 Å column, 150 mm (length) x 1 mm (internal diameter), particle size: 3µm (Phenomenex, USA) at a flow rate of 50 µL/min. Lipid separation was achieved using a LC gradient of the following mobile phases: tetrahydrofuran (THF):MeOH:water (supplemented with 10 mM ammonium acetate; A: 3:2:5 v/v/v; B: 7:2:1 v/v/v on the Ultimate^{TM} 3000 HPLC system (Dionex, USA). The mobile phases were de-gassed in an ice sonicating bath to minimise solvent evaporation for 10 min prior to use. The LC gradient was formulated as follows: 40% B for 4 min, 40% B to 60% B over 6 min, 60% B to 100% B over 15 min, and hold 100% B for 5 min, 100% B to 40% B over 2 min, then re-equilibrate to the 40% B over 13 min, with a total gradient time of 30 min in a 45 min LC run. A QTRAP® 5500 hybrid triple quadrupole/linear ion trap mass spectrometer with a with a Turbo V™ ion source (AB Sciex, UK) was utilised. The instrument parameters were described as per Section 2.19.4. Information-dependent acquisition (IDA) was employed to obtain MS/MS spectra during the LC run for structural characterisation of the lipid species. In practice, a general survey scan in the EMS mode (with DFT), at *m/z* 400-1000 Da was used to trigger IDA on one to two most intense ion peak(s) based on the following selection criteria: over *m/z* of 400 Da, 1000 cps, and 20 s; maximum occurrence of 2; mass tolerance of 250 mDa; excluding isotopes within 4 Da. This is followed by EPI scans (using the LIT) with a collision energy of 50 eV (positive ion mode) or 45 eV (negative ion mode).

LC-MS/MS analysis in the negative ion mode was also performed on a TripleTOF® 5600 hybrid quadrupole time-of-flight mass spectrometer equipped with the same

Turbo V™ ion source (AB Sciex, UK). The instrument parameters were as follows: curtain gas: 50 psi, ion spray voltage floating: -4.5 kV; temperature: 150°C; nebuliser gas (GS1): 13 psi; auxiliary/turbo gas (GS2): 0 psi; declustering potential: 50 V; entrance potential: 10 V; collision energy: 10 eV; accumulation time: 0.49 s, multichannel analysis (MCA): disabled. IDA was similarly employed to obtain MS/MS spectra during the LC run for structural characterisation of the lipid species. A general survey scan (*m/z* 500-1600) was used to trigger IDA on the most intense peak based on the following selection criteria: over *m/z* of 500 Da, 150 cps, and 20 s; maximum occurrence of 2; mass tolerance of 50 mDa; excluding isotopes within 4 Da; maximum accumulation of 2 s; collision energy: 45 eV; collision energy spread: 0 eV; ion release decay: 67 ms; ion release width: 25 ms.

In order to avoid sample carry over on the LC column, blank samples comprised of LC starting solvent were inserted between the lipid samples to access the background during initial method development (Cajka and Fiehn, 2014; Spickett *et al.,* 2011). Essentially, the sample carry over should be $\leq 2\%$. Subsequently, the inclusion of blank samples was also incorporated into the LC-MS runs. Care was taken to limit solvent evaporation (which can affect retention time) throughout the entire LC-MS run by ensuring tight connection on all HPLC fittings and adequate purging and priming of the HPLC pumps with every solvent changeover and/or replenishment.

2.19.7 Data analysis

Mass spectra inspection and data extraction involving relevant peak integration with Gaussian smoothing width of 0-2 points on each extracted ion chromatogram (XIC) were performed manually using the PeakView® 2.2 software (AB Sciex, UK). XICs display the extracted ion intensity of target analyte (specific *m/z* under a narrow mass tolerance window) from the entire LC-MS run, by plotting the total intensity of the target analyte at every LC time point. The identification and assignment of each phospholipid species and corresponding molecular structures were achieved with high confidence via the IDA LC-MS/MS analysis with subsequent data matching to the LIPID MAPS Structure Database - http://www.lipidmaps.org/data/databases.html (Sud *et al.,* 2007).

A two-step normalisation approach was exploited with the aim to remove systematic variations between the experimental conditions that are unrelated to biological differences. Firstly, the peak intensity for each phospholipid species was normalised against the peak intensity for the corresponding class-specific IS. The normalised data was then normalised against the total phospholipid ion intensity per sample/replicate or amount of protein for which lipid extraction was performed, in order to facilitate cross-sample comparison. In essence, the relative abundances of all the phospholipid species were determined by assuming the same instrument response factor for all the molecular species belonging to a given class.

2.20 Instrument optimisation

2.20.1 Calibration of ion optics

The QTRAP® 5500 mass spectrometer was calibrated periodically via direct infusion of appropriate tuning solutions, *i.e.* polypropylene glycol (PPG) 2 x 10^{-7} M (positive ion mode) or PPG 3 x 10^{-5} M (negative ion mode) at a flow rate of 10 µL/min to verify the mass accuracy. Both Q1 and Q3 quadrupoles were both calibrated at 200, 1000, and 2000 Da/s. The LIT was calibrated at 250, 1000, 10000 Da/s using the 100-fold diluted ES Tuning Mix (AB Sciex, UK). The instrument parameters during calibration were as follows: curtain gas: 35 psi, ion spray voltage; 5.5 kV (positive ion mode) or -4.5 kV (negative ion mode); temperature: 150°C; nebuliser gas (GS1): 15-20 psi; auxiliary/turbo gas (GS2): 0 psi; declustering potential: 50 V; entrance potential: 10 V; collision energy: 10 eV.

The TripleTOF® 5600 mass spectrometer was calibrated in the negative ion mode via direct infusion of either taurocholic acid (2 µg/mL) for a two-point calibration (*m/z* 79.956817 and 514.283851) or the 1000-fold diluted ESI Tuning Mix G2421A (Agilent Technologies, USA) for a four-point calibration with a larger *m/z* range: *m/z* 112.985590, 601.978980, 1033.988110, and 1633.949786, both in the MCA mode at a flow rate of 10 µL/min until a mass accuracy of < 5 ppm. The instrument parameters during calibration were as follows: curtain gas: 25 psi, ion spray voltage floating: -4.5 kV; temperature: 0°C; nebuliser gas (GS1): 12 psi; auxiliary/turbo gas (GS2): 0 psi; declustering potential: 50 V; collision energy: 10 eV.

2.20.2 Cleaning of LC column

The LC column was cleaned as per recommendation by the manufacturer (Phenomenex, USA) when significant increase in column back pressure was observed. The flow rate was set to half of the typical flow rate used, *i.e.* 25 µL/min. The first wash consisted of 95:5 v/v water:ACN; second wash of THF; and a third wash of 95:5 v/v water:ACN. All the washes were performed for 1-2 h. The column was then equilibrated to the starting LC solvent at 25 µL/min for 1 h prior to use. Note that back flushing of the column can be carried out if significant blockade of the LC column was suspected.

2.21 Univariate and multivariate analysis

2.21.1 Student's *t*-tests

Single and multiple *t*-test(s) were implemented in Prism® 7 (GraphPad Software, USA). For single unpaired *t*-test (parametric test with Gaussian distribution), both populations were assumed to have the same standard deviation. A statistical significance level of $\alpha = 0.05$ was employed. Multiple *t*-tests were conducted by analysing one unpaired *t*-test per row (phospholipid species), by assuming that all rows were sampled from the populations with the same scatter. A statistical significance level, $\alpha = 0.05$ was employed with Holm-Šídák correction for multiple comparisons.

2.21.2 One-way ANOVA

One-way analysis of variance (ANOVA) with Tukey's multiple comparisons test with a single pooled variance and assumed Gaussian distribution was implemented in Prism® 7 (GraphPad Software, USA). A statistical significance level, $\alpha = 0.05$ was employed.

2.21.3 Principal component analysis

Principal component analysis (PCA) was implemented via the PLS_Toolbox 5.2 (Eigenvector Research, USA) in MATLAB® 7.8.0 (R2009a) (MathWorks, USA) using mean-centred data.

Chapter 3: Method Development for the Characterisation of Local Lipid Environment of Bacterial Membrane Proteins

3.1 Background

One key advantage of employing the SMALP approach to study membrane proteins is the co-extraction of lipid moieties surrounding the target protein during the extraction and solubilisation process. It creates an attractive avenue to study the local (native) lipid environment of membrane proteins in relation to their structural and functional role due to this preservation of native protein-lipid interactions (Dörr *et al.*, 2016; Lee *et al.*, 2016a). Besides examining protein-lipid interactions in terms of potential influence on protein activity in the presence of specific lipids, the notion of specific lipid microdomains serving as spatial cues for targeted protein localisation within the cell to perform their function in the right spatiotemporal manner can be investigated.

It was found in a survey through published literatures to date (June 2017), only about a third (out of slightly over 20 primary SMALP publications) had reported some degree of lipid analysis. This is an obvious analytical area to address, calling for the development of robust methods to study the co-extracted membrane lipidome when exploiting the SMALP approach for membrane protein studies, which will be refer to as 'SMALP lipidomics' for the remainder of the thesis.

3.1.1 SMALP publications with lipid analysis

Long *et al.* (2013) first reported the extraction of functional mitochondrial membrane complexes from *Saccharomyces cerevisiae* with a 3:1 SMA copolymer. Based on the size and dimension of the discoidal particle of their SMALP-encapsulated complex IV holoenzyme, each disc was estimated to accommodate approximately 100 lipids per leaflet for a single copy of complex IV. Using TLC, they showed the presence of major mitochondrial lipids, *i.e.* PC, PE, and CL in the SMALPs (Long *et al.*, 2013). Similarly, with the use of a 3:1 SMA copolymer, Smirnova *et al.* (2016) extracted the multisubunit enzyme cytochrome oxidase (Cyt*c*O) from yeast mitochondria. TLC analysis revealed the presence of all the major inner mitochondrial membrane phospholipids, *i.e.* PC, PE, CL, PS and phosphatidylinositol. Each SMALP-Cyt*c*O disc was estimated to contain 100 lipids based on the cross-sectional information obtained with negative stain TEM,

which showed a surrounding ring of lipids of 1.5-2.5 nm from the enzyme. In comparison, detergent extraction using *n*-dodecyl β-D-maltoside (DDM) resulted in the loss of the regulatory proteins Rcf1 and 2, while SMALP extraction had retained both the regulatory proteins with Cyt*c*O (Smirnova *et al.*, 2016).

Postis *et al.* (2015) structurally characterised a secondary multidrug transporter, AcrB from *E. coli* that was extracted using a 2:1 SMA copolymer in its native trimeric state (~360 kDa) with negative stain TEM. Phosphate quantification revealed approximately 40 phospholipids per AcrB trimer. Using a similar phosphate quantification approach, Bresch *et al.* (2017) also reported approximately 32-35 lipids per dimer of CzcD, a zinc diffusion facilitator protein from *Cupriavidus metallidurans* CH34 that had been overexpressed in *E. coli* cells and extracted with the 2:1 and 3:1 SMA copolymers. Swainsbury *et al.* (2014) studied the photoreaction centre, an integral membrane protein-pigment complex of the purple bacterium - *Rhodobacter sphaeroides,* extracted with a 2:1 SMA copolymer. Increased stability of the photoreaction centre within SMALP was observed as compared to the detergent-solubilised counterparts. Based on TLC analysis, PE, PC, CL, PG, and sulphoquinovosyl diacylglycerol were identified as the main lipids, in similar proportion to the native membrane of *R. sphaeroides.* Notably, the photoreaction centre solubilised by the detergents - *N*,*N*-Dimethyldodecylamine *N*-oxide (LDAO) and DDM failed to show any lipid (even at five-fold higher protein concentration) upon TLC investigation, indicating that the lipids could have been stripped below detection limit by the detergent micelles. Approximately 150 lipids were estimated per photoreaction centre by phosphate quantification, which corresponded to an average of three layers of lipids surrounding the photoreaction centre within the disc (Swainsbury *et al.*, 2014).

Dörr *et al.* (2014) studied the recombinant *Streptomyces lividans* tetrameric potassium channel KcsA, overexpressed in *E. coli* and extracted using a 2:1 SMA copolymer. They discovered that SMALP-KcsA was more stable, both thermally and upon prolonged storage at 4°C, as compared to the DDM-solubilised counterpart. TLC analysis identified the lipids co-extracted with the protein from the host *E. coli* membrane, showing the three major phospholipids - PE, PG and CL. Interestingly, the SMALP-KcsA demonstrated a higher amount of the anionic lipids, PG and CL compared the total membrane extract control, corroborating the established preferential

interaction of KcsA with anionic lipids (Alvis *et al.*, 2003; Demmers *et al.*, 2003; Marius *et al.*, 2008). The fatty acid composition was investigated using GC, showing no specific changes in terms of fatty acid composition for SMALP-KcsA vs the membrane control (Dörr *et al.*, 2014).

The *E. coli* Sec translocon was examined by Prabudiansyah *et al.* (2015) using a 3:1 SMA copolymer. With SMALP encapsulation, the SecA ATPase motor protein was co-purified with the SecYEG complex. In contrast, detergent extraction disrupted the interaction of SecYEG with SecA. TLC analysis showed an enrichment of anionic lipids (at the expense of PE) with SMALP-SecYEG when compared to the total membrane extract control, supporting previous reports that anionic lipids are required to activate SecA during protein translocation across the cytoplasmic membrane (Breukink *et al.*, 1992; Ulbrandt *et al.*, 1992). In addition to TLC, they also employed LC-MS to better characterise and quantify the co-extracted membrane lipids. The lipid composition was found to be similar to the total membrane extract, despite the enrichment of anionic lipids seen in the TLC analysis. Consequently, they suggested that the protein-lipid interaction occurs mainly within the lipid headgroup, as no preference for lipids with specific acyl chain length was noted (Prabudiansyah *et al.*, 2015).

The successful isolation of the dynamic metabolon producing the plant defence compound - dhurrin in *Sorghum bicolor* was reported using a 2:1 SMA copolymer (Laursen *et al.*, 2016). They discovered that the catalytic efficiency of the enzyme, CYP71E1 was highly sensitive to anionic lipids, with optimal activity in the presence of 20-30% anionic lipids, matching the observed enrichment of PG (in place of the other two anionic lipids - PS and PI) in the affinity purified SMALP-sorghum microsomes through LC-MS analysis. Two types of LC (RPLC and HILIC) were used in their LC-MS analysis, with ten internal standards covering the different types of membrane lipids (Laursen *et al.*, 2016). Rehan *et al.* (2017) reported the isolation of a human equilibrative nucleoside transporter-1 (hENT1) overexpressed in Sf*9* insect cells using a 2:1 SMA copolymer. Lipid analysis was achieved by direct infusion-based ESI-MS and also GC-MS. A total of 16 PCs and two PEs were detected using class-specific targeted tandem MS scans, *i.e.* PIS 184 and NL 141 for PC and PE lipids respectively due to the noticeable suppression of many lipid peaks from the artefact peaks of the

SMA copolymer (in the absence of LC). Enrichment of long chain PC species and complete exclusion of polyunsaturated PE species were observed for the hENT1-SMALP when comparing the Sf9 membrane controls. GC-MS analysis also confirmed the presence of only saturated and monounsaturated fatty acyl chains in hENT1-SMALP (Rehan *et al.*, 2017).

In summary, it can be observed that phosphate quantification and TLC are commonly utilised for lipid analysis in the surveyed SMALP publications. GC and LC-MS are also gaining popularity in terms of lipid analysis, in particular MS-based techniques. So far, no lipid analysis using NMR or other spectroscopic techniques (*e.g.* Raman or FTIR) have been reported for the membrane proteins isolated in SMALP, most likely due to the relatively low sensitivity of these methods.

3.1.2 SMALP lipidomic method development and evaluation

In view of the clear limitations from other lipid analysis methods, MS was selected as the analytical method of choice for the SMALP lipidomic work in this thesis. In fact, a high sensitivity (low lipid loading requirement), coupled with comprehensive information (headgroup plus fatty acyl chains distribution) obtained for intact lipid profiling are the signatures of a MS-based lipidomic approach. It is the primary aim of the SMALP lipidomic approach to be an unbias profiling of the co-extracted lipidome of bacterial membrane proteins, targeting the key members participating in *E. coli* cell division. Thus, it is pivotal that the MS-based method developed ought to be capable of distiguishing the three major membrane phospholipids in *E. coli*, namely PE, PG and CL.

3.1.2.1 Analytical validation

For a quantitative (bio)analytical method to be reliable and reproducible for the intended applications (especially for biomedical research), it is important to validate key parameters such as accuracy, precision, sensitivity, selectivity, limits of detection and quantification, linearity range, recovery and stability (Sonawane *et al.*, 2014; Tiwari and Tiwari, 2010). Established guidelines from the Food and Drug Administration and European Medicines Agency are normally considered. In terms of sensitivity and selectivity, the use of MS surpasses the other common lipid analysis methods such as TLC and GC, as individual lipid species can be identified by their

unique *m/z*, coupled with characteristic fragmentation patterns upon CID when tandem MS is employed. MS-based lipid analysis also offers the best accuracy and precision, especially with the use of a well calibrated high resolution mass spectrometers, such as when Orbitrap or Fourier transform ion cyclotron resonance instruments are available. In the absence of these high resolution mass spectrometers, tandem MS is an effective alternative for other types of mass analysers such as triple quadrupoles or quadrupole-ion traps using the distinctive MS/MS fragmentaion patterns to accurately assign the lipids species.

In practice, once the robustness and validity of the developed analytical method has been established, a biological sample should only require a single analysis without the need for technical replication (Sonawane *et al.*, 2014; Tiwari and Tiwari, 2010). During method development, the analytical robustness of a method is often evaluated by examining the coefficient of variation, also known as the relative standard deviation (RSD) using the formula below with replicate analysis.

$$RSD = \frac{\sigma}{\mu} \, x \, 100\%$$

Normally, the RSD should be ≤ 20% for the developed analytical method to be robust enough for the intended application, in order to provide the confidence that the variation arising from the samples would be biologically significant and not due to the various technical variations imposed by the analytical method (Sonawane *et al.*, 2014; Tiwari and Tiwari, 2010).

3.1.3 Aim and objectives of chapter

The primary aim of the work described in this chapter was to develop a robust analytical method based on MS for the comprehensive analysis of the local lipid environment of bacterial membrane proteins encapsulated in SMALP. This effort was prompted by both the scarcity of primary literature relating to the direct analysis of local lipid environment of membrane proteins and the inherent advantage of the SMALP technology in the co-extraction of membrane lipidome during the protein isolation process. Much of the information available in terms of protein-lipid interactions in the literature were derived from crystallographic investigations whereby the tight binding

of non-annular lipid(s) to the membrane proteins (upon detergent extraction) still resulted in observable electron density in the crystal structures. Alternatively, mainstream protein-lipid investigations are often conducted by reconstituting the target membrane proteins into different liposomes to probe the biochemical and biophysical behaviours of these proteins using experiemental and/or computational approaches (Jensen and Mouritsen, 2004; Lee, 2011; van den Brink-van der Laan *et al.*, 2004; Yeagle, 2014). SMALP lipidomics is thus proposed to be a useful technique to complement the existing approaches to examine the target membrane protein in its native membrane milieu and to study its protein-lipid interaction.

Firstly, the feasibility of detection of membrane phospholipids co-extracted from SMALP-proteins using a modified Folch method for lipid extraction (Reis *et al.*, 2013) was examined. The identity of the extracted lipids were characterised by direct infusion MS. Once the feasibility of such lipid detection was established, the methodology was further improved by developing a LC-MS/MS method for SMALP lipidomics, with analytical robustness verification including limit of detection, intra- and inter-assay variations, linearity of response, and extraction effciency using known concentrations of synthetic and natural phospholipids.

3.2 Results and discussion

3.2.1 Direct infusion MS evaluation

In order to verify if the modified Folch extraction method (Reis *et al.*, 2013) was suitable to extract the membrane lipids co-extracted with the SMALP-proteins, one of the cell division protein, ZipA (encapsulated in SMALP) was subjected to lipid extraction using this modified Folch method and the resulting lipid extract was examined using direct infusion MS on a triple quadrupole/linear ion trap hybrid mass spectrometer - QTRAP® 5500. This shotgun lipidomic approach was used to evaluate the applicability of the modified Folch method to extract the membrane lipids from SMALP-proteins due to its high throughput nature with shorter MS data acquisition time and it is much simpler to implement than LC-MS-based methods. This modified Folch method was previously applied successfully to the extraction of yeast and mammalian lipids for the studies of lipid peroxidation (Alpesh Thakker, PhD Thesis, Aston University, 2017).

3.2.1.1 General survey scan

This shotgun lipidomic experiment was carried out in both positive and negative ion modes to facilitate the identification and characterisation of phospholipid speices. Using the general survey scan mode, a predetermined *m/z* range (that encompasses the common phospholipid region of *m/z* 650-800) was scanned to search for phospholipid species co-extracted with ZipA in SMALP. The mass spectrum of SMALP-ZipA lipid extract (in the negative ion mode) is depicted in Figure 3.1. The phospholipids were tentatively identified based on the *m/z* of the molecular ion by comparing to the LIPID MAPS online database (Sud *et al.*, 2007). As depicted in Figure 3.1, the most readily detected phospholipid species were from the PE and PG classes, with even and odd *m/z* value respectively. PE 32:1, PE 33:1, PE 34:2, PE 34:1, PE 36:2, PG 32:1, PG 34:1, and PG 36:2 were among the variety of lipid species observed in the SMALP-ZipA lipid extract, comprising of fatty acyl chains ranging from 32-36 carbon atoms, with 1-2 double bonds. No CL species was identified in the SMALP-ZipA lipid extract using this shotgun lipidomic approach. Without tandem MS, no structural information regarding individual fatty acyl chain was available with this general survey scan.

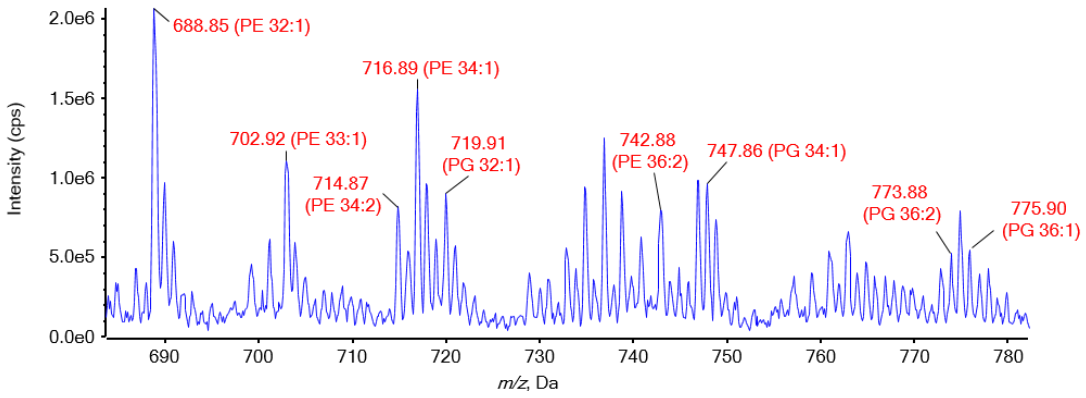

Figure 3.1 Mass spectrum of SMALP-ZipA lipid extract with direct infusion MS in negative ion mode using a general survey scan. A total of five PE and three PG lipid species were identified within the common phospholipid *m/z* range, all as singly deprotonated species $[M-H]^-$.

3.2.1.2 Tandem MS scans

Besides performing a general survey scan, the use of the QTRAP® 5500 also facilitated the use of targeted tandem MS scan modes, for example the frequently used precursor

ion scan and neutral loss scans to increase the instrument selectively for lipid analysis (Brügger *et al.*, 1997; Myers *et al.*, 2011; Spickett *et al.*, 2011). Figure 3.2 depicts the mass spectra of SMALP-ZipA lipid extract using PIS 281 scan in the negative ion mode, targeting the C18:1 fatty acyl moeity (*m/z* 281) on specific phospholipid species and NL 141 scan in positive ion mode, targeting the phosphoethanolamine ($H_2PO_4CH_2CH_2NH_2$) headgroup on PE species, providing a class-specific scan to selectively detect PE lipids. In Figure 3.2 (A), the scan for the C18:1 fatty acyl moiety which a common fatty acid in both prokaryotic and eukaryotic membrane phospholipids had isolated only the PE and PG species harbouring this fatty acid, *i.e.* PE 32:1, PE 34:2, PE 34:1, PE 36:2, PG 34:1, and PG 36:2. On the other hand, the NL 141 scan targeting the PE headgroup had specifically detected this class of lipids in the ZipA-SMALP sample, as depicted in Figure 3.2 (B). This targeted PE scan had identified three further PE species, namely PE 30:0, PE 33:1 and PE 35:1 that were not detected using the abovementioned general survey scan (Figure 3.1). The employment of targeted tandem MS scanning approaches increases the sensitivity of the mass spectrometer to the analytes of interest, which also resulted in better signal-to-noise (S/N) ratio, in other words a cleaner mass spectra, which is evident by comparing the mass spectra of the PIS and NL scans to the general survey scan of SMALP-ZipA lipid extract (Figure 3.1 vs 3.2)

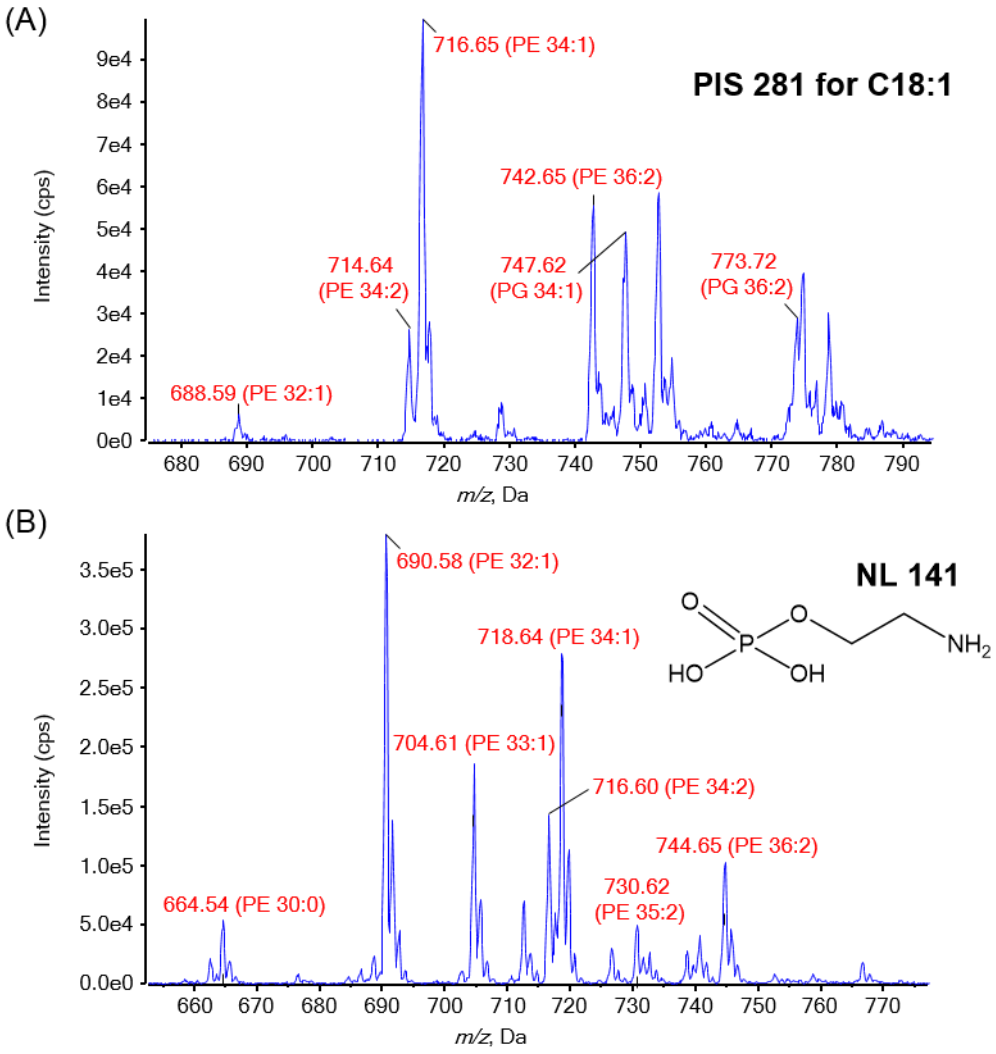

Figure 3.2 Mass spectra of SMALP-ZipA lipid extract with direct infusion MS using PIS and NL scans. (A) PIS 281 scan targeting the C18:1 fatty acyl moeity on the phospholipids in negative ion mode; (B) NL 141 scan targeting the phosphoethanolamine headgroup in positive ion mode, which is characteristic to PE lipids.

Product ion scans (in the negative ion mode) were utilised to structurally characterise the individual phospholipid molecular species (in terms of fatty acyl chain combinations). Figure 3.3 depicts the structural characterisation of PE 34:1, one of the phospholipid found in the ZipA-SMALP lipid extract. This particular lipid species was found to be composed of mainly three structural isomers, *i.e.* PE 16:0/18:1, cy17:0/17:0, and 18:0/16:1, as depicted in Figure 3.3 (A). From the CID fragmentation pattern as shown in Figure 3.3 (B), the different abundance of the isomeric species of PE 34:1 can be determined as follows (in the order of decreasing abundance): 16:0/18:1 > 18:0/16:1

≈ cy17:0/17:0. The peaks at *m/z* 140 and 196 are unique for PE lipids, whereas the fatty acyl peaks were observed at *m/z* 253 (C16:1), 255 (C16:0); 267 (cyC17:0), 269 (C17:0), 281 (C18:1), and 283 (C18:0) as highlighted in Figure 3.3(C). The peaks at *m/z* 434 and 452 are lyso-PE species, and the parent ion peak for PE 34:1 at *m/z* 716 can be observed.

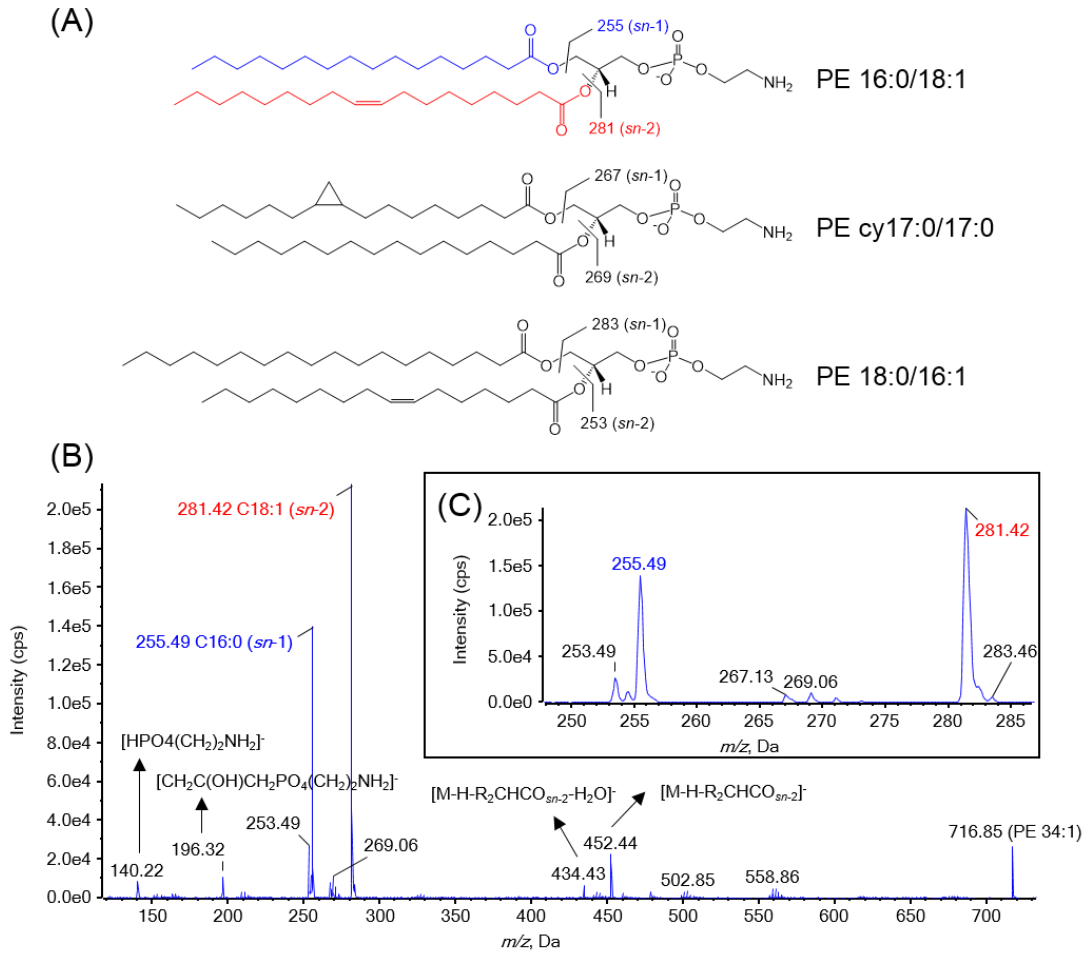

Figure 3.3 Product ion scan in negative ion mode of PE 34:1 (*m/z* 716) found in the SMALP-ZipA lipid extract. (A) Chemical structures of the three main isomeric species of PE 34:1. The molecular species with the highest abundance, *i.e.* PE 16:0/18:1 is highlighted with the C16:0 fatty acid (in blue) at the *sn*-1 position and C18:1 fatty acid (in red) at the *sn*-2 position on the glycerol backbone. (B) MS/MS spectrum of PE 34:1 showing the resulting fragment ion peaks as described in the text, (C) highlighting the fatty acyl combinations of this PE species.

3.2.1.3 Summary of direct infusion MS

The variety of PE and PG lipid species observed in the lipid extract of SMALP-ZipA (Figure 3.1 and 3.2) had supported the applicability of this lipid extraction method for

the analysis of co-extracted membrane lipidome from target SMALP-proteins and demonstrated the power of MS to provide detailed and comprehensive characterisation of the membrane phospholipids. The PE and PG lipids depicted in Figure 3.1 and 3.2 also matched the reported lipid species in a commercial *E. coli* polar lipid extracts using a similar experimental setup to the ones described in this chapter (Ilgü *et al.*, 2014). It is crucial to note that CL, as the minor anionic lipid constituent in *E. coli* membrane (Schlame, 2008) was not observed in the *E. coli* polar lipid extract (Ilgü *et al.*, 2014), as well as the SMALP-ZipA lipid extract. The detection of CL lipids was most likely masked by the other more abundant PE and PG lipids in the sample due to the employment of a shotgun lipidomic approach. It is a well known phenomemon that direct infusion MS experiments can often be hampered by ion suppression and/or enhancement effects by either the matrix (in particular when analysing biological materials), or the more abundant and/or better ionised species in the sample that compete for ionisation. This is due to the lack of a separation step prior to MS analysis in shotgun lipidomic approaches. Consequently, suboptimal ionisation of the lipid of interest can occur, which interfers with the detection of minor lipid species in the sample (Brouwers, 2011; Cajka and Fiehn, 2014; Pati *et al.*, 2016; Vaz *et al.*, 2014).

Given that the primary aim of the SMALP lipidomic approach is the unbias profiling of the co-extracted lipidome of bacterial membrane proteins in SMALP, the use of the SRM/MRM capability on the QTRAP® 5500 has not been discussed. Normally, these types of experiments would be more suited for targeted quantification of a small subset of analytes, rather than permiting a more exploratory global profiling exercise. Upon the evaluation of the modified Folch lipid extraction method using direct infusion MS, the SMALP lipidomic method was further developed to employ a LC-MS/MS approach (described in the next section of this chapter) due to the foreseeable limitations in using a shotgun lipidomic approach.

3.2.2 LC-MS/MS method development

The first step towards the development of a LC-MS method for lipid analysis is to systematically evaluate different LC columns (of different stationary phase chemistries) to find the best column to achieve the desired separation of target analytes. In the context of the work described in the thesis, the LC column selected has to be capable

of separating the three major classes of membrane phospholipids in *E. coli*, namely PE, PG and CL to facilitate their characterisation and quantification.

3.2.2.1 LC column evaluation

The numerous LC columns of different stationary phase chemistries (with the corresponding mobile phase combinations) tested during the development of the LC-MS/MS method are summarised in Table 3.1. During the evaluation of different LC columns, emphasis was placed on HILIC and RP-LC approaches, as they are both frequently employed for LC-MS-based lipidomic studies via ESI coupling.

Table 3.1 LC columns evaluation during LC-MS/MS method development.

LC column	LC condition	Experimental remark
ACE® SIL, HiChrom - Unbonded silica (stationary phase); 150 mm (length) x 3 mm (internal diameter); 3 µm (particle size); 1.06 mL (column volume)	Solvent A: Isopropyl alcohol (IPA)/ACN (1:4 v/v) Solvent B: IPA/20 mM ammonium formate (1:4 v/v) Gradient 1: 5% B for 1 min, 5-8% B over 4 min, 8-15% B over 5 min, 15-20% B over 3 min, 20-25% B over 3 min, 25-35% B over 7 min, hold 35% for 5 min, back to 5% B over 1 min, re-equilibrate at 5% B over 16 min	PG eluted around 3-7 min (too early), PE eluted around 13-15 min, PC eluted around 20-22 min, no information on CL
	Gradient 2: 5% B for 1 min, 5-10% B over 9 min, 10-20% B over 6 min, 20-35% B over 2 min, hold at 35% for 12 min, back to 5% B over 2 min, re-equilibrate at 5% B over 13 min	PG eluted around 5-8 min, CL eluted around 15-16 min, no information on PE
	Flow rate: 300 µL/min	
Synchronis™ HILIC, Thermo Fisher Scientific - Zwitterionic bonded silica (stationary phase), 150 mm (length) x 2.1 mm (internal diameter); 3 µm (particle size); 0.519 mL (column volume)	Solvent A: Isopropyl alcohol (IPA)/ACN (1:4 v/v) Solvent B: IPA/20 mM ammonium formate (1:4 v/v) Gradient: 5% B for 4 min, 5-10% B over 6 min, 10-20% B over 6 min, 20-35% B over 12 min, hold at 35% for 2 min, back to 5% B over 2 min, re-equilibrate at 5% B over 13 min	PG eluted around 2-3 min (too early), PE eluted around 11-12 min, CL eluted around 15 min
	Flow rate: 200 µL/min	

MAbPac™ RP, Thermo Fisher Scientific - Divinylbenzene copolymer (stationary phase); 100 mm (length) x 2.1 mm (internal diameter); 4 µm (particle size); 0.346 mL (column volume)	Solvent A: Water + 5 mM ammonium formate + 0.1% formic acid Solvent B: MeOH + 5 mM ammonium formate + 0.1% formic acid Gradient: 70% B for 4 min, 70-90% B over 11 min, 90-100% B over 5 min, hold at 100% B over 16 min, back to 70% B over 2 min, re-equilibrate at 70% B over 12 min Flow rate: 50 µL/min	PE and PG co-eluted around 30-34 min, cannot detect CL
ProSwift® Monolith RP 4H, Dionex - Ethylvinylbenzene divinylbenzene copolymer (stationary phase); 250 mm (length) x 1 mm (internal diameter); 5.14 µm (particle size); 0.196 mL (column volume)	A: Water + 5 mM ammonium formate + 0.1% formic acid B: MeOH + 5 mM ammonium formate + 0.1% formic acid Gradient 1: 70% B for 4 min, 70-90% B over 11 min, 90-100% B over 5 min, hold at 100% B over 16 min, back to 70% B over 2 min, re-equilibrate at 70% B over 12 min Gradient 2: 90% B for 4 min, 90-100% B over 16 min, hold at 100% B over 16 min, back to 90% B over 2 min, re-equilibrate at 90% B over 12 min Flow rate: 50 µL/min	PG eluted around 22-32 min, CL eluted around 31-32 min, no information on PE CL eluted around 15-19 min, no information on PE and PG

Luna® C18(2), Phenomenex - Octadecyl silane bonded silica (stationary phase); 150 mm (length) x 1 mm (internal diameter); 3 µm (particle size); 0.1178 mL (column volume)	A: Water/ACN (2:3 v/v) + 10 mM ammonium formate + 0.1% formic acid B: ACN/IPA (1:9 v/v) + 10 mM ammonium formate + 0.1% formic acid Gradient: 40% B for 2 min, 40-50% B over 8 min, 50-100% B over 20 min, hold at 100% B over 5 min, back to 40% B over 2 min, re-equilibrate at 40% B over 8 min Flow rate: 50 µL/min	PG eluted around 26-30 min, CL eluted around 34-35 min, no information on PE
Luna® C8(2), Phenomenex - Octyl silane bonded silica (stationary phase); 150 mm (length) x 1 mm (internal diameter); 3 µm (particle size); 0.1178 mL (column volume)	A: Water/ACN (2:3 v/v) + 10 mM ammonium formate + 0.1% formic acid B: ACN/IPA (1:9 v/v) + 10 mM ammonium formate + 0.1% formic acid Gradient: 70% B for 2 min, 70-80% B over 8 min, 80-100% B over 15 min, hold at 100% B over 5 min, back to 70% B over 2 min, re-equilibrate at 70% B over 13 min A: Tetrahydrofuran (THF)/MeOH:water (3:2:5 v/v/v) + 10 mM ammonium acetate B: THF/MeOH/water (7:2:1 v/v/v) + 10 mM ammonium acetate	PG eluted around 4-8 min, CL eluted around 15 min, no information on PE

	Gradient: 40% B for 2 min, 40-60% B over 8 min, 60-100% B over 15 min, hold at 100% B over 5 min, back to 40% B over 2 min, re-equilibrate at 40% B over 13 min Flow rate: 50 µL/min	PG eluted around 14-20 min, CL eluted around 25-27 min, no information on PE

Among the many LC columns and conditions tested (Table 3.1), the reverse-phase Luna® C8(2) provided the best separation capability of the different types of *E. coli* phospholipids, under a 30-min gradient of THF/MeOH/water with a total LC run time of 45 min. In RPLC and HILIC, water is commonly used, which benefits the ESI process in terms of its efficient conductivity. However, the relatively high viscosity and surface tension of water can sometimes affect the electrophoretic mobility of ions, as it increases the emitted droplet size. This could impede effective ion evaporation from the surface of the shrinking droplets, and thus hinders efficient charge separation during ESI. The use of volatile organic solvents, such as THF and MeOH in this case assisted the ESI process by expediting the solvent evaporation from the droplets, which in turns aids in ion formation (Brouwers, 2011).

Figure 3.4 depicts the total ion chromatogram (TIC) of a lipid extract from *E. coli* BL21(DE3) membrane (extracted and solubilised with the 2:1 SMA copolymer) when subjected to LC-MS/MS analysis using the C8 column under the developed THF/MeOH/water gradient. Essentially, a TIC represents the summed ion intensities detected by the mass spectrometer across the entire *m/z* range at every time point in the LC run. For complex biological samples containing a plethora of ionisable compounds, a TIC often only provides a limited amount of information as multiple compounds can elute concurrently, thus hindering the identification of individual species. The elution of the three phospholipid classes found in *E. coli* membrane was as follows: PG > PE > CL on the C8 column under a gradient of THF/MeOH/water.

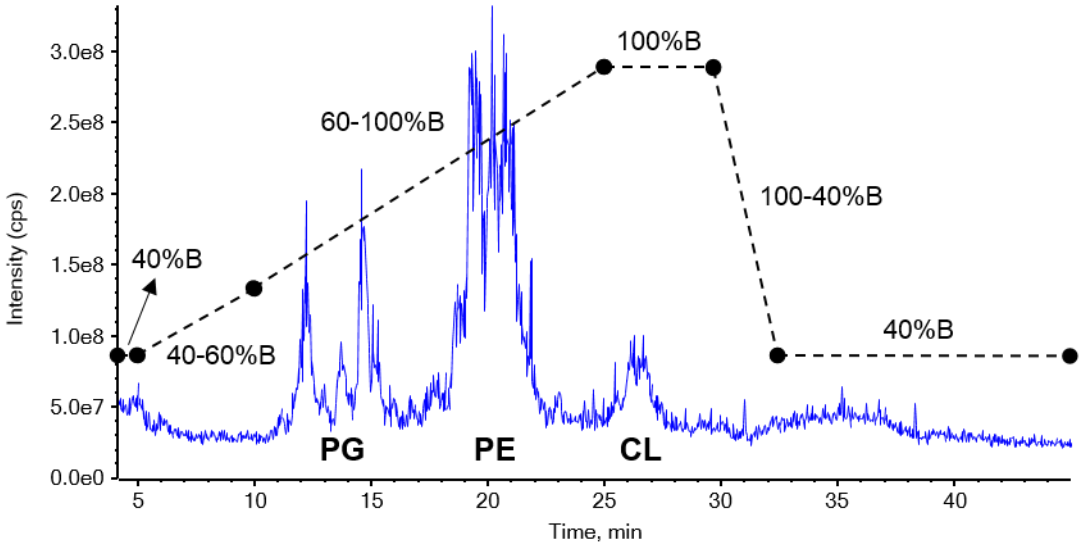

Figure 3.4 TIC of SMA-extracted *E. coli* BL21(DE3) membrane lipid extract on the Luna® C8(2) column under a THF/MeOH/water gradient. Dotted lines are added to indicate the change in gradient as solvent B percentage.

In terms of LC-MS, the viscosity of the solvents used (which is temperature-dependent) can influence the electrophoretic mobility of the ions and affect charge separation during ESI (Brouwers, 2011). Several other common physical properties of the LC solvents, *i.e.* THF, MeOH, and water used in the LC-MS/MS method developed are summarised in Table 3.2. In the developed LC-MS/MS method, the temperature of the C8 column was kept at 30°C (just slightly above room temperature) to maintain a constant LC temperature to minimise changes in the overall solvent viscosities throughout the entire experiment, which can last for a few days depending on the number of samples. The main consideration of setting the column temperature at 30°C and not higher is to prevent any undesirable degradation of membrane lipids throughout the experiment. The relatively high water content (34%) at the starting of the LC gradient could result in lipid precipitation issue when a high content of $CHCl_3$ is added, due to the immiscibility of $CHCl_3$ with water. Thus, the lipid extracts were reconstituted in 9:1 v/v MeOH:$CHCl_3$ (upon extraction), prior to diluting into the starting LC solvent for subsequent LC-MS/MS analysis. In the LC method developed, the amount of MeOH was kept constant (20%) throughout the LC run. It was the decrease in water (from 34% to 10%) and the concurrent increase in THF (46% to 70%) that eluted the different classes of phospholipids from the C8 column. In other words, the change in

polarity of the solvent was achieved by the exchange of water with THF for phospholipid elution.

Table 3.2 Common physical properties of the solvents used in the LC-MS/MS method developed (Source: Sigma-Aldrich).

Solvent	**Dielectric constant (at 25°C)**	**Polarity index (P')**	**Viscosity (at 20°C), mPa/s**	**Surface tension (at 20°C), mN/m**
Tetrahydrofuran	7.58	4.0	0.55	26.40
Methanol	32.7	5.1	0.59	22.55
Water	78.3	10.2	1.00	72.80

The ionisation efficiency of individual lipid species would rely on the electrical propensity in its own microenvironment during electrospray, either to gain or to lose a charge. For anionic lipids such as PG and CL, which carry a net negative charge at physiological pH, they tend to ionise quite efficiently in the negative ion mode. On the other hand, PE lipids carry only a negative charge at alkaline pH due to its zwitterionic nature, so it can either donate or accept a proton depending on the polarity of ionisation employed. Table 3.3 depicts the effect of fatty acyl chain on LC elution time on the C8 column under a THF/MeOH/water gradient. For the LC-MS/MS method developed, the addition of each methylene ($-CH_2$) group on the fatty acyl chains increases the retention time by about 1-1.5 min. Conversely, an increase in C=C unsaturation decreases the retention time by about 1-1.5 min. This is a typical phenomenon observed with RPLC columns (Damen *et al.*, 2014).

Table 3.3 Effect of fatty acyl chain on LC elution time on the C8 column under a THF/MeOH/water gradient.

Molecular species	*m/z* $[M-H]^-$	Average elution time (min)
PE 32:2	686	15.58
PE 32:1	688	16.99
PE 32:0	690	18.17
PE 33:2	700	16.65
PE 33:1	702	17.93
PE 33:0	704	14.99
PE 34:2	714	17.52
PE 34:1	716	18.62
PE 34:0	718	19.75
PE 35:2	728	18.35
PE 35:1	730	19.46

A partial overlap of the longer and less unsaturated PG species with the shorter and/or more unsaturated PE species was observed. However, based on the nitrogen rule, whereby nitrogen bearing lipids such as PE would register an even *m/z*, which can be used to contrast against PG lipids (without nitrogen) with odd *m/z*. In addition, the use of tandem MS scans produced different fragmentation patterns for PE and PG, which can be readily used to distinguish these two classes of lipids, therefore not hindering their identification. CLs were only eluted at the highest organic content, close to 100% solvent B (THF:MeOH:water, 7:2:1 v/v/v), and thus are well separated from the other phospholipids (as shown in Figure 3.4).

The inclusion of mobile phase additives, such as ammonia, trimethylamine, diisopropylamine, and piperidine have been reported to enhance ionisation in the negative ion mode, and also displaces sodium and potassium counterions in the positive ion mode which can simplify quantification (Wolf and Quinn, 2008). In terms of phospholipids, the addition of amine base can enhance the ionisation process in negative ion mode by inducing an efficient release and transfer of slightly acidic protons (Wolf and Quinn, 2008). Buffers including ammonium acetate, ammonioum formate, acetic acid and formic acid are commonly used to protonate or deprotonate the analytes of interest during LC-MS method development (Brouwers, 2011). Spickett *et al.* (2011) previously reported that ammonium acetate is an effective mobile phase additive on the ionisation of oxidised phospholipids. During the development of the LC-MS/MS method described in this chapter, ammonium formate, ammonium acetate, glacial

acetic acid and triethylamine had been tested with the LC solvents. Ammonium acetate was found to be the most effective on the ionisation of phospholipids in both positive and negative ion modes. The inclusion of acetic acid and triethylamine produced a peak tailing effect which was undesirable.

3.2.2.2 LC enables the separation of isobaric species

The presence of isobaric species (of very similar *m/z*) that complicate direct infusion MS analysis can be effectively resolved with the use of LC. For example, both PE 34:2 $[M-H]^-$ and CL 70:3 $[M-2H]^{2-}$ were present in the lipid extract of SMA-extracted *E. coli* BL21(DE3) and harbour a *m/z* 714 on the QTRAP® 5500 (Figure 3.5). With the use of the C8 column under the THF/MeOH/water gradient, these two isobaric species were effectively separated, as depicted in Figure 3.5 (A) for the extracted ion chromatogram (XIC) of *m/z* 714. Essentially, the XIC display the ion intensity of one or more analytes of interest, extracted or reconstructed from the entire data set for a chromatographic run, by plotting the intensity of the target analyte(s) at each time point. Furthermore, when tandem MS was employed as in the LC-MS/MS method developed for SMALP lipidomics, the distinct fragmentation pattern of both lipid species in the negative ion mode can be used to distinguish them. Figure 3.5 (B) and (C) depict the tandem mass spectra of PE 34:2 and CL 70:3 respectively, showing the characteristic peaks at *m/z* 140 and 196 that can be exploited to discern PE from CL and PG.

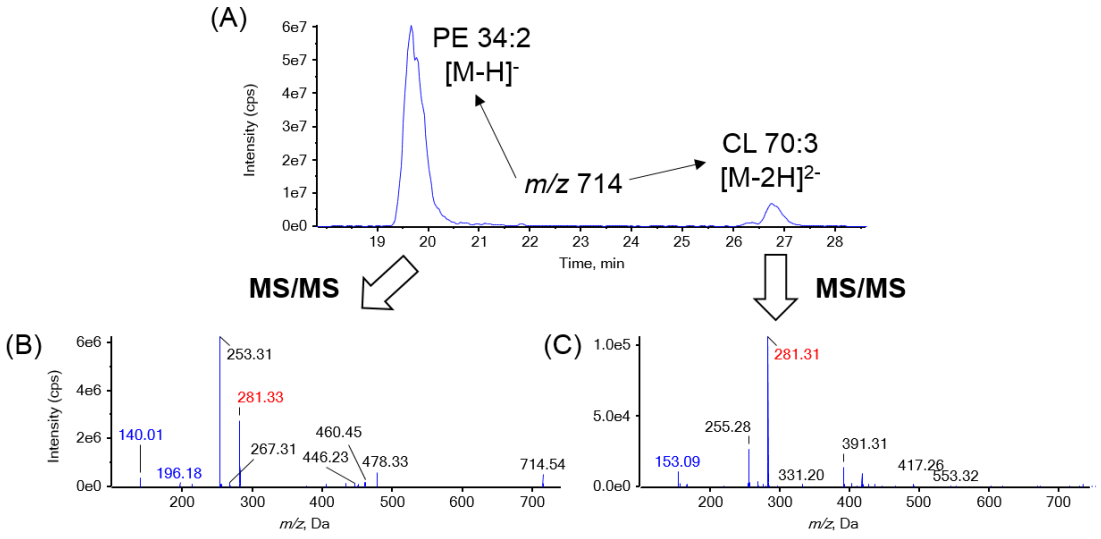

Figure 3.5 XIC of *m/z* 714 from SMA-extracted *E. coli* BL21(DE3) membrane lipid extract with corresponding tandem mass spectra in negative ion mode for the isobaric

pair - PE 34:2 and CL 70:3. (A) The XIC shows two distinct molecular species, *i.e.* PE 34:2 $[M-H]^-$ and CL 70:3 $[M-2H]^{2-}$, both harbouring a *m/z* of 714. The different fragmentation patterns of PE (B) and CL (C) upon CID in the negative ion mode can be used to distinguish these two isobaric species effectively in a tandem MS experiment.

Figure 3.6 (A) depicts the XIC of *m/z* 721 that corresponds to another isobaric pair - PG 32:0 and CL 71:3 in the same SMA-extracted *E. coli* BL21(DE3) membrane lipid extract. Without LC separation, the fragmentation patterns upon CID for these two isobaric species would be rather similar, as both lipid species show a peak at *m/z* 153 representing the dehydrated glycerophosphate $[C_3H_7O_2OPO_3H-H_2O]^-$, as depicted in Figure 3.6 (B) and (C), which is a common fragment for diacylglycerol phospholipids such as PG and CL (Brügger *et al.*, 1997). In fact, a PIS of *m/z* 153 in the negative ion mode can be used to selectively detect these lipid species from other types of membrane lipids. Both of these lipids also harbour the C16:0 fatty acid (*m/z* 255) and given that CL is synthesised from a PG precursor can further complicate the characterisation of these two isobaric pair in a shotgun lipidomic experiment. However, using the C8 column under a THF/MeOH/water gradient, PG 32:0 and CL 71:3 were effectively separated. Therefore, for the potential overlapping of CL peaks (of either odd or even *m/z* for doubly charged species) with PE and PG lipids, the use of an effective LC approach such as the one described in this chapter can effectively separate these isobaric pairs without resorting to the use of a mass spectrometer with a higher mass resolving power. The more abundant PE and PG species in *E. coli* membrane, which are isobaric to the CL species in doubly charged form can often mask its detection in a shotgun lipidomic experiment.

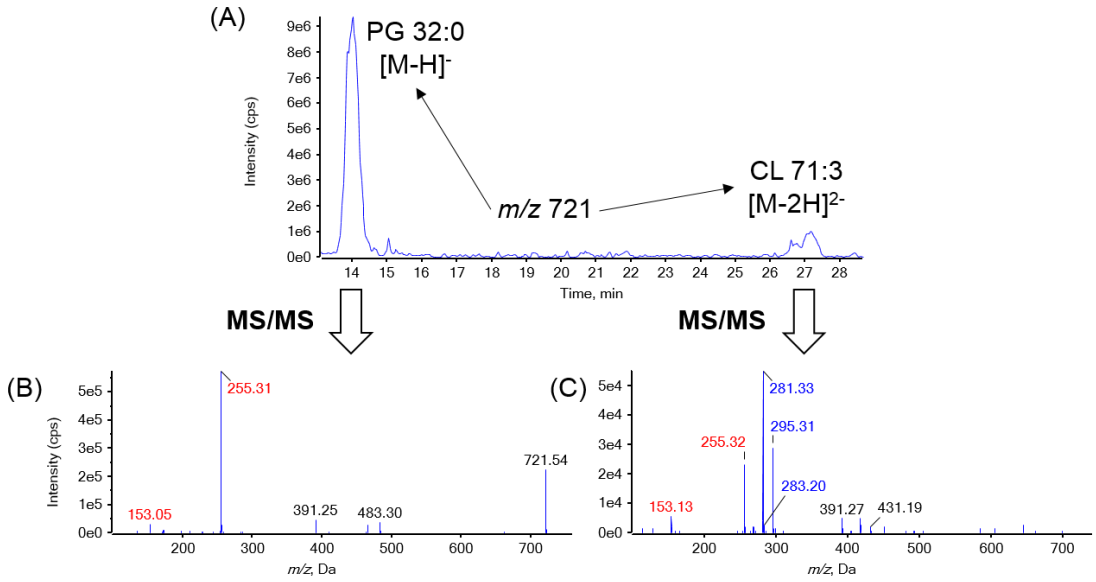

Figure 3.6 XIC of *m/z* 721 from SMA-extracted *E. coli* BL21(DE3) membrane lipid extract with corresponding tandem mass spectra in negative ion mode for the isobaric pair - PG 32:0 and CL 71:3. (A) The XIC shows two distinct molecular species, *i.e.* PG 32:0 $[M-H]^-$ and CL 71:3 $[M-2H]^{2-}$, both harbouring a *m/z* 721. The corresponding tandem mass spectra (B) and (C) for these isobaric pairs are rather similar as both lipid species show the dehydrated glycerophosphate peak at *m/z* 153, and C16:0 fatty acyl peak at *m/z* 255.

The use of RPLC was observed in this work to facilitate more accurate quantification of membrane phospholipids by allowing the separation of different molecular species based on their hydrophocity (fatty acyl chain length and degree of unsaturation), rather than headgroup polarity in HILIC-based separation. Figure 3.7 depicts the XICs of *m/z* 745 and 747 from an extracted egg PG sample in negative ion mode on the C8 column under the THF/MeOH/water gradient. The overlapping of the peak for the double ^{13}C isotope of PG 34:2 $[M-H+2]^-$ with the monoisotopic ^{12}C peak of PG 34:1 $[M-H]^-$ can be observed when the XIC was generated at *m/z* 747 (in pink trace). However, with effective RPLC separation, these overlapping isobaric species at *m/z* 747 can be distinguished by a retention time difference (*i.e.* 13.3 vs 14.7 min) to prevent misquantification by incorporating the amount of the double ^{13}C isotope of PG 34:2 $[M-H+2]^-$ into the quantification for PG 34:1.

The quantification strategy adopted in the LC-MS/MS method developed was based on the integration of the area under the curve (AUC) of the monoisotopic peak of the target phospholipid. For instance, the quantification for PG 34.2 in the extracted egg PG sample (Figure 3.7) was based on the integration of AUC of the monoisotopic peak at *m/z* 745 (*a*), whilst the amount of PG 34:1 was determined from the AUC of *m/z* 747 (*b*) as highlighted in the blue box in the Figure 3.7. The AUC resulting from the double ^{13}C isotope of PG 34:2 $[M-H+2]^-$ at *m/z* 747 (*c*) was not taken into account when quantifying PG 34:1 with the LC separation step, which has enabled a more accurate quantification of these PG species.

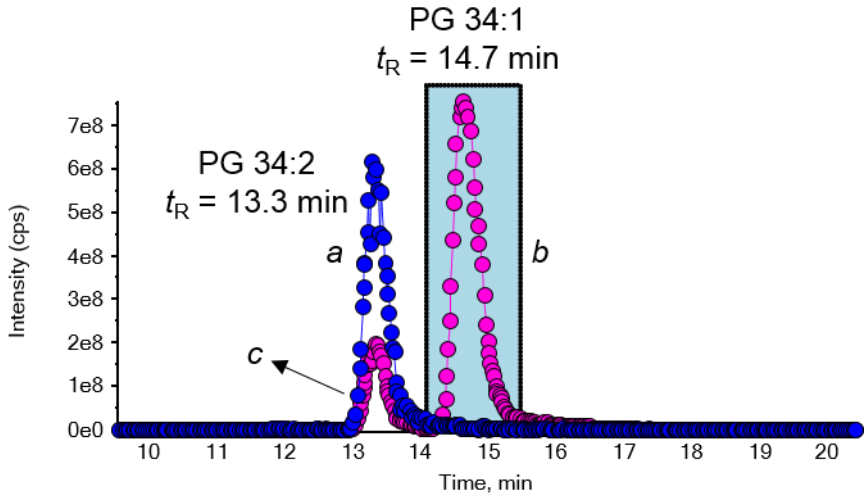

Figure 3.7 XICs of *m/z* 745 (PG 34:2) and *m/z* 747 (PG 34:1) from extracted egg PG in negative ion mode on the C8 column under a THF/MeOH/water gradient. The overlapping of the peak for the double ^{13}C isotope of PG 34:2 $[M-H+2]^-$ with the monoisotopic ^{12}C peak of PG 34:1 $[M-H]^-$ can be observed when the XIC was generated at *m/z* 747 (pink). The quantification of PG 34:2 and PG 34:1 was based on the integration of the AUCs for (*a*) and (*b*) respectively, and the AUC for the double ^{13}C isotope of PG 34:2 $[M-H+2]^-$ (*c*) was not taken into account when quantifying PG 34:1.

3.2.2.3 Verification of CL charged states

During the LC-MS/MS method development, the inherent limitation in mass range (*m/z* up to 1000) on the QTRAP® 5500, which could hamper the detection of CL in their singly charged states with *m/z* > 1000 was seriously considered and investigated. Instrument design has been previously reported to influence the charge states of CL lipids during ESI-MS analysis (Sparagna *et al.*, 2005). Therefore, the charge states of

CL was investigated using the QTRAP® 5500 and a hybrid quadrupole/time of flight TripleTOF® 5600 instrument from the same manufacturer (AB Sciex, UK) using a similar ESI source. Figure 3.8 depicts the examination of the predominant charge state of CL under the experimental setting using the TripleTOF® 5600 instrument. CL was largely detected as doubly charged species $[M\text{-}2H]^{2-}$ as depicted in Figure 3.8 (B), indicating that the CL lipids mostly lose two of its proton from the phosphates to be doubly deprotonated in the ESI source during the ionisation process, which is similar to the observation by several other groups (Garrett *et al.*, 2012, 2007; Han *et al.*, 2006; Hsu *et al.*, 2005; Tan *et al.*, 2012; Valianpour *et al.*, 2002). The +0.5 Da isotopologue pattern of the doubly charged CL $(M\text{-}2H)^{2-}$ vs the +1 Da increment in singly charged CL $[M\text{-}H]^{-}$ was clearly visible (Figure 3.8), and the abundance of these doubly charged species was 30-fold higher than the singly charged counterpart.

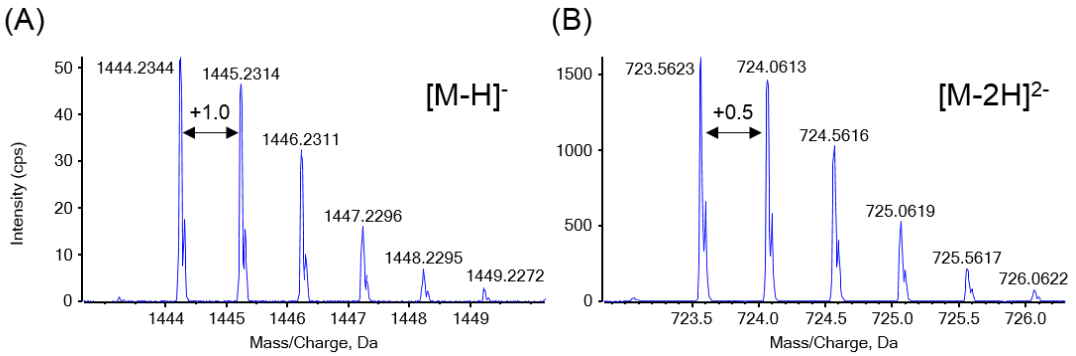

Figure 3.8 Verification of CL charge states using the TripleTOF® 5600 with similar ESI source as the QTRAP® 5500. Note the 30-fold differences in signal intensity between the (A) doubly $[M\text{-}2H]^{2-}$ and (B) singly charged $[M\text{-}H]^{-}$ species, indicating that CL was ionised predominantly in the doubly charged state under the experimental setting.

The pH-dissociation of characteristics of CL were previously investigated by Kates *et al.* (1993), with a pK_{a1} at 2.8 and pK_{a2} at 7.5-9.5. Thus, according to this study, in aqueous dispersions with a neutral pH, CL would normally harbour a single charge only, because one proton gets trapped in a bicyclic resonance structure formed by its two phosphates and the central hydroxyl group. It is only at pH greater than 7.5 that CL is a divalent anion (Kates *et al.*, 1993). This property was revisited by Olofssion and Sparr (2013), which reported a similar pK_{a1} around 2.5 (akin to phosphoric acid) but its pK_{a2}

was being determined to be only one unit or less larger than pK_{a1}. In effect, CL would carry two negative charges at pH 5.5-7.0 (Olofsson and Sparr, 2013). It is important to note that different types of CL samples were employed in both studies, in which natural samples of CL were used by Kates *et al.* (1993), while Olofsson and Sparr (2013) used synthetic CL.

Cole and Harrata (1993) had investigated the solvent effect on the charge state, signal intensity and stability of *E. coli* CLs on ESI-MS in the negative ion mode. They reported that solvents with high dielectric constant (which measures the electrical energy storage capability of a substance in an electric field) and polarity were better at stabilising multiply charged ions. The high polarity and dielectric constant of both water and MeOH used in the LC-MS/MS method developed have most likely contributed to the stabilisation of doubly charged CL in this work.

3.2.2.4 Co-elution of PC and PE

Despite the clear separation of PE, PG and CL lipids on the on the C8 column under the THF/MeOH/water gradient, PC and PE were found to co-elute in this LC method. This work was carried out to further evaluate the LC-MS/MS method developed for the application of other membrane lipids, such as PC, a zwitterionic phospholipid, commonly found in eukaryotic cell membranes (Aktas *et al.*, 2010; Fagone and Jackowski, 2008). Figure 3.9 (A) shows the various PC (red) and PE (blue) molecular species that had co-eluted within an elution window between 18-20 min for an extract of egg PC and soybean PE mixture subjected to LC separation using the method developed in this work. However, isobaric species such as PC 33:1 and PE 36:1 (*m/z* 746) were still separated in this RPLC method, with difference in retention time difference, *i.e.* 17.9 min for PC 33:1 and 21.3 min for PE 36:1. In addition, the application of tandem MS with the LC-MS/MS method developed has provided an additional dimension to distinguish these two isobaric species based on the characteristic MS/MS fragmentation pattern for these two zwitterionic phospholipids in the positive ion mode (Brügger *et al.*, 1997). As depicted in Figure 3.9 (B) and (C), the phosphocholine headgroup $[H_2PO_4CH_2CH_2N(CH_3)_3]^+$ at *m/z* 184 is the unique signature and an intense peak for PC lipids, while a NL of 141 of *m/z* 746 resulted in the *m/z* 605 peak as the most intense peak for this PE lipid.

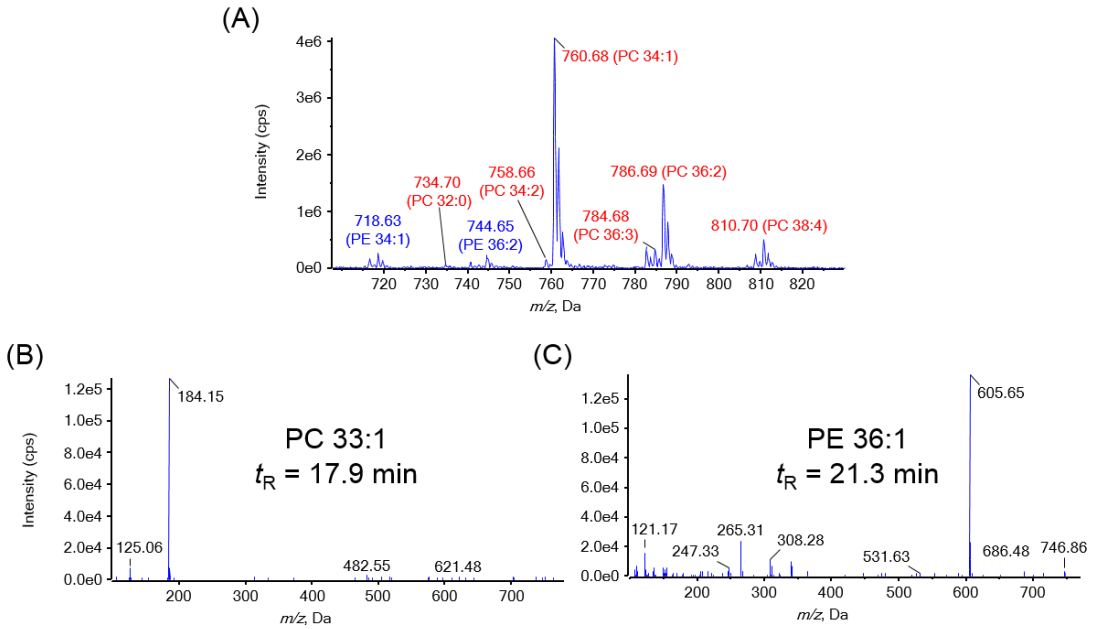

Figure 3.9 Mass spectrum of an extract of egg PC and soybean PE mixture with LC-MS/MS in positive ion mode on the C8 column under a THF/MeOH/water gradient, with corresponding tandem mass spectra for the isobaric species - PC 33:1 and PE 36:1. PC 33:1 and PE 36:1 (*m/z* 746) were separated using the LC-MS/MS developed with a retention time difference of around 3 min, and both phospholipids present different fragmentation patterns upon CID which can be used to distinguish them effectively with tandem MS in the positive ion mode.

3.2.3 Analytical validation of developed LC-MS/MS method

Upon the selection of LC column and the development of instrument parameters for the analysis of phospholipids, the developed LC-MS/MS method was further evaluated in terms of its robustness and validity for the intended characterisation of the co-extracted membrane lipidome of SMALP-proteins based on several key parameters as discussed in the following sections

3.2.3.1 Limit of quantification

The sensitivity of an analytical method measures the amount of analyte that can be detected under the experimental setting. The limit of detection (LoD) is typically defined as the lowest amount of analyte that can be detected (as opposed to be quantified) with a S/N ratio of 3. The S/N ratio measures the ratio of the height of a peak to the variability in the background signal/noise. On the other hand, the limit of quantification (LoQ) is defined as the lowest concentration of analyte that can be

reliably and precisely quantified under the experimental condition with a minimum S/N ratio of 10 (Sonawane *et al.*, 2014; Tiwari and Tiwari, 2010). For LoQ determination, normally five analyte concentrations are tested, with one near the LoQ, and one below the LoQ. Figure 3.10 depicts the comparison of two S/N ratios for one of the synthetic phospholipid - PG 34:1 at two different concentrations used in the LoQ determination experiment. A higher background noise at the lower concentration of this phospholipid (*i.e.* 0.039 ng) was observed with a corresponding lower S/N ratio at around 15, as depicted in Figure 3.10 (A). With approximately eight-fold increase in concentration at 0.31 ng, the S/N ratio increased five-fold, resulting from a lower background noise, as depicted in Figure 3.10 (B).

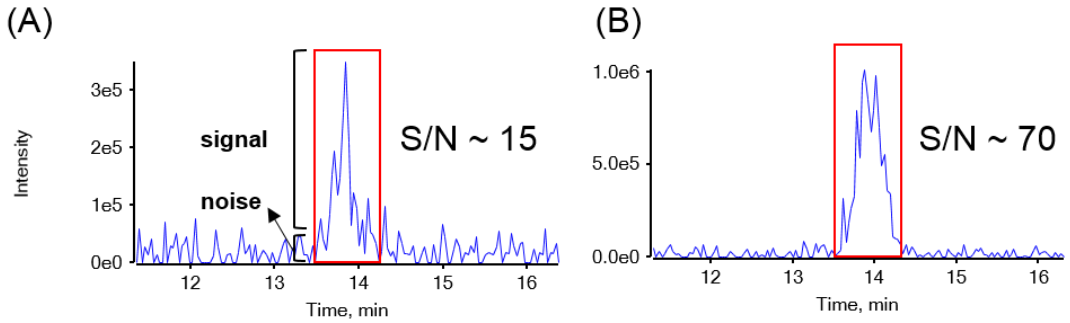

Figure 3.10 S/N ratios for PG 34:1 at two different concentrations used in the LoQ determination experiment. (A) The S/N ratio for PG 34:1 at 0.039 ng was measured to be around 15, while the S/N ratio increased to be around 70, with an increase in analyte concentration to 0.31 ng (B) as a result of lower background noise.

An exponential dilution series (in the concentration range of 0.039-2.5 ng per individual lipid) was employed to investigate the LoQ of the LC-MS/MS method developed. To simplify the examination of instrument response and downstream data analysis, synthetic phospholipid standards that encompass the three classes of membrane phospholipids were used. The LoQs for both PE 34:1 and PG 34:1 were determined to be between 0.039-0.078 ng, while CL 72:4 showed a LoQ approximately 10-fold higher than the PE and PG counterpart, at 0.31-0.63 ng.

3.2.3.2 Intra- and inter-assay variations

The intra-assay and inter-assay variations of the LC-MS/MS method developed were evaluated based on RSD using the same set of synthetic phospholipids - PE 34:1, PG

34:1 and CL 72:4. As shown in Table 3.4, the intra-assay (within-day) variation for the LC-MS/MS method was found to be only < 6%, with a very minimal retention time difference of ± 0.015-0.021 min. Although the RSD values were > 20% for the inter-assay (between-day) evaluation, the deviation in retention time was actually only very minimal at ± 0.12-0.30 min, signifying a lack of retention time drift over a period of five experimental days.

Table 3.4 Intra-assay and inter-assay variations of the LC-MS/MS method developed.

RSD (%)	PE 34:1		PG 34:2		CL 72:4	
	Peak	t_R	Peak	t_R	Peak	t_R
Intra-day: three replicates per day	2.62	0.07	5.83	0.13	1.14	0.18
Inter-day: five consecutive days	30.80	1.54	6.27	1.63	20.97	0.46

Note that the concentration of each synthetic phospholipid used was 0.1 µg.

3.2.3.3 Linearity of response

For a robust analytical method, the instrument response should be directly proportional to the concentration of the analytes within the range of the standard curve, spanning the concentrations expected to be measured in the samples (Sonawane *et al.*, 2014; Tiwari and Tiwari, 2010). In practice, a robust method should exhibit a linear detector response over a minimum of three orders of magnitude and it is crucial to verify the instrument detector response across a range of analyte concentrations to avoid saturating the detector into a non-linear readout. The linearity of response of the LC-MS/MS method developed was investigated using the same set of synthetic phospholipids, spanning a concentration range from 2 to 200 ng, as shown in Figure 3.11. The linearity observed for the three synthetic phospholipids has provided the confidence that there is enough dynamic range (up to 200 ng) for the characterisation and quantification of the co-extracted phospholipids from the SMALP-proteins. The range of individual phospholipid molecular species for the SMALP-protein samples analysed (discussed in Chapter 4 and 5) was found to be within the range of 0.2-150 ng, with only an exception being PgpB-SMALP (Chapter 5) that recorded two high abundance species, *i.e.* PE 34:1 and PE 33:1, around 220 and 250 ng respectively, just slightly over the 200 ng measured linearity range.

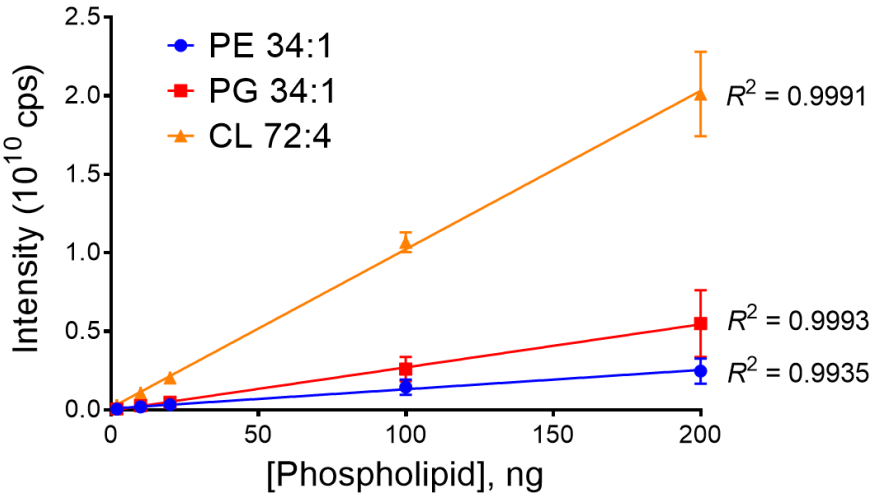

Figure 3.11 Linearity of response plot across three orders of magnitude (2-200 ng) for three synthetic phospholipid standards.

3.2.3.4 Extraction efficiency

The extraction efficiency of the modified Folch method used in the SMALP lipidomic approach was examined using naturally derived mixtures of phospholipid samples of egg yolk, soybean and bovine heart origins. The use of natural phospholipid mixtures to evaluate the extraction efficiency has dual benefits. Firstly, these natural phospholipid mixtures can better represent the diversity of lipid composition in a biological sample. Furthermore, they are available commercially at a cheaper price in larger bulk quantities than the synthetic equivalents. The four natural phospholipid mixtures employed in this work are commonly used for other lipid studies. For instance, bovine heart CL is a common lipid source for analytical studies involving CL (Mazzella *et al.*, 2004; Minkler and Hoppel, 2010; Samhan-Arias *et al.*, 2012; Sparagna *et al.*, 2005). As depicted in Figure 3.12, the extraction efficiencies for egg yolk PC and PG were found to be 82% and 81% respectively, while the extractions efficiencies for soybean PE was determined to be 77% and 63% for bovine heart CL.

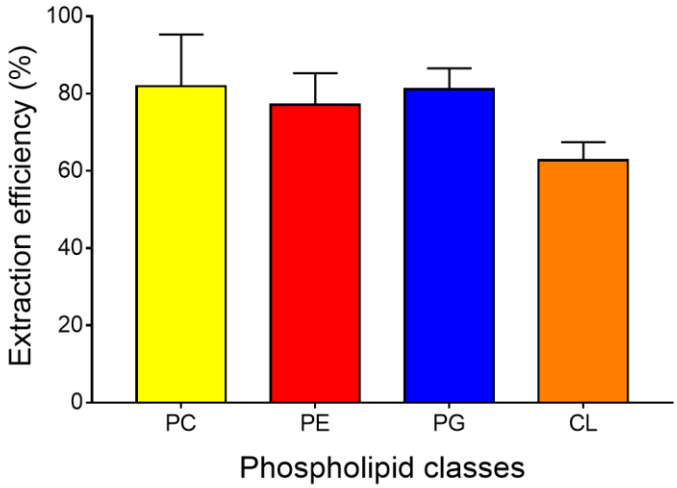

Figure 3.12 Extraction efficiencies for four natural phospholipid mixtures, encompassing egg yolk PC, soybean PE, egg yolk PG, and bovine heart CL.

In comparison to the extraction efficiencies of PC, PE and PG (around 80%), CL recorded a lower extraction efficiency. Similar observation was reported by Bird *et al.* (2011) while analysing mitochondrial CLs. They reported an extraction efficiency of 50% for the mitochondrial CLs, despite the application of strong organic solvents and sonication during the extraction process. The relatively low extraction efficiency of CL was said to account for two-thirds of the total variance in their assay and it was reasoned that many CLs in the mitochondrial samples could be protein-bound and hence lost with protein precipitation during the extraction process (Bird *et al.*, 2011). In the modified Folch lipid extraction protocol used in this work, the extraction efficiency for bovine heart CL was slightly better at 63%. In addition, the poor extraction efficiency of CL was proposed to account for the low amount of ions observed when lipid extracts from *E. coli* and *Bacillus* species were analysed using ESI-MS/MS in the negative ion mode (Smith *et al.*, 1995).

Sonaware *et al.* (2014) pointed out that the recovery of the target analyte need not necessary be 100%, but the extent of recovery of the analyte and the IS should at least be consistent and reproducible. When the extraction efficiency of the phospholipid IS added in three SMALP-protein samples was evaluated based on RSD, it was found that PE 25:0 and CL 57:4 recorded low RSD values at 2.78% and 4.77%, while PG 25:0 was higher at 13.31%. Nevertheless, the RSD values were still below the 20% guideline, indicating a consistent extraction of the three added phospholipid IS from the different

SMALP-samples and hence a reliable lipid extraction protocol for the SMALP-protein samples.

3.3 Concluding remark

In the work described in this chapter, the modified Folch method was successful in the extraction of phospholipids from the SMALP samples, as demonstrated by the direct infusion MS investigation of SMALP-ZipA lipid extract, which showed a variety of PE and PG lipids. A LC-MS/MS method employing a C8 column under a 30-min THF/MeOH/water gradient was further developed for the SMALP lipidomic strategy. The three classes of *E. coli* membrane phospholipids of interest, namely PE, PG and CL are separated effectively utilising the developed method. PE and PG ions were detected as $[M-H]^-$, while CL ions were detected in the doubly charged state as $[M-2H]^{2-}$ in the negative ion mode. The LC-MS/MS was also subjected to analytical validation to determine its robustness. Three synthetic phospholipid standards, *i.e.* POPE, POPG, and TOCL were employed for the LoQ, intra- and inter-assay variations, and linearity of response studies, while four natural phospholipid mixtures were used to determine the extraction efficiencies of the lipid extraction procedure. The LoQ for POPE and POPG was found to be 0.039-0.078 ng, while TOCL was 0.31-0.63 ng. The RSD values for the intra-assay (within-day) variation for the LC-MS/MS method were < 6%. Although RSD values > 20% were found for the inter-assay (between-day) evaluation, the deviation in retention time was only very minimal at ± 0.12-0.30 min, indicating a lack of retention time drift over a period of five experimental days. A linear response was observed for the three synthetic phospholipid standards at 2-200 ng, spanning three orders of magnitude. The extraction efficiencies for PC, PE and PG were found to be around 80%, while CL was lower at 63%.

Chapter 4: Lipidomic Analysis of *E. coli* Membranes and Key Bacterial Divisome Proteins - ZipA and FtsA

4.1 Background

The LC-MS/MS-based SMALP lipidomic approach developed in Chapter 3 was applied to characterise the local lipid environment of two essential cell division proteins in *E. coli* - ZipA and FtsA (Addinall and Lutkenhaus, 1996; Hale and de Boer, 1997). ZipA and FtsA both act as the anchor for the cytoskeletal bacterial tubulin homolog - FtsZ protein(s) to the cell membrane (as illustrated in Figure 4.1), forming the initial (minimal) proto-ring structure at the septum during cytokinesis within the cell division process (Ortiz *et al.*, 2016; Rico *et al.*, 2013). The presence of either of these two proteins is crucial for FtsZ filaments to organise into the Z-rings, although neither of them is needed for FtsZ proteins to nucleate and localise to the division site (Pichoff and Lutkenhaus, 2002). Recent immunofluorescent studies showed that each FtsZ protofilament consisted of approximately 27 FtsZ and is bound by four ZipA and five FtsA respectively (Vischer *et al.*, 2015).

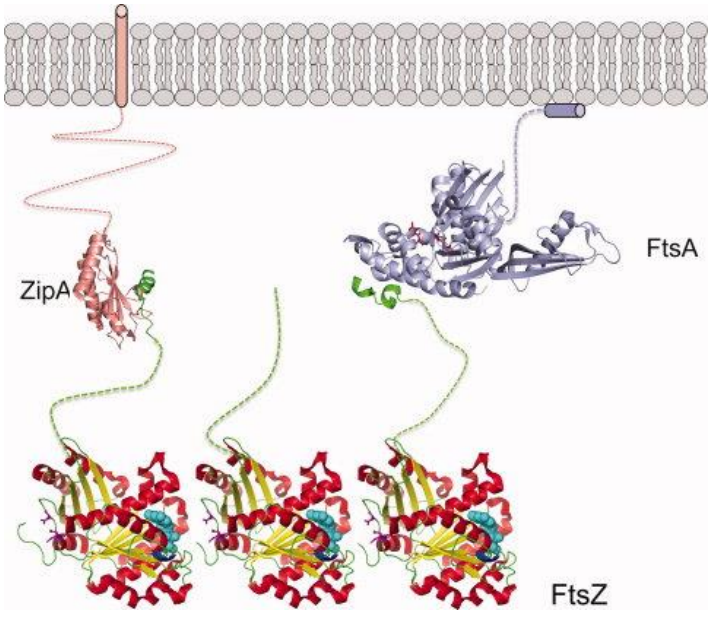

Figure 4.1 The tethering of FtsZ filaments (trimer is shown here) to the cell membrane by the essential proteins - ZipA (pink) and FtsA (blue) through the highly conserved carboxyl-terminal tail of FtsZ. This conserved C-terminal tail of FtsZ (green) connects to the main body of the FtsZ via a flexible linker (shown in dotted line). ZipA is connected to the cell membrane via its amino-terminal TM helix, while FtsA is

associated with the cell membrane through an amphipathic helix. Figure is adopted from Lutkenhaus *et al.* (2012) with permission.

4.1.1 Z-interacting protein A (ZipA)

ZipA is a biotopic membrane protein, harbouring a short N-terminal TM helix that is embedded into the cell membrane. It interacts with the C-terminal of FtsZ via its C-terminal globular domain, which is separated from its N-terminal TM helix by an unstructured linker region rich in proline and glutamine (termed the P/Q domain) (Mosyak *et al.*, 2000; Moy *et al.*, 2000; Ohashi *et al.*, 2002). The disruption of ZipA-FtsZ interaction was found to interrupt the cell division process (Mosyak *et al.*, 2000). The TM helix of ZipA plays no role in the interaction with FtsZ and the binding affinity of ZipA to FtsZ is not dependent on the nucleotide-binding or oligomerisation state of FtsZ (Hernández-Rocamora *et al.*, 2012b). However, the binding of ZipA to FtsZ has been demonstrated to alter the self-association of the FtsZ filaments within the proto-ring by inducing FtsZ fibre bundling (Hale *et al.*, 2000). ZipA seemed to respond to different membrane packing by varying its P/Q domain into a brush-like conformation, in order to act as a flexible tether for the FtsZ proteins (López-Montero *et al.*, 2013a). ZipA was also proposed to protect FtsZ from the ClpXP-directed degradation, and has been shown to stabilise the FtsZ spiral-like structures at the cell membrane (Pazos *et al.*, 2013).

A FtsZ-ZipA complex was previously investigated in giant spherical vesicles made of *E. coli* lipids (López-Montero *et al.*, 2013b). These complexes resulted in large vesicle dilation and enhanced elasticity, which led to the hypothesis that it was the hydrostatic expansion driven by the polymerisation of FtsZ inside the lumen of the vesicles that was causing this phenomenon. As a result, aside from its membrane tethering role, ZipA was assigned the role as a mechanical transducer for the eventual forces generated by the FtsZ filaments (López-Montero *et al.*, 2013b). Although studies on ZipA encapsulated in MSP-nanodiscs have been reported using *E. coli* polar lipid extract to reconstitute the inner membrane environment upon detergent extraction of ZipA, these studies do not rule out the possibility that ZipA was not investigated under the native lipid environment (Hernández-Rocamora *et al.*, 2012a, 2012b). Besides, even though ZipA encapsulated in MSP-nanodiscs can bind to FtsZ, no fibre bundling of FtsZ was observed. This thus presents an opportunity for using the SMALP technology to further

examine ZipA in its native lipid environment and its interaction with FtsZ (Lin, 2011). Given its membrane tethering role of ZipA towards FtsZ, the in-depth characterisation of the co-extracted lipidome of ZipA upon SMALP encapsulation is described in this chapter.

4.1.2 Filamentous temperature-sensitive protein A (FtsA)

FtsA is a member of the actin/Hsp70/hexokinase superfamily (van den Ent and Löwe, 2000), which was postulated to attach to the cell membrane through a C-terminal short amphipathic helix motif, termed the membrane targeting sequence (MTS) (Pichoff and Lutkenhaus, 2005). However, a hypermorph (gain-of-function) mutant, *i.e.* FtsA* (R286W) or FtsA tandem fusion have been shown to bypass this MTS requirement for cell membrane attachment (Shiomi and Margolin, 2008). Given that FtsA lacking the MTS can still localise to the Z-ring, it indicated that this amphipathic helix motif is not crucial for FtsZ assembly at the cell membrane, but was postulated to have other roles in ensuring the recruitment of downstream divisome proteins (Shiomi and Margolin, 2008). FtsA interacts with the C-terminal domain of FtsZ near its 2B domain and the interaction with the cell membrane is essential for its function in tethering FtsZ (Fujita *et al.*, 2014; Szwedziak *et al.*, 2012; van den Ent and Löwe, 2000). The 1C domain of FtsA was found to be important to recruit late-assembling division proteins, such as FtsN, and was also involved in its self-interaction (Busiek *et al.*, 2012; Rico *et al.*, 2004). Interaction with the cell membrane has been proposed to be essential for FtsA to regulate its interaction with the FtsZ filaments to form cooperative linkage of the FtsZ polymers into the Z-ring and for its self-interaction (Pichoff and Lutkenhaus, 2005). Nevertheless, strong self-interaction and membrane binding was not essential for the localisation of FtsA to the Z-ring (Shiomi and Margolin, 2008).

The FtsA* hypermorph mutant allows the bacterial cells to bypass the need for ZipA, and facilitates late-divisome assembly but cannot protect FtsZ from ClpXP-directed degradation (Geissler *et al.*, 2003; Pazos *et al.*, 2013). The stabilisation of FtsZ by FtsA was postulated to occur during the polymerisation stage of FtsZ, alluding that FtsA does not act on monomeric FtsZ (Pazos *et al.*, 2013). A report on the lipid-binding properties of *E. coli* FtsA demonstrated that it is the hydrophobic interactions that are involved in the association of purified FtsA to the lipid/membrane structures (Martos *et al.*, 2012). It has been shown that *E. coli* FtsA does not polymerise in the absence of lipids, but

forms polymeric structures on lipid/membrane-coated microbeads, with a ten-fold higher apparent binding affinity towards *E. coli* inner membrane than the added phospholipids (Martos *et al.*, 2012). This is akin to the observation in which *Thermotoga maritima* FtsA forms polymers on lipid monolayers *in vitro*, but not in the absence of lipids (Szwedziak *et al.*, 2012). By reconstituting *E. coli* FtsZ and FtsA into giant unilamellar vesicles made from *E. coli* inner membranes, the association of FtsA to the membrane within the vesicles was found to be modulated by the FtsZ polymers (Jiménez *et al.*, 2011). FtsA binds to adenosine triphosphate (ATP) and its polymerisation and membrane-association were said to be driven by this nucleotide-binding property (Krupka *et al.*, 2014; Szwedziak *et al.*, 2012). It has been proposed that FtsA exerts a dual function towards FtsZ, *i.e.* by tethering it to the cell membrane, and also destabilising the FtsZ polymers while rearranging the networks of the FtsZ filaments to allow the Z-ring to adapt its diameter during cytokinesis (Szwedziak *et al.*, 2012).

A recent report showed that it is the circumferential treadmilling action of the FtsAZ filaments around the division ring in *B. subtilis* that has guided the progressive insertion of new cell wall to create increasingly smaller concentric rings of peptidoglycan to eventually divide the cell (Bisson-Filho *et al.*, 2017). In this treadmilling model, the formation of this complex on the cytoplasmic side of the cell membrane is linked to the formation of the cell wall assembly enzymes on the outside of the cell membrane, thus providing a direct linkage between cell division and cell wall peptidoglycan assembly. So far, no report of FtsA in MSP-nanodisc or other membrane mimetics besides liposomes has been published. Given the intrinsic linkage to the cell membrane for the function of FtsA, the study of this key cell division protein in its native lipid environment is thus warranted, and the detailed characterisation of co-extracted lipidome of FtsA upon SMALP encapsulation is described in this chapter.

4.1.3 Aim and objectives of chapter

The primary aim of the work described in this chapter was to characterise the co-extracted membrane lipidome of *E. coli* ZipA and FtsA upon SMALP encapsulation, given their membrane tethering function towards FtsZ. The developed LC-MS/MS method was applied to the profiling and relative quantification of the co-extracted phospholipids. Given the postulation that some divisional proteins recognise a certain

membrane environment or local membrane curvature to localise (Barák and Muchová, 2013; Mileykovskaya and Dowhan, 2005; Ramamurthi, 2010), and the septal invagination process during cytokinesis might also require a specific local lipid composition to facilitate membrane curvature (Koppelman *et al.*, 2001), comparisons were made on the phospholipid profiles obtained for ZipA vs FtsA. Protein-lipid interaction (in terms of the differences of associated phospholipids) were investigated by comparing the phospholipid profiles of both proteins towards their respective membrane controls, in order to gain a better insight into whether specific phospholipid or membrane compositions are critical to the cell division process.

4.2 Results and discussion

4.2.1 LC-MS/MS analysis of *E. coli* BL21(DE3) membranes

In order to determine if the SMALP technology is a suitable tool for membrane lipidomic studies, the *E. coli* BL21(DE3) membranes were analysed using the developed LC-MS/MS method. This was to examine if there is any preferential extraction of certain membrane lipid types by the 2:1 SMA copolymer, prior to the application of the developed SMALP lipidomic approach to ZipA and FtsA. For this investigation, the *E. coli* BL21(DE3) membrane was separated into two fractions, one of which was subjected to SMALP treatment (and the other not), prior to lipid extraction using the modified Folch method.

The fact that MS is not inherently quantitative, *i.e.* the intensity for each analyte peak does not always directly correlate to its concentration due to the differences in ionisation efficiency, three specific IS, *i.e.* PE 12:0/13:0 (25:0), PG 12:0/13:0 (25:0) and CL 14:1/14:1/14:1/15:1 (57:4) have been added (prior to the lipid extraction) for the downstream data normalisation of each phospholipid class, so as to facilitate the relative quantification between phospholipid classes in this work. Figure 4.2 depicts the phospholipid profiles for both fractions of the *E. coli* BL21(DE3) membranes upon LC-MS/MS analysis. Multiple *t*-tests analysis was performed to assess any difference between the two phospholipid profiles. In general, the phospholipid profiles of *E. coli* BL21(DE3) membranes upon SMALP treatment demonstrated no significant difference in comparison to the non-treated membrane control. Significant differences ($p < 0.01$) were only detected for four out of the 52 molecular species, as depicted in Figure 4.2.

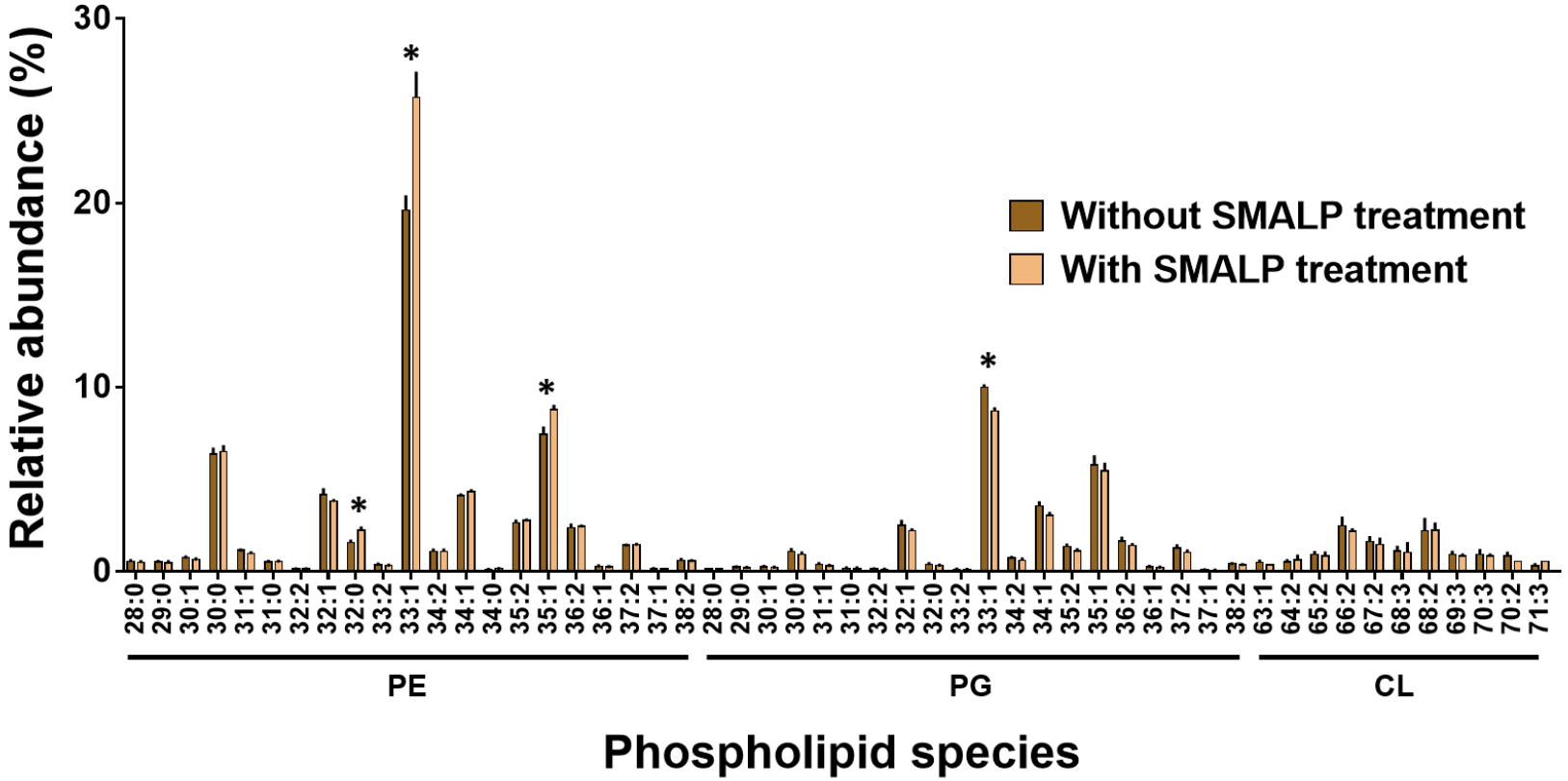

Figure 4.2 Comparison of phospholipid profiles of *E. coli* BL21(DE3) membranes with or without SMALP treatment upon LC-MS/MS analysis. The three classes of *E. coli* membrane phospholipids, *i.e.* PE, PG and CL were detected and relatively quantified. The phospholipid species showing significant differences based on multiple *t*-tests analysis ($p < 0.01$) are highlighted as *.

The RPLC method employed by Oursel *et al.* (2007b) only utilised one IS, *i.e.* PE 12:0/12:0 (24:0) to normalise the data obtained for the PE and PG lipids. Prabudiansyah *et al.* (2015) exploited the same IS for data normalisation and relative quantification for PE, PG and CL lipids. CL 57:4 was used as IS for the NPLC-MS analysis of *E. coli* CL by Garrett *et al.* (2012). The LC-MS/MS method developed in this work has built upon these studies and improve to incorporate three non-natural short chain IS, *i.e.* PE 25:0, PG 25:0 and CL 57:4 that have not been reported for *E. coli* membranes. This is to account for the differences in ionisation efficiency (during LC-MS/MS data normalisation) for each of the three major phospholipid class found in *E. coli* membranes, as the differences in ionisation efficiency across different classes of phospholipids should be addressed by a direct comparison to chemically similar standard(s). In this work, 52 phospholipid molecular species (without taking into account isomeric species) encompassing 21 PEs, 20 PGs and 11 CLs were detected. More molecular species within the PE and PG classes, in addition to a variety of CL species were detected in this work when compared to report by Oursel *et al.* (2007b). CL was observed as doubly charged species $[M-2H]^{2-}$ using the LC-MS/MS method developed in this work, which is akin to the NPLC-MS method reported by Garrett *et al.* (2012).

Essentially, the bulk physical state of the lipid membrane determines the solubilisation equilibrium, instead of the properties of individual lipid (Cuevas Arenas *et al.*, 2016; Dominguez Pardo *et al.*, 2017). In comparison to conventional mild detergents, the extraction of membrane lipids using the SMA copolymer has a lower free-energy penalty (Cuevas Arenas *et al.*, 2016). Based on the studies of model membranes, Scheidelaar *et al.* (2015) reported that interaction of the SMA copolymer with the lipid membrane was dependent on the lipid composition, with the solubilisation kinetics being modulated by physicochemical properties, for example surface charge, lipid packing, and lipid chain length. In this work, it was sufficient to state that there was essentially no preferential extraction of lipid types for the 2:1 SMA copolymer during *E. coli* membrane solubilisation. The observation in this work corroborated the findings from other groups which have also looked at the solubilisation of *E. coli* membrane lipids by the SMA copolymer (Dominguez Pardo *et al.*, 2017; Dörr *et al.*, 2014; Scheidelaar *et al.*, 2015). Furthermore, no preferential SMA extraction was reported for the cell membranes of *R. sphaeroides* (Swainsbury *et al.*, 2014), *S. cerevisiae*

mitochondria (Long *et al.*, 2013; Smirnova *et al.*, 2016) and synthetic PC/PE large unilamellar vesicles (Cuevas Arenas *et al.*, 2016). This fact highlighted the usefulness of the SMA copolymer as a good detergent-alternative for biological membrane solubilisation, which facilitates subsequent membrane lipid characterisation, especially the case for *E. coli*, which is a common host for recombinant protein production (Rosano and Ceccarelli, 2014).

It is critical and useful to know that SMA copolymer has been demonstrated to not perturb the membrane bilayer homogeneity and is both highly efficient and non-selective towards the extraction of lipids in homogenous fluid bilayers. However, recent studies by Dominguez Pardo *et al.* (2017) showed that the SMA copolymer does show a clear preference for lipids residing in the fluid phase than the gel phase in phase-separated lipid bilayers. Thus for eukaryotic cell membranes with liquid-ordered phase (L_o) containing sphingomyelin and cholesterol, lipid packing can play a major role in the resistance to the solubilisation by the SMA copolymer, in a manner analogous to the resistance to detergent extraction (Dominguez Pardo *et al.*, 2017). However, this limitation can be used to benefit the studies of membrane proteins too large to be extracted by the SMA copolymer or those that preferentially reside in lipid rafts (L_o phase). In fact, the SMA copolymer has been used as a solubilisation tool (in reverse) to selectively enrich the large Photosystem I-light harvesting chlorophyll II supercomplex from the spinach thylakoid membrane in the insoluble fraction upon SMA solubilisation (Bell *et al.*, 2015).

4.2.2 LC-MS/MS analysis of the local membrane environment of ZipA and FtsA

Upon confirming that the solubilisation of *E. coli* membranes by the 2:1 SMA copolymer used in this work is not bias to certain types of phospholipids, the developed LC-MS/MS method was extended to characterise the co-extracted membrane lipidomes of the ZipA and FtsA proteins. The phospholipid profiles of ZipA and FtsA in SMALP is depicted in Figure 4.3. For both proteins, slightly over 50 phospholipid molecular species (without taking into account of the different isomeric species) from the three phospholipids classes were detected. The spectrum of phospholipids is consistent with those depicted in Figure 4.2 as these cell division proteins were overexpressed using the *E. coli* BL21(DE3) strain. It also suggested that a vast diversity of native membrane

phospholipids which could have interacted with these two proteins during the cell division process have been co-extracted during SMALP encapsulation.

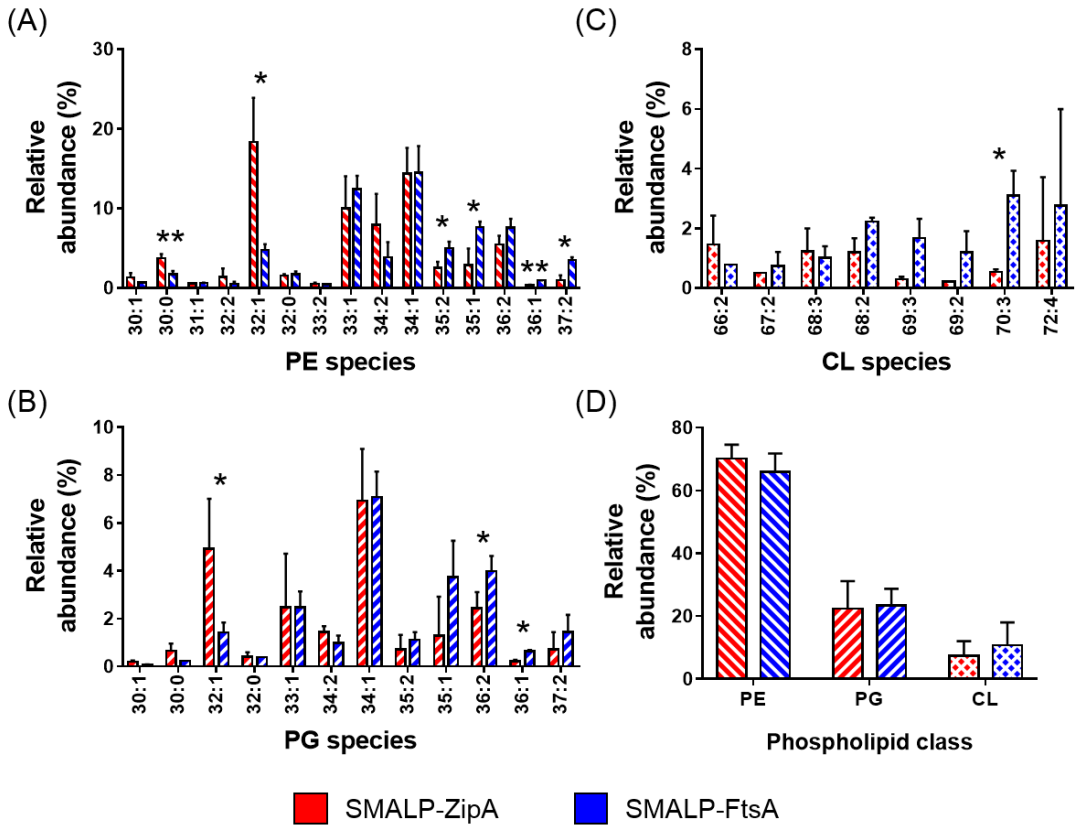

Figure 4.3. Comparison of phospholipid profiles between SMALP-ZipA and SMALP-FtsA upon LC-MS/MS analysis. The 35 common phospholipid species detected in the three classes of *E. coli* membrane phospholipids - (A) PE; (B) PG; and (C) CL are shown for both proteins. Significant differences based on unpaired *t*-tests analysis are highlighted as ** ($p < 0.01$); * ($p < 0.05$). (D) No significant difference was noted when comparing the total phospholipid composition for each phospholipids class. All phospholipid species were confirmed and assigned by tandem MS in the negative ion mode.

For the purified SMALP-ZipA proteins, a total of 22 PE, 21 PG, and 10 CL distinct molecular species (of different *m/z* ratio) were detected and relatively quantified upon LC-MS/MS analysis; 35 molecular species among the detected phospholipids that are were also found in SMALP-FtsA are depicted in Figure 4.3. In terms of phospholipid class composition, the zwitterionic PE contributed 70.2 ± 4.0%, while the anionic PG and CL were 22.5 ± 7.6% and 7.4 ± 4.1% respectively. On the other hand, a total of 26

PE, 21 PG, and 15 CL distinct molecular species were detected and relatively quantified by LC-MS/MS analysis for the purified SMALP-FtsA proteins. PE was found to be 65.9 ± 5.7%, while PG and CL were 23.4 ± 4.7% and 10.7 ± 6.7% respectively.

In general, the breakdown of total phospholipids of ZipA and FtsA resembles the native composition of *E. coli* membranes with 70% PE, 20-25% PG, and 5-10% CL (Mileykovskaya and Dowhan, 2005). The diversity of the co-extracted phospholipids can be observed from a combination of fatty acyl chains, ranging from 12-20 carbon atoms, each with 0-2 double bonds, and including cyclopropane fatty acids, *e.g.* cyC17:0 and cyC19:0, which are characteristics to *E. coli* membranes during stationary growth (Grogan and Cronan, 1997; Oursel *et al.*, 2007a). The presence of phospholipids harbouring these cyclopropane moieties is thus consistent with the fact that the *E. coli* cells were harvested during the stationary growth phase, a common end point for recombinant protein production. Given that the lipid composition has been reported to be dependent on the bacterial growth conditions and life cycle (Arneborg *et al.*, 1993; Cronan, 1968; Furse *et al.*, 2015b; Gidden *et al.*, 2009; Mozharov *et al.*, 1985), this resulted in a variation of approximately 5-6% between the three independent cultures, similar to the observation by Dörr *et al.* (2014).

The data reproducibility was assessed through three independent bacterial cultures and protein purification for ZipA and FtsA, which should cover for the natural variability of the biological samples to facilitate comparison between the phospholipid profiles of these two cell division proteins (Tiwari and Tiwari, 2010). The concentrations of the purified SMALP-ZipA used in this study ranged from 65 to 394.5 µg; whereas for the purified SMALP-FtsA, the concentrations were in the range of 122 to 404.3 µg. Despite a fairly wide range of protein concentrations tested, the profiling of co-extracted membrane phospholipids were successfully in all cases, reinforcing the sensitivity of the LC-MS/MS method developed.

It is important to note the existence of various naturally present isomeric species for each molecular species and tandem MS experiments embedded within the developed LC-MS/MS method have provided information on the individual fatty acid moieties and their structural positions (*sn*-1 vs *sn*-2). For example, the PE 34:1 lipid found in both ZipA and FtsA can be made up of different combination of isomeric species,

including 16:0/18:1, 18:0/16:1 and 17:0/cy17:0, and 15:0/cy19:0. The lack of CL detection using the direct infusion MS approach (as described in Chapter 3) was circumvented using the LC-MS/MS method developed. This refuted the notion of an absence of CL in the ZipA-SMALP lipid extract, but was in fact suppressed by the more abundant PE and PG species using the shotgun lipidomic approach without prior LC separation.

To ascertain the differences between the phospholipid profiles of these two cell division proteins, which have similar and overlapping proposed cellular function, their phospholipid profiles were further examined using statistical approaches. Different pairs of phospholipid species exhibiting significant differences in terms of relative abundance for both ZipA and FtsA are depicted in Figure 4.3 upon unpaired *t*-test analysis. Besides univariate analysis, a multivariate approach employing principal component analysis (PCA) was performed to determine if the phospholipid profiles of ZipA and FtsA are sufficiently distinctive to be clustered differently in the principal component space (as depicted in Figure 4.4). For the PCA of this work, exploiting two principal components were sufficed to explain 89.6% of the variance within the lipid dataset; with 73.5% variance from the first principal component (PC1) and 16.1% from the second principal component (PC2). Higher PC 1 loadings were found to discriminate ZipA over FtsA, in which FtsA was observed to cluster along the negative scale of PC1. The variations between the biological variations within ZipA was found to be larger than FtsA, but the variations in phospholipid profiles between these two cell division proteins were still large enough to discriminate between them and cluster them into two separate groups in the principal component space. It is suffice to state that although these two proteins have similar and likely overlapping function during the cell division process, their phospholipid profiles (as elucidated through SMALP lipidomics) were unique and distinct.

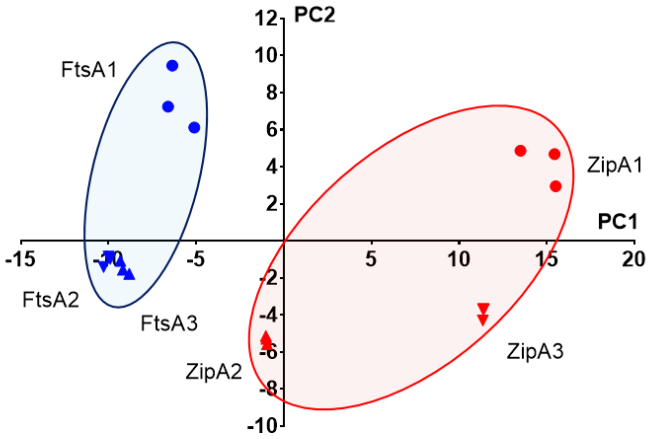

Highest PC1 loadings: ZipA	Lowest PC1 loadings: FtsA
PE 32:1	PE 35:1
PE 34:2	PE 33:1
PG 32:1	PG 35:1
PE 34:1	PE 35:2
PE 32:2	PE 37:2
PE 30:0	PG 36:2
PE 30:1	CL 70:3
CL 68:3	PG 33:1
PG 34:2	PG 37:2
CL 72:4	PE 36:2

Figure 4.4 PCA of SMALP-ZipA and SMALP-FtsA phospholipid profiles. (A) The PCA scores plot showing two distinct clusters for ZipA and FtsA based on their phospholipid profiles. (B) The ten highest and lowest phospholipid molecular species within PC1 loadings that differentiate ZipA from FtsA are listed.

It was observed that PE 30:0, PE 32:1, and PG 32:1 of the highest PC1 loadings (Figure 4.4) also corresponded to the significantly different molecular species between the two proteins (upon unpaired *t-test* analysis), with higher relative abundance in ZipA, especially for PE 32:1 and PG 32:1. In contrast, PE 35:2, PE 35:1, PE 36:1, PE 37:2, PG 36:2, PG 36:1, and CL 70:3 with the lowest PC1 loadings matched the significantly different molecular species between the two proteins with higher relative abundance in FtsA. The relatively high abundance of the fatty acyl combination of 32:1 from both the PE and PG classes in ZipA suggested that this particular fatty acyl combination could have provided the necessary hydrophobic matching to the N-terminal TM helix of ZipA within the lipid bilayer.

FtsA and other peripheral membrane proteins such as SpoVM and DivIVA (two curvature-sensitive proteins in *B. subtilis*) have been suggested to associate with the cell membrane by inserting the hydrophobic residues of their proposed amphiphatic helix into the cell membrane (Martos *et al.*, 2012; Ramamurthi, 2010). This could possibly explain why the phospholipid profile of FtsA is different from ZipA, showing a higher abundance of phospholipids with longer fatty acyl chains (35-37 carbons vs 32 carbons in ZipA). The longer fatty acyl chains could have facilitated the insertion of its amphiphatic helix into the inner leaflet of the cell membrane. Given that the overall phospholipid composition for ZipA and FtsA is essentially the same as depicted in

Figure 4.3 (D), while significant differences can be observed in terms of different fatty acyl profiles, this suggests a clear preference for different lipid chain lengths and/or degree of unsaturation (rather than headgroup) for these two cell division proteins.

The complex interaction between membrane proteins, lipids, and the physical forces applied to the membrane surface can generate membrane curvature which could serve as geometric cues for protein localisation. It has been proposed that proteins capable of sensing membrane curvature can themselves induce curvature and remodelling to the membrane through scaffolding action or by inserting their amphipathic helices into the lipid bilayer (Drin and Antonny, 2010; Zimmerberg and Kozlov, 2006). When the membrane curvature matches the shape of the peripheral proteins, the effective membrane binding energy is minimal, without the need for any local membrane deformation (Zimmerberg and Kozlov, 2006). In theory, it is possible that the insertion of the amphipathic helix of FtsA into the cell membrane can provide a stabilisation force for a negative curvature in the presence of right combination of membrane lipids. Moreover, the amphipathic helix could perturb the packing of the polar lipid headgroups in a wedge-like fashion, resulting in a local membrane deformation, thus inducing membrane curvature (Zimmerberg and Kozlov, 2006).

In addition, the formation of lipid domains triggered by the interaction of charged membrane-associating residues from peripheral membrane proteins, *e.g.* FtsA and MreB (another bacterial actin homologue involved in cell elongation) with the membrane lipids has been proposed (Lin and Weibel, 2016; Matsumoto *et al.*, 2015). Alterations in the membrane lateral pressure in relation to the formation of membrane insertion sites and the storage of curvature stress can affect the membrane binding of peripheral membrane proteins. According to van den Brink-van der Laan *et al.* (2004), when many peripheral membrane proteins insert into the lipid bilayer, it can give rise to an increased lipid headgroup lateral pressure that is likely to be compensated by a decrease in acyl chain lateral pressure to reduce the curvature stress.

4.2.3 Towards the investigation of cell division protein-lipid interaction

Upon the determination of the co-extracted membrane lipidomes for ZipA and FtsA, the next logical step was to compare their phospholipid profiles with respective membrane controls. *E. coli* BL21(DE3) membranes were prepared accordingly by

either inducing ZipA or FtsA overexpression or without protein induction. These control membranes were then subjected to SMALP solubilisation prior to lipid extraction to ensure consistency in the SMALP lipidomic approach. The induced membrane controls (with ZipA or FtsA overexpression but without protein purification) would represent a good comparison to the phospholipid profiles for the purified proteins in SMALP, to see if there is any specific sequestration of phospholipids during protein extraction and purification. On the other hand, the uninduced membrane controls could be used to examine the effect of harbouring the extrachromosal DNA plasmid encoding ZipA or FtsA towards the *E. coli* cells due to any leaky protein expression common to T7-based promoters used in this work (Rosano and Ceccarelli, 2014).

For statistical analysis, one-way analysis of variance (ANOVA) was carried out to uncover any significant differences between the phospholipid profiles for the purified SMALP-ZipA or SMALP-FtsA in comparison to their respective induced and uninduced membrane controls. Figure 4.5 and 4.6 depict the phospholipid profiles of SMALP-ZipA and SMALP-FtsA vs their respective membrane controls upon LC-MS/MS analysis. For the sake of simplicity, the significant differences (based on one-way ANOVA) for different molecular species within the three classes of phospholipids for the two cell division proteins vs their respective membrane controls are separately tabulated in Table 4.1.

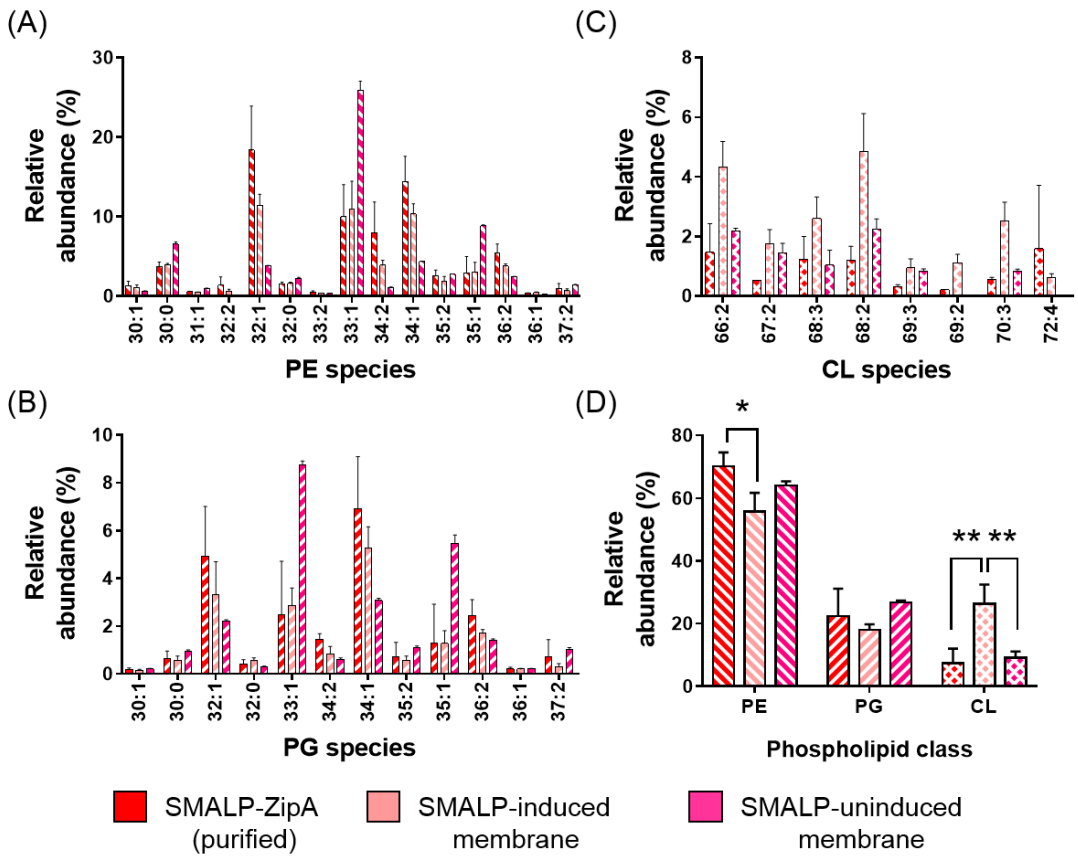

Figure 4.5 Comparison of phospholipid profiles between SMALP-ZipA with the respective induced and uninduced membrane controls upon LC-MS/MS analysis. The 35 common phospholipid species detected in the three classes of *E. coli* membrane phospholipids - (A) PE; (B) PG; and (C) CL are shown. (D) Significant differences (based on one-way ANOVA) for the total phospholipid composition for each phospholipids class were shown. All phospholipid species were confirmed and assigned by tandem MS in the negative ion mode.

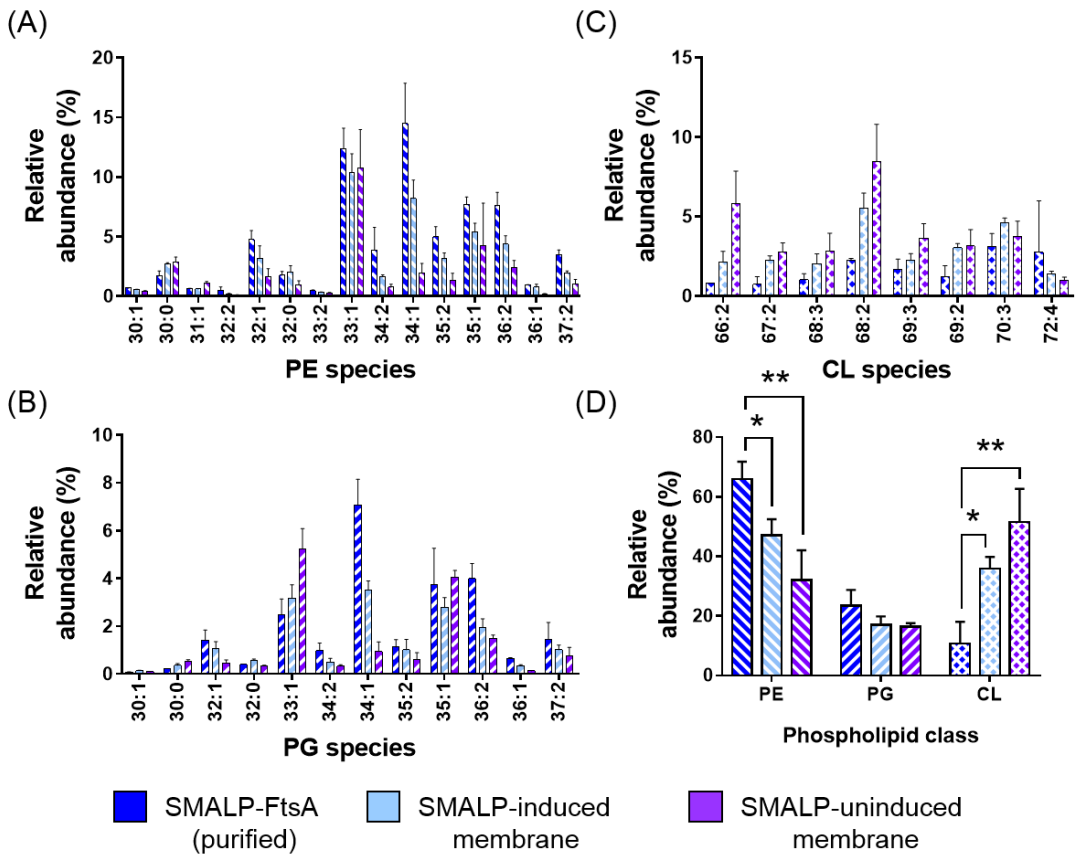

Figure 4.6 Comparison of phospholipid profiles between SMALP-FtsA with the respective induced and uninduced membrane controls upon LC-MS/MS analysis. The 35 common phospholipid species detected in the three classes of *E. coli* membrane phospholipids - (A) PE; (B) PG; and (C) CL are shown. (D) Significant differences (based on one-way ANOVA) for the total phospholipid composition for each phospholipids class were shown. All phospholipid species were confirmed and assigned by tandem MS in the negative ion mode.

Table 4.1 One-way ANOVA of the phospholipid profiles of SMALP-ZipA and SMALP-FtsA vs their respective membrane controls.

Phospho-lipid class	ZipA			FtsA		
	Purified vs induced	Purified vs uninduced	Induced vs uninduced	Purified vs induced	Purified vs uninduced	Induced vs uninduced
PE	N/A	30:0 ***	30:0 ***	30:1 *	30:1 **	30:0 *
		31:1 ***	31:1 ***	30:0 *	30:0 *	31:1 **
		32:1 **	32:0 *	34:1 *	31:1 **	32:0 *
		32:0 **	33:1 **	35:2 *	32:1 **	34:1 *
		33:2 *	34:1 *	36:2 **	33:2 *	35:2 *
		33:1 **	35:1 **	37:2 **	34:2 *	36:1 *
		34:2 *	36:1 *		34:1 **	37:2 *
		34:1**			35:2 **	
		35:1 **			36:2 ***	
		36:2 **			36:1 **	
					37:2 ***	
PG	34:2 *	33:1 **	33:1 **	30:1 *	30:0 *	30:1 *
		34:2 *	35:1 **	32:0 **	32:1 *	32:0 **
		34:1 *		34:1 **	33:1 **	33:1 *
		35:1 **		36:2 **	34:2 *	34:1 **
		36:2 *		36:1 **	34:1 ****	36:1 **
					36:2 ***	
					36:1 ****	
CL	66:2 **	N/A	66:2 *	67:2 *	67:2 *	66:2 *
	68:2 **		68:2 *		68:2 *	
	70:3 **		70:3 **		69:3 *	

Note that * ($p < 0.05$), ** ($p < 0.01$), *** ($p < 0.001$), **** ($p < 0.0001$)

4.2.3.1 ZipA vs membrane controls

There was essentially no difference (in terms of relative abundance) in the PE and PG classes of phospholipids for the purified SMALP-ZipA vs the induced membrane control, with only one difference detected for PG 34:2 which was higher in abundance in the purified SMALP protein sample. Differences were detected for CL 66:2, 68:2 and 70:3, in which the induced membrane control showed a higher abundance of these phospholipid species. More significant differences can clearly be observed when comparing the phospholipid profiles of the purified SMALP-ZipA vs the uninduced membrane control. Interestingly, two-thirds of these differences were also observed when comparing the phospholipid profiles of the induced and uninduced membrane controls. This indicates the overexpression of ZipA has exerted an effect on the membrane lipid composition of the host strain. In fact, the changes in lipid composition

were associated with ZipA, given the minimal differences in phospholipid profiles between the purified protein vs the induced membrane control.

It appears that the overexpression of ZipA has increased the overall CL content (at the expense of PE, as shown in Figure 4.5 (D). However, this increase in CL content did not seem to be locally associated with ZipA, as there was no significant difference between the CL profile for the purified SMALP-ZipA vs the uninduced membrane control. The overexpression and depletion of ZipA have been previously reported to inhibit cell division (Hale and de Boer, 1999). The overexpression of ZipA *in vivo* has also resulted in the observation of multilayered membrane inclusions within the cytoplasm. The overexpressed, excess ZipA was found to be distributed between these extra membrane structures, and displaced other cell division proteins, including FtsA, FtsN, and FtsZ from the septum, besides compromising the permeability barrier function of the cell membrane (Cabré *et al.*, 2013). Similar observation of extra membrane structures in the forms of cisterns, vesicles, tubules and invaginations were also reported for the overexpression of several other membrane proteins, including F_1F_o ATP synthase (Arechaga *et al.*, 2000; von Meyenburg *et al.*, 1984), fumarate reductase (Elmes *et al.*, 1986; Weiner *et al.*, 1984), glycerophosphate acyltransferase PlsB (Wilkison *et al.*, 1986), mannitol permease MltA (van Weeghel *et al.*, 1990), alkane hydrolase AlkB (Nieboer *et al.*, 1996, 1993), chemotaxis receptor Tsr (Lefman *et al.*, 2004), and lipid glycosyltransferases (Ariöz *et al.*, 2014; Eriksson *et al.*, 2009; van den Brink-van der Laan *et al.*, 2003).

In addition, the overexpression of ZipA in *E. coli* BL21(DE3) seemed to result in an enrichment of unsaturated fatty acyl chains, such as C16:1 and C18:1, at the expense of the cyclopropane counterpart - cyC17:0 and cyC19:0 in both PE and PG classes in this work. For example, the C16:1 containing PE 32:1 was more abundant than the cyC17:0 containing PE 33:1 when ZipA was overexpressed. By contrast, the cyC19:0 containing PG 35:1 was more abundant than the C18:1 containing PG 34:1 for the uninduced membrane control. Normally, upon entering the stationary growth phase, unsaturated fatty acids are converted into their cyclopropane counterparts as viable means to protect the double bonds in unsaturated fatty acyl chains from oxidation, or to protect the phospholipids from degradation when resynthesis becomes difficult during the stationary phase at a high energy cost (Cronan, 1968).

4.2.3.2 FtsA vs membrane controls

When comparing the phospholipid profiles of the purified SMALP-FtsA vs its induced membrane control, it was evident that the fatty acyl chain combinations of 34:1 and 36:2 in both PE and PG classes were significantly more abundant in the purified SMALP protein samples. The abundance of five molecular species, *i.e.* PE 34:1, PE 35:2, PE 37:2, PG 34:1 and PG 36:1 were significantly increased for the purified FtsA-SMALP sample vs its induced and uninduced membrane controls. This seemed to substantiate the preference of FtsA for longer fatty acyl chain combinations and thus resulting in the higher abundance for these phospholipid molecular species in its phospholipid profile.

Intriguingly, both the induced and uninduced membrane controls of FtsA showed a significant increase in CL content at the expense of PE, with the PG content remained relatively the same, as shown in Figure 4.6 (D). The uninduced membrane sample exhibited the largest amount of CL. It is known that the concentration of anionic lipids in bacterial membranes can vary in response to growth phase, pH, salinity, osmolality, and organic solvents (Lin and Weibel, 2016; Romantsov *et al.*, 2009). Although CL is only a trace membrane component during exponential growth in bacteria, it may increase to become the most dominant class under certain conditions that link to growth reduction (Schlame, 2008). Even a small amount of CL can decrease the lateral interaction within the lipid monolayer, resulting in a reduction of energy to stretch the membrane to favour the creation of membrane folds or invaginations. CL can also form domains or clusters and non-bilayer structures (Schlame, 2008). In the presence of divalent cations, such as Ca^{2+}, CL can induced the formation of inverse hexagonal (H_{II}) phase, analogous to the case for PE (Goldfine, 1984). Nevertheless, it should be noted that the CL content of the purified SMALP-FtsA resembled the reported native level of CL in *E. coli* cells. This suggests that the extra amount of CL induced by the presence of the FtsA plasmid was not sequestered by the protein during the solubilisation process. In other words, the overexpressed FtsA might not be located in a CL-rich domain in the host cells in this work.

The hypothesis for an enrichment in CL that associates with these two cell division proteins was not substantiated in this studies, as no significant increase in CL content was observed with either the purified SMALP-ZipA or SMALP-FtsA (Mileykovskaya

and Dowhan, 2005). Many reasons could refute this CL-enrichment idea, for example, CL does not specifically associated with ZipA and FtsA during the cell division process. The effects of protein overexpression could have also masked the association of CL to these proteins. It is important to note that the nature of the SMALP lipidomic approach developed could not provide spatial resolution in terms of lipid analysis, as the extracted lipidome represents an ensemble for all the extracted and purified SMALP protein in the sample. Nevertheless, the developed LC-MS/MS method has provided a sensitive and robust analytical tool for the detailed characterisation of membrane lipidomes of the target membrane proteins coupled with the SMALP technology.

4.3 Concluding remark

In the work described in this chapter, the LC-MS/MS method developed was applied to characterise the co-extracted membrane lipidomes of two key cell division proteins in *E. coli*, namely ZipA and FtsA. First and foremost, no preferential extraction was observed when analysing the phospholipid profiles of *E. coli* BL21(DE3) membranes with or without SMALP treatment, which substantiated the employment of SMALP lipidomics for the analysis of co-extracted membrane lipidomes of *E. coli* membrane proteins of interest. Subsequently, the first comprehensive characterisation of the co-extracted membrane lipidomes of ZipA and FtsA were reported, showing unique and distinct phospholipid profiles for these two cell division membrane proteins. ZipA was found to harbour a preference for the specific fatty acyl combination of 32:1 for both PE and PG in this work, which suggested that this particular fatty acyl combination could have provided the necessary hydrophobic matching to the N-terminal TM helix of ZipA within the lipid bilayer. In contrast, phospholipids with longer fatty acyl chains (35-37 carbons) were associated with FtsA in this work, suggesting that these longer fatty acyl chains could have facilitated the insertion of the amphiphatic helix of FtsA into the inner membrane of *E. coli*. In essence, clear preference for different lipid chain lengths and/or degree of unsaturation (rather than headgroup) for these two cell division proteins was elucidated in this work. In addition, the overexpression of ZipA exerted an effect on the membrane phospholipid composition of the host strain. The preference for FtsA for longer fatty acyl chain combinations was observed when comparing its corresponding membrane controls. The hypothesis for an enrichment in CL that associates with these two cell division proteins was not substantiated in this work, as

no significant increase in CL content was observed with either the purified ZipA or FtsA in SMALP.

Chapter 5: Detergent-Free Isolation and Characterisation of the Integral Membrane Lipid Phosphatase - PgpB

5.1 Background

Driven by the interesting insight of the unique and distinct membrane lipidomes for ZipA and FtsA (as described in Chapter 4) obtained through the LC-MS/MS method developed, the investigation was expanded to an *E. coli* integral membrane lipid phosphatase - PgpB. This membrane protein has six TM helices and was initially discovered for its phosphatase activity towards several phospholipids, including phosphatidylglycerol phosphate (PGP), phosphatidic acid (PA), lysophosphatidic acid (LPA) and diacylglycerol pyrophosphate (DGPP) (Dillon *et al.*, 1996; Funk *et al.*, 1992; Icho, 1988; Icho and Raetz, 1983). Subsequently, PgpB was also found to act on the glycan lipid carrier - undecaprenyl pyrophosphate (C_{55}-PP) (El Ghachi *et al.*, 2005; Touzé *et al.*, 2008), together with another phosphatase - BacA/UppP, with BacA/UppP being the primary C_{55}-PP phosphatase in *E. coli* (El Ghachi *et al.*, 2004). C_{55}-PP is synthesised by the successive addition of eight isopentyl pyrophosphates onto one farnesyl pyrophosphate, catalysed by the cytosolic undecaprenyl pyrophosphate synthase (UppS) (Fujihashi *et al.*, 2001). Given that both of these phosphatases act on C_{55}-PP on the periplasmic side of the inner membrane, the *de novo* formation of undecaprenyl phosphate (C_{55}-P) on the cytoplasmic side of the inner membrane in *E. coli* still remain an enigma (Chang *et al.*, 2014; Manat *et al.*, 2015, 2014; Teo and Roper, 2015).

PgpB belongs to the type 2 phosphatidic acid phosphatase (PAP2) superfamily which are Mg^{2+}-independent, with members such as YbjG and LpxT (both found to also act on C_{55}-PP), but is distinct to the Mg^{2+}-dependent BacA/UppP (Tatar *et al.*, 2007; Touzé *et al.*, 2008). A consensus motif of the acid phosphatase domain can be found on these PAP2 proteins, with signature residues facing the periplasmic region (Tatar *et al.*, 2007). The three distinct motifs are designated as C1: "KX_6RP"; C2: "PSGH"; and C3: "SRX_5HX_3D" (Stukey and Carman, 1997). In comparison to *E. coli* ZipA and FtsA, PgpB is much better structurally characterised. The first crystal structure of PgpB (in its apo form) was solved at 3.2 Å resolution (PDB: 4PX7) and was found to display similar folding topology with nearly identical active site to the other soluble PAP2

enzymes, but with differences in terms of their substrate-binding mechanism (Fan *et al.*, 2014). The lipid-bound form of PgpB was subsequently solved by Tong *et al.* (2016) at identical resolution of 3.2 Å (PDB: 5JWY) as illustrated in Figure 5.1. The binding of lipid substrates to PgpB was proposed to proceed via an induced fit mechanism. A cleft formed by a V-shaped TM helix pair - TM2 and TM3 was suggested to be the potential substrate entrance, facilitating the lateral movement of the lipid substrates to the active site of the enzyme from the cell membrane (Figure 5.1) (Fan *et al.*, 2014). However, recent mutational studies of PgpB by Tong *et al.* (2016) did not provide support for this route of substrate access.

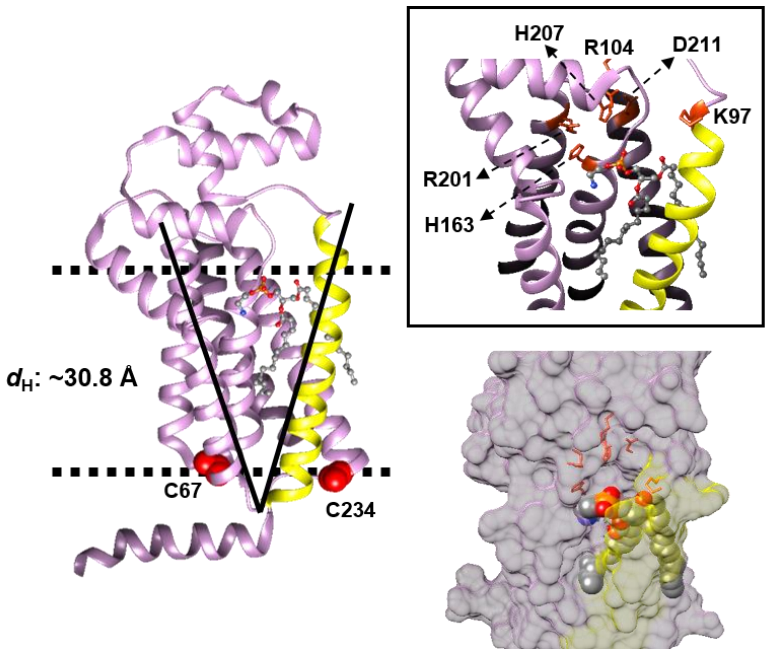

Figure 5.1 Crystal structure of the PE-bound form of *E. coli* PgpB (PDB: 5JWY). The angled-away TM3 (in yellow) resulting in the V-shaped groove below the active site and the membrane-embedded tunnel is shown. The key residues implied in catalysis are highlighted in the zoomed-in panel (top right). The two cysteine residues in PgpB (C67 and C234) are represented as red spheres. The boundaries of the lipid bilayer (30.8 Å) as an indication of its hydrophobic thickness are indicated as black dotted lines following the prediction using the Orientations of Proteins in Membranes (OPM) database (Lomize *et al.*, 2006). Figure was prepared using UCSF Chimera version 1.10.1 (Pettersen *et al.*, 2004).

In this lipid-bound structure of PgpB, the PE molecule was found in a narrow tunnel-like feature (termed TM3 tunnel) sandwiched between TM3 with TM4 and TM6. The

ethanolamine headgroup was stabilised by the residues, H163, Q50 and F166 in front of the catalytic site via cation-π interactions. The PE molecule was constrained in the tunnel by G89 (TM3) and G162 (C2 motif). Blocking the TM3 tunnel via bulky valine or phenylalanine residues was found to abolish PgpB activity. The *sn*-2 tail of PE was found to penetrate deeply into a narrow acyl pore, with the tip of the fatty acyl tail reaching out in front of TM2-3 groove. Based on molecular docking examination, this acyl pore was also found to accommodate the *sn*-1 tail of LPA and sphingosine-1-phosphate (S1P), besides the *sn*-2 tail of PA. Lastly, the double lysine residues - K93 and K97 (TM3) were proposed to be the sensor residues, deemed to be critical for lysolipid substrate recognition, but not for PGP (Tong *et al.*, 2016).

Figure 5.2 depicts the proposed catalytic mechanism of PgpB (Fan *et al.*, 2014). In reference to other PAP2 enzymes, H207 and D211 were presented as the charge-relay pair for nucleophilic attack and the formation of the phosphoenzyme intermediate, which could then be stabilised by H163 that catalyses the cleavage of the phosphate group. The lipid substrate is thought to project its phosphate head into the bottom of the active site pocket of PgpB, towards the nucleophilic H207. This engagement could stabilise the phosphoenzyme complex, allowing H163 to complete the dephosphorylation step in recruiting a water molecule from the solvent-accessible side of the enzyme active site. In addition, R104 was suggested to interact with H207 and potentially with the lipid substrate, while R201 could interact with H163 (Fan *et al.*, 2014).

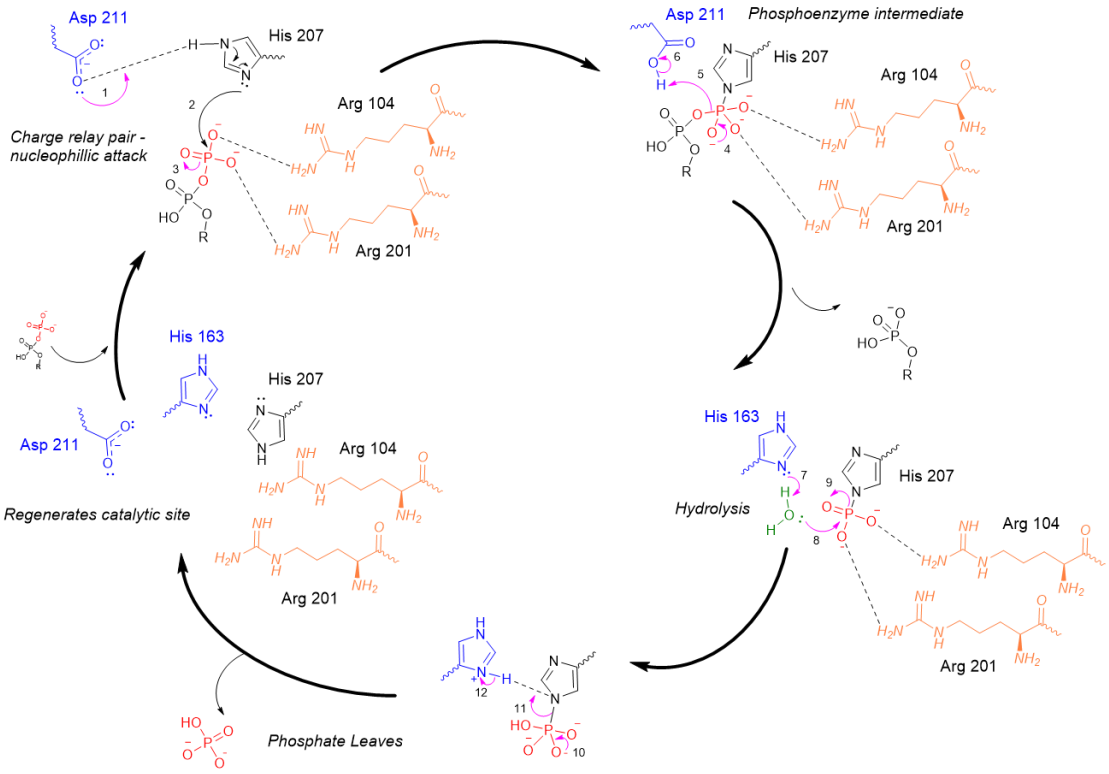

Figure 5.2. The proposed catalytic mechanism of *E. coli* PgpB (Fan *et al.*, 2014). Figure was prepared in ChemDraw Processional version 15.0 with the help of Dr. M. Quareshy.

The proposed catalytic mechanism involving the catalytic triad - H207, D211, and H163 was found to be important for the dephosphorylation of PA, LPA, and S1P, but was not for PGP, as H207 was the only residue demonstrated to be essential for catalysis. Specific conformational changes were thus suggested to enable PgpB to accommodate the large PGP headgroup, for example by shifting the imidazole ring of H163 away from the entry point of the enzyme catalytic site. A water molecule may be allocated as the H^+ donor to initiate the hydrophilic attack. In addition, the bulky phosphoglycerol moeity of PGP (as a replacement of H163) at the catalytic entry site could serve as an alternative H^+ donor to the terminal phosphate group to facilitate self-catalysis, therefore explaining the different specificity of PgpB for PGP vs the other lipid substrates (Tong *et al.*, 2016).

DGPP, which is commercially available in different fatty acyl chain lengths (*e.g.* 8:0/8:0 and 18:1/18:1) has been demonstrated to be a good *in vitro* substrate for PgpB (Touzé *et al.*, 2008). The addition of 8:0/8:0 DGPP stimulated the activity of PgpB on C_{55}-PP in a dose-dependent manner *in vitro*. The addition of PE, PG and CL also

enhanced the activity of PgpB towards C_{55}-PP, especially the anionic phospholipids - PG and CL (by five-fold). The stimulating effect was most pronounced with C_{55}-PP, when compared to other shorter isoprenoid pyrophosphate substrates such as C_{15}-PP and C_{35}-PP (Touzé *et al.*, 2008). They reasoned that C_{55}-PP is the preferred substrate for PgpB as the addition of 8:0/8:0 DGPP did not inhibit its activity towards C_{55}-PP but rather stimulated it. This observation led them to the hypothesis that the C_{55}-PP substrate might be presented in a non-native conformation or orientation in the detergent micelles, thus preventing the charged pyrophosphate headgroup from being correctly presented to the active site of PgpB. The addition of DGPP or other membrane phospholipids could have rendered the detergent micelles more 'native membrane-like' and consequently stimulated the activity of PgpB towards C_{55}-PP (Touzé *et al.*, 2008).

According to the surface dilution kinetics model, enzymes that act on lipid substrates are operating in an environment in which both three dimensional bulk interactions in solution and two dimensional surface interactions occur. Both of these interactions thus need to be considered as the surface concentration of the lipid substrates and their bulk concentration would play crucial roles during kinetic characterisation (Carman *et al.*, 1995). With TM proteins solubilised in detergent micelles, for instance PgpB in DDM, there are two existing interacting surfaces, with one containing the enzyme and the other containing the lipid substrate. The enzyme-micelle complexes *in vitro* can maintain its integrity, bouncing from micelle to micelle, or alternatively the enzyme-micelle complex can fuse with other lipid-micelle complexes. The alteration of lipid headgroup and/or fatty acyl chain composition of a lipid substrate could result in considerable changes in the interface characteristics, which affect the activity of lipid-dependent enzymes. An observed difference in the activity of an enzyme acting on two different lipid substrates could either be a reflection of true specificity or an indirect consequence of physicochemical changes in the surface characteristics (Carman *et al.*, 1995).

The activity of PgpB has been demonstrated to depend on the acyl chain length of the lipid substrates, as no activity was detected for the water soluble substrates, including glycerol-3-phosphate, glucose-6-phosphate and *p*-Nitrophenyl phosphate (Tong *et al.*, 2016; Touzé *et al.*, 2008). It was deemed that the long fatty acyl chain is essential for both substrate binding and enzyme catalysis (Tong *et al.*, 2016).

5.1.1 Aim and objectives of chapter

The primary aim of the work described in this chapter was to examine the feasibility of studying *E. coli* PgpB using the SMALP technology. The effort was prompted by the lack of published report to-date of any integral membrane lipid phosphatase of such nature to be studied in a detergent-free membrane mimetic system. The *E. coli* PgpB was overexpressed recombinantly with a C-terminal polyhistine tag to facilitate downstream affinity purification. The overexpressed His-tagged PgpB was extracted from the host membrane using the conventional detergent approach with DDM and also the SMALP technology utilising a 2:1 SMA copolymer. The affinity purified SMALP-PgpB and DDM-PgpB were subsequently subjected to biophysical and biochemical analyses. In addition, the co-extracted membrane lipidomes of PgpB (in SMALP and DDM) was characterised by exploiting the LC-MS/MS method developed and the corresponding phospholipid profiles were compared to assess the delipidation effect of DDM as the membrane solubilising agent.

5.2 Results and discussion

5.2.1 Overexpression and purification of the C-terminally hexahistidine tagged PgpB in SMALP and DDM

Based on the overexpression protocol by Touzé *et al.* (2008), recombinant *E. coli* PgpB was successfully overexpressed in the *E. coli* C43(DE3) cells and subsequently extracted from the host membrane utilising either the 2:1 SMA copolymer or DDM. PgpB has been previously characterised in DDM (Touzé *et al.*, 2008) and both the apo and PE-bound forms of PgpB were crystallised in DDM (Fan *et al.*, 2014; Tong *et al.*, 2016), thus DDM was selected as the benchmark detergent of choice for the comparative examination of PgpB in SMALP. The host strain used in this study, *i.e. E. coli* C43(DE3) is one of the Walker strains derived from the commonly used expression strain - BL21(DE3). *E. coli* C43(DE3) has been genetically characterised with mutations in the *lac*UV5 promoter region, which resulted in a weaker wild-type-like promoter, thus reducing the overall level of T7 RNA polymerase that facilitated greater membrane protein production, possibly by reducing the pressure of the *E. coli* cells from the overexpression of target membrane proteins (Wagner *et al.*, 2008).

The overexpressed PgpB was successfully solubilised and purified using the SMALP technology (as shown in Figure 5.3), demonstrating the first report of SMALP

encapsulation of this integral membrane lipid phosphatase. The overall purity of PgpB was considerably higher in SMALP when compared to the DDM-solubilised PgpB even after one-step immobilised metal affinity (IMAC) purification using the Ni-NTA resin (as shown in Figure 5.3), which corroborated similar observations from previous reports from the Rothnie group (Gulati *et al.*, 2014; Morrison *et al.*, 2016). A reduction in the number of purification steps could prevent the loss of protein, which is advantageous for the already much lower yield of membrane proteins vs the soluble counterparts. It can be observed that some PgpB was left in the insoluble fraction upon solubilisation with the SMA copolymer. Thus, the extraction protocol could be optimised in the future to maximise the yield of the membrane protein.

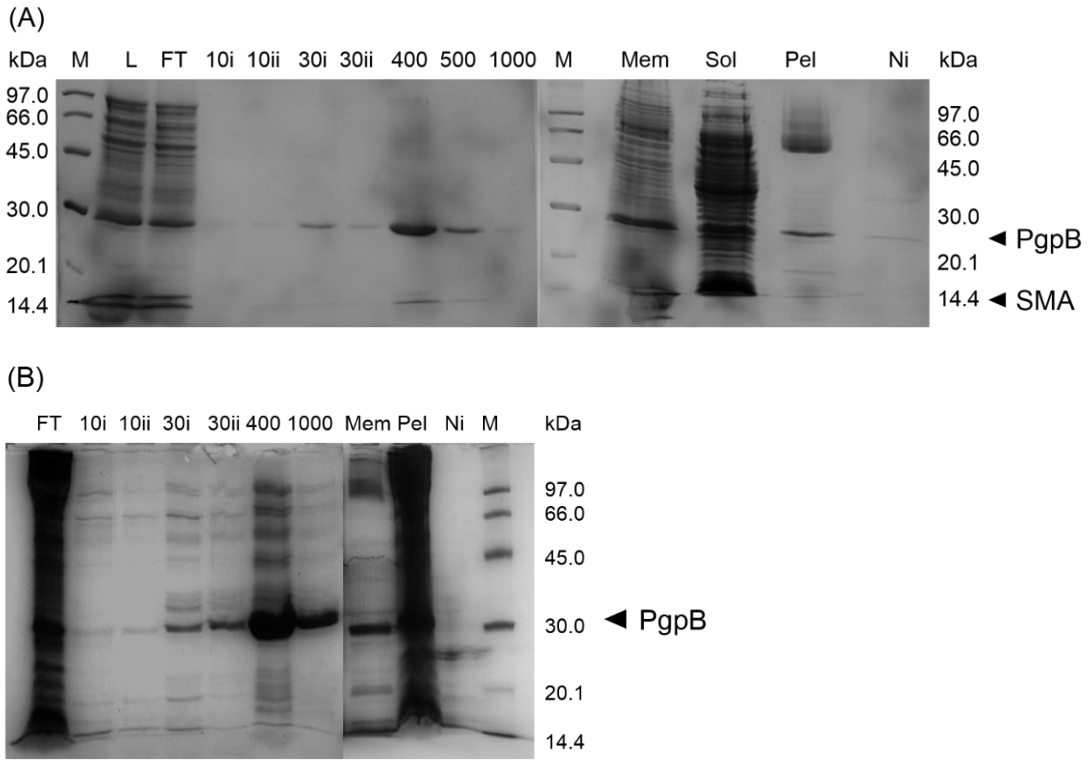

Figure 5.3 SDS-PAGE gels showing the purification of *E. coli* PgpB in SMALP and DDM. (A) With a single IMAC purification, PgpB in SMALP was found to be in higher purity than the DDM counterpart as shown in (B). M: Molecular marker; L: IMAC load; FT: IMAC flow through; 10i: 10 mM imidazole wash 1; 10ii: 10 mM imidazole wash 2; 30i: 30 mM imidazole wash 1; 30ii: 30 mM imidazole wash 2; 400: 400 mM imidazole elution; 500: 500 mM imidazole elution; 1000: 1 M imidazole elution; Mem: *E. coli* C43(DE3) membrane for SMALP or DDM solubilisation; Sol: Solubilised membrane for Ni-NTA IMAC purification; Pel: Insoluble fraction upon SMALP or

DDM solubilisation; Ni: Ni-NTA resin post IMAC purification. Note that the SMA copolymer can often be observed as a band below the dye front (at approximately 10 kDa) under denaturing electrophoretic separation condition.

The solubilisation efficiency of the 2:1 SMA copolymer used in this work has been reported to be comparable to DDM (around 55%) for several bacterial membrane proteins overexpressed in *E. coli*, namely ZipA, BmrA (a multidrug efflux pump from *B. subtilis*), and LeuT (an amino acid:Na^+ symporter from *Aquifex aeolicus*). However, a lower overall yield of purified protein was noted when employing the SMALP technology, suggesting future improvement in the protein solubilisation and purification protocol (Morrison *et al.*, 2016). Several other variants of the SMA copolymers which differ in the S:MA ratio and molecular weight were also evaluated by Morrison *et al.* (2016) and they found that the 2:1 variant (used in this work) gave the best yield, purity and functional conservation of target membrane proteins upon a single step of IMAC purification.

5.2.2 CD analysis of PgpB in SMALP and DDM

CD is a common spectroscopic technique employed to characterise the secondary structure composition of polypeptide to infer folding or conformational change of a protein in solution by measuring the differential absorption of left- and right-handed circularly polarised light (Kelly *et al.*, 2005; Miles and Wallace, 2016). In comparison to the MSP-nanodisc system, whereby the α-helical signal from the MSP can skew the CD measurement of membrane protein of interest, the exploitation of the SMA copolymer (although still absorb in the UV range) can facilitate the acquisition of good quality CD spectra given the low amount of polymer associated with SMALP-proteins upon purification (Dörr *et al.*, 2016). The percent helicity calculated from the CD spectra is often a useful indicator for stability monitoring of membrane proteins. However, it can be challenging to obtain good quality CD spectra below 200 nm (far-UV region) for membrane proteins, especially the presence of chloride ions in the buffer above 200 mM can absorb light. Thus, a buffer of low chloride concentration (< 50 mM) has been suggested for SMALP protein studies (Lee *et al.*, 2016b).

In this work, PgpB was observed to retain its proper folding in SMALP (as shown in Figure 5.4), similar to the observations by other groups investigating different TM

proteins (Dörr *et al.*, 2014; Gulati *et al.*, 2014; Jamshad *et al.*, 2015a). The CD spectrum for PgpB in DDM micelles was analogous to the one in SMALP (as shown in Figure 5.4). The characteristic α-helical signals (with negative minima at 208 and 222 nm) signified that PgpB was predominantly α-helical, which corresponds to its six TM helices, and thus indicates that the protein was very likely to be correctly folded in both solubilisation system.

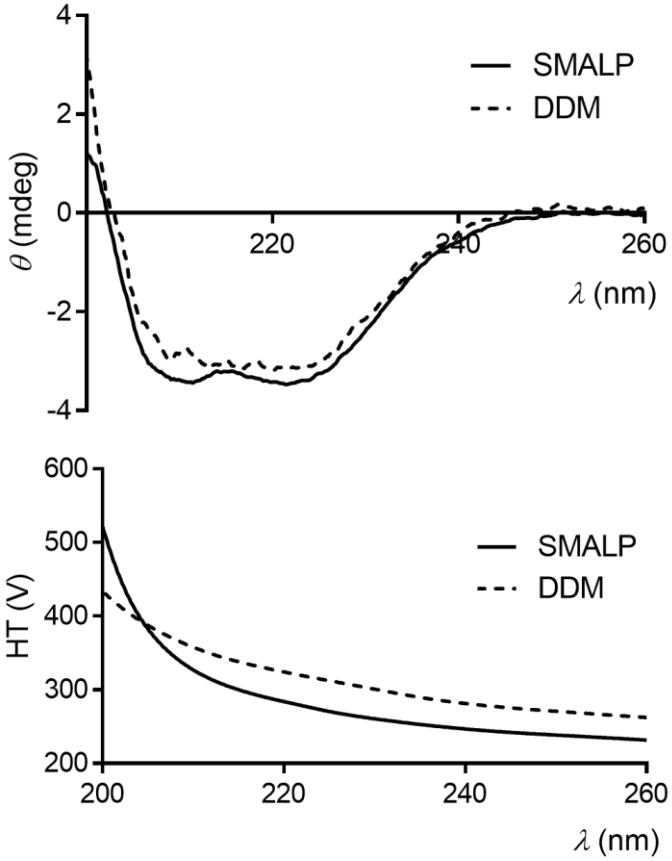

Figure 5.4 CD spectra of purified PgpB (0.02 mg/mL) in SMALP and DDM, with high tension (HT) cut-off at 600V. The CD spectra have been corrected for the buffer signal.

5.2.3 TEM analysis of PgpB in SMALP

Besides CD, TEM is another biophysical technique being employed for the imaging of purified SMALP-protein particles, especially through the negative staining approach (Bersch *et al.*, 2017; Dörr *et al.*, 2014; Gulati *et al.*, 2014; Knowles *et al.*, 2009; Laursen *et al.*, 2016; Li *et al.*, 2015; Long *et al.*, 2013; Paulin *et al.*, 2014; Postis *et al.*, 2015; Smirnova *et al.*, 2016; Swainsbury *et al.*, 2014; Zhang *et al.*, 2017). In this work, the purified SMALP-PgpB was characterised by TEM with negative staining. Regularly

sized and monodisperse particles around 10±2 nm in size were observed (as shown in Figure 5.5). This observation is similar to several other reported SMALP-proteins, substantiating that the SMALP encapsulation results defined sized particles (Dörr *et al.*, 2014; Gulati *et al.*, 2014; Laursen *et al.*, 2016; Long *et al.*, 2013; Smirnova *et al.*, 2016; Swainsbury *et al.*, 2014).

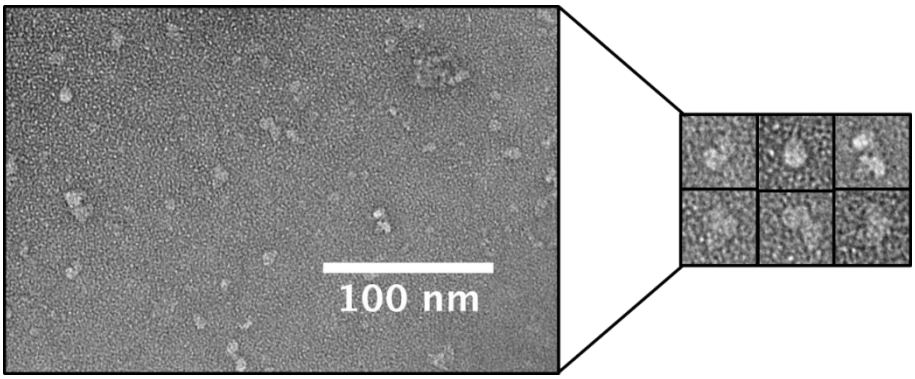

Figure 5.5 Negative stained TEM image (x 30000) of affinity purified SMALP-PgpB (0.1 mg/mL). Representative close-up images are shown on the right.

It is important to note that the TEM examination (with negative staining) performed in this work was primarily to visualise the state and size of the purified SMALP-PgpB, and thus the different projections and orientations of the particles could not be deciphered without further in-depth structural analysis. For future work, Ni-NTA functionalised gold nanoparticles could be utilised to label and positively identify the SMALP-PgpB in solution to aid structural analysis, as per reported by Swainsbury *et al.* (2014).

With the current revolution of cryo-electron microscopy, an increasing number of proteins which previously resisted X-ray crystallography or other structural biology approaches have been successfully characterised to high resolution using this technique (Callaway, 2015). Thus, the detergent-free encapsulation of PgpB in SMALP is potentially beneficial for future structural characterisation efforts of this functionally intriguing lipid phosphatase using advance cryo-EM technique to complement the crystallographic data obtained on this enzyme. Nevertheless, the lower size limit of cryo-EM (around 300 kDa) renders it inherently a technique more suitable for large and stable molecular machineries and/or complexes that can withstand electron bombardment. Thus, this size limitation must be overcome when working with a

relatively small membrane protein such as PgpB (Callaway, 2015; Kühlbrandt, 2014). Given the notion that 'structure is function', further structural investigation of PgpB in its native lipid environment (in SMALP) could perhaps aid in deciphering how this enzyme participates in the multiple biochemical pathways in *E. coli*.

5.2.4 Thermal stability analysis of PgpB in SMALP and DDM

Previously, the thermal stability of DDM-PgpB was investigated using a fluorescence-based thermal shift assay by employing the thiol-specific probe, 7-Diethylamino-3-(4-maleimidophenyl)-4-methylcoumarin (CPM) (Fan *et al.*, 2014). This technique has also been applied to examine the thermal stability of recombinant SMALP-P-glycoprotein, which was overexpressed in yeast cells (Routledge *et al.*, 2016). The assay is based on the binding of the CPM dye to cysteine residues (normally within the TM segment or interior of membrane protein) or other exposed hydrophobic patches upon heat-induced protein unfolding (Alexandrov *et al.*, 2008; Wang *et al.*, 2015). PgpB has two cysteine residues, *i.e.* C67 (TM2) and C234 (TM6), both of which are close to the inner leaflet of the cytoplasmic membrane (as depicted in Figure 5.1).

The thermal stability of PgpB in SMALP and DDM was investigated based on the method by Sonoda *et al.* (2011). Based on their method, the time whereby half of the maximum fluorescence is recorded (defined as its half-life, $t_{1/2}$) of 17 min or longer at 40°C signifies adequate membrane protein stability such that it can be exchanged into LDAO from DDM for crystallisation trials. Essentially, membrane proteins with an unfolding rate longer than approximately 17 min at 40°C are sufficiently stable for crystallisation trials in that detergent, however it is crucial to note that protein stability in this scenario does not equate to an absolute guarantee to crystallisation. The stability of membrane proteins is predominantly intrinsic to the polypeptide itself and it is often not conferred by detergent or being detergent-specific (Sonoda *et al.*, 2011).

In this work, the steady increase in fluorescence, shown in the *y*-axis as relative fluorescence unit (RFU) for SMALP-PgpB was observed, with a half-life > 17 min (RFU of 10000 around 60 min), indicating that the PgpB in SMALP was relatively stable in the buffer employed (as shown in Figure 5.6). In contrast, the DDM-solubilised PgpB has most likely aggregated and crashed out of solution in the buffer used, thus a reduction in fluorescence was observed after 150 min. It is also likely that

the presence of the reducing agent - β-ME included the DDM buffer has reacted with the CPM dye in some ways (Alexandrov *et al.*, 2008).

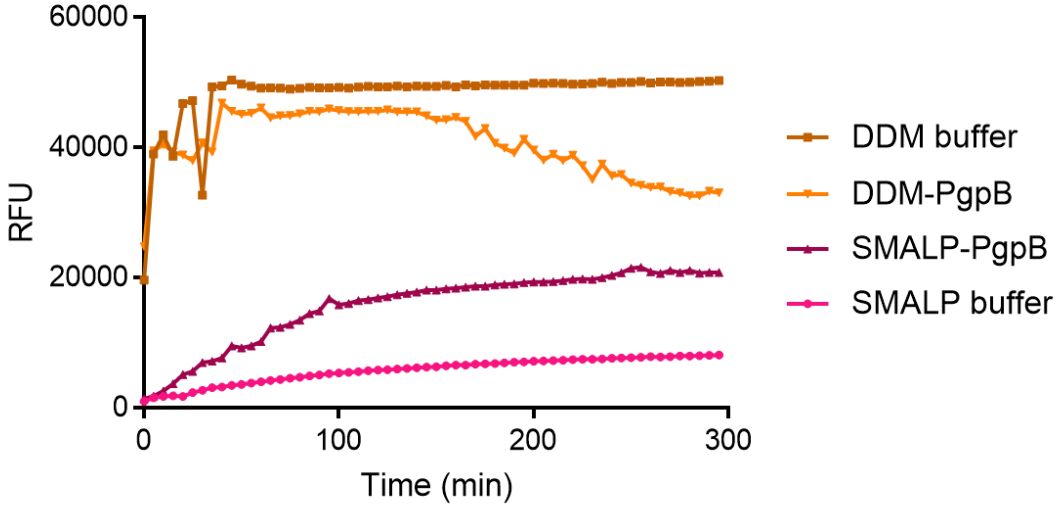

Figure 5.6 Thermal stability of PgpB in SMALP and DDM as monitored by the CPM assay at 40°C over a five-hour period.

This preliminary stability analysis of PgpB utilising the CPM assay has demonstrated its applicability to this protein in the SMALP context. However, more work ought to be conducted to validate the findings besides exploiting this assay for ligand screening purposes. The CPM assay employed in this work was based on the method by Sonoda *et al.* (2011) to monitor the changes in fluorescence over a prolonged period at 40°C. Alternatively, a temperature sweep approach can be employed to examine the melting temperature of PgpB by monitoring its unfolding (with concominant surge in fluorescence) as the temperature increases.

5.2.5 Towards *in vitro* biochemical characterisation of PgpB in SMALP

Previous biochemical studies on PgpB have utilised either radiolabelled substrate for TLC-based assay (Touzé *et al.*, 2008) or colorimetric reagents, including ammonium molybdate and malachite green to assess the desphosphorylation activity of PgpB (Fan *et al.*, 2014; Tong *et al.*, 2016). These are end-point assays with a fixed incubation time providing limited information on the kinetics of the enzymatic reaction. By contrast, an enzyme-coupled phosphate release assay (Webb, 1992) was adopted in this work to

facilitate a continuous time course monitoring of phosphate release by PgpB in the presence of the lipid substrate as described in Figure 2.1 in Chapter 2.

Fan *et al.* (2014) previously tested the activity of PgpB (in DDM) on various lipid substrates, including 18:1 LPA, 18:1/18:1 PA, 8:0/8:0 and 18:1/18:1 DGPP, but neither PGP nor C_{55}-PP were examined despite both of them being claimed to be the 'native' substrates of PgpB. This was probably due to the fact that PGP and C_{55}-PP were not commercially available. Touzé *et al.* (2008) managed to obtain the C_{55}-PP substrate and other variants through the Institute of Biochemistry and Biophysics of the Polish Academy of Sciences, while Tong *et al.* (2016) resorted to custom-made PGP for their biochemical studies. The availability of these substrates in the commercial market should support future biochemical studies with PgpB.

In this work, the commercially available 18:1/18:1 DGPP was exploited to investigate the activity of PgpB in SMALP and DDM. When DGPP was added to DDM-PgpB, an immediate dephosphorylation of the lipid substrate (with concomitant phosphate release) was observed (as depicted in Figure 5.7). However, no dephosphorylation activity (in the form phosphate release) was detected for SMALP-PgpB using the same lipid substrate solubilised in DDM micelles (as depicted in Figure 5.7). An attempt to present the lipid substrate in DMSO also led to the same observation. DGPP was also added to 1% w/v SMA copolymer to be presented to the SMALP-PgpB, but no dephosphorlation activity was recorded. Despite the addition of excess SMALP-PgpB and/or lipid substrate, no phosphate release was observed after prolonged and repeated investigations. As a result, the MESG/PNP coupling system was validated by the addition of inorganic phosphates, which recorded an immediate 'phosphate jump' (as depicted in Figure 5.7), indicating a robust reporting system. Thus, the inactivity of PgpB in SMALP was not due to a defective coupling system.

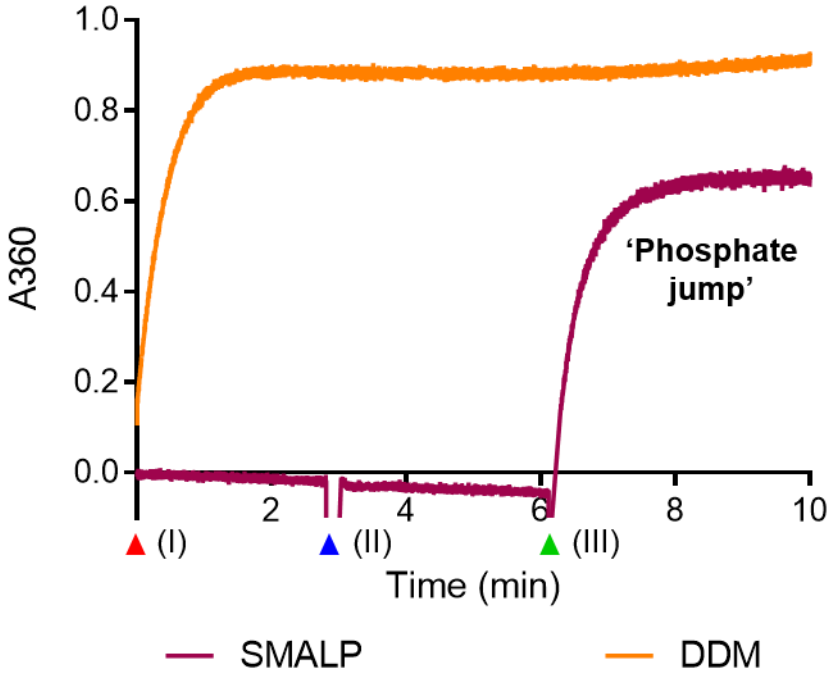

Figure 5.7 Biochemical characterisation of PgpB *in vitro* using the enzyme-coupled phosphate release assay. The reaction was initiated with the addition of 1 µM PgpB in SMALP or DDM (I). For SMALP-PgpB, 4.15 µM enzyme was further added at *t* around 3 min to re-examine its activity (II), and upon prolonged and repeated observations of SMALP-PgpB inactivity, the MESG/PNP coupling system was validated with the addition of 2 mM phosphate at *t* around 6 min (III) to validate the MESG/PNP coupling system.

These observations led to the hypothesis that the SMA copolymer belt was preventing PgpB from accessing the the lipid substrate presented in detergent micelles, rather than the protein itself being denatured as the CD spectrum of SMALP-PgpB (Figure 5.4) indicated a proper folding. It should be noted that ligand binding studies using water soluble ligands have been successfully performed on G-protein-coupled receptors encapsulated in SMALP (Gulati *et al.*, 2014; Jamshad *et al.*, 2015a). Thus, the possibility of a 'blocked' enzyme in SMALP towards the water-insoluble lipid substrates rather than an inactivated enzyme seems more likely.

5.2.5.1 Release and reconstitution of SMALP-PgpB (de-SMALP)

In order to investigate the hypothesis that the SMA copolymer was blocking the encapsulated PgpB from accessing the lipid substrate, the idea of releasing it from the SMA copolymer

belt was tested, in other words to 'de-SMALP' the protein. To maintain the solubility of the de-SMALPed PgpB in solution, an attempt to resolubilise the protein was investigated with the addition of detergents, *i.e.* DDM in this work. It was the main goal of this experiment to examine the possibility of releasing a SMALP encapsulated protein with subsequent reconstitution into another membrane mimetic system or solubilisation agent. Although the concept of de-SMALP has been suggested and briefly tested for SMALP-ZipA (Lin, 2011), no optimised de-SMALP procedure has been reported for other SMALP-protein.

There are two potential approaches to achieve this releasing of encaspsulated protein from the SMA copolymer belt; either based on the pH-driven SMALP encapsulation process or the sensitivity of the SMA copolymer to divalent cations (as depicted in Figure 5.8) (Jamshad *et al.*, 2011; Knowles *et al.*, 2009). By reducing the pH of the solution, the SMA copolymer would be protonated as the first pK_a of the 2:1 SMA copolymer is around 6 and the second pK_a around 10. At low pH, this SMA copolymer is essential uncharged; while at neutral pH, one of the carboxyl group would be charged; and at alkaline pH, both of the carboxyl groups would be charged. Electrostatic repulsions between the carboxylate groups is deemed to dominate the hydrophobic effect at neutral and high pH, leading to the SMA copolymer adopting a random coil conformation and thus dissolves relatively easily in aqueous solution. When the pH is reduced below the pK_a of the SMA copolymer, the protonation of the carboxyl group(s) would result in the inherent loss of its charge repulsion property, *i.e.* making the SMA copolymer less amphipathic, which leads to a globular conformation and consequently precipitate as aggregates in solution. In essence, the structural transition of the SMA copolymer in solution in the defined pH range would depend on the polymer composition and the ionic strength of the solution (Dörr *et al.*, 2016; Lee *et al.*, 2016a). On the other hand, the sensitivity of the SMA copolymer towards divalent cations, such as Mg^{2+} could be exploited to destabilise the polymer-protein interaction, wherein the Mg^{2+} ions bind and chelate the carboxylic acid groups of the SMA copolymer, leading to the precipitation of the polymer and protein out of solution (Lee *et al.*, 2016b; Morrison *et al.*, 2016).

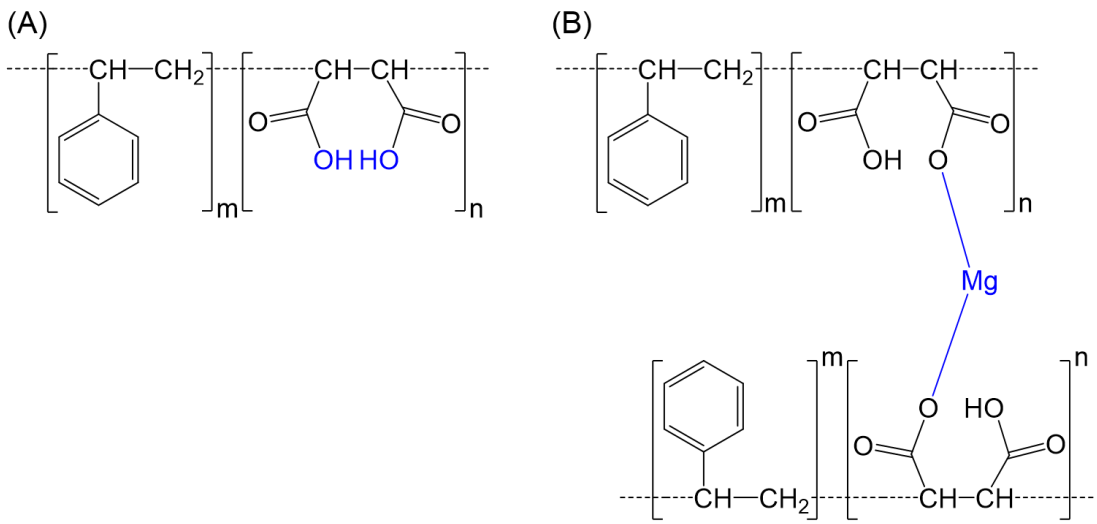

Figure 5.8 The two proposed de-SMALP mechanisms. (A) With a reduction in pH below the pK_a of the SMA copolymer, the protonation of the carboxylic acid group(s) will occur and (B) the binding and chelation of divalent cations (for example Mg^{2+} ion is shown here) to the carboxylic acid groups, which in both cases the SMA copolymer loses its charge property and thus solubility in solution (*i.e.* becoming less amphiphilic) and consequently precipitating out of solution.

It was recently reported that SMALP-ZipA can tolerate up to 4 mM Mg^{2+} (Morrison *et al.*, 2016), thus a Mg^{2+}concentration of 10 mM was used in this work to fully de-SMALP PgpB in the presence of DDM at various concentrations above its critical micelle concentration (around 0.0087%) as the resolubilisation agent. In this preliminary de-SMALP attempt, PgpB was released from SMALP and reconstituted into DDM micelles even at the lowest concentration of DDM tested, *i.e.* 0.5%. No visible amount of protein was found in the insoluble pellet upon ultracentrifugation, indicating that this de-SMALP approach was rather successful (as shown in Figure 5.9).

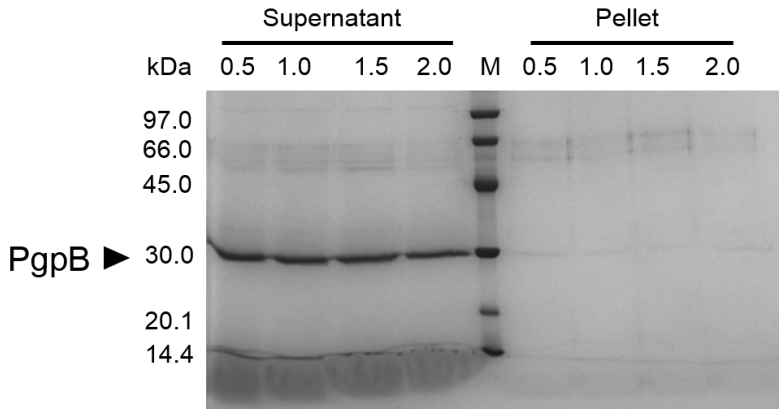

Figure 5.9 SDS-PAGE gel showing PgpB (upon de-SMALP with 10 mM $MgCl_2$) in the soluble fraction after ultracentrifugation, at different percentages of DDM employed (0.5-2.0%). This observation indicates that the PgpB has been successfully released from SMALP and reconstituted into DDM micelles across the range of DDM concentrations tested.

In addition, there was a strong indication that the de-SMALPed PgpB has retained its proper folding based on subsequent CD investigation (as shown in Figure 5.10). Characteristic α-helical signals with negative minima at 208 and 222 nm, which was similar to the CD spectra of SMALP-PgpB and DDM-PgpB were recorded for the de-SMALPed PgpB. It signified that PgpB has been reconstituted into DDM micelles upon the release from SMALP. However, it should be noted that a positive α-helical signature might not always represent the correct folding of a membrane protein in solution, as loose helical bundles can also result in strong α-helical signals (Wang *et al.*, 2015). Thus, the CD spectra should be interpreted with caution and the de-SMALPed PgpB was further examined for activity utilising the phosphate release assay.

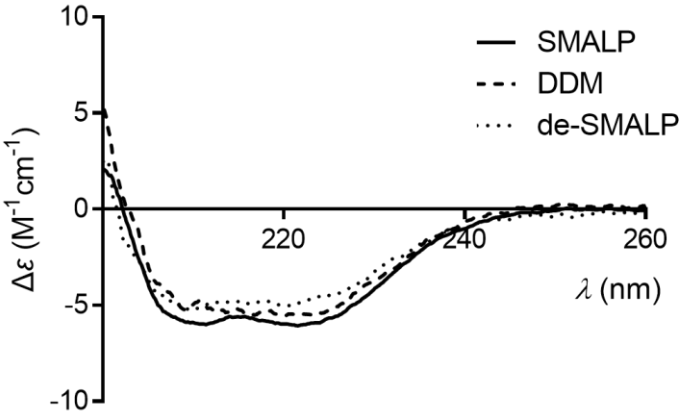

Figure 5.10 CD spectra of de-SMALPed PgpB vs PgpB in SMALP and DDM. The *y*-axis is plotted as $\Delta\varepsilon$ for concentration-independent comparison of CD spectra.

With the successful reconstitution of de-SMALPed PgpB into DDM micelles, its activity was investigated at various enzyme and lipid substrate concentration (as depicted in Figure 5.11). In all cases, the de-SMALPed PgpB recorded dephosphorylation activity as observed by the steady increase in absorbance at 360 nm, indicating the release of phosphate, which was not observed when the protein was encapsulated in SMALP (as depicted in Figure 5.7). This preliminary de-SMALP work thus provided a strong indication that the proposed hypothesis of the SMA copolymer blocking the access of this enzyme towards the lipid substrate was correct. In other words, active PgpB was encapsulated in SMALP; however the lipid substrate was inaccessible to the SMALP-PgpB *in vitro*. Therefore, by releasing PgpB from the SMA copolymer into detergent micelles, it is now able to interact and act on the lipid substrates.

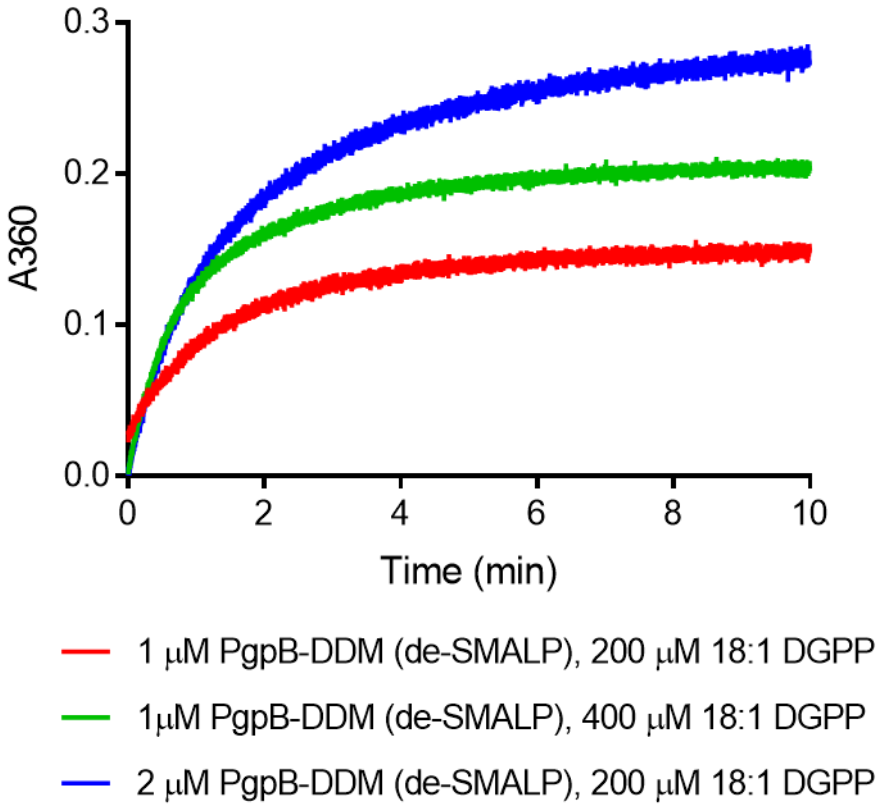

Figure 5.11 Biochemical characterisation of de-SMALPed PgpB at different enzyme and lipid substrate concentrations using the enzyme-coupled phosphate release assay. In all three cases, dephosphorylation activity were recorded for the de-SMALPed PgpB, indicating the viability of the de-SMALP approach.

However, the activity of the de-SMALPed PgpB was noted to be considerably lower than the DDM-PgpB benchmark (as depicted in Figure 5.7). Given that this preliminary de-SMALP attempt was more of a proof-of-principle investigation, which was far from optimised, this could account for the considerably lower activity of the de-SMALPed PgpB. During de-SMALP, the proteins could have been destabilised (to a certain degree) and thus lost their function upon de-SMALP and DDM reconstitution. The reduction in activity of the de-SMALPed PgpB should not be a result of any residual metal effect (due to the use of Mg^{2+} ions for the de-SMALP attempt), given that PgpB is not a metal-dependent enzyme (Fan *et al.*, 2014; Tong *et al.*, 2016; Touzé *et al.*, 2008). This was part of the reason that PgpB was initially selected for this work to explore the SMALP technology, as the other lipid phosphatase - BacA/UppP is dependent on divalent metal ions for activity (Chang *et al.*, 2017, 2014; Manat *et al.*, 2015).

Subsequent studies could examine the effect of buffer pH towards PgpB to develop the de-SMALP method via the pH reduction approach by exploiting CD spectroscopy and/or CPM assay to screen different buffer conditions. However, it should be noted for pH investigations, the maleimide-based thiol-reactive CPM dye has an optimal pH of 6-8, and thus with reduced reactivity at pH below 6, and impaired selectivity above pH 8 (Alexandrov *et al.*, 2008). Alternatively, the effect of divalent cations towards the de-SMALP of PgpB can also be examined using similar CD and/or CPM assays.

5.2.6 LC-MS/MS analysis of the local membrane environment of PgpB

Utilising the LC-MS/MS method developed (as described in Chapter 3 and 4), the phospholipid content and composition of SMALP-PgpB and DDM-PgpB were examined and compared to specifically investigate the much acclaimed delipidation effect of detergents towards the solubilised membrane proteins (Ilgü *et al.*, 2014). Figure 5.12 depicts the phospholipid profiles of PgpB in both SMALP and DDM. The phospholipid profiles obtained for PgpB, which was overexpressed in *E. coli* C43(DE3) strain resemble the phospholipid profile for the BL21(DE3) strain it derived from. Interestingly, PgpB being an integral membrane protein with six TM helices, its phospholipid composition is more similar to ZipA (a bitopic membrane protein) than FtsA (a peripheral membrane protein), with a high abundance in monounsaturated phospholipid species, *i.e.* 32:1, 33:1 and 34:1 in both the PE and PG classes (as depicted in Figure 5.12). There were more CL species detected for PgpB vs the two cell division proteins - ZipA and FtsA, which could indicate a preference towards anionic phospholipids for PgpB that has resulted in the co-extraction of more CLs.

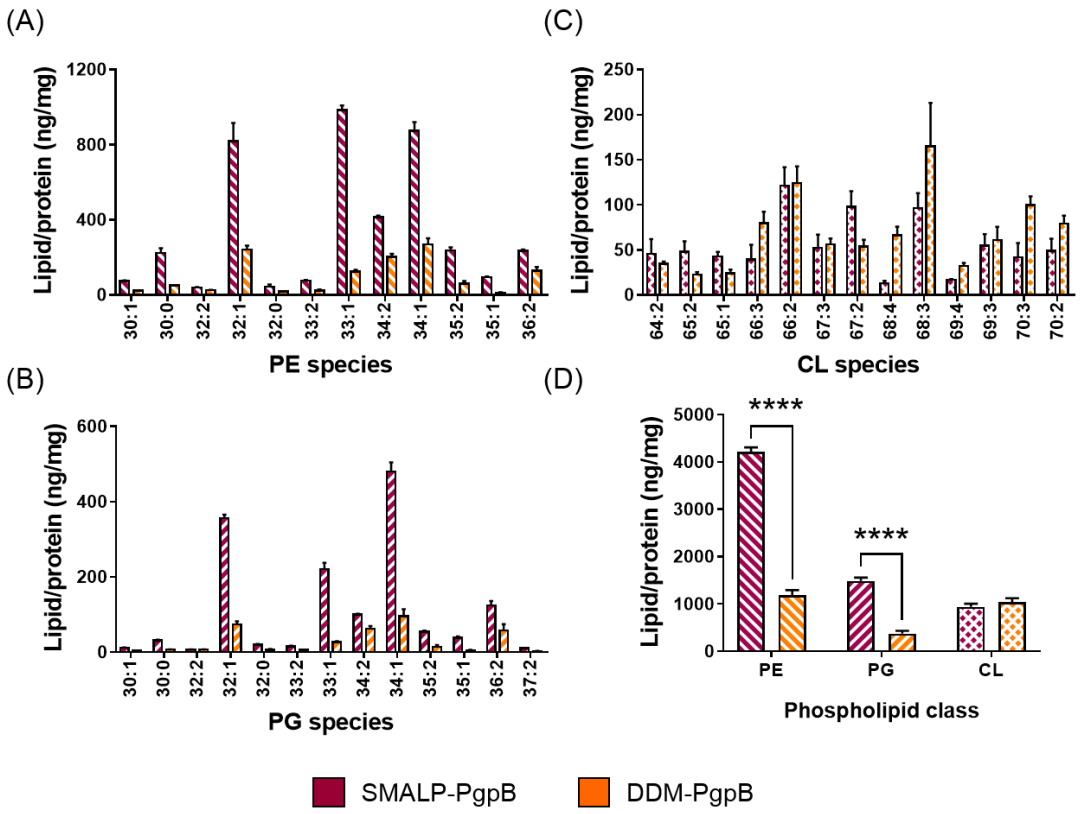

Figure 5.12 Comparison of phospholipid profiles between SMALP-PgpB and DDM-PgpB upon LC-MS/MS analysis. The 38 phospholipid species (distinct *m/z*) detected in the three classes of *E. coli* membrane phospholipids - (A) PE; (B) PG; and (C) CL are shown. (D) Significant differences when comparing the total phospholipid composition for each phospholipids class based on unpaired *t*-tests analysis ($p < 0.0001$) are highlighted as ****. All phospholipid species was confirmed and assigned by tandem MS in negative ion mode.

The lipid sequestering effect of detergents was very evident when comparing the total composition for each phospholipids class, as depicted in Figure 5.12 (D). Noticeably, there was a 2.5-fold greater presence of phospholipids co-extracted in SMALP than the DDM counterpart, with phospholipids in both PE and PG classes showing a marked reduction. No significant differences in the CL content was observed for both SMALP-PgpB and DDM-PgpB, and thus it is likely to allude to the preference or affinity of PgpB towards this particular class of anionic phospholipid. CL could have bound more tightly at the non-annular sites of this enzyme, and thus not lost during the detergent extraction process. This investigation into the delipidation effect of detergents by comparing the co-extracted phospholipid profiles of PgpB in the context of SMALP

and DDM has corroborated previous notion that the SMALP encapsulation process is better at retaining the native membrane environment of the target proteins than detergents, at least it was true for DDM as demonstrated in this work.

It was also apparent in this lipidomic investigation that the use of detergents to solubilise membrane proteins do not result in the total stripping of the membrane lipids surrounding the proteins. It is thus important to note that the solubilisation of membrane proteins by detergents would result in soluble complexes of membrane proteins in mixed micelles containing detergents and varying amounts of membrane lipids, rendering the membrane lipids as 'minority surfactants' (Otzen, 2011). Ilgü *et al.* (2014) have previously observed that among the several alkyl matosides tested for the purification of *Desulfovibrio vulgaris* urea transporter, *E. coli* L-arginine/agmatine antiporter, AdiC and lactose permease, LacY, the employment of DDM retained the most phospholipids. By contrast, *n*-Octyl β-D-maltoside (OM) stripped the most lipids from the urea transporter and AdiC; while *n*-Decyl β-D-maltoside retained only one phospholipid for LacY (Ilgü *et al.*, 2014). In addition, a strong reduction in PE lipids was observed when AdiC was purified with OM vs DDM, with the level of PG lipids remained similar. They thus concluded that DDM being the mildest non-ionic detergent in comparison to the other two related alkyl maltosides (Ilgü *et al.*, 2014).

When comparing the lipid profile of PgpB (in SMALP) to that of BL21(DE3) (Figure 4.2), differences in terms of relative abundance can be observed in a variety of molecular species in the PE and PG classes. No difference was observed for CL molecular species. However, a higher relative abundance in total CL lipids (with concurrent less PG lipids) was detected for the purified PgpB proteins vs the BL21(DE3) control. It is to note that PgpB was overexpressed using the *E. coli* C43(DE3) strain, which is a derivative of the BL21(DE3) strain (Miroux and Walker, 1996), and upon IPTG induction, no temperature alteration (*i.e.* lowering to 25°C as per ZipA and FtsA) was employed prior to cell harvest. In the future, a control C43(DE3) membrane lipid extracts should be examined to serve as a better comparison of lipid profiles to investigate any specific enrichment of phospholipid species by the PgpB proteins.

The activity of PgpB was reported to be inhibited by 70% with the addition of 3 mM POPE (16:0/18:1), with no apparent inhibition from POPG (16:0/18:1) or CL at the

similar concentration when 18:1 LPA was employed as the substrate (Tong *et al.*, 2016). To establish that the ethanolamine headgroup is critical for this inhibition of PgpB, Tong *et al.* (2016) tested the inhibitory effect of DOPC (18:1/18:1), a related zwitterionic phospholipid with an additional trimethyl moiety on ethanolamine to give the choline headgroup. However, no noticeable inhibition effect was found. They thus questioned whether PgpB rests in a lipid-occluded state in the native membrane given that PE was found to harbour such an inhibitory effect. However, a lipid-occluded TM3 tunnel was deemed energetically unfavourable based on their studies and thus might require the presence of membrane lipids (Tong *et al.*, 2016). Judging from the lipidomic investigation in this work, the relative abundance of the three classes of phospholipids for PgpB in SMALP that comprises of approximately 63.4% PE, 22.4% PG and 14.2% CL resemble the native membrane of *E. coli* (Mileykovskaya and Dowhan, 2005). It is thus reasonable to arrive at the same postulation as Tong *et al.* (2016) that PE could serve as a molecular regulator for PgpB activity at a physiologically required threshold to balance the amount of zwitterionic and anionic phospholipids in the cell membrane necessary for *E. coli* survival and growth, in the light of the newly discovered knowledge of the phospholipid profile of PgpB in this work.

Annular lipid molecules are reported to exchange with the surrounding bulk membrane lipids. In which case whereby there is no specific protein-lipid interaction or selective lipid binding, the annular lipid composition of a membrane protein would reflect the composition of the surrounding bulk (Landreh *et al.*, 2016). The size of SMALPs could technically be tuned using different SMA copolymers of different S:MA ratio (Craig *et al.*, 2016; Morrison *et al.*, 2016). Further effort could be directed to investigate the use of different SMA copolymers to solubilise PgpB into smaller particle size (with less surrounding membrane phospholipids being captured), to potentially reflect its annular phospholipid composition for the examination of its apparent affinity towards CL. On the other hand, the delipidation of other commonly used mild detergents for membrane protein studies, including *n*-Octyl-β-D-glucoside, LDAO and CHAPS can be tested in tandem in a systematic manner using the LC-MS/MS method developed and then compare against the result established for SMALP-PgpB and DDM-PgpB in this work.

5.3 Concluding remark

In the work described in this chapter, the advantages and drawbacks of using the SMALP technology for the studies of an integral membrane lipid phosphatase were examined. First and foremost, the overexpressed *E. coli* PgpB was successfully extracted and purified with the SMALP technology using a 2:1 SMA copolymer. Upon a single-step IMAC purification, higher purity was observed for PgpB in SMALP in comparison to the DDM benchmark. PgpB was found to retain its native folding in both SMALP and DDM as demonstrated by CD spectroscopy. The purified SMALP-PgpB formed discrete nanoparticles of approximately 10 nm in size as characterised using negative stained TEM. Besides, it was demonstrated to be thermally stable in the buffer employed using a CPM thermal stability assay. Biochemical characterisation (in terms of phosphate release) was unsuccessful for PgpB in the SMALP context. The hypothesis of the SMA copolymer blocking the lipid substrate access to PgpB in SMALP was tested by devising a preliminary de-SMALP procedure based on the sensitivity of the SMA copolymer towards divalent cations. The SMALP-PgpB was de-SMALPed with 10 mM Mg^{2+} to release the encapsulated PgpB from the SMA copolymer belt with concurrent reconstitution into DDM micelles, which subsequently allowed its biochemical characterisation. Lipidomic analysis of PgpB in both SMALP and DDM revealed the significant delipidation effect of DDM for both PE and PG classes of phospholipids. However, DDM did not strip away all the phospholipids from PgpB during the extraction and solubilisation process. The CL content was similar for PgpB in both SMALP and DDM, suggesting a preferential association and/or affinity of PgpB towards this class of anionic lipids that warrants further investigation.

Chapter 6: General Discussion and Conclusion

6.1 General discussion

6.1.1 Challenges in membrane protein production and purification

It has been estimated that 30% of the prokaryotic and eukaryotic genomes encode for membrane proteins and these proteins represent the target for over 50% of modern medicinal drugs (Overington *et al.*, 2006). However, the low natural abundance of most membrane proteins, which inevitably hinder the purification of sufficient amount of target proteins for downstream analytical studies, still remains the main bottleneck towards their structural and functional characterisation. In addition, the toxic effects towards the host cells frequently accompanied with the overexpression of recombinant membrane proteins can further exacerbate this matter (Hardy *et al.*, 2016; Parmar *et al.*, 2016).

The introduction of the green fluorescent protein-fusion technology has allowed the rapid screening for the optimal condition to overexpress membrane proteins in different growth media, inducer level, aeration, temperature, *etc.* (Drew *et al.*, 2006). Besides, fluorescence-detection SEC can be employed for detergent screening to monitor the stability and monodispersity of the solubilised membrane proteins in different detergents (Backmark *et al.*, 2013). The development of cell-free expression systems as an alternative to recombinant protein expression in host cells, albeit being more technically challenging, can offer another viable means to produce membrane proteins of interest without being limited by the intrinsic membrane space of the host cells (Bernhard and Tozawa, 2013).

6.1.2 Exploiting the SMALP technology for bacterial membrane proteins studies

In the work of this thesis, the membrane proteins being studied were successfully overexpressed in *E. coli* BL21(DE3) and C43(DE3) strains which have facilitated subsequent SMALP encapsulation, followed by conventional purification prior to downstream analytical studies. The development of different membrane mimetics (as discussed in Chapter 1) has offer the protein scientists alternative strategies to encapsulate the target membrane proteins in solution upon extraction for *in vitro* studies.

The SMALP technology was selected as the membrane mimetic of choice for the work in this thesis, due to two key advantages of this technique.

Firstly, the SMA copolymer can be exploited as a solubilisation agent to extract target membrane proteins from biological and synthetic membranes directly in the total absence of detergents. Secondly, the surrounding membrane lipids are preserved and co-extracted during the solubilisation process, limiting the delipidation effect often encountered by the use of detergents. This particular attribute was capitalised in the work of this thesis and as a result a robust LC-MS/MS method was developed (Chapter 3) to characterise the co-extracted membrane lipidomes of target bacterial membrane proteins. The detailed phospholipid profiles of *E. coli* ZipA, FtsA, and PgpB were reported in this work (Chapter 4 and 5). However, as with all other techniques, limitation was observed during the biochemical analysis of PgpB in SMALP, whereby the SMA copolymer belt was preventing the access of the lipid substrate to the enzyme (Chapter 5). Consequently, a de-SMALP approach based on the sensitivity of the SMA copolymer to divalent cations was investigated to release the encapsulated proteins from SMALP into solution to be reconstituted into detergent micelles for subsequent activity analysis.

6.1.2.1 LC methodology

For the LC-MS/MS method developed (as described in Chapter 3), volatile organic solvents, including THF and MeOH were employed. This can result in elution time drift over prolonged LC runs due to the change in overall solvent composition due to unwanted solvent evaporation. However, this phenomenon was not observed, with no elution time drift observed over the entire experimental period. Essentially, the ideal solvent combination for LC-MS should have sufficient conductivity to enable optimal charge separation at the MS ion source emitter, coupled with a low viscosity to maintain the electrophoretic mobility of the analytes. The solvent combination should also promote the formation of small droplets, volatile enough for the quick evaporation of solvents and subsequently the analyte ions, in addition to displaying a high proton affinity to facilitate ion formation through gas-phase chemistry (Brouwers, 2011). When a gradient elution is employed, the change in solvent composition can affect the ionisation efficiency of analytes throughout the LC run (Brouwers, 2011). For the LC-MS/MS method developed, effcient ionisation effiencies of the three classes of

phospholipids (*i.e.* PE, PG and CL) were observed throughout the LC run. Ion suppresion is also less prevalent in RPLC (as employed in this work) in comparison to NPLC or HILIC, due to the effective separation of phospholipid molecular species based on hydrophobicity, with less frequent overlapping of peaks (Brouwers, 2011).

A relative long gradient time of 30 min (total LC run of 45 min) was employed to separate the phospholipids in the LC-MS/MS method developed, which is less capable of high throughput analysis of large amount of samples. For future method improvement, LC column with sub-2µm particles can be evaluated utilising an appropriate HPLC system to shorten the overall LC gradient to enable a faster analysis and turnaround (Brouwers, 2011; Cajka and Fiehn, 2014). Alternatively, supercritical fluid chromatography (SFC) using supercritical carbon dioxide (sCO_2) as the mobile phase, coupled with ESI-MS can be investigated. Lísa and Holčapek (2015) recently reported a rapid separation of 30 nonpolar and polar lipid classes just within 6 min and managed to identify a total of 436 lipid species using a ultrahigh performance SFC-MS system. When used as the mobile phase, sCO_2 has the same polarity as hexane, but the polarity of this mobile phase can be tuned using a suitable modifier, for instance MeOH to achieve the desired separation of lipids (Cajka and Fiehn, 2014).

One limitation to the LC-MS/MS method developed is that CLs were found to elute at the highest precentage of solvent B, which inherently limited the separation between the molecular species of CL. Essentially, this suboptimal separation of CL is similar to NPLC or HILIC methods of separation by class rather than molecular species. Nevertheless, CL was still effectively separated from PE and PG, which was the primary goal of the LC strategy. This is in contrast to the method employed by Oursel *et al.* (2007) which failed to detect CL, necessitating the development of a separate method for CL investigation (Garrett *et al.*, 2007). The efficient separation of CL from PE and PG has aided the relative quantification of this minor class of membrane phospholipid in *E. coli*, without worrying about ion suppressions from the other more abundant phospholipids.

In the future, for improved LC separation with complex biological samples containg multiple types of lipids, two-dimensional (2D) LC can be considered, whereby a combination of NPLC or HILIC and RPLC separations is exploited to maximise the

separaiton of lipids (Cajka and Fiehn, 2014; Minkler and Hoppel, 2010; Samhan-Arias *et al.*, 2012). Normally for 2D LC, the lipids are separated based on their headgroup characteristics in the first dimension, followed by the separation based on their fatty acyl chain characteristics (carbon chain length and unsaturation) in the second dimension.

6.1.2.2 MS ion polarity

The developed LC-MS/MS method used to characterise the co-extracted membrane lipidomes of the target membrane proteins was mainly conducted in the negative ion mode, which is commonly used for lipid analysis as it provides the greatest structural information (including fatty acyl chains distribution) for the membrane phospholipids under investigation upon MS/MS analysis. PE, PG and CL were all found to ionise effectively in the negative ion mode, validating this ion mode as the polarity of choice. During the initial method development stage, positive ion mode was also considered due to the potential employment of targeted tandem MS scan modes, such as NL 141 scan to specifically target the PE lipids. However, no suitable targeted scans in the positive ion mode can be used to target PG and CL lipids (Brügger *et al.*, 1997), and this ion polarity was therefore dropped from further evaluation. Although the PIS 196 scan can be used in negative ion mode to target the PE lipids, PG and CL (due to their structural and chemical similarities) cannot be specifically targeted using the PIS 153 scan (Brügger *et al.*, 1997).

6.1.2.3 Phospholipid isomerism

Although the *sn* regioisomers of the phospholipids under investigation can be readily inferred through the LC-MS/MS method developed, by examining the relative ratio of the carboxylate ions upon MS/MS, the other isomeric forms could not be readily distinguished. As with many other conventional LC-MS/MS methods, the LC-MS/MS method developed in this work does not provide information on methyl-branched fatty acyl chains or the double bond position and geometry in unsaturated chains (Hancock *et al.*, 2017). One way to obtain more structural information on these fatty acyl chains would be to exploit ozone-induced dissociation, whereby the fragmentation from the resultant ozonides produces ions to reveal the double bond positions (Kozlowski *et al.*, 2015; Thomas *et al.*, 2008). The LC-MS/MS method developed in this work is also 'chirally blind', thus could not distinguish between the *R*- or *S*-enantiomers. Ion

mobility is another MS technique offering a further orthogonal separation based on the differences in collisional cross-sections of the lipid ions besides their mass and charge characteristics (Cajka and Fiehn, 2014; Damen *et al.*, 2014). It works by the principle that ions travel with different mobilities in low to high electric fields, which could be useful in the separation of isobaric species (Cajka and Fiehn, 2014).

6.1.2.4 Surface sampling for phospholipid analysis

Other MS-based methods using surface sampling under both ambient or vaccum conditions, such as desorption electrospray ionisation, liquid extraction surface analysis, MALDI, and SIMS have all been utilised for the analysis of bacterial samples (Fang and Dorrestein, 2014; Watrous and Dorrestein, 2011), in which membrane phospholipids represent the major ions being detected (Shu *et al.*, 2012; Wehrli *et al.*, 2016; Zhang *et al.*, 2011). If the SMALP-proteins can be suitably immobilised onto a surface, for instance through the polyhistidine tags on the recombinant proteins, there could be enromous potential in the future to employ these surface sensitive analysis techniques for the direct analysis of co-extracted membrane lipids, without the need for prior lipid extraction and/or separation (Ellis *et al.*, 2013).

6.1.2.5 Inclusion of quality control samples

For prolonged LC-MS experiments, QC samples (normally made up of a consistent analyte composition representative to the target analytes of interest, *e.g.* pooled sample mixtures) are often included and inserted at multiple intervals within the LC-MS runs. These samples serve to mainly assess any run-to-run variation and subsequently facilitate the correction of any run-to-run effect when deemed necessary (Bird *et al.*, 2011; Hewelt-Belka *et al.*, 2016; Vaz *et al.*, 2014). For the LC-MS/MS method developed, QC samples which composed of a mixture of POPE, POPG and TOCL (in equal mass ratio) were inserted before, in between, and after the samples to assess the instrument response, due to the relatively long LC run time employed (45 min). As a matter of fact, it can often takes several days (with overnight batches) to complete the entire experiment, which can complicate downstream data analysis with potential shifts in chromatographic retention and/or MS response over the course of experiment. However, no substantial run-to-run effect was observed during the course of the experiments in this work.

6.1.2.6 Inclusion of internal standards for data normalisation

The primary goal of data normalisation is to remove unwanted systematic variation in ion intensities between measurements, while retaining interesting biological variation (Cajka and Fiehn, 2014; Katajamaa and Orešič, 2007). Due to the enormous chemical diversity of lipids, which can inherently lead to different recoveries during the extraction process or ionisation responses in the mass spectrometer, the separation of interesting biological variation and unwanted systematic bias can be very difficult without appropriate data normalisation (Katajamaa and Orešič, 2007). The addition of IS allows for the ratiometric comparison of different lipid classes and/or molecular species (within each class) to support quantitative analysis (Vaz *et al.*, 2014). In the LC-MS/MS method developed, three IS (one for each class) were employed to normalise the ion intensities for each of the phospholipid molecular species under each respective class. The normalisation approach employed in this work was to first normalise the ion intensities of each phospholipid molecular species (within each class) against its internal standard. Subsequently, to facilitate sample-to-sample comparison, the normalised ion intensities were normalised against the total lipid intensities in each sample to obtain their relative abundance.

IS comprising of odd chain fatty acids are frequently used to study eukaryotic lipids (Myers *et al.*, 2011). However, prokaryotic bacteria including *E. coli* contain phospholipids harbouring odd chain fatty acids, *e.g.* C13:0 and C15:0, thus the IS chosen should not be present in the samples (*i.e.* non-natural), which requires *a priori* information about the sample nature. Ideally, the IS should cover the span of carbon chain lengths and degree of unsaturation of the native lipids but are not present in the sample under investigation (Myers *et al.*, 2011). Although the LC-MS/MS method developed in this work represent an improvement over the methods by Oursel *et al.* (2007) and Prabudiansyah *et al.* (2015), whereby only one short chain PE (12:0/12:0) was used for data normalisation, the employment of IS that contain short and odd chain fatty acids (C12:0 to C15:1) in this work was still deemed not ideal to cover the whole range of native carbon chain lengths and degree of unsaturation. The use of stable isotope labelled IS could have been a better approach. However, it is inherently more costly to be employed and not all classes of lipids have stable isotope labelled IS. For example, the deuterated version of PE and PG can be commercially sourced, but deuterated CL is not available. In an ideal experiment, multiple IS should be used to

flank a lipid class, but this is often not feasible due to availability and cost concerns. Therefore, at least one IS for each class of phospholipid was chosen in this work, whereby the fatty acyl combinations are out of the natural range of targeted phospholipids under investigation.

6.1.2.7 Lipidomic data analysis routine

Lipidomics is an interdisciplinary field of research, thus it has to be appreciated that experts from different fields, encompassing biochemistry, analytical chemistry, and bioinformatics will each play a different role in a lipidomic team. Constructive collaboration between the different disciplines would be the key to obtain the best lipidomic results (Vaz *et al.*, 2014). Within the 'omics' fields, one of the biggest challenge is inevitably the ability to translate the vast amounts of information generated into useful knowledge to advance the understanding of biological phenomena. The development of appropriate bioinformatic tools to facilitate the extraction of useful information from the dataset is thus needed to fill this gap (Orešič, 2011). Judging from the unique and distinct membrane lipidomes of ZipA, FtsA, and PgpB (Chapter 4 and 5) obtained in this work, new informatics and computational approaches would almost certainly be useful to further investigate and/or model the complex regulation of membrane phospholipids and their interactions with the membrane proteins of interest.

In this work, manual peak assignment and integration with subsequent data normalisation were implemented upon the LC-MS/MS data acquisition. It was a rather labour-intensive approach and required prior domain expert knowledge. The adoption of such data analysis strategy was prompted by the lack of high mass resolution data, thus DDA/IDA experimental design was exploited to utilise the tandem MS data for high confidence peak assignment. A typical data processing pipeline comprises of peak filtering, integration, alignment, identification and normalisation (Katajamaa and Orešič, 2007; Orešič, 2011). The selection of data processing parameters can directly impact the outcome (*i.e.* peak list) and thus potentially influence biological interpretation. For future improvement of the data processing and analysis workflow of the LC-MS/MS method developed in this work, a more automated approach to minimise human error and to speed up the process is very much desired. For example, the use of a higher mass resolution instrument to acquire high mass accuracy spectra and the development of new algorithms or in-house scripts can facilitate the data

processing and analysis workflow. However, it should be noted that there is still no established standard in the procedure and platform for lipidomic data acquisition, in addition to the absence of a uniform data processing strategy.

6.1.2.8 SMALP lipidomic investigation of *E. coli* ZipA, FtsA, and PgpB

In this work, one of the major challenge towards the analysis of the co-extracted membrane lipidome of the target SMALP-proteins was the small amount of purified membrane protein samples (and thus limited number of co-extracted phospholipids), in comparison to the bulk cell membranes used in typical lipidomic studies. In fact, a large amount of target cells can be cultured with their cell membranes harvested relatively easily and straightforward, but the purification of recombinantly overexpressed membrane protein of interest is not as straightforward and the yield is often very low (Hardy *et al.*, 2016). Thus, even with a sensitive lipid analysis technique such as MS, the limitation of starting materials can still be very challenging.

Although extrachromosomal plasmids have been utilised to produce sufficient amount of recombinant membrane proteins of interest for subsequent *in vitro* analyses, such as the work described in this thesis for ZipA, FtsA and PgpB, it poses a potential drawback to the investigation of lipid moeities surrounding the target membrane proteins. Normally, the overexpressed proteins are purifed from the host cells in the stationary growth phase, as was the case for ZipA, FtsA, and PgpB. Although this growth phase is a common end point for recombinant protein production, it is pivotal to note that the cell division process would have terminated. Thus, any biological inference in terms of protein-lipid interaction should be taken with due consideration, and subjected to further experimental validations. For ZipA and FtsA, a reduction of culture temperature (from 37°C to 25°C) upon IPTG induction was employed, which could have also influenced the membrane lipid composition.

Multiple reports on the formation of extra membrane structures upon the overexpression of membrane proteins (Arechaga, 2013) should be taken into account when contemplating the biological relevance of the data obtained through SMALP lipidomics. In addition, the SMALP sampling approach could not provide any spatio-temporal information on the phospholipid profiles of the target membrane proteins if they are not located at a fixed cellular location during the harvesting stage. Therefore,

in vivo fluorescence imaging studies utilising specific lipophilic dyes, such as NAO could be conducted in the future to complement the SMALP lipidomic investigations described in this thesis.

Specific lipid enrichment reported by previous SMALP studies have suggested that the existence of preferential protein-lipid interactions that were preserved by the SMALP technology (Dörr *et al.*, 2014; Prabudiansyah *et al.*, 2015). This means that the co-extracted lipidomes are not merely a snapshot of the native biological membrane at the time of solubilisation, but reflect specific protein-lipid interaction, which strongly support the notion of exploiting the SMALP lipidomic approach to probe protein-lipid interactions. Importantly, the observation that the co-extracted membrane lipid profiles for the three *E. coli* membrane proteins investigated in this work are different to the bulk membrane controls is a reassurance to use the SMALP technology (in conjunction with current recombinant protein production protocols) as a valid means to examine the unique membrane lipidome of target membrane proteins.

It is worth exploring the generation of overexpression strains whereby the chromosomal gene encoding for the target membrane protein has been deleted, so that all the target proteins are expressed through the inducible extrachromosomal plasmid. There has been reports of temperature-senstive strains for *zipA* and *ftsA* (Pichoff and Lutkenhaus, 2002), *E. coli zipA* deletion strains (Haeusser *et al.* 2015, Gessier *et al.* 2003, Pichoff *et al.* 2012) and *B. subtilis ftsA* deletion strain (Jensen *et al.* 2005). However, no report on the construction of the deletion of *zipA* or *ftsA* for *E. coli* BL21(DE3) or other relevant expression strains has been reported, thus the feasibility of such approach has to be further examined thoroughly.

Alternatively, the protein purification protocol could be modified to employ a co-immunoprecipitation approach exploiting specific antibodies against ZipA or FtsA, analogous to the purification of *S. aureus* native PBP2/2a complex (Paulin *et al.*, 2014) and *E. coli* holo-translocon complex (Komar *et al.*, 2016), instead of using plasmid-encoded proteins with conventional purification tags. However, the low natural abundance of these two cell division proteins might preclude such an approach to obtain sufficient amount of purified protein sample for lipidomic analysis. In the future, a bioreactor could be utilised (if available) to scale up the bacterial cell cultures, in order

to harvest enough cells (and hence target proteins) at the exponential growth phase, whereby cell division is still taking place. In addition, immunoaffinity purification (with appropriate antibodies) can be exploited in tandem to purify target (non-recombinant) cell division membrane proteins in a more native manner (T. den Blaauwen & Y. Chen, personal communication, 2017). The LC-MS/MS method developed in this work is applicable to the analysis of co-extracted membrane lipidomes of native protein samples, as long as the target membane protein is adequately purified to an acceptable yield and the co-extracted membranes are sufficient for LC-MS/MS detection and quantification. PC, PE, PG, and CL are the four classes of membrane phospholipids readily detected using the LC-MS/MS method developed, and this method can be further evaluated and/or modified for the detection of other membrane lipids such as PA, PS, and PI.

To validate the specific phospholipid profile obtained for *E. coli* FtsA in this work, one approach would be to fuse the MTS of FtsA to other proteins (*e.g.* FtsZ or MreB) and re-examine the corresponding phospholipid profiles (T. den Blaauwen, personal communication, 2016). It has been reported that a chimera FtsZ fused with the MTS of MinD was still functional and capable of attaching to the cell membrane (Osawa *et al.*, 2008; Osawa and Erickson, 2013). The MTS of FtsA was reported to be replaceable by that of MinD and *vice versa* (Pichoff and Lutkenhaus, 2005). The MTS of FtsA can also be replaced by the first TM helix of the maltose transporter, MalF (Shiomi and Margolin, 2008). Essentially, it appears that as long as there is a MTS, FtsA can bind to the cell membrane. Therefore, it would be insightful to investigate the phospholipid profiles of chimera FtsA with different MTS to ascertain if there is any lipid specificity towards each MTS. Other alternative techniques, for example fluorescence imaging, protein reconstitution and biochemical analysis should be implemented to supplement and/or validate the lipidomic findings reported in this work. Additionally, the existence of extra membrane structures could be inspected for the BL21(DE3) strains overexpressing ZipA and FtsA through conventional microscopic studies. Nevertheless, the SMALP lipidomic investigations performed in this work could complement other existing protein-lipid interaction studies, for example utilising native MS, whereby the target membrane proteins are analysed at intact or near intact from (without prior protease digestion) to interrogate the structure and dynamics of protein-lipid binding (Bechara *et al.*, 2015; Cong *et al.*, 2016; Landreh *et al.*, 2016).

6.1.2.9 Release and reconstitution (de-SMALP) of *E. coli* PgpB

Although in this work (as described in Chapter 5), PgpB was not amenable to conventional biochemical analysis in the context of SMALP, there is no reported precedent studies for other related PAP2 enzymes in a detergent-free alternative membrane mimetic system. The preliminary de-SMALP attempt conducted in this work thus demonstrated the first possibility of releasing such integral membrane lipid phosphatase into detergent micelles and potentially into other membrane mimetic systems upon SMALP encapsulation. With future de-SMALP method development and optimisation, it presents the opportunity to directly solubilise membrane proteins of interest using the SMA copolymer to capitalise on the benefits of the SMALP technology, while affording the flexibility for subsequent protein release and reconstitution into other membrane mimetic systems to facilitate downstream analyses (Dörr *et al.*, 2016).

Dörr *et al.* (2014) previously reported the spontaneous transfer of SMALP-KcsA into planar lipid bilayers to enable downstream electrophysiological characterisation, motivated by the fact that ion transport measurements are not feasible without compartment-forming bilayers. However, in their work, the target membrane protein was not a lipid-dependent enzyme such as PgpB, and the transfer of SMALP-KcsA into the planar lipid bilayers was not via a de-SMALP approach. Similarly, the transfer of the SMALP-bacteriorhodopsin to monoolein LCP for subsequent crystallographic investigation was not achieved through a de-SMALP approach.

In this work, liposomes have been considered as the alternative membrane mimetic to SMALP during the de-SMALP method development. However, the reconstitution of PgpB into liposomes would necessitate the use of detergents (with subsequent careful removal) to form the proteoliposomes. Besides, the lipid substrates would need to be solubilised and presented to PgpB in the liposomes for dephosphorylation to occur. Taking these technical considerations into account, coupled with the reasonable activity of PgpB from direct detergent resolubilisation (upon de-SMALP), it was deemed not the method of choice during the de-SMALP investigation for PgpB. It would be more pragmatic to examine the activity of PgpB (in the form of proteoliposomes) using detergent-solubilised PgpB instead of the de-SMALPed proteins.

Cuevas Arenas *et al.* (2016) have demonstrated the reincorporation of phospholipids from SMALPs into vesicular bilayer membrane by adding excess lipids to shift the equilibrium back into the purely vesicular range. Hazell *et al.* (2016) also reported the exchange of lipids from SMALPs with lipid monolayers absorbed at either solid-liquid or air-liquid interfaces, with the lipid exchange being medicated by the monomeric diffusion of PC lipids through the aqueous medium and not through collisions with the SMALPs. Cuevas Arenas *et al.* (2017) further observed that lipid exchange of PC/PE SMALPs can occur not only by monomer diffusion but also by fast collisional transfer. This lipid exchange was implied through a hydrophobic continuum enabled by the flexible nature of the SMA copolymer, advocating a dynamic nature of the PC/PE SMALPs. These observations suggested that the formation of freely diffusing SMALPs is a dynamic yet reversible process. However, in this work, the addition of the lipid substrate - DGPP did not result in the spontaneous transfer into SMALP-PgpB. It is also important to note that the abovementioned spontaneous lipid transfer and exchange were investigated using SMALPs without the presence of membrane protein.

Nevertheless, future reconstitution effort of membrane proteins in SMALP into other membrane mimetic systems could explore the feasibility of spontaneous lipid transfer and exchange, rather than employing the 'harsher' methods of pH reduction or divalent cations to de-SMALP the target proteins. DGPP could be mixed with bilayer forming lipids to explore this spontaneous lipid transfer and exchange means of presenting the lipid substrate to SMALP-PgpB. Alternatively, the newly discovered and commercially available - diisobutylene/maleic acid copolymer, which was found to be less sensitive to divalent cations (up to 20 mM Mg^{2+} and Ca^{2+}) could be tested as an alternative to the SMA copolymer due to their similar membrane solubilising properties (Oluwole *et al.*, 2017).

6.1.2.10 Towards a 'SMALP divisome'

Trip and Scheffers (2015) have recently observed a 1 MDa *E. coli* divisome complex on native PAGE, containing seven of the essential cell division proteins, namely FtsZ, ZipA, FtsK, FtsQ, FtsL, FtsB, and FtsN. The use of membrane isolation methods, such as sonication or French press followed by ultracentrifugation was noted to disrupt this dynamic, fragile and temporal divisome complex. Since the SMALP technology has already been reported to encapsulate multiprotein complexes (up to 36 TM helices), it

harbours the potential to encapsulate these divisome members for the interrogation of protein-protein interactions in the divisome context (Komar *et al.*, 2016; Paulin *et al.*, 2014; Postis *et al.*, 2015). In particular, the ACEMBL system, which is an advanced recombinant DNA technique, developed in the Berger group to produce challenging multiprotein complexes (Bieniossek *et al.*, 2009; Komar *et al.*, 2015) could be utilised to co-express the different divisome components concurrently to facilitate the subsequent encapsulation of these proteins towards a 'SMALP divisome' in the future.

6.2 Conclusion

The primary aim for the work in this thesis to develop appropriate analytical approaches and tools for the *in vitro* analysis of bacterial membrane proteins was firstly achieved by the development of a LC-MS/MS method for the characterisation of co-extracted membrane lipidomes of target membrane proteins from *E. coli* (as described in Chapter 3). The developed LC-MS/MS method was also analytically validated to be robust for the intended SMALP lipidomic application, which has allowed the elucidation of the co-extracted membrane lipidomes of three *E. coli* membrane proteins, namely ZipA, FtsA and PgpB (as described in Chapter 4 and 5), representing the first report of its kind for these membrane proteins. Protein-lipid interaction in the divisome context was investigated based on established phospholipid profiles for ZipA and FtsA; while the delipidation effect upon detergent (DDM) extraction and solubilisation was examined for the case of PgpB.

It is important to note that the lipid profiling was conducted under a lack of *a priori* knowledge regarding any specific protein-lipid interaction for the three target membrane proteins, unlike previous published studies for the potassium ion channel, KcsA and the bacterial Sec translocon, which have been examined for their preferential association with anionic membrane lipids (Dörr *et al.*, 2014; Prabudiansyah *et al.*, 2015). The work in this thesis thus showcased the power and novelty of the SMALP lipidomic approach to facilitate the characterisation of the local lipid environment of the membrane proteins of interest to gain valuable insight into the unknown or yet to be discovered protein-lipid interaction.

Furthermore, even though ZipA and FtsA are structurally different (bitopic vs peripheral membrane protein), both of them were amenable to the SMALP lipidomic

investigation, highlighting the applicability of the SMA copolymer to extract and solubilised both types of membrane proteins from their native membrane environment. It was demonstrated in this work that the SMALP approach did not preferentially extract specific types of lipids from the native *E. coli* membranes and thus preserved the surrounding lipid moeities during the solubilisation and purification process. However, it is still too early to draw a definite conclusion regarding the protein-lipid interaction in the context of *E. coli* cell division with regards to ZipA and FtsA from this investigation, and further work is warranted in this area of research. Nonetheless, the pioneering studies reported in this thesis has provided the first exploitation of the detergent-free membrane solubilisation approach using the SMA copolymer to facilitate the detail investigation of the native membrane phospholipid compositions of these proto-ring components.

With the timely establishment of the LC-MS/MS method developed in this work, it will provide the analytical tool needed to extend such SMALP lipidomic studies to other divisome members. The establishment of membrane phospholipid profiles for the membrane proteins of interest could be used to guide further biophysical and biochemical analyses, especially in terms of protein-lipid interactions. Complementing this SMALP lipidomic approach with other techniques to decipher protein-lipid interaction in the divisome context is likely play a critical role in identifying mechanisms and targets for the development of next-generation antimicrobial compounds.

The SMALP technology was demonstrated to be applicable to the solubilisation and purification of the *E. coli* PgpB in this work (Chapter 5), which represented the first report to-date of an integral membrane lipid phosphatase of such nature to be directly extracted and studied in a detergent-free membrane mimetic system. This has provided a suitable tool to benchmark previous studies of PgpB in a detergent context (Fan *et al.*, 2014; Tong *et al.*, 2016; Touzé *et al.*, 2008). Upon extraction and purification, PgpB was found to be properly folded (comparable to the DDM-extracted counterpart), with a size around 10 nm in SMALP. Although challenges arise in terms of biochemical characterisation of PgpB in SMALP, but the preliminary devised de-SMALP method has managed to release the encapsulated PgpB using Mg^{2+} ions with concurrent

reconstitution into DDM micelles to enable subsequent biochemical analysis using the lipid substrate - DGPP.

It is pivotal to note that no membrane mimetic system represent a perfect solution to the replacement of detergent. In fact, the advantages and drawbacks to the studies of PgpB in SMALP were pragmatically demonstrated in this work. Future efforts in optimising the de-SMALP procedure is warranted to capitalise on the SMA copolymer as the initial solubilisation and purification agent for target membrane proteins, but also allowing subsequent transfer (upon de-SMALP) into other membrane mimetic system to facilitate other downstream analyses as required. The proof-of-concept de-SMALP studies demonstrated in this work could serve a basis for future reconstitution studies when the target membrane proteins (*e.g.* those acting on lipid substrates) are not amenable to downstream assays or applications within the SMALP context.

During bacterial cell division, the constriction of septum involved efficient separation of the cell envelope components, including the cell membranes and peptidoglycan cell wall into the two daughter cells (Egan and Vollmer, 2013; Haeusser and Margolin, 2016). The biophysical, biochemical and lipidomic characterisation of PgpB reported in this work could set the foundation for its future *in vitro* and *in vivo* studies (and other related integral membrane lipid phosphatases) to shed light on the exact functional role of PgpB, which has been demonstrated to be involved in several pathways from the biosynthesis of phospholipids to various cell wall polysaccharides (Manat *et al.*, 2014; Teo and Roper, 2015).

Chapter 7: Bibliography

Addinall, S.G., Lutkenhaus, J., 1996. FtsA is localized to the septum in an FtsZ-dependent manner. J. Bacteriol. 178, 7167–7172.

Adosraku, R.K., Choi, G.T.Y., Constantinou-Kokotos, V., Anderson, M.M., Gibbons, W.A., 1994. NMR lipid profiles of cells, tissues, and body fluids: proton NMR analysis of human erythrocyte lipids. J. Lipid Res. 35, 1925–1931.

Akbarzadeh, A., Rezaei-Sadabady, R., Davaran, S., Joo, S.W., Zarghami, N., Hanifehpour, Y., Samiei, M., Kouhi, M., Nejati-Koshki, K., 2013. Liposome: classification, preparation, and applications. Nanoscale Res. Lett. 8, 102.

Aktas, M., Wessel, M., Hacker, S., Klüsener, S., Gleichenhagen, J., Narberhaus, F., 2010. Phosphatidylcholine biosynthesis and its significance in bacteria interacting with eukaryotic cells. Eur. J. Cell Biol. 89, 888–894.

Alexandrov, A.I., Mileni, M., Chien, E.Y.T., Hanson, M.A., Stevens, R.C., 2008. Microscale fluorescent thermal stability assay for membrane proteins. Structure 16, 351–359.

Alvis, S.J., Williamson, I.M., East, J.M., Lee, A.G., 2003. Interactions of anionic phospholipids and phosphatidylethanolamine with the potassium channel KcsA. Biophys. J. 85, 3828–3838.

Arechaga, I., 2013. Membrane invaginations in bacteria and mitochondria: Common features and evolutionary scenarios. J. Mol. Microbiol. Biotechnol. 23, 13–23.

Arechaga, I., Miroux, B., Karrasch, S., Huijbregts, R., de Kruijff, B., Runswick, M.J., Walker, J.E., 2000. Characterisation of new intracellular membranes in *Escherichia coli* accompanying large scale over-production of the b subunit of F_1F_o ATP synthase. FEBS Lett. 482, 215–219.

Ariöz, C., Götzke, H., Lindholm, L., Eriksson, J., Edwards, K., Daley, D.O., Barth, A., Wieslander, Å., 2014. Heterologous overexpression of a monotopic glucosyltransferase (MGS) induces fatty acid remodeling in *Escherichia coli* membranes. Biochim. Biophys. Acta 1838, 1862–1870.

Arneborg, N., Salskov-Iversen, A., Mathiasen, T., 1993. The effect of growth rate and other growth conditions on the lipid composition of *Escherichia coli*. Appl. Microbiol. Biotechnol. 39, 353–357.

Backmark, A.E., Olivier, N., Snijder, A., Gordon, E., Dekker, N., Ferguson, A.D., 2013.

Fluorescent probe for high-throughput screening of membrane protein expression. Protein Sci. 22, 1124–32.

Barák, I., Muchová, K., 2013. The role of lipid domains in bacterial cell processes. Int. J. Mol. Sci. 14, 4050–4065.

Bayburt, T.H., Grinkova, Y. V., Sligar, S.G., 2002. Self-assembly of discoidal phospholipid bilayer nanoparticles with membrane scaffold proteins. Nano Lett. 2, 853–856.

Bechara, C., Nöll, A., Morgner, N., Degiacomi, M.T., Tampé, R., Robinson, C. V., 2015. A subset of annular lipids is linked to the flippase activity of an ABC transporter. Nat. Chem. 7, 255–262.

Bell, A.J., Frankel, L.K., Bricker, T.M., 2015. High yield non-detergent isolation of photosystem I-light-harvesting chlorophyll II membranes from spinach thylakoids: Implications for the organization of the PS I antennae in higher plants. J. Biol. Chem. 290, 18429–18437.

Benamara, H., Rihouey, C., Abbes, I., Ben Mlouka, M.A., Hardouin, J., Jouenne, T., Alexandre, S., 2014. Characterization of membrane lipidome changes in *Pseudomonas aeruginosa* during biofilm growth on glass wool. PLoS One 9, e108478.

Bernhard, F., Tozawa, Y., 2013. Cell-free expression-making a mark. Curr. Opin. Struct. Biol. 23, 374–380.

Bersch, B., Dçrr, J.M., Hessel, A., Killian, J.A., Schanda, P., 2017. Proton-detected solid-state NMR spectroscopy of a zinc diffusion facilitator protein in native nanodiscs. Angew. Chemie Int. Ed. 56, 2508–2512.

Bieniossek, C., Nie, Y., Frey, D., Olieric, N., Schaffitzel, C., Collinson, I., Romier, C., Berger, P., Richmond, T.J., Steinmetz, M.O., Berger, I., 2009. Automated unrestricted multigene recombineering for multiprotein complex production. Nat. Methods 6, 447–450.

Bird, S.S., Marur, V.R., Sniatynski, M.J., Greenberg, H.K., Kristal, B.S., 2011. Lipidomics profiling by high-resolution LC-MS and high-energy collisional dissociation fragmentation: Focus on characterization of mitochondrial cardiolipins and monolysocardiolipins. Anal. Chem. 83, 940–949.

Bisson-Filho, A.W., Hsu, Y.-P., Squyres, G., Kuru, E., Wu, F., Jukes, C., Dekker, C., Holden, S., VanNieuwenhze, M., Brun, Y., Garner, E., 2017. Treadmilling by FtsZ filaments drives peptidoglycan synthesis and bacterial cell division. Science 355,

739–743.

Bligh, E.G., Dyer, W.J., 1959. A rapid method of total lipid extraction and purification. Can. J. Biochem. Physiol. 37, 911–917.

Breukink, E., Demel, R.A., de Korte-Kool, G., de Kruijff, B., 1992. SecA insertion into phospholipids is stimulated by negatively charged lipids and inhibited by ATP: A monolayer study. Biochemistry 31, 1119–1124.

Broecker, J., Eger, B.T., Ernst, O.P., 2017. Crystallogenesis of membrane proteins mediated by polymer-bounded lipid nanodiscs. Structure 25, 384–392.

Broughton, C.E., van Den Berg, H.A., Wemyss, A.M., Roper, D.I., Rodger, A., 2016. Beyond the discovery void: New targets for antibacterial compounds. Sci. Prog. 99, 153–182.

Brouwers, J.F., 2011. Liquid chromatographic-mass spectrometric analysis of phospholipids. Chromatography, ionization and quantification. Biochim. Biophys. Acta 1811, 763–775.

Brügger, B., Erben, G., Sandhoff, R., Wieland, F.T., Lehmann, W.D., 1997. Quantitative analysis of biological membrane lipids at the low picomole level by nano-electrospray ionization tandem mass spectrometry. Proc. Natl. Acad. Sci. U. S. A. 94, 2339–2344.

Busiek, K.K., Eraso, J.M., Wang, Y., Margolin, W., 2012. The early divisome protein FtsA interacts directly through its 1c subdomain with the cytoplasmic domain of the late divisome protein FtsN. J. Bacteriol. 194, 1989–2000.

Buszewski, B., Noga, S., 2012. Hydrophilic interaction liquid chromatography (HILIC)-a powerful separation technique. Anal. Bioanal. Chem. 402, 231–247.

Cabré, E.J., Sánchez-Gorostiaga, A., Carrara, P., Ropero, N., Casanova, M., Palacios, P., Stano, P., Jiménez, M., Rivas, G., Vicente, M., 2013. Bacterial division proteins FtsZ and ZipA induce vesicle shrinkage and cell membrane invagination. J. Biol. Chem. 288, 26625–26634.

Cajka, T., Fiehn, O., 2014. Comprehensive analysis of lipids in biological systems by liquid chromatography-mass spectrometry. Trends Anal. Chem. 61, 192–206.

Callaway, E., 2015. The revolution will not be crystallized. Nature 525, 172–174.

Calvano, C.D., Italiano, F., Catucci, L., Agostiano, A., Cataldi, T.R.I., Palmisano, F., Trotta, M., 2014. The lipidome of the photosynthetic bacterium *Rhodobacter sphaeroides* R26 is affected by cobalt and chromate ions stress. Biometals 27, 65–73.

Carman, G.M., Deems, R.A., Dennis, E.A., 1995. Lipid signaling enzymes and surface dilution kinetics. J. Biol. Chem. 270, 18711–14.

Chan, Y.H.M., Boxer, S.G., 2007. Model membrane systems and their applications. Curr. Opin. Chem. Biol. 11, 581–587.

Chang, H.-Y., Chou, C.-C., Hsu, M.-F., Wang, A.H.J., 2014. Proposed carrier lipid-binding site of undecaprenyl pyrophosphate phosphatase from *Escherichia coli*. J. Biol. Chem. 289, 18719–18735.

Chang, H.-Y., Chou, C.-C., Wu, M.-L., Wang, A.H.J., 2017. Expression, purification and enzymatic characterization of undecaprenyl pyrophosphate phosphatase from *Vibrio vulnificus*. Protein Expr. Purif. 133, 121–131.

Checa, A., Bedia, C., Jaumot, J., 2015. Lipidomic data analysis: Tutorial, practical guidelines and applications. Anal. Chim. Acta 885, 1–16.

Cole, R.B., Harrata, A.K., 1993. Solvent effect on analyte charge state, signal intensity, and stability in negative ion electrospray mass spectrometry; implications for the mechanism of negative ion formation. J Am Soc Mass Spectrom 4, 546–556.

Cong, X., Liu, Y., Liu, W., Liang, X., Russell, D.H., Laganowsky, A., 2016. Determining membrane protein-lipid binding thermodynamics using native mass spectrometry. J. Am. Chem. Soc. 138, 4346–4349.

Contreras, F.-X., Ernst, A.M., Wieland, F., Brügger, B., 2011. Specificity of intramembrane protein-lipid interactions. Cold Spring Habor Perspect. Biol. 3, a004705.

Craig, A.F., Clark, E.E., Sahu, I.D., Zhang, R., Frantz, N.D., Al-Abdul-Wahid, M.S., Dabney-Smith, C., Konkolewicz, D., Lorigan, G.A., 2016. Tuning the size of styrene-maleic acid copolymer-lipid nanoparticles (SMALPs) using RAFT polymerization for biophysical studies. Biochim. Biophys. Acta 1858, 2931–2939.

Cronan, J.E., 1968. Phospholipid alterations during growth of *Escherichia coli*. J. Bacteriol. 95, 2054–2061.

Cuevas Arenas, R., Danielczak, B., Martel, A., Porcar, L., Breyton, C., Ebel, C., Keller, S., 2017. Fast collisional lipid transfer among polymer-bounded nanodiscs. Sci. Rep. 7, 45875.

Cuevas Arenas, R., Klingler, J., Vargas, C., Keller, S., 2016. Influence of lipid bilayer properties on nanodisc formation mediated by styrene/maleic acid copolymers. Nanoscale 8, 15016–15026.

Damen, C.W.N., Isaac, G., Langridge, J., Hankemeier, T., Vreeken, R.J., 2014.

Enhanced lipid isomer separation in human plasma using reversed-phase UPLC with ion-mobility/high-resolution MS detection. J. Lipid Res. 55, 1772–1783.

de Boer, P.A.J., 2010. Advances in understanding *E. coli* cell fission. Curr. Opin. Microbiol. 13, 730–737.

Demmers, J.A.A., Van Dalen, A., De Kruijff, B., Heck, A.J.R., Killian, J.A., 2003. Interaction of the K^+ channel KcsA with membrane phospholipids as studied by ESI mass spectrometry. FEBS Lett. 541, 28–32.

den Blaauwen, T., Andreu, J.M., Monasterio, O., 2014. Bacterial cell division proteins as antibiotic targets. Bioorg. Chem. 55, 27–38.

den Blaauwen, T., Hamoen, L.W., Levin, P.A., 2017. The divisome at 25: the road ahead. Curr. Opin. Microbiol. 36, 85–94.

Dillon, D.A., Wu, W., Riedel, B., Wissing, J.B., Dowhan, W., Carman, G.M., 1996. The *Escherichia coli pgpB* gene encodes for a diacylglycerol pyrophosphate phosphatase activity. J. Biol. Chem. 271, 30548–30553.

Dominguez Pardo, J.J., Dörr, J.M., Iyer, A., Cox, R.C., Scheidelaar, S., Koorengevel, M.C., Subramaniam, V., Killian, J.A., 2017. Solubilization of lipids and lipid phases by the styrene–maleic acid copolymer. Eur. Biophys. J. 46, 91–101.

Dörr, J.M., Koorengevel, M.C., Schäfer, M., Prokofyev, A. V., Scheidelaar, S., van der Cruijsen, E.A.W., Dafforn, T.R., Baldus, M., Killian, J.A., 2014. Detergent-free isolation, characterization, and functional reconstitution of a tetrameric K^+ channel: The power of native nanodiscs. Proc. Natl. Acad. Sci. U. S. A. 111, 18607–18612.

Dörr, J.M., Scheidelaar, S., Koorengevel, M.C., Dominguez, J.J., Schäfer, M., van Walree, C.A., Killian, J.A., 2016. The styrene-maleic acid copolymer: a versatile tool in membrane research. Eur. Biophys. J. 45, 3–21.

Doubsky, J., 2009. Acid-base-driven matrix-assisted mass spectrometry for targeted metabolomics. Proc. Natl. Acad. Sci. U. S. A. 106, 10092–10096.

Dowhan, W., Mileykovskaya, E., Bogdanov, M., 2004. Diversity and versatility of lipid-protein interactions revealed by molecular genetic approaches. Biochim. Biophys. Acta 1666, 19–39.

Drew, D., Lerch, M., Kunji, E., Slotboom, D.-J., de Gier, J.-W., 2006. Optimization of membrane protein overexpression and purification using GFP fusions. Nat. Methods 3, 303–313.

Drin, G., Antonny, B., 2010. Amphipathic helices and membrane curvature. FEBS Lett. 584, 1840–1847.

Dumas, F., Lebrun, M.C., Tocanne, J.F., 1999. Is the protein/lipid hydrophobic matching principle relevant to membrane organization and functions? FEBS Lett. 458, 271–277.

Dürr, U.H.N., Gildenberg, M., Ramamoorthy, A., 2012. The magic of bicelles lights up membrane protein structure. Chem. Rev. 112, 6054–6074.

Egan, A.J.F., Vollmer, W., 2013. The physiology of bacterial cell division. Ann. N. Y. Acad. Sci. 1277, 8–28.

El Ghachi, M., Bouhss, A., Blanot, D., Mengin-Lecreulx, D., 2004. The *bacA* gene of *Escherichia coli* encodes an undecaprenyl pyrophosphate phosphatase activity. J. Biol. Chem. 279, 30106–30113.

El Ghachi, M., Derbise, A., Bouhss, A., Mengin-Lecreulx, D., 2005. Identification of multiple genes encoding membrane proteins with undecaprenyl pyrophosphate phosphatase (UppP) activity in *Escherichia coli*. J. Biol. Chem. 280, 18689–18695.

Ellis, S.R., Brown, S.H., In Het Panhuis, M., Blanksby, S.J., Mitchell, T.W., 2013. Surface analysis of lipids by mass spectrometry: More than just imaging. Prog. Lipid Res. 52, 329–353.

Elmes, M.L., Scraba, D.G., Weiner, J.H., 1986. Isolation and characterization of the tubular organelles induced by fumarate reductase overproduction in *Escherichia coli*. J. Gen. Microbiol. 132, 1429–1439.

Engelman, D.M., 2005. Membranes are more mosaic than fluid. Nature 438, 578–580.

Eriksson, H.M., Wessman, P., Ge, C., Edwards, K., Wieslander, Å., 2009. Massive formation of intracellular membrane vesicles in *Escherichia coli* by a monotopic membrane-bound lipid glycosyltransferase. J. Biol. Chem. 284, 33904–33914.

Fagone, P., Jackowski, S., 2008. Membrane phospholipid synthesis and endoplasmic reticulum function. J. Lipid Res. 50, S311–S316.

Fan, J., Jiang, D., Zhao, Y., Liu, J., Zhang, X.C., 2014. Crystal structure of lipid phosphatase *Escherichia coli* phosphatidylglycerophosphate phosphatase B. Proc. Natl. Acad. Sci. U. S. A. 111, 7636–7640.

Fang, J., Barcelona, M.J., 1998. Structural determination and quantitative analysis of bacterial phospholipids using liquid chromatography/electrospray ionization/mass spectrometry. J. Microbiol. Methods 33, 23–35.

Fang, J., Dorrestein, P.C., 2014. Emerging mass spectrometry techniques for the direct analysis of microbial colonies. Curr. Opin. Microbiol. 19, 120–129.

Folch, J., Lees, M., Sloane Stanley, G.H., 1957. A simple method for the isolation and

purification of total lipides from animal tissues. J. Biol. Chem. 226, 497–509.

Fuchs, B., Süß, R., Teuber, K., Eibisch, M., Schiller, J., 2011. Lipid analysis by thin-layer chromatography - A review of the current state. J. Chromatogr. A 1218, 2754–2774.

Fujihashi, M., Zhang, Y.W., Higuchi, Y., Li, X.Y., Koyama, T., Miki, K., 2001. Crystal structure of cis-prenyl chain elongating enzyme, undecaprenyl diphosphate synthase. Proc. Natl. Acad. Sci. U. S. A. 98, 4337–4342.

Fujita, J., Maeda, Y., Nagao, C., Tsuchiya, Y., Miyazaki, Y., Hirose, M., Mizohata, E., Matsumoto, Y., Inoue, T., Mizuguchi, K., Matsumura, H., 2014. Crystal structure of FtsA from *Staphylococcus aureus*. FEBS Lett. 588, 1879–1885.

Funk, C.R., Zimniak, L., Dowhan, W., 1992. The *pgpA* and *pgpB* genes of *Escherichia coli* are not essential: Evidence for a third phosphatidylglycerophosphate phosphatase. J. Bacteriol. 174, 205–213.

Furse, S., Egmond, M.R., Killian, J.A., 2015a. Isolation of lipids from biological samples. Mol. Membr. Biol. 32, 55–64.

Furse, S., Wienk, H., Boelens, R., de Kroon, A.I.P.M., Killian, J.A., 2015b. *E. coli* MG1655 modulates its phospholipid composition through the cell cycle. FEBS Lett. 589, 2726–2730.

Garavito, R.M., Ferguson-Miller, S., 2001. Detergents as tools in membrane biochemistry. J. Biol. Chem. 276, 32403–32406.

Garrett, T.A., Kordestani, R., Raetz, C.R.H., 2007. Quantification of cardiolipin by liquid chromatography-electrospray ionization mass spectrometry. Methods Enzymol. 433, 213–230.

Garrett, T.A., O'Neill, A.C., Hopson, M.L., 2012. Quantification of cardiolipin molecular species in *Escherichia coli* lipid extracts using liquid chromatography/electrospray ionization mass spectrometry. Rapid Commun. Mass Spectrom. 26, 2267–2274.

Geissler, B., Elraheb, D., Margolin, W., 2003. A gain-of-function mutation in *ftsA* bypasses the requirement for the essential cell division gene zipA in *Escherichia coli*. Proc. Natl. Acad. Sci. U. S. A. 100, 4197–202.

Gidden, J., Denson, J., Liyanage, R., Ivey, D.M., Lay, J.O., 2009. Lipid compositions in *Escherichia coli* and *Bacillus subtilis* during growth as determined by MALDI-TOF and TOF/TOF mass spectrometry. Int. J. Mass Spectrom. 283, 178–184.

Gifford, S.M., Meyer, P., 2015. Enzyme function is regulated by its localization.

Comput. Biol. Chem. 59, 113–122.

Goddard, A.D., Dijkman, P.M., Adamson, R.J., dos Reis, R.I., Watts, A., 2015. Reconstitution of membrane proteins: a GPCR as an example. Methods Enzymol. 556, 405–424.

Goldfine, H., 1984. Bacterial membranes and lipid packing theory. J. Lipid Res. 25, 1501–1507.

Greenhalgh, T., 1997. Statistics for the non-statistician. I: Different types of data need different statistical tests. Br. Med. J. 315, 364–366.

Grogan, D.W., Cronan, J.E.J., 1997. Cyclopropane ring formation in membrane lipids of bacteria. Microbiol. Mol. Biol. Rev. 61, 429–441.

Gulati, S., Jamshad, M., Knowles, T.J., Morrison, K.A., Downing, R., Cant, N., Collins, R., Koenderink, J.B., Ford, R.C., Overduin, M., Kerr, I.D., Dafforn, T.R., Rothnie, A.J., 2014. Detergent-free purification of ABC (ATP-binding-cassette) transporters. Biochem J. 461, 269–78.

Haeusser, D.P., Margolin, W., 2016. Splitsville: structural and functional insights into the dynamic bacterial Z ring. Nat. Rev. Microbiol. 14, 305–319.

Hale, C.A., de Boer, P.A.J., 1997. Direct binding of FtsZ to ZipA, an essential component of the septal ring structure that mediates cell division in *E. coli*. Cell 88, 175–185.

Hale, C.A., de Boer, P.A.J., 1999. Recruitment of ZipA to the septal ring of *Escherichia coli* is dependent on FtsZ and independent of FtsA. J. Bacteriol. 181, 167–176.

Hale, C.A., Rhee, A.C., De Boer, P.A.J., 2000. ZipA-induced bundling of FtsZ polymers mediated by an interaction between C-terminal domains. J. Bacteriol. 182, 5153–5166.

Han, X., Gross, R.W., 2003. Global analyses of cellular lipidomes directly from crude extracts of biological samples by ESI mass spectrometry: a bridge to lipidomics. J Lipid Res 44, 1071–1079.

Han, X., Yang, K., Gross, R.W., 2012. Multi-dimensional mass spectrometry-based shotgun lipidomics and novel strategies for lipidomic analyses. Mass Spectrom. Rev. 31, 134–178.

Han, X., Yang, K., Yang, J., Cheng, H., Gross, R.W., 2006. Shotgun lipidomics of cardiolipin molecular species in lipid extracts of biological samples. J. Lipid Res. 47, 864–879.

Hancock, S.E., Poad, B.L.J., Batarseh, A., Abbott, S.K., Mitchell, T.W., 2017.

Advances and unresolved challenges in the structural characterization of isomeric lipids. Anal. Biochem. 524, 45–55.

Hankin, J.A., Barkley, R.M., Murphy, R.C., 2007. Sublimation as a method of matrix application for mass spectrometric imaging. J. Am. Soc. Mass Spectrom. 18, 1646–1652.

Hardy, D., Bill, R.M., Jawhari, A., Rothnie, A.J., 2016. Overcoming bottlenecks in the membrane protein structural biology pipeline. Biochem. Soc. Trans. 44, 838–844.

Harkewicz, R., Dennis, E.A., 2011. Applications of mass spectrometry to lipids and membranes. Annu. Rev. Biochem. 80, 301–325.

Hazell, G., Arnold, T., Barker, R.D., Clifton, L.A., Steinke, N.-J., Tognoloni, C., Edler, K.J., 2016. Evidence of lipid exchange in styrene maleic acid lipid particle (SMALP) nanodisc systems. Langmuir 32, 11845–11853.

Henrich, E., Ma, Y., Engels, I., Münch, D., Otten, C., Schneider, T., Henrichfreise, B., Sahl, H.-G., Dötsch, V., Bernhard, F., 2015. Lipid requirements for the enzymatic activity of MraY translocases and in vitro reconstitution of lipid II synthesis pathway. J. Biol. Chem. 291, 2535–2546.

Hernández-Rocamora, V.M., García-Montañés, C., Rivas, G., Llorca, O., 2012a. Reconstitution of the *Escherichia coli* cell division ZipA-FtsZ complexes in nanodiscs as revealed by electron microscopy. J. Struct. Biol. 180, 531–538.

Hernández-Rocamora, V.M., Reija, B., García, C., Natale, P., Alfonso, C., Minton, A.P., Zorrilla, S., Rivas, G., Vicente, M., 2012b. Dynamic interaction of the *Escherichia coli* cell division ZipA and FtsZ proteins evidenced in nanodiscs. J. Biol. Chem. 287, 30097–30104.

Hewelt-Belka, W., Nakonieczna, J., Belka, M., Bączek, T., Namieśnik, J., Kot-Wasik, A., 2016. Untargeted lipidomics reveals differences in the lipid pattern among clinical isolates of *Staphylococcus aureus* resistant and sensitive to antibiotics. J. Proteome Res. 15, 914–922.

Hrast, M., Sosič, I., Šink, R., Gobec, S., 2014. Inhibitors of the peptidoglycan biosynthesis enzymes MurA-F. Bioorg. Chem. 55, 2–15.

Hsu, F.-F., Turk, J., 2001. Studies on phosphatidylglycerol with triple quadrupole tandem mass spectrometry with electrospray ionization: Fragmentation processes and structural characterization. J. Am. Soc. Mass Spectrom. 12, 1036–1043.

Hsu, F.-F., Turk, J., 2006. Characterization of cardiolipin from *Escherichia coli* by electrospray ionization with multiple stage quadrupole ion-trap mass

spectrometric analysis of $[M-2H+Na]^-$ ions. J. Am. Soc. Mass Spectrom. 17, 420–429.

Hsu, F.F., Turk, J., Rhoades, E.R., Russell, D.G., Shi, Y., Groisman, E. a, 2005. Structural characterization of cardiolipin by tandem quadrupole and multiple-stage quadrupole ion-trap mass spectrometry with electrospray ionization. J. Am. Soc. Mass Spectrom. 16, 491–504.

Icho, T., 1988. Membrane-bound phosphatases in *Escherichia coli*: sequence of the *pgpB* gene and dual subcellular localization of the *pgpB* product. J. Bacteriol. 170, 5117–5124.

Icho, T., Raetz, C.R.H., 1983. Multiple genes for membrane-bound phosphatases in *Escherichia coli* and their action on phospholipid precursors. J. Bacteriol. 153, 722–730.

Ilgü, H., Jeckelmann, J.M., Gachet, M.S., Boggavarapu, R., Ucurum, Z., Gertsch, J., Fotiadis, D., 2014. Variation of the detergent-binding capacity and phospholipid content of membrane proteins when purified in different detergents. Biophys. J. 106, 1660–1670.

Ishida, Y., Madonna, A.J., Rees, J.C., Meetani, M.A., Voorhees, K.J., 2002. Rapid analysis of intact phospholipids from whole bacterial cells by matrix-assisted laser desorption/ionization mass spectrometry combined with on-probe sample pretreatment. Rapid Commun. Mass Spectrom. 16, 1877–1882.

Jamshad, M., Charlton, J., Lin, Y., Routledge, S.J., Bawa, Z., Knowles, T.J., Overduin, M., Dekker, N., Dafforn, T.R., Bill, R.M., Poyner, D.R., Wheatley, M., 2015a. G-protein coupled receptor solubilization and purification for biophysical analysis and functional studies, in the total absence of detergent Bioscience Reports. Biosci. Rep. 35, 1–10.

Jamshad, M., Grimard, V., Idini, I., Knowles, T.J., Dowle, M.R., Schofield, N., Sridhar, P., Lin, Y., Finka, R., Wheatley, M., Thomas, O.R.T., Palmer, R.E., Overduin, M., Govaerts, C., Ruysschaert, J.M., Edler, K.J., Dafforn, T.R., 2015b. Structural analysis of a nanoparticle containing a lipid bilayer used for detergent-free extraction of membrane proteins. Nano Res. 8, 774–789.

Jamshad, M., Lin, Y.-P., Knowles, T.J., Parslow, R. a, Harris, C., Wheatley, M., Poyner, D.R., Bill, R.M., Thomas, O.R.T., Overduin, M., Dafforn, T.R., 2011. Surfactant-free purification of membrane proteins with intact native membrane environment. Biochem. Soc. Trans. 39, 813–818.

Janmey, P.A., Kinnunen, P.K.J., 2006. Biophysical properties of lipids and dynamic membranes. Trends Cell Biol. 16, 538–546.

Jensen, M.Ø., Mouritsen, O.G., 2004. Lipids do influence protein function - The hydrophobic matching hypothesis revisited. Biochim. Biophys. Acta 1666, 205–226.

Jiménez, M., Martos, A., Vicente, M., Rivas, G., 2011. Reconstitution and organization of *Escherichia coli* proto-ring elements (FtsZ and FtsA) inside giant unilamellar vesicles obtained from bacterial inner membranes. J. Biol. Chem. 286, 11236–11241.

Jouhet, J., 2013. Importance of the hexagonal lipid phase in biological membrane organization. Front. Plant Sci. 4, 494.

Kaneda, T., 1991. Iso- and anteiso-fatty acids in bacteria: biosynthesis, function, and taxonomic significance. Microbiol. Rev. 55, 288–302.

Katajamaa, M., Orešič, M., 2007. Data processing for mass spectrometry-based metabolomics. J. Chromatogr. A 1158, 318–328.

Kates, M., Syz, J.Y., Gosser, D., Haines, T.H., 1993. pH-dissociation characteristics of cardiolipin and its 2'-deoxy analogue. Lipids 28, 877–882.

Kawazura, T., Matsumoto, K., Kojima, K., Kato, F., Kanai, T., Niki, H., Shiomi, D., 2017. Exclusion of assembled MreB by anionic phospholipids at cell poles confers cell polarity for bidirectional growth. Mol. Microbiol. 104, 472–486.

Kelly, S.M., Jess, T.J., Price, N.C., 2005. How to study proteins by circular dichroism. Biochim. Biophys. Acta 1751, 119–139.

Knol, J., Sjollema, K., Poolman, B., 1998. Detergent-mediated reconstitution of membrane proteins. Biochemistry 37, 16410–16415.

Knowles, T.J., Finka, R., Smith, C., Lin, Y.-P., Dafforn, T., Overduin, M., 2009. Membrane proteins solubilized intact in lipid containing nanoparticles bounded by styrene maleic acid copolymer. J. Am. Chem. Soc. 131, 7484–7485.

Köfeler, H.C., Fauland, A., Rechberger, G.N., Trötzmüller, M., 2012. Mass spectrometry based lipidomics: an overview of technological platforms. Metabolites 2, 19–38.

Komar, J., Alvira, S., Schulze, R., Martin, R., Lycklama a Nijeholt, J., Lee, S., Dafforn, T., Deckers-Hebestreit, G., Berger, I., Schaffitzel, C., Collinson, I., 2016. Membrane protein insertion and assembly by the bacterial holo-translocon SecYEG-SecDF-YajC-YidC. Biochem. J. 473, 3341–3354.

Komar, J., Botte, M., Collinson, I., Schaffitzel, C., Berger, I., 2015. ACEMBLing a multiprotein transmembrane complex: The functional SecYEG-SecDF-YajC-YidC holotranslocon protein secretase/insertase. Methods Enzymol. 556, 23–49.

Koppelman, C.-M., den Blaauwen, T., Duursma, M.C., Heeren, R.M.A., Nanninga, N., 2001. *Escherichia coli* minicell membranes are enriched in cardiolipin. J Bacteriol. 183, 6144–6147.

Kozlowski, R.L., Mitchell, T.W., Blanksby, S.J., 2015. A rapid ambient ionization-mass spectrometry approach to monitoring the relative abundance of isomeric glycerophospholipids. Sci. Rep. 5, 9243.

Krupka, M., Cabré, E.J., Jiménez, M., Rivas, G., Rico, A.I., Vicente, M., 2014. Role of the FtsA C terminus as a switch for polymerization and membrane association. MBio 5, 1–9.

Kühlbrandt, W., 2014. Cryo-EM enters a new era. Elife 3, e03665.

Laemmli, U.K., 1970. Cleavage of structural proteins during the assembly of the head of bacteriophage T4. Nature.227, 680-685.

Landreh, M., Marty, M.T., Gault, J., Robinson, C. V., 2016. A sliding selectivity scale for lipid binding to membrane proteins. Curr. Opin. Struct. Biol. 39, 54–60.

Laursen, T., Borch, J., Knudsen, C., Bavishi, K., Torta, F., Martens, H.J., Silvestro, D., Hatzakis, N.S., Wenk, M.R., Dafforn, T.R., Olsen, C.E., Motawia, M.S., Hamberger, B., 2016. Characterization of a dynamic metabolon producing the defense compound dhurrin in sorghum. Science 354, 890–893.

Layre, E., Moody, D.B., 2013. Lipidomic profiling of model organisms and the world's major pathogens. Biochimie 95, 109–115.

Lee, A.G., 2004. How lipids affect the activities of integral membrane proteins. Biochim. Biophys. Acta 1666, 62–87.

Lee, A.G., 2011. Lipid–protein interactions. Biochem. Soc. Trans. 39, 761–766.

Lee, S.C., Khalid, S., Pollock, N.L., Knowles, T.J., Edler, K., Rothnie, A.J., R.T.Thomas, O., Dafforn, T.R., 2016a. Encapsulated membrane proteins: A simplified system for molecular simulation. Biochim. Biophys. Acta 1858, 2549–2557.

Lee, S.C., Knowles, T.J., Postis, V.L.G., Jamshad, M., Parslow, R.A., Lin, Y., Goldman, A., Sridhar, P., Overduin, M., Muench, S.P., Dafforn, T.R., 2016b. A method for detergent-free isolation of membrane proteins in their local lipid environment. Nat. Protoc. 11, 1149–1162.

Lee, S.C., Pollock, N.L., 2016. Membrane proteins: is the future disc shaped? Biochem. Soc. Trans. 44, 1011–1018.

Lefman, J., Zhang, P., Hirai, T., Robert, M., Juliani, J., Bliss, D., Kessel, M., Bos, E., Peters, P.J., Subramaniam, S., Weis, R.M., 2004. Three-dimensional electron microscopic imaging of membrane invaginations in *Escherichia coli* overproducing the chemotaxis teceptor Tsr. J Bacteriol. 186, 5052–5061.

Li, D., Li, J., Zhuang, Y., Zhang, L., Xiong, Y., Shi, P., Tian, C., 2015. Nano-size uni-lamellar lipodisq improved *in situ* auto-phosphorylation analysis of *E. coli* tyrosine kinase using ^{19}F nuclear magnetic resonance. Protein Cell 6, 229–233.

Li, L., Han, J., Wang, Z., Liu, J., Wei, J., Xiong, S., Zhao, Z., 2014. Mass spectrometry methodology in lipid analysis. Int. J. Mol. Sci. 15, 10492–10507.

Lin, T., Weibel, D.B., 2016. Organization and function of anionic phospholipids in bacteria. Appl. Microbiol. Biotechnol. 100, 4255–4267.

Lin, Y.-P., 2011. Over-expression and biophysical characterisation of membrane proteins solubilised in a styrene maleic acid polymer. PhD Thesis, University of Birmingham.

Lindhoud, S., Carvalho, V., Pronk, J.W., Aubin-Tam, M.-E., 2016. SMA-SH: Modified styrene-maleic acid copolymer for functionalization of lipid nanodiscs. Biomacromolecules 17, 1516–1522.

Lísa, M., Holčapek, M., 2015. High-throughput and comprehensive lipidomic analysis using ultrahigh-performance supercritical fluid chromatography-mass spectrometry. Anal. Chem. 87, 7187–7195.

Lomize, M.A., Lomize, A.L., Pogozheva, I.D., Mosberg, H.I., 2006. OPM: Orientations of proteins in membranes database. Bioinformatics 22, 623–625.

Long, A.R., O'Brien, C.C., Malhotra, K., Schwall, C.T., Albert, A.D., Watts, A., Alder, N.N., 2013. A detergent-free strategy for the reconstitution of active enzyme complexes from native biological membranes into nanoscale discs. BMC Biotechnol. 13, 41.

López-Montero, I., López-Navajas, P., Mingorance, J., Rivas, G., Vélez, M., Vicente, M., Monroy, F., 2013a. Intrinsic disorder of the bacterial cell division protein ZipA: coil-to-brush conformational transition. FASEB J. 27, 3363–3375.

López-Montero, I., López-Navajas, P., Mingorance, J., Vélez, M., Vicente, M., Monroy, F., 2013b. Membrane reconstitution of FtsZ-ZipA complex inside giant spherical vesicles made of *E. coli* lipids: Large membrane dilation and analysis of membrane

plasticity. Biochim. Biophys. Acta 1828, 687–698.

Lutkenhaus, J., Pichoff, S., Du, S., 2012. Bacterial cytokinesis: From Z ring to divisome. Cytoskeleton 69, 778–790.

Manat, G., El Ghachi, M., Auger, R., Baouche, K., Olatunji, S., Kerff, F., Touzé, T., Mengin-Lecreulx, D., Bouhss, A., 2015. Membrane topology and biochemical characterization of the *Escherichia coli* BacA undecaprenyl-pyrophosphate phosphatase. PLoS One 10, e0142870.

Manat, G., Roure, S., Auger, R., Bouhss, A., Barreteau, H., Mengin-Lecreulx, D., Touzé, T., 2014. Deciphering the metabolism of undecaprenyl-phosphate: the bacterial cell-wall unit carrier at the membrane frontier. Microb. Drug Resist. 20, 199–214.

Mancia, F., Love, J., 2010. High-throughput expression and purification of membrane proteins. J. Struct. Biol. 172, 85–93.

Marius, P., Zagnoni, M., Sandison, M.E., East, J.M., Morgan, H., Lee, A.G., 2008. Binding of anionic lipids to at least three nonannular sites on the potassium channel KcsA is required for channel opening. Biophys. J. 94, 1689–1698.

Markgraf, D.F., Al-Hasani, H., Lehr, S., 2016. Lipidomics - Reshaping the analysis and perception of Type 2 diabetes. Int. J. Mol. Sci. 17, 1841.

Martos, A., Monterroso, B., Zorrilla, S., Reija, B., Alfonso, C., Mingorance, J., Rivas, G., Jiménez, M., 2012. Isolation, characterization and lipid-binding properties of the recalcitrant FtsA division protein from *Escherichia coli*. PLoS One 7, e39829.

Matsumoto, K., Hara, H., Fishov, I., Mileykovskaya, E., Norris, V., 2015. The membrane: transertion as an organizing principle in membrane heterogeneity. Microb. Physiol. Metab. 6, 572.

Matyash, V., Liebisch, G., Kurzchalia, T. V, Shevchenko, A., Schwudke, D., 2008. Lipid extraction by methyl-*tert*-butyl ether for high-throughput lipidomics. J. Lipid Res. 49, 1137–46.

Mazzella, N., Molinet, J., Syakti, A.D., Dodi, A., Doumenq, P., Artaud, J., Bertrand, J.-C., 2004. Bacterial phospholipid molecular species analysis by ion-pair reversed-phase HPLC/ESI/MS. J. Lipid Res. 45, 1355–1363.

McMahon, H.T., Gallop, J.L., 2005. Membrane curvature and mechanisms of dynamic cell membrane remodelling. Nature 438, 590–596.

Meetani, M., Shin, Y.-S., Zhang, S., Mayer, R., Basile, F., 2007. Desorption electrospray ionization mass spectrometry of intact bacteria. J. Mass Spectrom. 42,

1186–1193.

Miles, A.J., Wallace, B.A., 2016. Circular dichroism spectroscopy of membrane proteins. Chem. Soc. Rev. 14, 1130–1135.

Mileykovskaya, E., Dowhan, W., 2005. Role of membrane lipids in bacterial division-site selection. Curr. Opin. Microbiol. 8, 135–142.

Mileykovskaya, E., Dowhan, W., 2009. Cardiolipin membrane domains in prokaryotes and eukaryotes. Biochim. Biophys. Acta 1788, 2084–2091.

Milne, S., Ivanova, P., Forrester, J., Alex Brown, H., 2006. Lipidomics: An analysis of cellular lipids by ESI-MS. Methods 39, 92–103.

Minkler, P.E., Hoppel, C.L., 2010. Separation and characterization of cardiolipin molecular species by reverse-phase ion pair high-performance liquid chromatography-mass spectrometry. J. Lipid Res. 51, 856–865.

Morrison, K.A., Akram, A., Mathews, A., Khan, Z.A., Patel, J.H., Zhou, C., Hardy, D.J., Moore-Kelly, C., Patel, R., Odiba, V., Knowles, T., Javed, M.–.-H., Chmel, N.P., Dafforn, T.R., Rothnie, A.J., 2016. Membrane protein extraction and purification using styrene-maleic acid (SMA) co-polymer: Effect of variations in polymer structure. Biochem. J. 473, 4349–4360.

Mosyak, L., Zhang, Y., Glasfeld, E., Haney, S., Stahl, M., Seehra, J., Somers, W.S., 2000. The bacterial cell-division protein ZipA and its interaction with an FtsZ fragment revealed by X-ray crystallography. EMBO J. 19, 3179–3191.

Moy, F.J., Glasfeld, E., Mosyak, L., Powers, R., 2000. Solution structure of ZipA, a crucial component of *Escherichia coli* cell division. Biochemistry 39, 9146–9156.

Mozharov, A., Shchipakin, V., Fishov, I., Evtodienko, Y.V., 1985. Changes in the composition of membrane phospholipids during the cell cycle of *Escherichia coli*. FEBS Lett. 186, 103–106.

Mrsny, R.J., Volwerk, J.J., Griffith, O.H., 1986. A simplified procedure for lipid phosphorus analysis shows that digestion rates vary with phospholipid structure. Chem. Phys Lipids 39, 185–191.

Murphy, R.C., Gaskell, S.J., 2011. New applications of mass spectrometry in lipid analysis. J. Biol. Chem. 286, 25427–25433.

Myers, D.S., Ivanova, P.T., Milne, S.B., Brown, H.A., 2011. Quantitative analysis of glycerophospholipids by LC-MS: acquisition, data handling, and interpretation. Biochim. Biophys. Acta 1811, 748–757.

National Audit Office, 2004. Improving patient care by reducing the risk of hospital

acquired infection: A progress report.

Nieboer, M., Kingma, J., Witholt, B., 1993. The alkane oxidation system of Pseudomonas oleovorans: induction of the *alk* genes in *Escherichia coli* W3110(pGEc47) affects membrane biogenesis and results in overexpression of alkane hydroxylase in a distinct cytoplasmic membrane subtraction. Mol. Microbiol. 8, 1039–1051.

Nieboer, M., Vis, A.J., Witholt, B., 1996. Overproduction of a foreign membrane protein in *Escherichia coli* stimulates and depends on phospholipid synthesis. Eur. J. Biochem. 241, 691–696.

O'Neill, J., 2014. Review on Antimicrobial Resistance. Antimicrobial Resistance: Tackling a Crisis for the Health and Wealth of Nations.

Ohashi, T., Hale, C.A., De Boer, P.A.J., Erickson, H.P., 2002. Structural evidence that the P/Q domain of ZipA is an unstructured, flexible tether between the membrane and the C-terminal FtsZ-binding domain. J. Bacteriol. 184, 4313–4315.

Oliver, P.M., Crooks, J.A., Leidl, M., Yoon, E.J., Saghatelian, A., Weibel, D.B., 2014. Localization of anionic phospholipids in *Escherichia coli* cells. J. Bacteriol. 196, 3386–3398.

Olofsson, G., Sparr, E., 2013. Ionization constants pK_a of cardiolipin. PLoS One 8, e73040.

Oluwole, A.O., Danielczak, B., Meister, A., Babalola, J.O., Vargas, C., Keller, S., 2017. Solubilization of membrane proteins into functional lipid-bilayer nanodiscs using a diisobutylene/maleic acid copolymer. Angew. Chemie Int. Ed. 56, 1917–1924.

Orešič, M., 2011. Informatics and computational strategies for the study of lipids. Biochim. Biophys. Acta 1811, 991–999.

Ortiz, C., Natale, P., Cueto, L., Vicente, M., 2016. The keepers of the ring: regulators of FtsZ assembly. FEMS Microbiol. Rev. 40, 57–67.

Orwick, M.C., Judge, P.J., Procek, J., Lindholm, L., Graziadei, A., Engel, A., Gröbner, G., Watts, A., 2012. Detergent-free formation and physicochemical characterization of nanosized lipid-polymer complexes: Lipodisq. Angew. Chemie Int. Ed. 51, 4653–7.

Osawa, M., Anderson, D.E., Erickson, H.P., 2008. Reconstitution of contractile FtsZ rings in liposomes. Science 320, 792–794.

Osawa, M., Erickson, H.P., 2013. Liposome division by a simple bacterial division machinery. Proc. Natl. Acad. Sci. U. S. A. 110, 11000–11004.

Otzen, D., 2011. Protein-surfactant interactions: A tale of many states. Biochim. Biophys. Acta 1814, 562–591.

Oursel, D., Loutelier-Bourhis, C., Orange, N., Chevalier, S., Norris, V., Lange, C.M., 2007a. Identification and relative quantification of fatty acids in *Escherichia coli* membranes by gas chromatography/mass spectrometry. Rapid Commun. Mass Spectrom. 21, 3229–3233.

Oursel, D., Loutelier-Bourhis, C., Orange, N., Chevalier, S., Norris, V., Lange, C.M., 2007b. Lipid composition of membranes of *Escherichia coli* by liquid chromatography/tandem mass spectrometry using negative electrospray ionization. Rapid Commun. Mass Spectrom. 21, 1721–1728.

Overington, J.P., Al-Lazikani, B., Hopkins, A.L., 2006. How many drug targets are there? Nat. Rev. Drug Discov. 5, 993–996.

Parmar, M.J., Lousa, C.D.M., Muench, S.P., Goldman, A., Postis, V.L.G., 2016. Artificial membranes for membrane protein purification, functionality and structure studies. Biochem. Soc. Trans. 44, 877–882.

Parsons, J.B., Rock, C.O., 2013. Bacterial lipids: Metabolism and membrane homeostasis. Prog. Lipid Res. 52, 249–276.

Pati, S., Nie, B., Arnold, R.D., Cummings, B.S., 2016. Extraction, chromatographic and mass spectrometric methods for lipid analysis. Biomed. Chromatogr. 30, 695–709.

Paulin, S., Jamshad, M., Dafforn, T.R., Garcia-Lara, J., Foster, S.J., Galley, N.F., Roper, D.I., Rosado, H., Taylor, P.W., 2014. Surfactant-free purification of membrane protein complexes from bacteria: application to the staphylococcal penicillin-binding protein complex PBP2/PBP2a. Nanotechnology 25, 285101.

Pazos, M., Natale, P., Vicente, M., 2013. A specific role for the ZipA protein in cell division: Stabilization of the FtsZ protein. J. Biol. Chem. 288, 3219–3226.

Perozo, E., Kloda, A., Cortes, D.M., Martinac, B., 2002. Physical principles underlying the transduction of bilayer deformation forces during mechanosensitive channel gating. Nat. Struct. Biol. 9, 696–703.

Pettersen, E.F., Goddard, T.D., Huang, C.C., Couch, G.S., Greenblatt, D.M., Meng, E.C., Ferrin, T.E., 2004. UCSF Chimera - a visualization system for exploratory research and analysis. J. Comput. Chem. 25, 1605–1612.

Phillips, R., Ursell, T., Wiggins, P., Sens, P., 2009. Emerging roles for lipids in shaping membrane-protein function. Nature 459, 379–385.

Pichoff, S., Lutkenhaus, J., 2002. Unique and overlapping roles for ZipA and FtsA in

septal ring assembly in *Escherichia coli*. EMBO J. 21, 685–693.

Pichoff, S., Lutkenhaus, J., 2005. Tethering the Z ring to the membrane through a conserved membrane targeting sequence in FtsA. Mol. Microbiol. 55, 1722–1734.

Postis, V., Rawson, S., Mitchell, J.K., Lee, S.C., Parslow, R.A., Dafforn, T.R., Baldwin, S.A., Muench, S.P., 2015. The use of SMALPs as a novel membrane protein scaffold for structure study by negative stain electron microscopy. Biochim. Biophys. Acta 1848, 496–501.

Prabudiansyah, I., Kusters, I., Caforio, A., Driessen, A.J.M., 2015. Characterization of the annular lipid shell of the Sec translocon. Biochim. Biophys. Acta 1848, 2050–2056.

Rajesh, S., Knowles, T., Overduin, M., 2011. Production of membrane proteins without cells or detergents. N. Biotechnol. 28, 250–254.

Ramamurthi, K.S., 2010. Protein localization by recognition of membrane curvature. Curr. Opin. Microbiol. 13, 753–757.

Rehan, S., Paavilainen, V.O., Jaakola, V., 2017. Functional reconstitution of human equilibrative nucleoside transporter-1 into styrene maleic acid co-polymer lipid particles. Biochim. Biophys. Acta 1859, 1059–1065.

Reis, A., Rudnitskaya, A., Blackburn, G.J., Fauzi, N.M., Pitt, A.R., Spickett, C.M., 2013. A comparison of five lipid extraction solvent systems for lipidomic studies of human LDL. J. Lipid Res. 54, 1812–1824.

Renner, L.D., Weibel, D.B., 2012. MinD and MinE interact with anionic phospholipids and regulate division plane formation in *Escherichia coli*. J. Biol. Chem. 287, 38835–38844.

Rico, A.I., García-Ovalle, M., Mingorance, J., Vicente, M., 2004. Role of two essential domains of *Escherichia coli* FtsA in localization and progression of the division ring. Mol. Microbiol. 53, 1359–1371.

Rico, A.I., Krupka, M., Vicente, M., 2013. In the beginning, *Escherichia coli* assembled the proto-ring: An initial phase of division. J. Biol. Chem. 288, 20830–20836.

Rigaud, J., Levy, D., 2003. Reconstiution of Membrane Proteins into Liposomes. Methods Enzymol. 372, 65–86.

Rilfors, L., Lindblom, G., 2002. Regulation of lipid composition in biological membranes - biophysical studies of lipids and lipid synthesizing enzymes. Colloids Surfaces B Biointerfaces 26, 112–124.

Ringnér, M., 2008. What is principal component analysis? Nat Biotechnol 26, 303–304.

Romantsov, T., Guan, Z., Wood, J.M., 2009. Cardiolipin and the osmotic stress responses of bacteria. Biochim. Biophys. Acta 1788, 2092–2100.

Rosano, G.L., Ceccarelli, E.A., 2014. Recombinant protein expression in *Escherichia coli*: Advances and challenges. Front. Microbiol. 5, 1–17.

Rothnie, A.J., 2016. Detergent-free membrane protein purification. Methods Mol. Biol. 1432, 261–267.

Rouser, G., Fleischer, S., Yamamoto, A., 1970. Two dimensional thin layer chromatographic separation of polar lipids and determination of phospholipids by phosphorus analysis of spots. Lipids 5, 494–496.

Routledge, S.J., Mikaliunaite, L., Patel, A., Clare, M., Cartwright, S.P., Bawa, Z., Wilks, M.D.B., Low, F., Hardy, D., Rothnie, A.J., Bill, R.M., 2016. The synthesis of recombinant membrane proteins in yeast for structural studies. Methods 95, 26–37.

Samhan-Arias, A.K., Ji, J., Demidova, O.M., Sparvero, L.J., Feng, W., Tyurin, V., Tyurina, Y.Y., Epperly, M.W., Shvedova, A.A., Greenberger, J.S., Bayır, H., Kagan, V.E., Amoscato, A.A., 2012. Oxidized phospholipids as biomarkers of tissue and cell damage with a focus on cardiolipin. Biochim. Biophys. Acta 1818, 2413–2423.

Santos, T., Capelo, J.L., Santos, H.M., Oliveira, I., Marinho, C., Gonçalves, A., Araújo, J.E., Poeta, P., Igrejas, G., 2015. Use of MALDI-TOF mass spectrometry fingerprinting to characterize *Enterococcus* spp. and *Escherichia coli* isolates. J. Proteomics 127, 321–331.

Sato, S., Kawamoto, J., Sato, S.B., Watanabe, B., Hiratake, J., Esaki, N., Kurihara, T., 2012. Occurrence of a bacterial membrane microdomain at the cell division site enriched in phospholipids with polyunsaturated hydrocarbon chains. J. Biol. Chem. 287, 24113–24121.

Scheidelaar, S., Koorengevel, M.C., Pardo, J.D., Meeldijk, J.D., Breukink, E., Killian, J.A., 2015. Molecular model for the solubilization of membranes into nanodisks by styrene maleic acid copolymers. Biophys. J. 108, 279–290.

Scheidelaar, S., Koorengevel, M.C., van Walree, C.A., Dominguez, J.J., D??rr, J.M., Killian, J.A., 2016. Effect of polymer composition and pH on membrane solubilization by styrene-maleic acid copolymers. Biophys. J. 111, 1974–1986.

Schindelin, J., Arganda-Carreras, I., Frise, E., Kaynig, V., Longair, M., Pietzsch, T., Preibisch, S., Rueden, C., Saalfeld, S., Schmid, B., Tinevez, J.-Y., White, D.J.,

Hartenstein, V., Eliceiri, K., Tomancak, P., Cardona, A., 2012. Fiji: an open-source platform for biological-image analysis. Nat. Methods 9, 676–682.

Schlame, M., 2008. Cardiolipin synthesis for the assembly of bacterial and mitochondrial membranes. J. Lipid Res. 49, 1607–1620.

Schwalbe-Herrmann, M., Willmann, J., Leibfritz, D., 2010. Separation of phospholipid classes by hydrophilic interaction chromatography detected by electrospray ionization mass spectrometry. J. Chromatogr. A 1217, 5179–5183.

Sebastián, M., Smith, A.F., González, J.M., Fredricks, H.F., Van Mooy, B., Koblížek, M., Brandsma, J., Koster, G., Mestre, M., Mostajir, B., Pitta, P., Postle, A.D., Sánchez, P., Gasol, J.M., Scanlan, D.J., Chen, Y., 2016. Lipid remodelling is a widespread strategy in marine heterotrophic bacteria upon phosphorus deficiency. ISME J. 10, 968–978.

Seddon, A.M., Curnow, P., Booth, P.J., 2004. Membrane proteins, lipids and detergents: not just a soap opera. Biochim. Biophys. Acta 1666, 105–117.

Serebryany, E., Zhu, G.A., Yan, E.C.Y., 2012. Artificial membrane-like environments for *in vitro* studies of purified G-protein coupled receptors. Biochim. Biophys. Acta 1818, 225–233.

Shevchenko, A., Simons, K., 2010. Lipidomics: coming to grips with lipid diversity. Nat. Rev. Mol. Cell Biol. 11, 593–598.

Shiomi, D., Margolin, W., 2008. Compensation for the loss of the conserved membrane targeting sequence of FtsA provides new insights into its function. Mol. Microbiol. 67, 558–569.

Shu, X., Li, Y., Liang, M., Yang, B., Liu, C., Wang, Y., Shu, J., 2012. Rapid lipid profiling of bacteria by online MALDI-TOF mass spectrometry. Int. J. Mass Spectrom. 321–322, 71–76.

Silver, L.L., 2013. Viable screening targets related to the bacterial cell wall. Ann. N. Y. Acad. Sci. 1277, 29–53.

Singer, S.J.J., Nicolson, G.L.L., 1972. The fluid mosaic model of the structure of cell membranes. Science 175, 720–731.

Smirnova, I.A., Sjöstrand, D., Li, F., Björck, M., Schäfer, J., Östbye, H., Högbom, M., von Ballmoos, C., Lander, G., Ädelroth, P., Brzezinski, P., 2016. Isolation of yeast complex IV in native lipid nanodiscs. Biochim. Biophys. Acta 1858, 2984–2992.

Smith, P.B., Snyder, a P., Harden, C.S., 1995. Characterization of bacterial phospholipids by electrospray ionization tandem mass spectrometry. Anal. Chem.

67, 1824–1830.

Smith, P.K., Krohn, R.I., Hermanson, G.T., Mallia, A.K., Gartner, F.H., Provenzano, M.D., Fujimoto, E.K., Goeke, N.M., Olson, B.J., Klenk, D.C., 1985. Measurement of protein using bicinchoninic acid. Anal. Biochem. 150, 76–85.

Sonawane, L. V, Poul, B.N., Usnale, S. V, Waghmare, P. V, Surwase, L.H., 2014. Bioanalytical method validation and its pharmaceutical application- A review. Pharm. Anal. Acta 5, e1000288.

Song, Y., Talaty, N., Tao, W.A., Pan, Z., Cooks, R.G., 2007. Rapid ambient mass spectrometric profiling of intact, untreated bacteria using desorption electrospray ionization. Chem. Commun. (Camb). 10, 61–63.

Sonoda, Y., Newstead, S., Hu, N.J., Alguel, Y., Nji, E., Beis, K., Yashiro, S., Lee, C., Leung, J., Cameron, A.D., Byrne, B., Iwata, S., Drew, D., 2011. Benchmarking membrane protein detergent stability for improving throughput of high-resolution X-ray structures. Structure 19, 17–25.

Sotirhos, N., Herslöf, B., Kenne, L., 1986. Quantitative analysis of phospholipids by ^{31}P-NMR. J. Lipid Res. 27, 386–392.

Sparagna, G.C., Johnson, C.A., McCune, S.A., Moore, R.L., Murphy, R.C., 2005. Quantitation of cardiolipin molecular species in spontaneously hypertensive heart failure rats using electrospray ionization mass spectrometry. J. Lipid Res. 46, 1196–1204.

Spickett, C.M., Reis, A., Pitt, A.R., 2011. Identification of oxidized phospholipids by electrospray ionization mass spectrometry and LC-MS using a QQLIT instrument. Free Radic. Biol. Med. 51, 2133–2149.

Stewart, J.C.M., 1980. Colorimetric determination of phospholipids with ammonium ferrothiocyanate. Anal. Biochem. 104, 10–14.

Stukey, J., Carman, G.M., 1997. Identification of a novel phosphatase sequence motif. Protein Sci. 6, 469–472.

Sud, M., Fahy, E., Cotter, D., Brown, A., Dennis, E.A., Glass, C.K., Merrill, A.H., Murphy, R.C., Raetz, C.R.H., Russell, D.W., Subramaniam, S., 2007. LMSD: LIPID MAPS structure database. Nucleic Acids Res. 35, D527-532.

Swainsbury, D.J.K., Scheidelaar, S., van Grondelle, R., Killian, J.A., Jones, M.R., 2014. Bacterial reaction centers purified with styrene maleic Acid copolymer retain native membrane functional properties and display enhanced stability. Angew. Chemie Int. Ed. 53, 11803–11807.

Szwedziak, P., Wang, Q., Freund, S.M., Löwe, J., 2012. FtsA forms actin-like protofilaments. EMBO J. 31, 2249–2260.

Tan, B.K., Bogdanov, M., Zhao, J., Dowhan, W., Raetz, C.R.H., Guan, Z., 2012. Discovery of a cardiolipin synthase utilizing phosphatidylethanolamine and phosphatidylglycerol as substrates. Proc. Natl. Acad. Sci. U. S. A. 109, 16504–16509.

Tatar, L.D., Marolda, C.L., Polischuk, A.N., van Leeuwen, D., Valvano, M.A., 2007. An *Escherichia coli* undecaprenyl-pyrophosphate phosphatase implicated in undecaprenyl phosphate recycling. Microbiology 153, 2518–2529.

Teo, A.C.K., Roper, D.I., 2015. Core steps of membrane-bound peptidoglycan biosynthesis: Recent advances, insight and opportunities. Antibiot (Basel). 4, 495–520.

Thomas, M.C., Mitchell, T.W., Harman, D.G., Deeley, J.M., Nealon, J.R., Blanksby, S.J., 2008. Ozone-induced dissociation: Elucidation of double bond position within mass-selected lipid ions. Anal. Chem. 80, 303–311.

Tiwari, G., Tiwari, R., 2010. Bioanalytical method validation: An updated review. Pharm. Methods 1, 25–38.

Tong, S., Lin, Y., Lu, S., Wang, M., Bogdanov, M., Zheng, L., 2016. Structural insight into substrate selection and catalysis of lipid phosphate phosphatase PgpB in the cell membrane. J. Biol. Chem. 291, 18342–18352.

Touzé, T., Blanot, D., Mengin-Lecreulx, D., 2008. Substrate specificity and membrane topology of *Escherichia coli* PgpB, an undecaprenyl pyrophosphate phosphatase. J. Biol. Chem. 283, 16573–16583.

Tribet, C., Audebert, R., Popot, J.L., 1996. Amphipols: polymers that keep membrane proteins soluble in aqueous solutions. Proc. Natl. Acad. Sci. U. S. A. 93, 15047–15050.

Trip, E.N., Scheffers, D.-J., 2015. A 1 MDa protein complex containing critical components of the *Escherichia coli* divisome. Sci. Rep. 5, 18190.

Typas, A., Banzhaf, M., Gross, C.A., Vollmer, W., 2012. From the regulation of peptidoglycan synthesis to bacterial growth and morphology. Nat. Rev. Microbiol. 10, 123–136.

Ulbrandt, N.D., London, E., Oliver, D.B., 1992. Deep penetration of a portion of *Escherichia coli* SecA protein into model membranes is promoted by anionic phospholipids and by partial unfolding. J. Biol. Chem. 267, 15184–15192.

Valianpour, F., Wanders, R.J.A., Barth, P.G., Overmars, H., Gennip, A.H. Van, 2002. Quantitative and compositional study of cardiolipin in platelets by electrospray ionization mass spectrometry: Application for the identification of Barth Syndrome Patients. Clin. Chem. 48, 1390–1397.

van den Brink-van der Laan, E., Antoinette Killian, J., de Kruijff, B., 2004. Nonbilayer lipids affect peripheral and integral membrane proteins via changes in the lateral pressure profile. Biochim. Biophys. Acta 1666, 275–288.

van den Brink-van der Laan, E., Boots, J.-W.P., Spelbrink, R.E.J., Kool, G.M., Breukink, E., Killian, J.A., de Kruijff, B., 2003. Membrane interaction of the glycosyltransferase MurG: a special role for cardiolipin. J Bacteriol. 185, 1–7.

van den Ent, F., Löwe, J., 2000. Crystal structure of the cell division protein FtsA from *Thermotoga maritima*. EMBO J. 19, 5300–7.

van Weeghel, R.P., Keck, W., Robillard, G.T., 1990. Regulated high-level expression of the mannitol permease of the phosphoenolpyruvate-dependent sugar phosphotransferase system in *Escherichia coli*. Proc. Natl. Acad. Sci. U. S. A. 87, 2613–2617.

Vargas, C., Cuevas Arenas, R., Frotscher, E., Keller, S., 2015. Nanoparticle self-assembly in mixtures of phospholipids with styrene/maleic acid copolymers or fluorinated surfactants. Nanoscale 7, 20685–20696.

Vaz, F.M., Pras-Raves, M., Bootsma, A.H., van Kampen, A.H.C., 2014. Principles and practice of lipidomics. J. Inherit. Metab. Dis. 38, 41–52.

Vischer, N.O.E., Verheul, J., Postma, M., van den Berg van Saparoea, B., Galli, E., Natale, P., Gerdes, K., Luirink, J., Vollmer, W., Vicente, M., den Blaauwen, T., 2015. Cell age dependent concentration of *Escherichia coli* divisome proteins analyzed with ImageJ and ObjectJ. Front. Microbiol. 6, 586.

von Meyenburg, K., Jørgensen, B.B., van Deurs, B., 1984. Physiological and morphological effects of overproduction of membrane-bound ATP synthase in *Escherichia coli* K-12. EMBO J 3, 1791–1797.

Wagner, S., Klepsch, M.M., Schlegel, S., Appel, A., Draheim, R., Tarry, M., Högbom, M., van Wijk, K.J., Slotboom, D.J., Persson, J.O., de Gier, J.-W., 2008. Tuning *Escherichia coli* for membrane protein overexpression. Proc. Natl. Acad. Sci. U. S. A. 105, 14371–6.

Wang, Z., Ye, C., Zhang, X., Wei, Y., 2015. Cysteine residue is not essential for CPM protein thermal-stability assay. Anal. Bioanal. Chem. 407, 3683–3691.

Warschawski, D.E., Arnold, A.A., Beaugrand, M., Gravel, A., Chartrand, É., Marcotte, I., 2011. Choosing membrane mimetics for NMR structural studies of transmembrane proteins. Biochim. Biophys. Acta 1808, 1957–1974.

Watrous, J.D., Dorrestein, P.C., 2011. Imaging mass spectrometry in microbiology. Nat. Rev. Microbiol. 9, 683–694.

Webb, M.R., 1992. A continuous spectrophotometric assay for inorganic phosphate and for measuring phosphate release kinetics in biological systems. Proc. Natl. Acad. Sci. U. S. A. 89, 4884–4887.

Wehrli, P.M., Angerer, T.B., Farewell, A., Fletcher, J.S., Gottfries, J., 2016. Investigating the role of the stringent response in lipid modifications during the stationary phase in *E. coli* by direct analysis with ToF-SIMS. Anal. Chem. 88, 8680–8688.

Wehrli, P.M., Lindberg, E., Angerer, T.B., Wold, A.E., Gottfries, J., Fletcher, J.S., 2014. Maximising the potential for bacterial phenotyping using time-of-flight secondary ion mass spectrometry with multivariate analysis and Tandem Mass Spectrometry. Surf. Interface Anal. 46, 173–176.

Weiner, J.H., Lemire, B.D., Elmes, M.L., Bradley, R.D., Scraba, D.G., 1984. Overproduction of fumarate reductase in *Escherichia coli* induces a novel intracellular lipid-protein organelle. J Bacteriol. 158, 590–596.

Wheatley, M., Charlton, J., Jamshad, M., Routledge, S.J., Bailey, S., La-Borde, P.J., Azam, M.T., Logan, R.T., Bill, R.M., Dafforn, T.R., Poyner, D.R., 2016. GPCR-styrene maleic acid lipid particles (GPCR-SMALPs): their nature and potential. Biochem. Soc. Trans. 44, 619–623.

WHO, 2014. Antimicrobial Resistance: Global Report on Surveillance. doi:1.4.2014

Wilkison, W.O., Walsh, J.P., Corless, J.M., Bell, R.M., 1986. Crystalline arrays of the *Escherichia coli sn*-glycerol-3-phosphate acyltransferase, an integral membrane protein. J. Biol. Chem. 261, 9951–9958.

Wilm, M., 2011. Principles of electrospray ionization. Mol. Cell. Proteomics 10, M111.009407.

Wolf, C., Quinn, P.J., 2008. Lipidomics: Practical aspects and applications. Prog. Lipid Res. 47, 15–36.

Worley, B., Powers, R., 2013. Multivariate analysis in metabolomics. Curr. Metabolomics 1, 92–107.

Yang, K., Han, X., 2011. Accurate quantification of lipid species by electrospray

ionization mass spectrometry - Meets a key challenge in lipidomics. Metabolites 1, 21–40.

Yeagle, P.L., 2014. Non-covalent binding of membrane lipids to membrane proteins. Biochim. Biophys. Acta 1838, 1548–1559.

Zhang, J.I., Talaty, N., Costa, A.B., Xia, Y., Tao, W.A., Bell, R., Callahan, J.H., Cooks, R.G., 2011. Rapid direct lipid profiling of bacteria using desorption electrospray ionization mass spectrometry. Int. J. Mass Spectrom. 301, 37–44.

Zhang, R., Sahu, I.D., Bali, A.P., Dabney-Smith, C., Lorigan, G.A., 2017. Characterization of the structure of lipodisq nanoparticles in the presence of KCNE1 by dynamic light scattering and transmission electron microscopy. Chem. Phys. Lipids 203, 19–23.

Zhang, R., Sahu, I.D., Liu, L., Osatuke, A., Comer, R.G., Dabney-Smith, C., Lorigan, G.A., 2015. Characterizing the structure of lipodisq nanoparticles for membrane protein spectroscopic studies. Biochim. Biophys. Acta 1848, 329–333.

Zhang, Y.-M., Rock, C.O., 2008. Membrane lipid homeostasis in bacteria. Nat. Rev. Microbiol. 6, 222–233.

Zhou, X., Arthur, G., 1992. Improved procedures for the determination of lipid phosphorus by malachite green. J. Lipid Res. 33, 1233–1236.

Zimmerberg, J., Kozlov, M.M., 2006. How proteins produce cellular membrane curvature. Nat. Rev. Mol. Cell Biol. 7, 9–19.

Zoonens, M., Popot, J.L., 2014. Amphipols for each season. J. Membr. Biol. 247, 759–796.

Appendix A

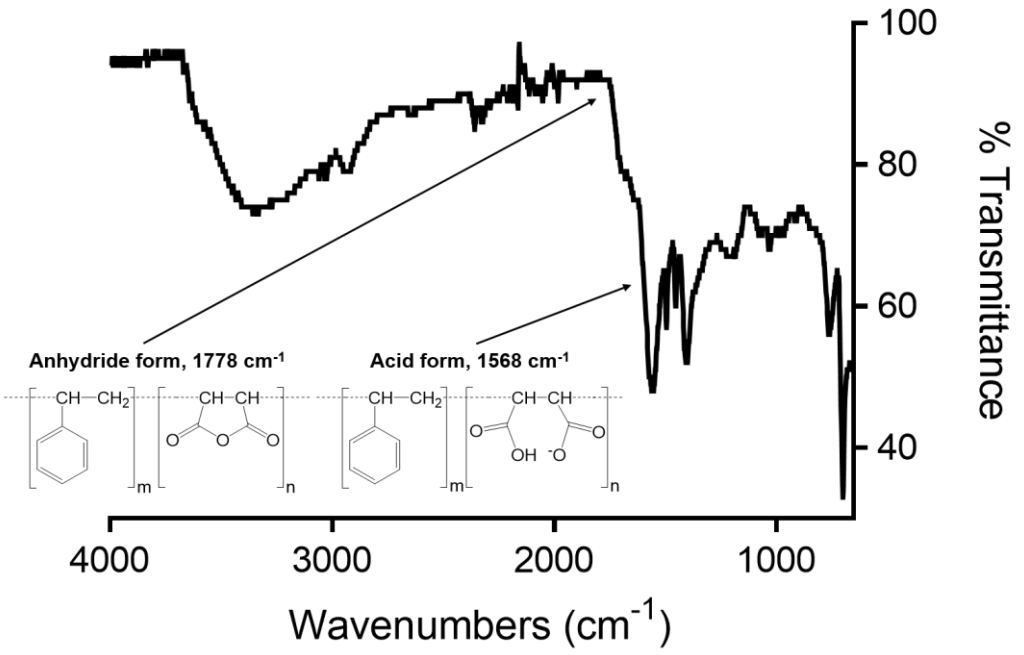

Figure A1. ATR-FTIR analysis of the freeze-dried SMA powder (used in the work in this thesis) showing the disappearance of the anhydride peak at 1778 cm^{-1}, with the concurrent appearance of the carboxylic acid peak at 1568 cm^{-1}.

Appendix B

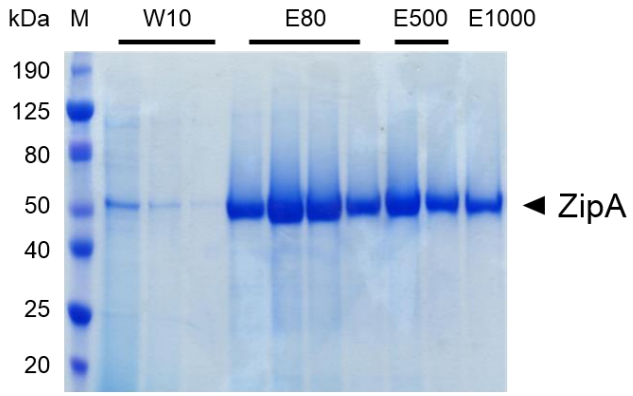

Figure B1. SDS-PAGE gel showing the purification of *E. coli* ZipA in SMALP. SMALP-ZipA was found to be high in purity with a single IMAC purification. M: Molecular marker; W10: 10 mM imidazole washes; E80: 80 mM imidazole elutions; E500: 500 mM imidazole elutions; E1000: 1 M imidazole elution. Figure courtesy of Zoe Stroud, University of Birmingham. Note that Figure 4 in Lee *et al*. (2016) also showcased the purity of SMALP-ZipA obtained upon Ni-NTA IMAC and SEC purification.

Appendix C

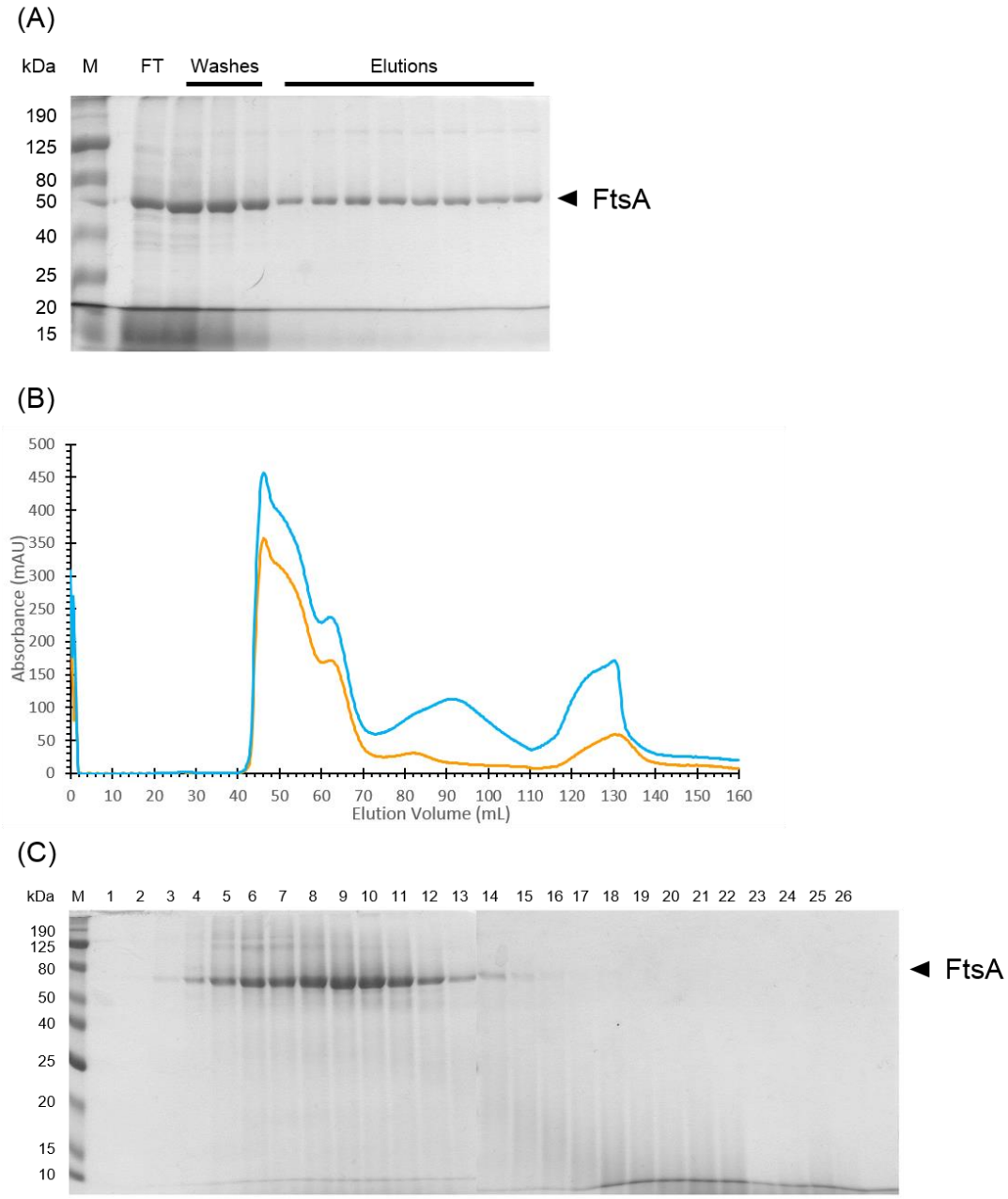

Figure C1. Purification of *E. coli* FtsA in SMALP. (A) SDS-PAGE gel showing SMALP-FtsA was found to elute in high purity after a single Ni-NTA purification. M: Molecular marker; FT: IMAC flow through; Washes: 20 mM imidazole; Elutions: 300 mM imidazole. (B) Elution profile of IMAC-purified SMALP-FtsA using a Superdex 200 16/600 column a flow rate of 1 mL/min. SMALP-FtsA was eluted in 50 mM Tris-HCl, 200 mM NaCl, pH 8. Orange trace corresponds to absorbance at 280 nm while blue trace represents absorbance at 254 nm. (C) SDS-PAGE gel showing selected SEC fractions. Lane 3 to 15 cover the elution volume from 40 to 66 mL (fraction volume of

2 mL), while lane 16 to 26 cover the elution volume from 68 to 88 mL (showing the absence of SMALP-FtsA). Figure courtesy of Stephen Hall, University of Birmingham.